

THE SYNTHESIS AND PROPERTIES OF SOME METALLOCENE  
CONTAINING MACROCYCLES AND THEIR ANALOGUES

by

JONATHAN PAUL KNYCHALA

A Thesis  
presented for the Degree of  
DOCTOR OF PHILOSOPHY  
in the Faculty of Science of the  
UNIVERSITY OF LONDON



Bedford College, London

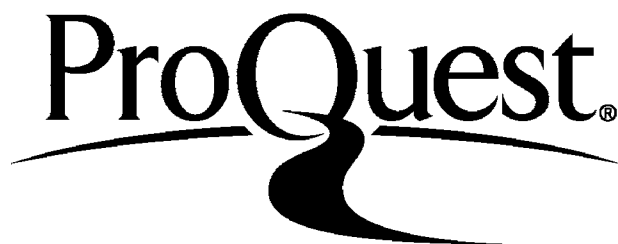
ProQuest Number: 10098532

All rights reserved

INFORMATION TO ALL USERS

The quality of this reproduction is dependent upon the quality of the copy submitted.

In the unlikely event that the author did not send a complete manuscript and there are missing pages, these will be noted. Also, if material had to be removed, a note will indicate the deletion.



ProQuest 10098532

Published by ProQuest LLC(2016). Copyright of the Dissertation is held by the Author.

All rights reserved.

This work is protected against unauthorized copying under Title 17, United States Code.  
Microform Edition © ProQuest LLC.

ProQuest LLC  
789 East Eisenhower Parkway  
P.O. Box 1346  
Ann Arbor, MI 48106-1346

CONTENTS

	Page
ABSTRACT	7
ACKNOWLEDGEMENTS	9
	<u>INTRODUCTION</u>
	11
<u>CHAPTER 1.</u> CROWN-ETHERS AND CRYPTANDS	11
1.1	Introduction 11
1.2	Synthesis 12
1.3	Structure and selective ion-binding 16
1.4	The effect of the ligand on the properties of the cation 23
<u>CHAPTER 2.</u> A REVIEW OF THE CURRENT LITERATURE ON THE USES OF CROWN-ETHERS AND CRYPTANDS	26
2.1	Chemical 26
2.2	Biochemical 47
	<u>DISCUSSION</u>
<u>CHAPTER 3.</u> DISCUSSION	56
3.1	Aims of the project 56
3.2(i)	Structure and physical properties of ferrocene and ruthenocene 58
3.2(ii)	Electrochemistry 61
3.3	The design of ferrocene and ruthenocene macrocycles containing ion-binding ligands 65

	Page
<u>CHAPTER 4.</u> THE SYNTHESIS OF FERROCENE AND RUTHENOCENE DERIVATIVES AND CRYPTANDS	69
4.1 Reactions of ferrocene and 1,1'-disubstituted derivatives	69
(i) Friedel-crafts acylation and subsequent reactions	69
(ii) Lithiation and subsequent reactions	73
4.2(i) Preparation of ruthenocene	78
4.2(ii) The preparation of ruthenocene-1,1'-dicarboxylate and 1,1'-ruthenocene bis acid chloride	84
4.3 Preparation of binding ligands	92
(i) Aliphatic $\alpha$ , $\omega$ -diamines and diaza crown-ethers	92
(ii) Other amines	98
<u>CHAPTER 5.</u> THE CONDENSATION OF METALLOCENE BIS ACID CHLORIDES WITH 'AMINES'	101
5.1 Preparation	101
5.1(i) Introduction	101
5.1(ii) Simple 'amides'	102
5.1(iii) Macrocyclic amides, ferrocene crown-ethers, metallocene cryptands	102
5.2 n.m.r.	109
5.2.1(i) Ferrocene and ruthenocene amides	109
5.2.1(ii) Other ferrocene and ruthenocene amides	126
5.2.2 Ferrocene crown-ethers	129
5.2.3 Metallocene cryptands monomers	133
5.2.3(i) Ruthenocene[2.2]cryptand (monomer) and ferrocene[2.2]cryptand (monomer)	133
5.2.3(ii) Metallocene cryptands (monomers)	146

	Page
5.2.3(iii) Metallocene cryptands (dimers)	151
5.2.4 Dynamic n.m.r.	155
5.2.4(i) Introduction	155
5.2.4(ii) Discussion	158
(a) 'Simple' metallocene amides	158
(b) Cryptands (monomers)	177
(c) Cryptands (dimers)	189
5.3 Ion binding	202
<u>CHAPTER 6.</u> CYCLIC VOLTAMMETRIC STUDIES OF SOME FERROCENE DERIVATIVES	205
6.1 Introduction	206
6.2 Instrumentation	212
6.3 Results and discussion	213
<u>CHAPTER 7.</u> PHOTOELECTRON SPECTROSCOPIC STUDIES OF SOME SUBSTITUTED FERROCENES	234
7.1 Introduction	234
7.2 The molecular orbital bond system for ferrocene	239
7.3 Results and discussion	244
7.4 The correlation of oxidation potentials, ionisation energies (and $\sigma$ Hammett values)	258
<u>CHAPTER 8.</u> FUTURE DEVELOPMENTS AND CONCLUSIONS	266
<u>CHAPTER 9.</u> EXPERIMENTAL	270

	Page
APPENDIX 1. Infra-red spectroscopic results	309
APPENDIX 2. Ruthenium n.m.r.	311
APPENDIX 3. n.m.r. definitions	316
APPENDIX 4. The thermodynamic relationship between the first ionisation energy and the half wave potential.	317
REFERENCES	321

TO DEBRA

ABSTRACT

The objectives of this work were (i) to prepare a number of mono- and bi-cyclic cryptands in which one of the bridges is either a ferrocene or ruthenocene unit and (ii) to investigate the properties of these compounds by a variety of techniques with a view to assessing their ion-binding selectivity and electronic interactions which might occur between the metallocene moiety and the bound metal ion.

The macro bi-cycles were prepared from the parent metallocenes by a number of synthetic routes. The 1,1'-disubstituted ferrocene and ruthenocene were investigated; these materials were then converted by established pathways to the target molecules. Intermediates and the final products of these preparations were fully characterised by a wide variety of spectroscopic and other techniques. Particular attention was paid to the temperature dependence of the n.m.r. spectra of the cryptands themselves, which showed remarkable flexibility. The energetics of these processes were investigated.

The final cyclic reactions leading to the cryptands also afforded in each case quantities of dimeric material which were also isolated and characterized. Some initial investigations were also carried out on the ion-binding properties of these materials.



These cryptands offer the possibility of significant electronic interaction between the metallocene unit and the included metal ion, in such a manner that the degree and nature of the ion-binding may be externally detected. The efficiency of this process relies on the electronic properties of the metallocene itself and these have therefore been investigated by a number of techniques including cyclic voltammetry and photo electron spectroscopy.

ACKNOWLEDGEMENTS

My sincere thanks are due to Dr. M.C. Grossel for his encouragement and direction in the supervision of this work.

To my co-workers Dr. P.J. Hammond and Dr. C.D. Hall (King's College, London) I offer thanks for their arduous efforts and for the publication of our first joint paper.<sup>193</sup>

I am indebted to Mr. D. Parkinson for the detailed variable temperature n.m.r. studies and to Dr. E.A. Seddon, *Mr. Aladin Al Saeed* and Miss. S. Tompkins (University of Sussex) for their cyclic voltammetric and photoelectron spectroscopic studies.

I am grateful to Prof. G.H. Williams for the opportunity of working in this department.

To my colleagues and to all members of the technical, administrative and academic staffs at Bedford and Royal Holloway Colleges I offer my thanks for their help and friendship during my stay.

To Mrs. S. Greenwood I offer my thanks for her patience and typing skills in producing this thesis.

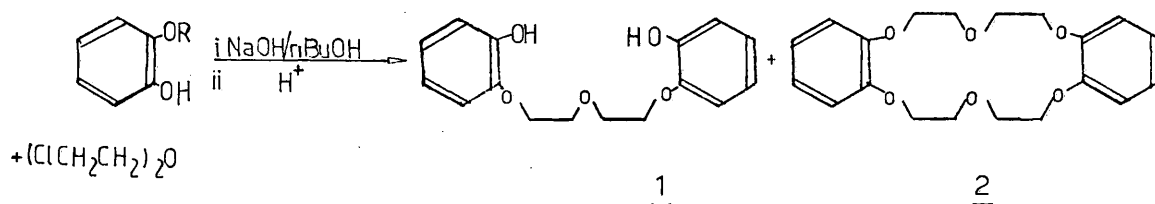
Finally I would like to thank Debra for her support and love while I have been completing this work.

**CHAPTER 1: INTRODUCTION**

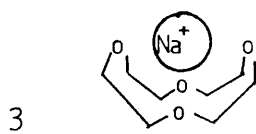
## CHAPTER 1

INTRODUCTION, CROWN ETHERS AND CRYPTANDS1.1. INTRODUCTION

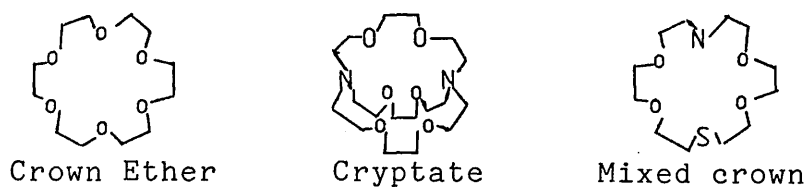
In 1967, Pedersen<sup>1</sup>, reported the synthesis of a group of macrocyclic polyethers, now termed, crown polyethers. Pedersen discovered these compounds while investigating new vanadium containing catalysts for the polymerization of olefins. In attempting to synthesize the phenolic derivative (1), in the reaction scheme below, he obtained as a by-product a 0.4% yield of (2) dibenzo [18] crown-6, which was a white crystalline fibrous solid [Reaction 1.1].

Reaction 1.1

The formation of dibenzo [18] crown-6, arose from the reaction of residual unprotected catechol with the chloroether. It was found to be insoluble in hydroxylic solvents, but, in the presence of added alkali or salt, the compound readily dissolved. Pedersen termed these compounds crown ethers because of their resemblance, in models, to royal crowns and because of their ability to 'crown' alkali metal cations (3).



It was soon recognized that these neutral synthetic compounds were capable of forming selective stable complexes with salts of the alkali metals and this has now opened up a new area of chemistry<sup>2,3</sup>.



The nomenclature adopted is as follows; for (2)dibenzo [18] crown-6, dibenzo- describes the non-ethyleneoxy content; 18, the total number of atoms in the crown ring and 6, the number of heteroatoms in the ring. The crown compounds which display selective ion-binding properties are normally, mono-, bi-, or multicyclic structures consisting of a basic  $-\text{CH}_2\text{CH}_2\text{x}-$  repeat unit, where x the heteroatom is often, oxygen, nitrogen or sulphur<sup>4,13</sup>. Monocyclic structures are known as crown ethers whereas polycyclic structures are known as cryptands.

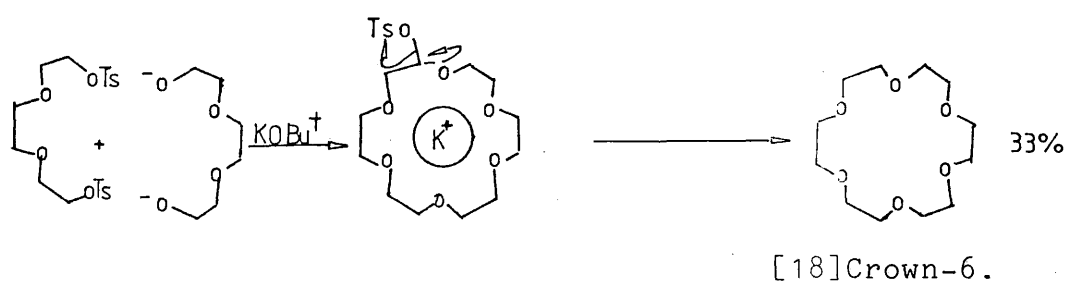
## 1.2. SYNTHESIS

There are only two general methods by which a macrocycle may be prepared: i. the intramolecular nucleophilic displacement of tosyl or halide groups by anions; and ii. the condensation of acid carbonyls with amines.

There are many factors which influence the yield from each method. These include the nature of the bonds being formed and the conformational effects

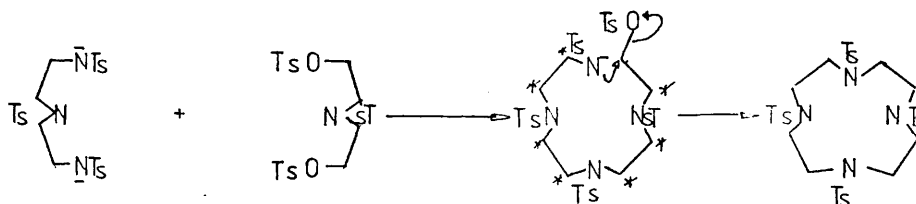
of molecular geometry and template action. Metal-ion coordination plays a major role in organising starting materials or intermediates so as to direct the course of the reaction in favour of cyclisation. This is called the "Template effect"<sup>5-8</sup>. For example the  $K^+$  ion has been shown to act as a template in reaction [1.2] but, not before one tosyl group has

Reaction 1.2.



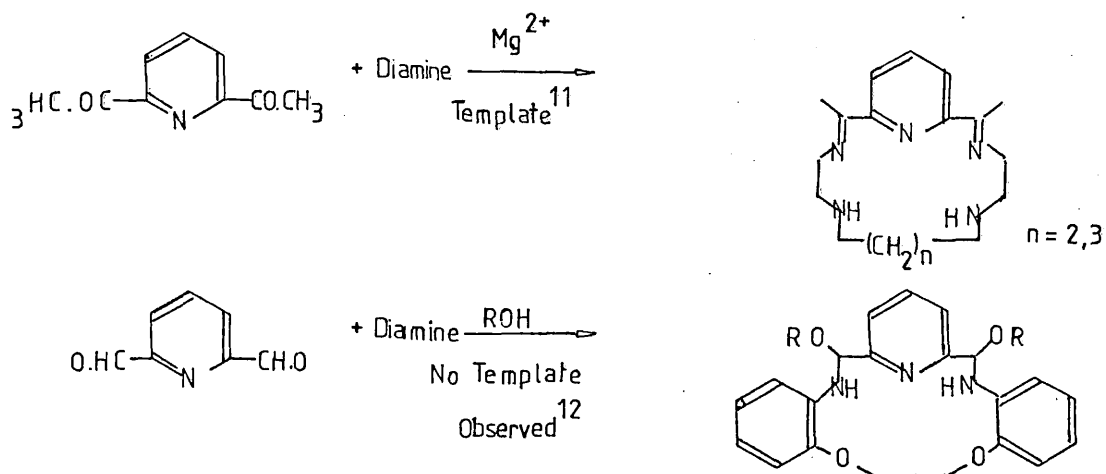
been eliminated i.e. the  $K^+$  only acts by following the linear chain into the correct orientation to cyclise. When the macrocycle contains heteroatoms other than oxygen e.g. sulphur and nitrogen, transition metals have been found to be more useful as templates. The cations  $Ni^{2+}$  and  $Cu^{2+}$  are particularly effective for generating macrocycles containing four donor nitrogen atoms arranged in a plane<sup>6</sup>. The template effect is just one of the factors influencing the internal entropy change on cyclisation. The 80% yield of the macrocycle obtained in reaction [1.3], which shows no template effect has been explained in terms of the internal difference between the half-reacted species and the macrocycle<sup>9</sup>. The restricted rotation about the groups

Reaction 1.3



marked \* caused by the size of the tosyl groups ensures that the internal entropy of the half-reacted molecule is low. Consequently the decrease in entropy for cyclisation is small. The other main factor to be taken into account is the rigidity of the components of the macrocycle's precursors. Any steric compression which reduces the number of conformational degrees of freedom of a molecule must decrease the entropy difference between the reactants and the products. If the effects are such that conformations favourable to cyclisation in the pre-cyclisation intermediate are promoted, the macrocyclic formation may be facile<sup>4</sup>. This is termed, "The rigid group principle"<sup>10</sup> and is illustrated by scheme [1.1].

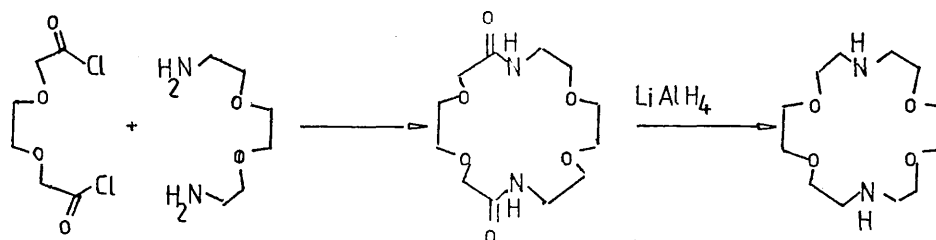
Scheme 1.1



Aza crowns are prepared by a different method from those already mentioned and it is with these that the second part of this project will be mainly concerned.

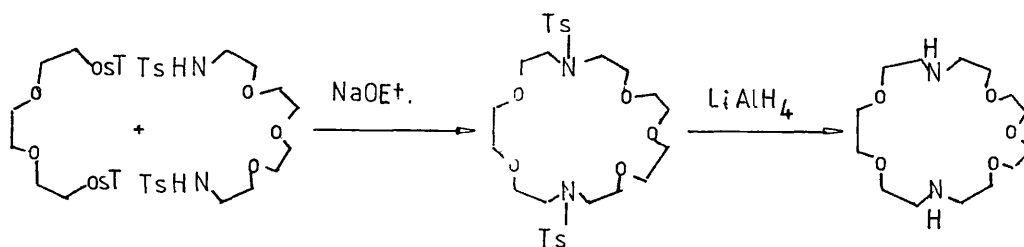
Macrocyclic diamides can be prepared from diacid chlorides and diamines. The diamide is then reduced to form the aza crown [Reaction 1.4]<sup>2,4,13,14,15</sup>. Such compounds may also contain sulphur and/or oxygen heteroatoms in the ring. Further details of the precursors are given in Chapter 4, Section 4.3.

Reaction 1.4



An alternative route to these compounds proceeds by reaction of the glycolditosylate e.g. triethylene glycol ditosylate with the sodium salt of the glycol-diamineditosylate e.g. tetraethyleneglycoldiamine ditosylate [Reaction 1.5]. The cyclic ditosylate is then reduced to form the aza crown. Further details

Reaction 1.5



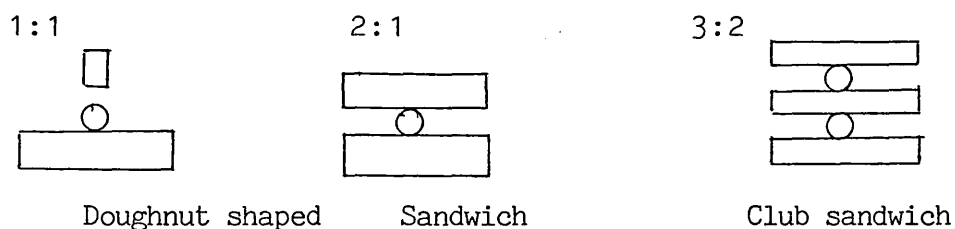
of the precursors and the preferred route are described in Chapter 4, Section 4.3.



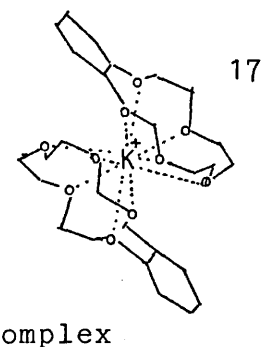
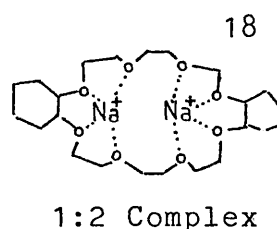
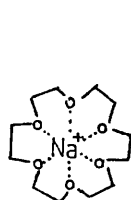
### 1.3. STRUCTURE AND SELECTIVE ION-BINDING

The structures of many macrocyclic compounds have already been investigated by x-ray crystallography<sup>2,3</sup>. In general alkali and alkaline earth metal cations prefer to reside in a symmetrical coordination sphere which reflects their surface charge distribution. For example, in the potassium cation dibenzo[30]crown-10 complex the flexible crown ring encapsulates the cation with all ten oxygen atoms coordinating to the metal ion. Where the ligand does not provide sufficient donor atoms or is inflexible, additional coordination from another crown ether is observed. For example with small crown ethers e.g. dibenzo[15]crown-5, the potassium cation forms a 1:1 complex with one molecule of water coordinated to the potassium. While sodium forms a 1:2 complex, the cation being sandwiched between two rings [Diagram 1.1]. No evidence has yet been obtained for the 3:2 complex in the solid state.

Diagram 1.1

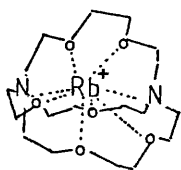


Other crystalline crown ether complexes;



X-ray crystallography of cryptands e.g.  $\text{Rb}^+[\text{2.2.2}]$  cryptate, show the cation to be completely embedded in the cavity of the ligand [Diagram 1.2]. Further evidence from N.M.R., deprotonation and kinetics of dissociation in cryptand(II)<sup>20,21</sup> reveals that there is no interaction between complexed cation and solvent.

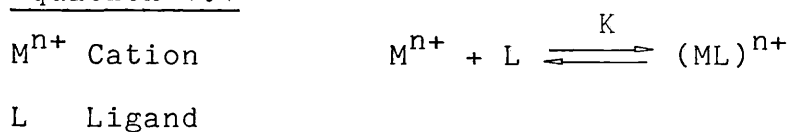
Diagram 1.2



19

This suggests that the cryptate shields the cation from the environment by the ligand skin. The heteroatoms in macrocyclic complexes are capable of replacing most, if not all of the ion's solvation sphere. The degree of complex formation is quantified in terms of the equilibrium constant for the equation [1.1].

Equation 1.1

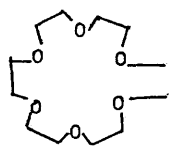
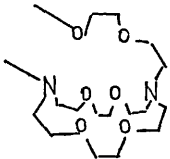
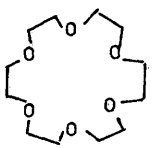
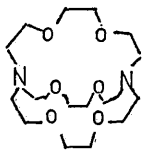


The equilibrium constant  $K$  is the stability constant  $K_s$ , or the association constant  $K_a$ .

It is easily seen that crown ether cation complexes have larger association constants than their open chain analogues because of the greater degree of encapsulation, "The macrocyclic effect"<sup>22,21</sup> [Table 1.1]. A three-dimensional encapsulation would give rise to an even greater association constant and this can

be seen with cryptands e.g. the  $K^+[2.2.2]$  cryptate is more stable than the  $K^+$ -complexes of its corresponding monocyclic coronand by a factor of  $10^5$  and even  $10^4$  times more stable than the  $K^+$  complex of valinomycin (a natural ionophor). This is known as "The cryptate effect"<sup>21</sup>.

Table 1.1

	$\frac{\text{LOG } K_a}{\text{Na}^+ \quad 1.5}$ $\text{K}^+ \quad 2.2$		$\frac{\text{LOG } K_a}{\text{K}^+ \quad 4.8}$
	$\text{Na}^+ \quad 4.3$ $\text{K}^+ \quad 6.1$		$\text{K}^+ \quad 9.7$
The macrocycle effect <sup>22</sup>		The cryptate effect <sup>21</sup>	

$K_a$  in  $\text{lm}^{-1}$  in methanol @  $25^\circ\text{C}$ .

It has been suggested that the unfavourable entropy decrease which the open chain compounds must suffer in order to match the conformations of their cyclic analogues is responsible for the difference in complex stabilities. However, it has been shown that for cryptates there is a large favourable enthalpy increase and that the internal entropy actually decreases due to increased structuring of the solvent upon complex formation. The selectivity of the macrocycle will depend upon, the charge and size of the heteroatoms, and the ligand structure and complexation. The degree of complex formation between a cation and a macrocycle

reflects the compatibility of the ligand cavity size with the size of the ion, i.e. the cation which fits best into the cavity is the most strongly bound [Table 1.2].

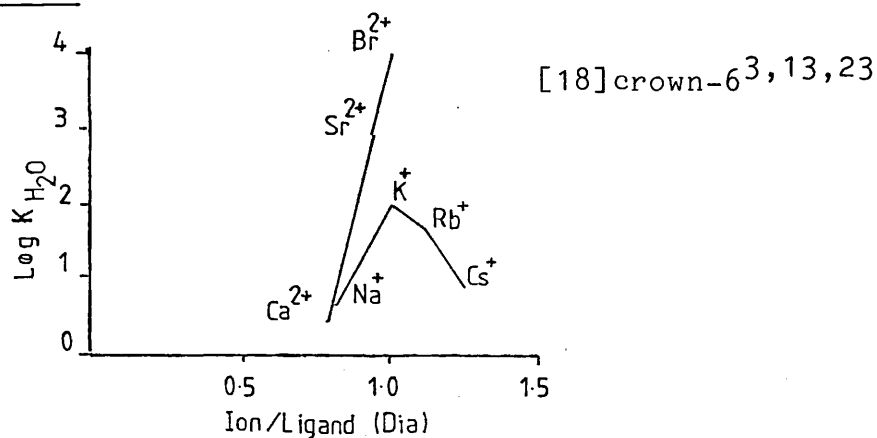
Table 1.2. Stability constants for crown alkali cation complexes<sup>2,13</sup>

Complex	Inside diameter of cavity crown Å	log <sub>10</sub> K in CH <sub>3</sub> OH 25°C		
		Na <sup>+</sup>	K <sup>+</sup>	C <sub>s</sub> <sup>+</sup>
[12]crown-4	1.2-1.5	2.2	1.3	-
[15]crown-5	1.7-2.2	3.7	3.6	2.8
[18]crown-6	2.6-3.2	4.3	6.1	4.6
[21]crown-7	3.4-4.3	2.4	4.3	4.2
Diameter of ion Å		1.94	2.66	3.34

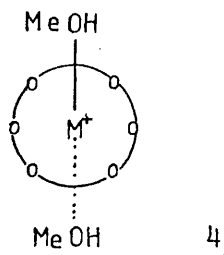
Thus [18]crown-6 which has a cavity diameter of 2.6-3.2 Å prefers to complex with K<sup>+</sup><sup>26</sup>. The limited flexibility of smaller ligands ensures that only cations within a narrow size range can be accommodated in the cavity whereas larger more flexible macrocycles while showing a preference for large cations have much less discriminative powers. For maximum stability the ion-size to crown-size ratio for univalent cations is about 0.9. For divalent ions, the stability constant is larger than that for univalent ions because of the greater polarizing power of the cation. The optimum ratio for the divalent ions is about 0.8 rather than

0.9 or 1.0 which reflects the larger enthalpy changes for the ligation of divalent ions than for monovalent ions [Graph 1.1].

Graph 1.1



It is important to note that when discussing the binding properties of crown ethers reference is made to the solvent in which the experiments are being run. If similar experiments are run in aqueous and methanolic solutions, it is found that the crown ether is less cation selective in aqueous solutions. The reason is that solvation enthalpies ( $\Delta H$ ) for the ions are much larger in water than in methanol. Therefore, the crowns compete much better with methanol than with water for the cations. Methanol has another effect on the crown ether complexes, because the crown ligands are large lipophilic molecules and their metal ion complexes are appreciably soluble in organic solvents e.g. toluene. However, if a small amount of methanol is present the solubility increases greatly. This could result from methanol molecules binding to the ion thus resulting in a more spherically symmetrical distribution of ligands and therefore increased solubility in organic media (4).



The complexation of cryptands with alkali and alkaline earth cations is even more selective than that for crown ethers and their complexes show enhanced stabilities with respect to the crown ethers [Table 1.3]. The  $K^+$  complex of [2.2.2.] cryptand is a factor

Table 1.3

Stability constants  $\log K_{H_2O}$  for various cryptates.<sup>4</sup>

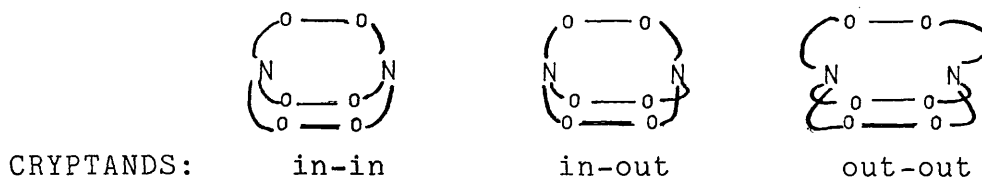
Cryptates		Stability constants $\log K_{H_2O}$								
Ligand	$\text{\AA}$ radius Size	$Li^+$	$Na^+$	$K^+$	$Rb^+$	$Cs^+$	$Mg^{2+}$	$Ca^{2+}$	$Si^{2+}$	$Ba^{2+}$
		0.86	1.12	1.44	1.58	1.84		1.18	1.32	1.49
[2.1.1.]*	0.80	4.3	2.8	<2.0	<2.0	<2.0		2.8	<2.0	<2.0
[2.2.1.]*	1.15	2.5	5.4	4.0	2.6	2.0	<2.0	7.0	7.4	6.3
[2.2.2.]*	1.40	<2.0	3.9	5.4	4.4	<2.0	<2.0	4.4	8.0	9.5
[3.2.2.]*	1.80	<2.0	<2.0	2.2	2.1	2.2	<2.0	2.0	3.4	6.0

\*Size with Nitrogens endo-endo.

of  $10^5$  more stable than the corresponding diaza[18]crown-6 complex and by a factor of 4 when compared with the valinomycin complex (an ionophorous antibiotic).

The cryptands also exhibit a peak selectivity for metal cations which agrees with the ion-cavity size concept i.e. the cation that fits best into the ligand cavity will be most tightly bound.

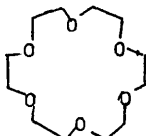
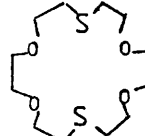
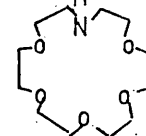
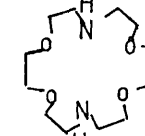
In the bicyclic oligo ethers the two nitrogen atoms serve as bridgeheads. Each of these may be oriented either inward or outward with respect to the central cavity, leading to three possible stereoisomeric forms: in-in, in-out, out-out.<sup>24</sup>



The most favourable isomer for complex formation is the in-in form as the result of electronic lone pairs in the nitrogen atoms pointing towards the metal ion. This has been found by X-ray crystallographic methods in the cation complexes of cryptands and also for the uncomplexed [2.2.2.] cryptand.<sup>25</sup>

Apart from the cavity geometry the nature of the donor heteroatoms of the ligand has a large effect on the cation-selectivity.<sup>4</sup> When oxygen is replaced by sulphur (soft), the ligands show an increased preference for metals with more covalent bond character (soft transition metal ions e.g.  $\text{Ag}^+$ ) and a weakening of binding to alkali and alkaline earth (hard) metal cations.<sup>27,28</sup> Nitrogen as a heteroatom plays the role of a mediator by promoting the complexation of transition metal ions,  $\text{Ag}^+$  without discriminating against alkali metals as well.<sup>27</sup> [Table 1.4].

Table 1.4. A comparison of various  $\log K_s$  values.<sup>2</sup>

Ligand				
$K^+CH_3OH$	6.10	1.15	3.90	2.04
$Ag^+H_2O$	1.60	4.34	3.30	7.80

Further possibilities for new binding site-controlled cation selectivities may be found by the incorporation of phosphorous or arsenic donor atoms into the ligand rings of which, only a few cases have been reported.<sup>29,30</sup>

#### 1.4. THE EFFECT OF THE LIGAND ON THE PROPERTIES OF THE CATION

The effects of neutral macrocyclic ligands on the properties of the cation, other than solubility in organic media (i.e. acting as a super-heavy alkali cation which stabilizes unusually anionic species (Section 1.1.)) has not received much attention.

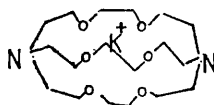
Busch<sup>31</sup> has investigated square planar tetraaza-macrocyclic complexes of neutral, mono and dianionic ligands with transition metals. These complexes show a relationship between the macrocyclic ligand field strengths and the difference between the normal or preferred metal-donor distance (acyclic systems) and the metal-donor distance imposed by the ring size.



When the metal ion is a perfect fit in the ligand cavity, the complex is stable and relatively inert to reactions involving a change in ring size, but when the cation and ligand cavity sizes do not match, reactions leading to a more favourable ionic size, (i.e. oxidation-reduction, change in spin state or movement of the cation out of the plane of the ligand), are promoted by relief of the strain. It is this last observation that can be exploited to great advantage in electrochemistry by changing chemical potentials (Section 4.1, Diag. 1) and thus permitting unusual reactions.

The potentials of  $\text{Ni}^{\text{II}}/\text{Ni}^{\text{III}}$  couples of various tetraazamacrocyclic complexes were shown to vary over a wide range: 1.8 v. Similar behaviour has been reported for  $\text{Fe}^{\text{II}}/\text{Fe}^{\text{III}}$  and  $\text{Co}^{\text{I}}/\text{Co}^{\text{II}}$  systems.

Peter & Cross<sup>32</sup> have reported reduction potentials for  $\text{Na}^+$ ,  $\text{K}^+$  and  $\text{Rb}^+$  cryptates in polycarbonate solution. The complexes were all more difficult to reduce than the free ion, e.g. the reduction potential for the  $\text{K}^+$  cryptate of (5) was 0.9 V more negative than for  $\text{K}^+(\text{aq})$ .



CHAPTER 2: A REVIEW OF THE LITERATURE ON THE USES  
OF CROWN ETHERS AND CRYPTANDS

CHAPTER 2A REVIEW OF THE LITERATURE ON THE USES OF  
CROWN ETHERS AND CRYPTANDS2.1: CHEMICAL

The interest in these compounds arises from their potential usefulness in a variety of fields, physical, chemical and biochemical.

Crown ethers and cryptates represent a new approach to the study of ionic solvation, since they provide cations isolated in coordination shells whose binding sites and geometry may be modified at will. The alkali metal ( ${}^7\text{Li}$ ,  ${}^{23}\text{Na}$ ,  ${}^{133}\text{Cs}$ )<sup>75,80,81,82,83</sup> N.M.R. signals of the crown ethers complexes and cryptates are markedly shifted from those of the free solvated cation. The  ${}^{23}\text{Na}$  nuclear quadrupole coupling constants  $\chi$  of several cryptates obey a linear relationship between<sup>82</sup>  $\chi$  and the  ${}^{23}\text{Na}$  shift  $\delta(\chi = \delta 0.05 + 1.65 \text{ MHz})$ . Thus, measuring  ${}^{23}\text{Na}$  shifts and relaxation times allows a detailed study of  $\text{Na}^+$  solvation in various media. This method should be extendable to other quadrupolar nuclei and enhance the study of field gradients and cation mobility.

Crown ethers and cryptates open a route to a reliable scale of single-ion free energies of transfer<sup>84</sup> and have electrochemical uses.<sup>85</sup> Electrochemical reduction of crown-ether and cryptate complexes occurs

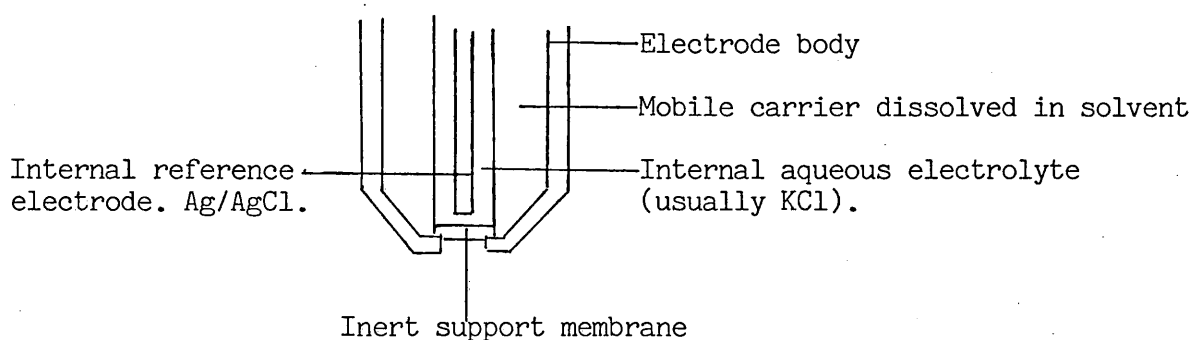
at appreciably more negative potentials than those of the free cations.<sup>86</sup> Macrocyclic compounds can also be used in ion-selective electrodes. These can be divided into three classes; solid ion exchangers, liquid ion exchangers and neutral sequestering agents. The solid ion exchangers, include glass electrodes and solid-state crystal electrodes. The glass electrodes are made from mixtures of silicon oxides with other metal oxides. The selectivity of the electrode results from the type of defect in the glass and is modified by varying the glass composition. Macrocyclic additives will not commonly affect these electrodes.<sup>87</sup>

Liquid ion exchange electrodes are based on a liquid membrane containing a mobile carrier. Examples of mobile carriers include phosphate esters, fatty acids and amines. The first commercial liquid membrane electrode was calcium selective and used didecylphosphate. The selectivity of these electrodes is based on the specific reaction between the carrier and the solute being studied. The mobile carriers in this case are charged. Macrocyclic molecules may be effectively used as mobile carriers in these electrodes.<sup>88</sup>

Neutral sequestering electrodes also use membranes containing a mobile carrier, but this carrier is uncharged. Their selectivity depends totally on the specificity of the reaction between the carrier and the solute being studied. Macrocyclic additives which act as mobile carriers are most useful for this type of electrode.

There are two problems with ion exchange and neutral carrier type, liquid membrane ion-selective electrodes: mechanical stability and reasonable response times. The stability problem is easily overcome by use of an inert support for the liquid e.g. a porous glass frit [Diag. 2.1]. The support is thin enough to allow for rapid establishment of the potential across the membrane.

Diagram 2.1. Liquid membrane electrode.<sup>89</sup>

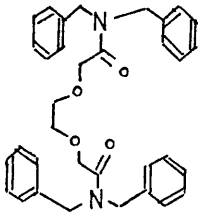
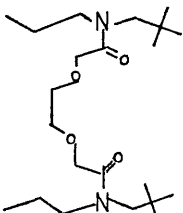
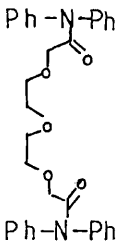


Synthetic macrocycles and natural antibiotics have been used in these electrodes. Most of the work with natural antibiotics, "ionophorous antibiotics", has centred on cation-selective electrodes for the alkali and alkaline earth ions. The earliest electrode was based on valinomycin which showed a selectivity for potassium over sodium 10-100 times greater than the commercial glass electrode.<sup>90</sup> Other neutral antibiotics nonactin, actin, enniatins, gramicidin and tetralactones show potassium selectivity. Nonactin<sup>91</sup> was found to have a selectivity of 750 for potassium over sodium with a glass frit support membrane. Charged

antibiotics behave in a similar manner, nigericin is selective for sodium and monensin is selective for potassium.<sup>92</sup> Since synthetic macrocycles complex ions selectively, they can be substituted for antibiotics. Again the selectivity of the resulting electrode depends on two main factors; the relative equilibrium constant for formation of the ion-macrocylic complex and the membrane solvent. Only crown ethers have been studied extensively. Nitrobenzene solutions of dicyclohexyl[18]crown-6<sup>93</sup> were found to have equilibrium constants for complexation, with potassium, which agreed with the selectivity for the electrode. However the selectivity of potassium over sodium was found to be much less than that of the analogous antibiotic valinomycin electrode. Mascini and Pallozi<sup>94</sup> repeated the same experiment using a different support, polyvinyl chloride, and they found the same result when they compared dibenzo[18]crown-6 with valinomycin. Since then Simon<sup>95</sup> has developed a calcium-selective electrode that can be used in the presence of sodium, potassium and magnesium [Table 2.1]. The carrier here is not cyclic or a polyether but is very similar to them. The selectivity of the carrier (7) for  $\text{Ca}^{2+}$ , compared to those for  $\text{Mg}^{2+}$  and  $\text{Zn}^{2+}$ , is very striking and important for the differentiation of blood sera.<sup>96</sup> Particularly favourable is the fact that the membrane electrode does not interact with  $\text{Na}^+$  and  $\text{K}^+$  under physiological conditions. For similar reasons carriers which are selective for  $\text{Na}^+$  (6) in the presence of

protons are interesting, (6) permits the intracellular determination of  $\text{Na}^+$  in blood serum.<sup>98</sup> Many macrocyclic ligands have not been used but their potential is greater than the natural antibiotics because they can be synthesized with properties specific to the ion to be measured.

Table 2.1. Selectivity constants of carrier molecules in P.V.C. matrices in acidic solution.<sup>97</sup>

<u>6</u>	<u>7</u>	<u>8</u>
		
$\text{Mg}^{2+} \gg \text{Ca}^{2+} > \text{Ba}^{2+} \gg \text{Na}^+ <$ $\text{K}^+ \ll \text{NH}_4^+$	$\text{Mg}^{2+} \gg \text{Ca}^{2+} \ll \text{Ba}^{2+} \ll \text{Na}^+ \approx$ $\text{K}^+ \approx \text{NH}_4^+ < \text{Zn}^{2+}$	$\text{Mg}^{2+} > \text{Ca}^{2+} \gg \text{Ba}^{2+} \ll$ $\text{Na}^+ \approx \text{K}^+ \approx \text{NH}_4^+$
$\text{Na}^+$ selective	$\text{Ca}^{2+}$ selective	$\text{Ba}^{2+}$ selective

The complexing properties of macrocyclic compounds can be utilized as photometric reagents and for other electrochemical determinations; potentiometry, conductometry, polarography.

All picrate extractions by cyclic polyethers and cryptands offer the possibility of direct photometric determination of the extracted salts. Another route involves the introduction of a chromophoric substituent into the macrocycle. 4'-Picrylamino benzo[15]crown-5 forms with  $\text{K}^+$  a reddish-yellow ion pair which is only moderately soluble in water but can be dissolved in organic solvents. In order to separate  $\text{K}^+$  or  $\text{Rb}^+$

from  $\text{Na}^+$ , the aqueous solution is extracted by chloroform containing 0.002 M 4'-picrylamino-benzo[15]crown-5 and 1 M triethylamine.<sup>99</sup> From the difference between the absorption of the chloroform solution before and after extraction the content of  $\text{K}^+$  or  $\text{Rb}^+$  is determined. The determination of 10-400 ppm  $\text{K}^+$  is possible in the presence of 2000 ppm  $\text{Na}^+$ .

$\text{Na}^+$  and  $\text{K}^+$  can be titrated with aqueous solutions of cryptand[2.2.1.] and cryptand[2.2.2.] using an ion selective electrode.<sup>100</sup> The titration is in alkaline solution, the pH of which is adjusted to 9-10 by triethanolamine. Good results are achieved with alkali salt concentrations of  $10^{-3}$  -  $10^{-4}$  mol/l. For  $\text{Li}^+$  the cryptand[2.2.1.] is used. However, the potential drop is small. The [2.2.1.]cryptand will be more suitable for the determination of  $\text{Ag}^+$  because the pK of the complex is 10.6 but this still requires further investigation.<sup>101</sup>

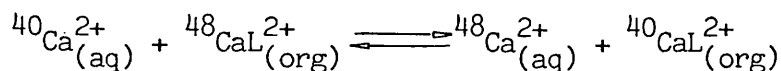
Caesium chloride (0.001 mol/l) can be determined by conductimetric titration in methanol/chloroform (90/60 v/v) with [18]crown-6 or polyvinyl[18]crown-6. The decrease of conductivity at the end point of the titration with polyvinyl[18]crown-6 is particularly high since the mobility of the  $\text{Cs}^+$  complex with the linear polyether is less than with the monomeric polyether.<sup>102,103</sup>  $\text{Na}^+$  can be titrated with dicyclohexano[18]crown-6. However, there is no sharp end point.<sup>104</sup> The conductivities of the single-protonated cryptands[2.1.1.], [2.2.1.] and [2.2.2.] in water are almost equal.<sup>105</sup>



The stability constants of the complexes of dicyclohexano[18]crown-6 with sodium or potassium salts can be determined polarographically. A stability constant of  $1.4 \times 10^3$  is found in acetonitrile for the complex of [18]crown-6 and HgO.<sup>107</sup> Cations complexed by the crown compounds or cryptands are strongly adsorbed on the dropping mercury electrode.<sup>85</sup> The polarographic behaviour of the complex cryptand[2.2.2.] with Tl<sup>+</sup> and K<sup>+</sup> in propylene has also been investigated.<sup>106</sup>

Crown ethers and cryptand complexation now provide a useful method by which cations can be extracted for use industrially, medicinal, chemically and analytically. Because of pollution and increases in the prices of raw materials, the purification and recovery of metals from wastes becomes more important. Cryptands and crown-ethers may be of use in specific cases, if they are fixed on polymer supports for easy recovery.<sup>76</sup> Cryptand[2.2.2.] has already provided a simple extraction method for purifying radioactive  $^{127}\text{Cs}^+$ . Isotope separation was envisaged and good results were obtained for  $^{22}\text{Na}/^{24}\text{Na}$  with cryptand[2.2.1.] in methanol.<sup>75</sup> Other cases, such as  $^6\text{Li}/^7\text{Li}$  and  $^{40}\text{Ca}/^{44}\text{Ca}$ <sup>116</sup> are now under investigation with cryptands. Crown ethers have also been studied in detail for calcium isotope enrichment. For example the separation of calcium-48 from calcium-44 is outlined below;<sup>77</sup> [Reaction 2.1].

Reaction 2.1.



L = macrocyclic polyether.

This reaction tends to go preferentially to the right as written, and therefore, calcium-40 is preferentially enriched in the organic phase. For dicyclohexyl[18]crown-6, the equilibrium separation factor is:  $1.0080 \pm 0.0016$ .

Almost any commercially available counter current extractor can be used to obtain multiple-stage separation with such a separation factor. For example, six columns 60' long and 1.5-6" in diameter can enrich approximately 1000 g of calcium per year from natural abundance.

Closed reflux of these columns can be accomplished by removing the calcium from the calcium polyether complex at one end of the column and reforming the complex at the other end of the column. In a system containing an aqueous solution of calcium chloride and a chloroform solution of dicyclohexyl[18]crown-6 calcium complex. The organic phase is more dense and the bottom reaction is  $\text{CaL}^{2+}_{\text{org}} + \text{H}_2\text{O} \rightleftharpoons \text{L}_{\text{org}} + \text{Ca}^{2+}_{\text{aq}}$ .

This occurs because the calcium ions prefer the dilute aqueous environment to the polyether complex in the organic solution. The equilibrium ratio of  $[\text{Ca}]^{2+}_{\text{aq}}$  to  $[\text{Ca}^{2+}\text{L}]_{\text{org}}$  was found to be: 20-130. The calcium-polyether complex is formed in the separation column by using high calcium concentrations 5 M in the aqueous phase compared to 0.2 M in the organic phase. The reaction at the top of the column is;

$\text{Ca}^{2+}_{\text{aq}} + \text{L}_{\text{org}} \longrightarrow \text{CaL}^{2+}_{\text{org}} + \text{Ca}^{2+}_{\text{aq}}$ . Before recycling the aqueous calcium chloride some reconcentration is required before complexation with the polyether.

[Table 2.2]

Table 2.2.

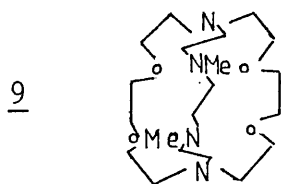
Calculated calcium isotope enrichments from a six-column production cascade using dicyclohexyl[18]crown-6.

Isotope	Natural abundance %	Product concentration %
Calcium-48	0.185	10.0
Calcium-46	0.0033	0.1
Calcium-44	2.06	40.0
Calcium-43	0.145	1.8
Calcium-42	0.64	2.0
Calcium-40	96.97	46.0

This theoretical cascade system has many advantages over other calcium isotope separation methods. It is easier to operate than the mercury amalgam approach<sup>78,79</sup> and avoids the toxicity problems. It is also superior to an ion exchange method in that it is simpler and the single-stage separation factor is considerably larger.<sup>79</sup> Besides isotope separation, liquid-liquid extractions have possible applications for expensive chemical separations, e.g. Lanthanides, aminoacids and optically active isomers.

The development of neoselective crown-ethers and cryptates is important in the treatment of heavy metal poisoning and for decontamination from radioactive metals. The cryptand[2.2.2.] binds with  $\text{Sr}^{2+}$ ,  $\text{Ba}^{2+}$ ,  $\text{Pb}^{2+}/\text{Ca}^{2+}$  and has been tested on rats to remove Strontium-85 and radium-224; it is also effective

for the removal of lead. Cryptand(9) displays a very high selectivity  $10^6$ - $10^7$  for  $\text{Cd}^{2+}$  with respect to  $\text{Zn}^{2+}$  and  $\text{Ca}^{2+}$ , with even higher ratios for lead and mercury. This striking feature is due to the operation of a double-parameter discrimination (cavity size and binding sites) for whilst the nitrogen sites favour both  $\text{Cd}^{2+}$  and  $\text{Zn}^{2+}$  over  $\text{Ca}^{2+}$ , its cavity is too large



for any strong complexation of  $\text{Zn}^{2+}$ . At present there seems to be no other ligand displaying such high selectivities for the heavy metal cations.

"Cryptatotherapy"<sup>21</sup> may become important for the medical treatment of heavy metal poisoning and pollution control from smelters.

The cryptand[2.2.1.] is able to dissolve sodium urate and therefore may have a bright future in the treatment of gout!

There are many other examples of extractions using macrocyclic and polymeric macrocyclic systems. Alkali salts with organic anions e.g. picrates, are easily complexed and extracted by careful choice of the crown-ether any particular cation can be extracted [Table 2.3].

Table 2.3: Extraction coefficients follow the order  
in the benzene/water system

Metal I picrates<sup>109,110</sup>

[15]crown-5	$\text{Ag}^+ > \text{Na}^+ > \text{Tl}^+ \gg \text{K}^+ > \text{Rb}^+ > \text{Cs}^+ > \text{Li}^+$
[18]crown-6	$\text{Tl}^+ > \text{K}^+ > \text{Rb}^+ > \text{Ag}^+ > \text{Cs}^+ > \text{Na}^+ \gg \text{Li}^+$
Dibenzo[24]crown-8	$\text{Tl}^+ > \text{Cs}^+ > \text{Ag}^+ > \text{Rb}^+ > \text{Na}^+ \gg \text{Li}^+$ and $\text{Ba}^{2+} \gg \text{Pb}^{2+} > \text{Sr}^{2+} > \text{Ca}^{2+}$

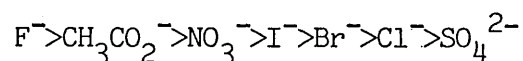
Metal II picrates<sup>111</sup>

[15]crown-5	$\text{Pb}^{2+} > \text{Sr}^{2+} > \text{Ba}^{2+} > \text{Ca}^{2+}$
[18]crown-6	$\text{Pb}^{2+} \gg \text{Ba}^{2+} = \text{Sr}^{2+} > \text{Hg}^{2+} > \text{Ca}^{2+}$
Dibenzo[18]crown-6	$\text{Pb}^{2+} > \text{Hg}^{2+} > \text{Sr}^{2+} > \text{Ca}^{2+}$

The separation of  $\text{Sr}^{2+}$  from  $\text{Ca}^{2+}$ ,  $\text{Mg}^{2+}$  and  $\text{Cs}^{2+}$  in an acetate-buffered solution (pH 4-7) is achieved by using dicyclohexano[18]crown-6 in chloroform. Coextracted  $\text{Ca}^{2+}$  is removed by using a picrate solution buffered with 0.015 mol/l  $\text{NH}_4\text{Cl}$  and the  $\text{Sr}^{2+}$  is finally re-extracted into an aqueous solution containing 2 mol/l HCl and 2 mol/l  $\text{NH}_4\text{Cl}$ .<sup>108</sup>

Alkali salts with hard anions are only slightly soluble in most organic solvents. In order to increase the extraction of these salts by crown ethers, hydrogen-bonding compounds e.g. alcohols and phenols, are added to the organic solvent.<sup>112</sup> An impressive example of high  $\text{Sr}^{2+}$  selectivity is shown when the diester of binaphthyl[18]crown-6 is hydrolyzed by a ten fold excess of barium hydroxide. The selectivity of the crown is so high that only the 0.8% of  $\text{Sr}^{2+}$  present in the barium hydroxide is extracted.<sup>113</sup> The separation

of  $\text{Sr}^{2+}$  and  $\text{Ca}^{2+}$  from milk is performed with dicyclohexano[18]crown-6 in chloroform and this method is now used for the determination of  $\text{Sr}^{2+}$  in milk.<sup>114</sup> For potassium salts and dicyclohexano[18]crown-6, the extraction coefficients decrease in the order;<sup>112</sup>



Extractions with linear polymeric crown compounds show extraction coefficients up to 250 times higher than those of the corresponding monomers.<sup>115</sup>

Polyvinyl[15]crown-5 and polyvinyl[18]crown-6 are easily soluble in most organic media. In the water/dichloromethane system the extraction coefficients with polyvinyl[15]crown-5 are 5 times higher and with polyvinyl[18]crown-6 are 250 times higher than the corresponding monomers. The selectivities are listed in Table [2.4.].

Table 2.4. The selectivity of picrates extraction for polymeric polyethers

Polyvinyl[15]crown-5	$\text{K}^+ > \text{Rb}^+ > \text{Cs}^+ > \text{NH}_4^+ > \text{Na}^+ > \text{Li}^+$
Polyvinyl[18]crown-6	$\text{Cs}^+ > \text{K}^+ > \text{Rb}^+ > \text{NH}_4^+ > \text{Na}^+ > \text{Li}^+$

Many of the liquid, liquid extraction systems may be applied to chromatographic separations; Column chromatography; Extraction; Elution; Exchangers; thin-layer chromatography and thin-layer electrophoresis. The macrocycle may be in the stationary phase or in the mobile phase. Silica gel is employed as a solid

support for dibenzo[18]crown-6 in the separation of radioactive ions. The elution is accomplished with 0.01 mol/l  $\text{NH}_4\text{SCN}$  in water at  $40^\circ\text{C}$  and pH 7. The alkali ions appear in the eluate in the order  $\text{Li}^+$ ,  $\text{Na}^+$ ,  $\text{Rb}^+$ ,  $\text{K}^+$ ,  $\text{Cs}^+$ .<sup>117</sup> Even the separation of isotopes  $^{40}\text{Ca}^{2+}/^{44}\text{Ca}^{2+}$  as mentioned earlier is possible.<sup>116</sup>

Optically active primary amino ester salts are adsorbed on silica gel from an aqueous solution and are separated by elution with chloroform solutions of different derivatives of di/binaphthyl[18]crown-6. The enantiomers are completely separated in this process.<sup>118</sup> A similar method has been used with  $\alpha$ -phenylethylamine and again the pure enantiomers were obtained. The chiroselective properties of some bicyclic and tricyclic cryptands in which the naphthyl group is bound via the bridging oxygen atoms can be analytically exploited.<sup>119</sup> The ligands are deformed by the cations of the different alkali elements to varying degrees so that the complex stabilities differ from each other. The stability constants of their alkali complexes are higher than those of the complexes with all the other polyethers.<sup>120</sup> [15]crown-5, [18]crown-6, and the cryptands[2.1.2.], [2.2.1.], [2.2.2.] are suitable for the separation of cis- and trans-dimethylsemdion.<sup>121</sup> Numerous cross-linked polymeric cyclic polyether exchangers are available which are able to bind particular inorganic salts or organic compounds. These polymeric exchangers can be prepared

by a number of reactions [Table 2.5]. Some of the more notable properties of these exchangers when

Table 2.5. Synthesis of exchangers containing cyclic polyethers as anchoring groups.<sup>2</sup>

Type of synthesis	Matrix	Starting materials	
		Anchor groups	Cross-linking agents
Condensation	Methylene bridges	Dibenzo-crown, and cryptands	Formaldehyde
	Methylene bridges-cross-linking agent	Monobenzo-crown and cryptands	Formaldehyde Toluene, (xylene, phenol, resorcinol)
Polymerization Substitution	Polystyrene		
	Polystyrene		Chloro-methylated polystyrene
	Polystyrene		
	Amino bridges		
	Ether bridges		
	Silica gel, methoxy bridges		Silica gel
	Alkane bridges		

compared with those of commercially available exchangers are: high resistance to chemicals, temperature and radiolysis. They have neutral ligands as anchoring groups which can simultaneously take up cations and anions to maintain electroneutrality. They can strip off the solvent shell of the cation and anion and the binding of the ions is achieved in solvents which are less polar than water. The stability of the polyether complexes depends on cation, anion, solvent,



the size of the polyether ring and on the number, type and position of the heteroatoms. They are also able to activate the anions. Elution by pure solvents and under changing pH conditions causes no pollution of the eluate, except when oxygen and nitrogen are the heteroatoms of the crowns and cryptands. These are pH dependent and at  $\text{pH} < 3$  there is leakage into the solvent.

Cyclic polyether-containing exchangers have many applications in inorganic and organic chemistry, e.g. the separation of cations, anions, non-salt-like organic compounds; trace enrichment of radionuclides; the determination of water in inorganic and organic compounds and various column chromatography techniques.

Cyclic polyethers bound to silica gel or polystyrene are useful in ion-chromatography. In contrast to stationary phases used until now, these permit separation of the cations and anions over the whole pH range in pure solvents e.g. water. A suppressor column is unnecessary and therefore conductivity detectors can be applied without any problems.

The exchangers can also be applied as adsorbents in thin-layer chromatography and electrophoresis. Polyethylene terephthalate sheets<sup>122</sup> are coated with suspensions of powdered exchangers in polyvinyl alcohol solutions. The exchanger layers are non-abrasive and resistant to fracture and most organic solvents can be used except - dichloromethane, chloroform,

and dioxane. An example of the results obtained by thin-layer electrophoresis on exchange layers compared with those obtained by paper electrophoresis for neutral amino acids can be seen in Table [2.6].

Table 2.6. Electrophoresis of neutral amino acids<sup>2</sup>

Solid support electrolyte buffer	Paper Pyridine acetate	Paper 0.75 mol/l formic acid 1.0 mol/l acetic acid(1:1)	D.B[18]C-6 1.09 mol/l formic acid 2.6 mol/l acetic acid
pH	3.6	2.25	1.6
Voltage	100 V/cm	55 V/cm	40 V/cm
Time duration	180 min	150 min	60 min
$R_B$ VALUES                      D.B = Dibenzo			
Gly.	133	143	97
$\alpha$ ABS	107	-	135
Ser.	68	102	156
Val.	100	100	100
Ileu.	-	97	33
Pro.	51	81	135
Phe.	79	79	20
Tyr.	79	70	135
Trif.	88	59	3

It is possible to separate certain amino acids eg, isoleucine, valine, serine and  $\alpha$ -aminobutyric acid, which show non-resolved zones on paper, even when applying a higher voltage or longer separation times.

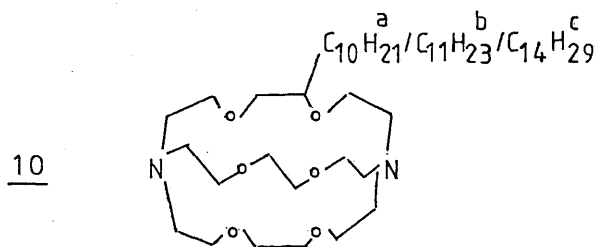
Cryptates and crown ethers complexed with cations have been discussed as separate entities, however, as a single entity, a counter-ion, they do have some interesting properties. To the environment, the anions and the solvent, the complex appears as a spheroidal

cationic species of very large size  $10 \text{ \AA}$  diameter and of low surface charge density which reacts with anions and solvent molecules much more weakly than the largest alkali cation  $\text{Cs}^+$ . They therefore behave as a, "super-heavy" alkali cations,<sup>21</sup> eg.  $\text{K}^+$ -cryptand[2.2.2]. This may result in strong anion activation since stabilization of anions by ion pairing or by solvation is greatly reduced, especially in solvents of low polarity in which cryptate formation causes the increased solubility of insoluble salts. Whereas the cation in crown complexes is still accessible from "top" and "bottom" of the complex, this is much more difficult with the well-encased cations of the cryptates. As a result cation-anion separation is more complete and dissociation constants in solvents of low polarity are much larger. This difference in exposure to the environment, between a partial and complete "organic skin" should affect the properties of the accompanying anion. In ideal conditions complete ion-pair separation in non-polar media should enable the study of gas-phase type chemistry in solution.

Both macrocyclic polyethers and cryptands like [2.2.2.] solubilize alkali metals but, only the latter yields solvated electrons in large concentrations.<sup>21,72</sup> The ability of cryptate counterions to stabilize unusual species is seen in the first salt containing an alkali metal anion  $[\text{Na}^+\text{cryptand}[2.2.2.]\text{Na}^-]$ , as gold-coloured crystals.<sup>72</sup> The  $^{23}\text{Na}$  N.M.R. spectrum contains a narrow

upfield  $\text{Na}^-$  resonance.<sup>73</sup> The electrone (Na<sup>+</sup>cryptand [2.2.2.]e<sup>-</sup>) and (K<sup>+</sup>cryptand[2.2.2.]K<sup>-</sup>) have also been observed.<sup>21</sup> Cryptate counterions are useful in the determination of the crystal structure of polyatomic anionic clusters of the heavy post-transition metals,<sup>74</sup>  $\text{Sb}_7^{3-}$ ,  $\text{Pb}_5^{2-}$ ,  $\text{Sn}_7^{4-}$ . Complexation of Na<sup>+</sup> by cryptate [2.2.2.] prevents reversion to the starting Na/metal alloy phase.

Strong basic systems<sup>123</sup> can be obtained by the addition of cryptate[2.2.2.] to a solution of tert-amylate in benzene or butyllithium in hexane. The pKa of tert-amylate anion with the potassium cation complexed by cryptand (10) is approximately 37.<sup>124</sup>



The highly hindered ester, methyl mesitoate, is hydrolyzed at room temperature by cryptand[2.2.2.] with powdered potassium hydroxide suspended in dry benzene or much more rapidly by concentrated solutions of potassium hydroxide in dimethyl sulphoxide in the presence of cryptand[2.2.2.].<sup>123</sup>

Macrocycles are useful in phase-transfer catalysis,<sup>125</sup> assisting transfer from solid to liquid or from liquid to liquid. Catalytic amounts of the macrocycle can bring about numerous reactions from solid salts<sup>26,123</sup>

under unusual solvent conditions thus preventing side reactions. Cryptands or derivatives immobilized on a polymer support were found to be efficient for salt solubilization and for liquid to liquid phase transfer catalysis for a variety of simple substitution reactions [Table 2.7].

Table 2.7.

Substrate	Product	Catalyst + Reaction medium	Yield %
1. n-C <sub>8</sub> H <sub>17</sub> Br	n-C <sub>8</sub> H <sub>17</sub> I	KI CR.Ic 60°C 0.2 hr	100
2. n-C <sub>8</sub> H <sub>17</sub> Cl	n-C <sub>8</sub> H <sub>17</sub> CN	KCN CR.Ic.	93
3. n-C <sub>8</sub> H <sub>17</sub> Br	n-C <sub>8</sub> H <sub>17</sub> SPh	PhSNa CR.Ic.	100

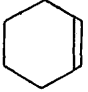
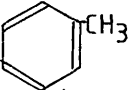
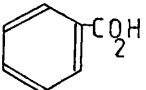
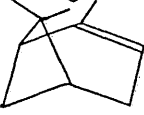
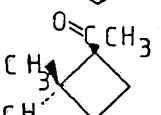
CR - Cryptand; CE - Crown Ether; L - liquid; S - solid

Crown ethers have found more specific use in phase transfer catalysis and are especially useful for synthetic organic reactions; oxidations, reductions, displacements, alkylations, and eliminations [Table 2.8].

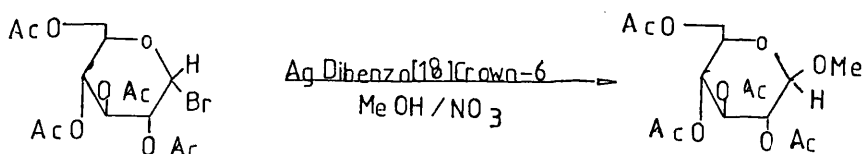
Oxidizing anionic species, transferred into an organic medium by a crown ether normally show much higher reactivity than under classical conditions. For example oxidations with potassium permanganate where the anion  $\text{MnO}_4^-$  is transferred into a non-polar organic medium like benzene (to give "purple benzene") by complexed macrocyclic polyethers occur both in liquid, liquid and solid, liquid phase transfer systems. This procedure eliminates the self-catalyzed decomposition

of  $\text{MnO}_4^-$  which occurs with the evolution of oxygen. Olefins, alcohols, alkylated arenes etc. are thus oxidized to carboxylic acids, ketones, aldehydes or glycols. The reactions are generally exothermic. However, the oxidation is extremely sensitive to the pH of the aqueous phase.

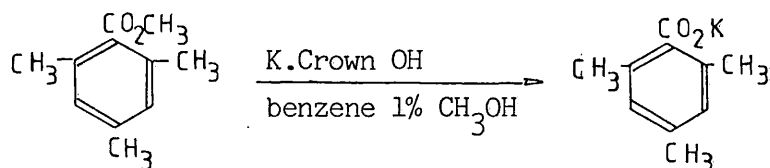
Table 2.8. Reactions using crown ethers as a phase transfer catalysis.<sup>2</sup>

Substrate	Product	Catalyst and reaction medium	Yield %
	$\text{HO}_2\text{C}(\text{CH}_2)_4\text{CO}_2\text{H}$	C.E. $\text{KMnO}_4$ S.L	100
		C.E. $\text{KMnO}_4$ S.L	78-100
		C.E. $\text{KMnO}_4$ S.L	90
Rx	RCN	CE or CR NaCN L.L	85-98
Rx	RHalogen	CE Halogen L.L	77-100
$\text{CH}_2(\text{CO}_2\text{Et})_2$	$\text{RCH}(\text{CO}_2\text{Et})_2$	CE $\text{K}_2\text{CO}_3$ RHalogen S.L	94
$\text{R-CH}_2\text{CH}_2\text{Halogen}$	$\text{RCH}=\text{CH}_2$	CE $\text{Ba}^+\text{OK}$ S.L	73-97
$\text{RCH}=\text{CH}_2$		CE NaOH $\text{CHClBr}_2$ L.L	44-62
$\text{NH}_2\text{NH}_2$	$\text{CH}_2\text{N}_2$	CE NaOH $\text{CHCl}_3$ L.L	48

Dibenzo[18]crown-6 has been used to solubilize silver nitrate in alcohols so that the synthesis of glycosides from  $\alpha$ -bromo sugars is possible under homogeneous conditions. The silver ion of silver nitrate is bound strongly enough to form a stable soluble crown ether

Reaction 2.2

complex [Reaction 2.2]. However, the binding energy is not as strong as the AgBr/ClHiCl energy. (If it were, the driving force for the reaction would be lost.) Crown ethers will dissolve sodium and potassium hydroxide in benzene and if traces of methanol are present concentrations up to 1 M may be achieved. These solutions are powerful reagents for the saponification of highly hindered water-insoluble esters eg. mesitoic acid [Reaction 2.3].

Reaction 2.3

Crown ethers and cryptands can be used for the reduction of carbonyl compounds to alcohols with NaBH<sub>4</sub> in a two-phase aqueous-organic system. However, the reaction will proceed slowly because in the homogeneous organic phase, complexation of LiAlH<sub>4</sub> or NaBH<sub>4</sub> by specific cryptands ([2.1.1.] for Li and [2.2.1.] for Na) inhibits the reduction of ketones, due to the absence of the electrophilic activation by the inorganic cation. There are many other examples of the uses of phase transfer catalysts and crown ethers and cryptands which may be found in the reviews.

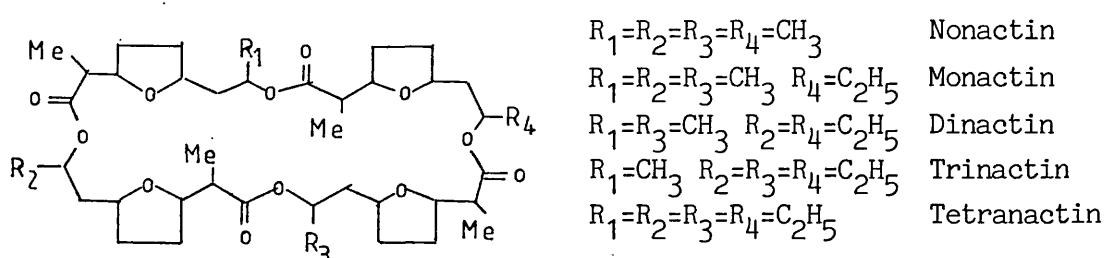
## 2.2. BIOCHEMICAL USES OF CROWN ETHERS AND CRYPTANDS

The close similarity of crown ethers and cryptands to ionophorous or ion-carrying antibiotics offers a great potential in biochemical reactions. The essential metals of the human body (~70 Kg) may be divided into two categories; "Bulk" metals - sodium, potassium (~170 g), magnesium and calcium, which constitute about 1% of the human body weight and "Trace" metals - iron (~5 g), manganese, copper, iron, cobalt, zinc, vanadium, chromium, and molybdenum, which constitute less than 0.01% of the human body. However, it is the trace metals that have been studied most during recent investigations of metal ions in biological processes. This is because, the bulk metals have very few spectroscopic properties. They have no unpaired electrons and cannot be studied by magnetic measurements or electron spin resonance spectroscopy. However some complexes of  $^{23}\text{Na}$  and  $^{44}\text{Ca}$ ,  $^{75}\text{Fe}$ ,  $^{80}\text{Zn}$ ,  $^{81}\text{Zn}$ ,  $^{82}\text{Zn}$ ,  $^{83}\text{Zn}$  can be studied by nuclear magnetic resonance spectroscopy. The alkali metal cations are concerned in vivo with the maintenance of normal water balance and distribution, the conduction of nerve impulses, and neuromuscular activity. Potassium helps the heart to relax between beats. These roles are related to the ionic character and mobility of the cations. Sodium and potassium are also required to activate certain enzymes by mechanisms which are as yet undefined. Sodium and potassium have a great difference in their location and this is easily seen in mammalian blood cells.  $\text{Na}^+$  is principally



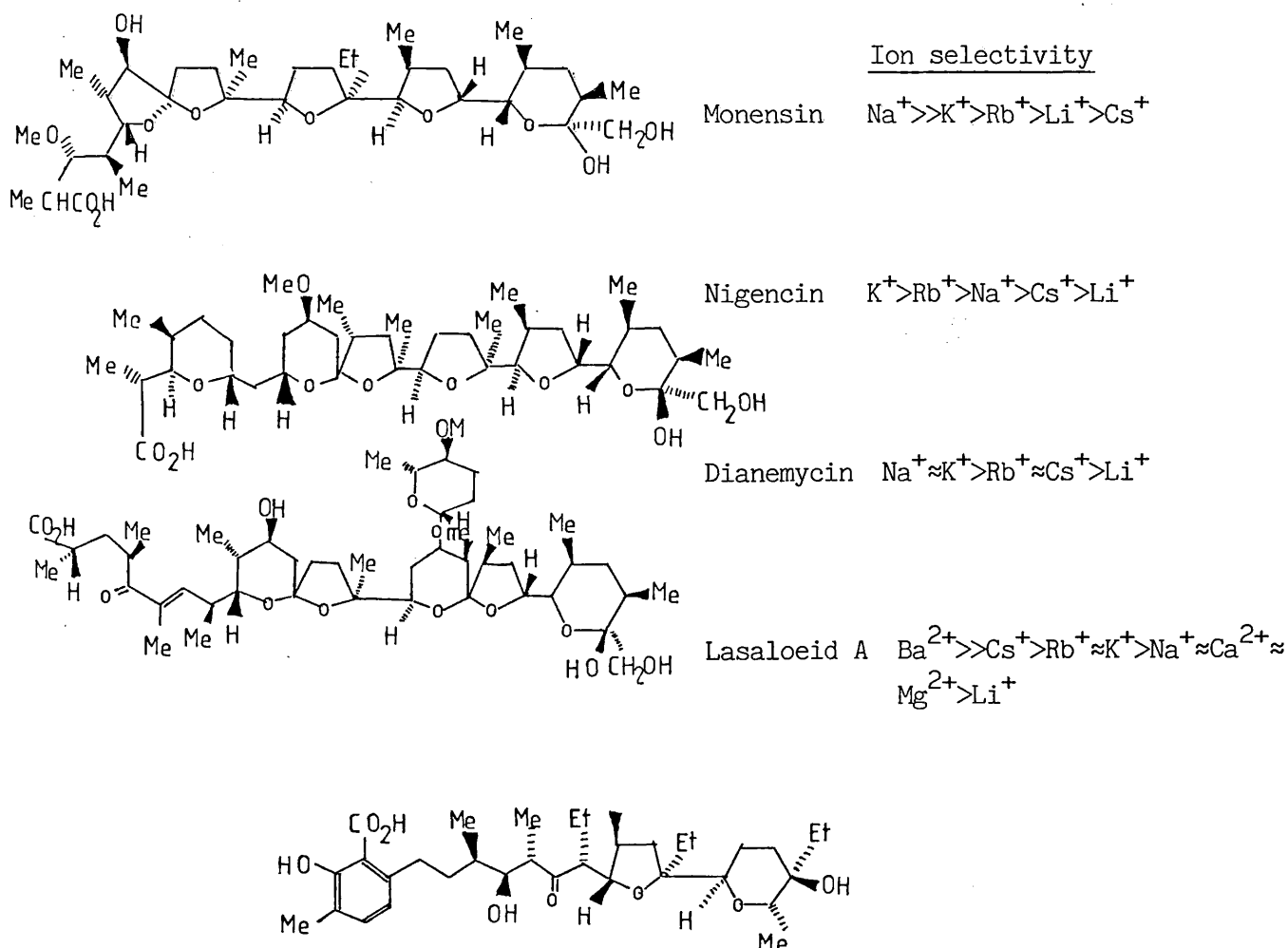
extra-cellular ( $143 \text{ mM Kg}^{-1} \text{Na}^+$  compared with  $5 \text{ mM Kg}^{-1} \text{K}^+$  for blood plasma) and  $\text{K}^+$  is intra-cellular ( $105 \text{ mM Kg}^{-1} \text{K}^+$  compared with  $10 \text{ mM Kg}^{-1} \text{Na}^+$  for red blood cells). There is, therefore, a discriminatory mechanism which controls the selective uptake of  $\text{K}^+$  across the membrane into the cell from the plasma. To reach the inside of the cell any alkali metal must cross the lipid bylayer which is a layer of low dielectric constant. This is unfavourable because of the high electrostatic energy required to transfer an ion from high dielectric aqueous solution into the low dielectric hydrocarbon. To overcome this two main mechanisms have been proposed; the cations can cross the membrane in association with organic molecules or by pores in the membrane. It is the first mechanism that is of great importance since if a macrocycle can be found which can achieve five simple requirements - selective cation binding; crossing of cell membranes; water solubility; an indicator change when bound to a cation; and non-toxicity - it will be possible to investigate the internal mechanism of the cell and measure accurately the internal free-unbound concentration of various cations.<sup>126</sup> One immediate use would be in detecting tumour cells since tumour cells have much larger concentrations of  $\text{Ca}^{2+}$  than normal cells.

Table 2.9. Thenactins - ionophorous antibiotics<sup>3</sup>



The antibiotics nigencens, lasaloeids and nactins [Table 2.9] were the first naturally occurring ionophores to be isolated in 1951 from streptomyces cultures.<sup>127</sup> These compounds were subsequently investigated and it was found that they had outstanding properties as selective cation carriers and were neutral at physiological pH. They could increase the permeability of black-lipid films and were found to increase the selective movement of  $K^+$  into rat liver mitochondria. All of these antibiotics either possess or can fold up to form a large ring of fourteen or more members resulting in a symmetrical arrangement of  $-CO-$ ,  $-NH-$ , or  $-O-$  groups which act as ligands towards the central cation.

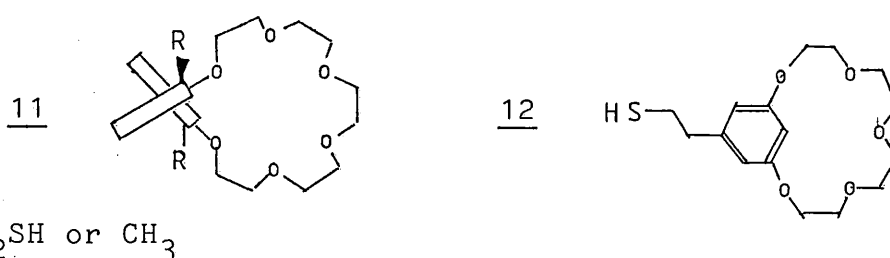
Table 2.10. Polyether antibiotics. The nigencins<sup>127,3</sup>



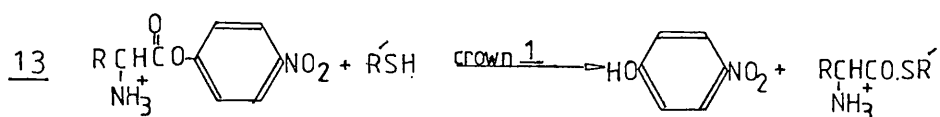
The ion-selectivities of the polyether antibiotics given in Table [2.10] are lower than those of the nactins, (see ion-selective electrodes) but are still large. The ionophorous antibiotics have a limited human use because they are highly toxic to mammalian cells, although monensin and others are used in poultry foods.<sup>3,126</sup> The main function here is to cause potassium ion leakage which results in the eventual death of the cell. For this reason of leakage they have been studied as a system by which ion gradients could be altered to control biological functions via ion transport through membranes. The discovery of a calcium transporting antibiotic, lasaloeid A, started numerous studies into its physiological properties. It was found to release  $\text{Ca}^{2+}$  down a concentration gradient from loaded vesicles prepared from muscle sarcoplasmic reticulum. An immediate application of this property was as a cardiovascular reagent. Tests on guinea pig and rabbit heart preparations resulted in an increase in the contractile force and spontaneous beat frequency. Studies on dogs produced a three-fold increase of the contractility index, after an intravenous dose of 2.0 mg/Kg. Similar effects were also seen with monovalent ionophores, monensin. At low concentrations 50  $\mu\text{g}/\text{Kg}$  (2.25  $\mu\text{g}/\text{Kg}$  totally specific response) monensin produces a relaxation of smooth muscle of the coronary arteries which results in increased coronary blood flow. At higher concentrations 0.2 mg/Kg monensin produces an initial dilatation of the systemic arteries and an increase in cardiac

contractility (blood pressure and heart rate). These clinical applications are hampered by the toxicity of the ionophore. However, due to the possible commercial applications, extensive research is still being continued with these natural polyether antibiotics.<sup>126</sup>

Other natural products that have specific binding properties can be seen in enzymes, carbohydrates and proteins all of which are found in metabolic processes which are essential for life. The enzymes protease<sup>128</sup> and transacylase are imitated by certain types of crown compounds (11) and (12) which are able to bind ammonium salts and introduce sulphur nucleophiles at the proper



position to attack an activated carbonyl group in the ammonium substrate<sup>129</sup> eg. ammonium salts of activated amino acid esters (13). The major contributing factor

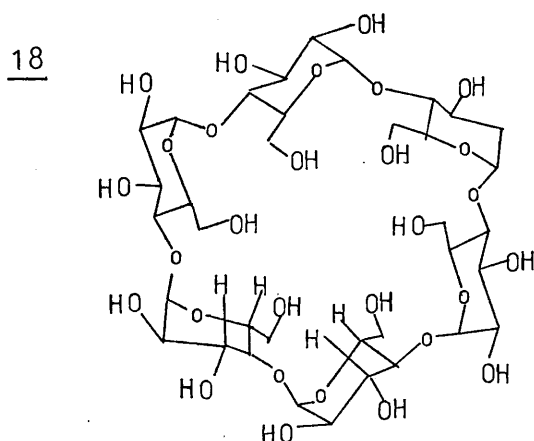


to enzyme catalysis is the polarization of the carbonyl group by an electrophile, in metabolic processes.

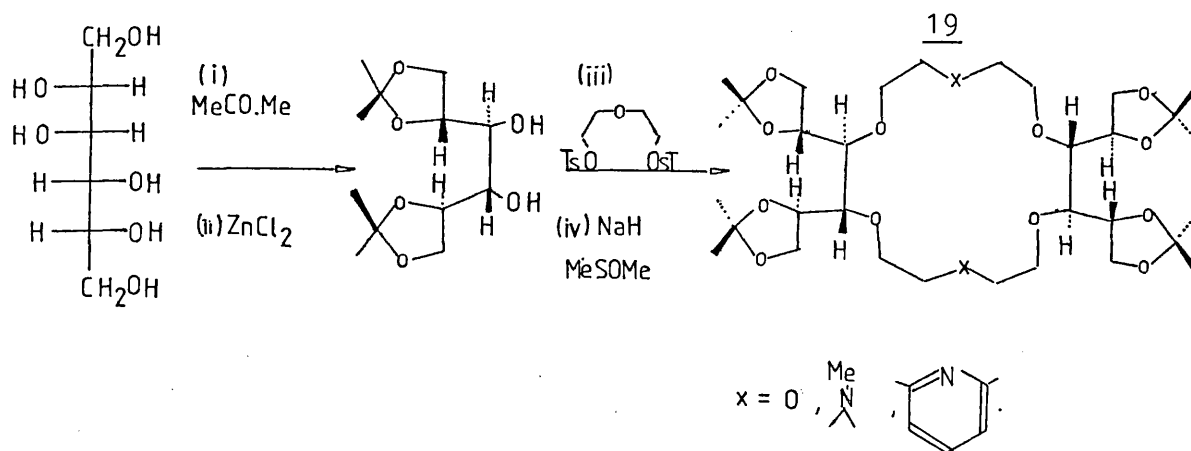
This occurs by an imidazole group or a zinc ion in a peptide chain.<sup>3</sup> Synthetic dihydropyridines<sup>130,131</sup> with complexed magnesium ions are the best synthetic electrophilic catalysts and are now being incorporated into crown ethers (14)(15).



Crown ether and cryptate analogues can also be seen in carbohydrates, polysaccharides and proteins. Amylose, a polysaccharide compound which forms 20% of starch can form cyclohexa-amylose<sup>136</sup> (18), which has a diameter cavity of 4.5 Å. This is large enough for a benzene ring and it can serve as a host molecule in aqueous solutions for organic guest molecules.



The cyclohexa-amylose complexes have a high association constant  $10^2$ - $10^4$   $\text{l.mol}^{-1}$  due to hydrophobic bonding and have been shown to exhibit covalent catalysis, (the hydrolysis of *m*-*t*-butylphenylacetate is accelerated 260 times) and non-covalent catalysis, (the *p*-chlorination of anisole with hypochlorous acid is accelerated 5.3 times with high regioselectivity, *para*:*ortho*: 96:4). Other examples of new chiral crown-ether carbohydrates are, the D,D. tetra-*O*-isopropylidenedi-D-mannito[18]crown-6 derivative<sup>135</sup> (19) prepared from D. diethyleneglycol bistosylate in 24% yield together with the [9]crown-3 and [27]crown-9 homologues. Other similar carbohydrates with pyridine and nitrogen substituents in the crown ether ring have also been prepared.<sup>135</sup>



This brief introduction has reviewed some of the applications and potentials of crown ether and cryptand type compounds. It is clear that they are becoming an essential part of modern chemistry and that they will soon be invaluable in industry and medicine.

CHAPTER 3: DISCUSSION



CHAPTER 3DISCUSSION3.1. AIMS OF THE PROJECT

The aim of this work is to find a system capable of both complexing a metal ion in organic and aqueous solutions and also effecting or facilitating electron transfer to or from the complexed cation.

Such a process may occur spontaneously, thermally or be initiated photochemically. One way this has been envisaged is by using a macrocyclic system already containing an oxidisable metal ion locked in a  $\pi/\sigma$ -bond framework of a metallocene. In order to complex the second metal ion (the cation) it was decided to use a monodentate and bidentate macrocyclic ligands of a crown-ether type.

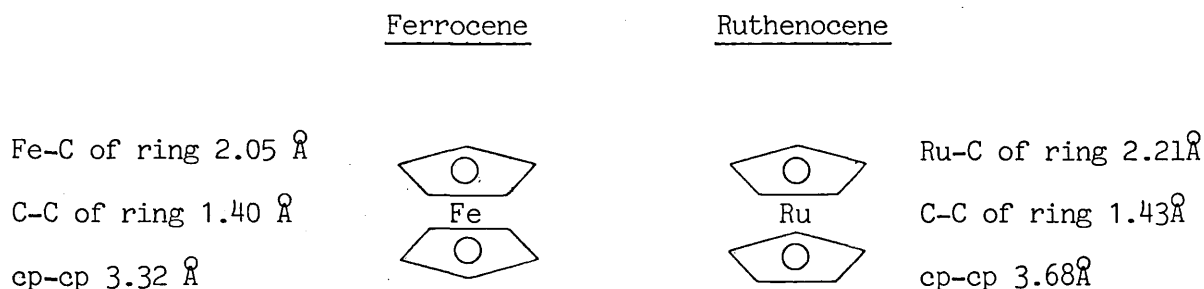
The molecules being prepared in this work will consist of a metallocene bridged by a macrocyclic ligand and because of good documentation, air insensitivity and relative ease of preparation of their derivatives ferrocene and ruthenocene were chosen as the metallocene unit.

Ferrocene and ruthenocene display two important features essential for this work: i) a metal atom capable of releasing an electron and ii) two cyclopentadienyl rings which can be readily functionalised

(Chapter 4). Ruthenocene is of particular interest since it has two n.m.r.  $^{138,139}$  active isotopes,  $^{99}\text{Ru}$  and  $^{101}\text{Ru}$ , with a relative natural abundance of 13 and 17% which may facilitate the investigation of the metallocene/bound metal ion (cation) interaction. The iron in ferrocene also has one n.m.r. active isotope  $^{57}\text{Fe}$  (2.2% abundance) and the signal for ferrocene  $^{137}$  has been found. However, due to its low abundance and sensitivity it would be a poor n.m.r. probe.

3.2.i. STRUCTURE AND PHYSICAL PROPERTIES OF FERROCENE  
AND RUTHENOCENE

In the solid state monoclinic crystals of ferrocene<sup>140</sup> have the planar antiprismatic (staggered) configuration\*, whereas orthorombic crystals of ruthenocene<sup>46</sup> has the planar prismatic (eclipsed) configuration. This suggests that the inter-ring repulsive forces in ruthenocene are less than in ferrocene which agrees with their larger inter-ring distance (x-ray diffraction).



Electron diffraction of ferrocene<sup>140,141,142</sup> in the gas phase has found that it has an eclipsed prismatic configuration and a barrier to rotation of only  $3.8 \pm 1.3 \text{ kJ mol}^{-1}$ . Hence the rings are almost free to rotate and the configuration adopted in the crystal is susceptible to packing forces. Electron diffraction of ruthenocene<sup>25,41</sup> gave consistent data for the prismatic structure but, were insufficiently accurate to permit calculation of the internal rotation barrier of the cyclopentadienyl rings. However, calorimetric and x-ray diffraction measurements between  $77^\circ$  and  $300^\circ \text{ K}$  indicate the absence of any phase transition, in contrast to ferrocene.<sup>45</sup> Three independent studies

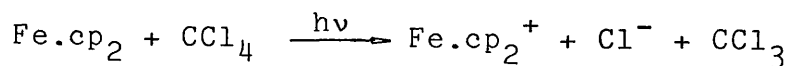
\* SEE REFERENCE 174 for the latest information.

of ruthenocene in the solid state by  $^1\text{H}$  n.m.r. have yielded three different values for the activation enthalpy for ring rotation: 7.53; 9.62; and 18.87  $\text{kJ mol}^{-1}$ . These results indicate that the rotational barrier is due to a combination of bonding forces within the molecule and crystal packing forces and the non-bonding interactions between the rings are small. However, monosubstituted and 1,1'-disubstituted derivatives of ruthenocene all have significantly higher activation energies towards ring rotation. Calorimetric studies on ferrocene have shown that there is a  $\lambda$  point transition at  $163.9^\circ\text{K}$  ( $\lambda$  range  $125\text{-}200^\circ\text{K}$ ). N.m.r. studies on solid ferrocene over the range  $50\text{-}425^\circ\text{K}$  show that the line width varies on cooling, as would be expected during a transition from a 'liquid' situation to a 'rigid' solid. The data suggests that there is a considerable reorientation of the molecule between  $60\text{-}80^\circ\text{K}$ . However, in the range  $115\text{-}225^\circ\text{K}$  (also  $\lambda$  range) there is an anomalous line-width broadening with increasing temperature. These observations are due to reorientations of the molecule in the lattice and transitions between eclipsed and staggered configurations of ferrocenes.<sup>143</sup> Low-temperature crystallographic studies show no large changes of unit-cell constants in the  $\lambda$  region but there are torsional vibrations in the crystals.

Cell constants

Ferrocene <sup>140</sup> Å		Ruthenocene <sup>46</sup> Å	
a	10.561	a	7.13
b	7.567	b	8.99
c	5.952	c	12.81
2 molecules per unit cell		4 molecules per unit cell	

Ruthenocene and ferrocene have been studied extensively by ir, raman<sup>47-50</sup> and electronic spectroscopy<sup>41</sup> under a variety of experimental conditions and physical states. The infrared spectra and enthalpy of formation indicates the ring-metal bond strength : ruthenocene > ferrocene. It is of interest to note that both ferrocene and ruthenocene are inert in hydrocarbon solvents but not in chlorinated solvents. Irradiation of ferrocene in carbontetrachloride produces a free radical breakdown of the solution in which the ferricenium ion can be detected and isolated [Dig. 3.1]. Similar irradiation

DIG. 3.1.

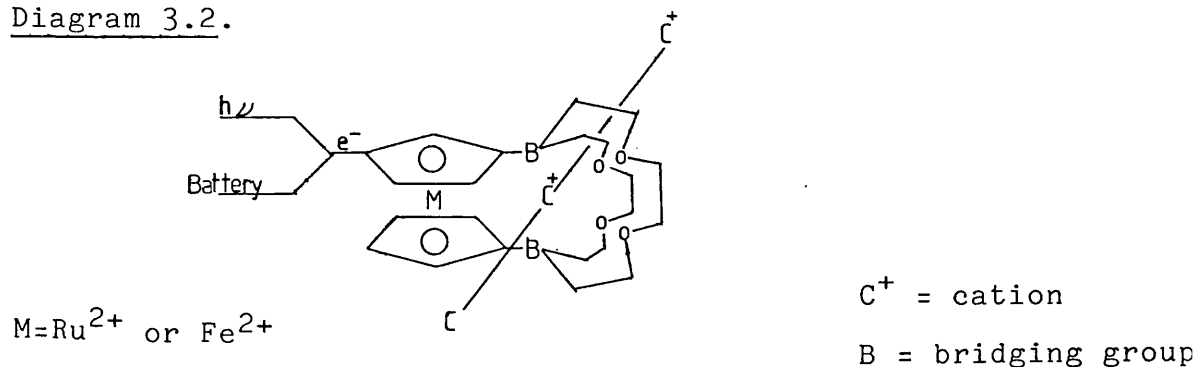
of ruthenocene in chlorinated hydrocarbons again produces photo-oxidation reportedly to the ruthenocenium ion and prolonged photolysis in 1,2-dichloroethane is claimed to produce a (Ru cp<sub>2</sub>)(Ru CCl<sub>4</sub>) complex. However, due to the lack of evidence of the ruthenocenium ion electrochemically and the absence of any assignable

i.r.  $\nu(\text{RuCl})$  peak, magnetic and e.s.r. measurements the identity must be regarded as suspect. It should be noted that the electronic spectrum of ruthenocene in carbontetrachloride is more complicated and this is probably due to the formation of a 1:1 charge-transfer complex.

### 3.2.ii. ELECTROCHEMISTRY

If the two cyclopentadienyl rings of ferrocene or ruthenocene were bridged by a macrocyclic crown-ether, a cryptand is obtained one bridge of which consists of the metallocene unit. When this binds a metal cation, the latter may be brought into close proximity with the metal ion of the metallocene allowing possible electron exchange between the two metal ions to occur. This leads to reduction of the bound metal ion and oxidation of the metallocene. If the metallocene ring is also attached to an external electron source eg. an electrode or photo-electrode the metallocene ring merely plays the role of an electron transfer agent which is part of an ion-selective cathode (the cryptand) [Diagram 3.2].

Diagram 3.2.



There are many natural examples of this type of reduction. Nitrogen fixing ferredoxins as found in the root hairs of plants, have  $\text{Fe}^{2+}$  ions which are believed to give electrons which reduce nitrogen bound to molybdenum. If the process were endorganic i.e. the chemical potential of the system would rise this general process would be particularly significant. Whether or not a metal ion complexed in a ferrocenyl or ruthenocenyl macrocycle would accept an electron must depend on the nature of that cation in the unusual environment of a crown-ether, in which there may be considerable changes in its properties i.e. Redox potential.

Electron exchange studies via n.m.r. line broadening have shown that the electron transfer reaction:  $\text{Fe cp}_2 \rightleftharpoons \text{Fe cp}_2^+$ , is very rapid and does not vary markedly with the dielectric properties of the solvent or if the ring is substituted. The oxidation of substituted ferrocenes have been studied by quarter-wave potentials determined by chronopotentiometry. From the results it can be seen that ferrocenes which contain electron-donating groups are more easily oxidized than ferrocenes which contain electron-withdrawing groups which were more resistant to oxidation than ferrocene itself. This result is not surprising since amino-ferrocene and hydroxyferrocene are slowly oxidized on exposure to air.

Oxidation of ferrocene to give ferricenium salts may be effected electrolytically by the action of various

oxidants e.g. picric acid, and also photochemically. Neutral and basic solutions of this cation are unstable resulting in the formation of iron hydroxide and ferrocene. The ferricenium cation is easily reduced back by a number of reagents, e.g. sodium thiosulphate, ascorbic acid.

The electrochemistry of ruthenocene is not analogous to the simple one electron reversible ferrocene couple  $\text{Fe cp}_2/\text{Fe cp}_2^+$   $E_0 = 0.56 \text{ V}^{141}$  (vs. SHE). The electrochemical oxidation of ruthenocene at a mercury anode was reported to yield the ruthenocenium ion. However, the product has since been characterised<sup>69</sup> as  $[(\text{cp})_2\text{Ru} \dots \text{Hg} \dots \text{Ru}(\text{cp})_2]^{2+}$  where the redox potential observed corresponds to the electrochemical oxidation of mercury  $\text{Hg}^0$  to  $\text{Hg}^{2+}$  and not the ruthenocene.

At a platinum electrode,<sup>69,70,71</sup> it is suggested from chromopotentiometric measurements that ruthenocene undergoes a two-electron, one step irreversible oxidation at an  $\approx E_{\frac{1}{2}}$  of 0.934 V (vs. SHE) in ethanenitrile. There have also been reports of polarographic oxidation at platinum with  $E_{\frac{1}{2}}$  of 1.02 V and 1.05 V (vs. SHE) in ethanenitrile. No electrolytic oxidation products of ruthenocene at a platinum electrode have yet been isolated. It is important to note that there is no electrochemical evidence for the ruthenocenium ion and all attempts to oxidise ruthenocene have produced ruthenocenium IV complexes. It has however been suggested that the two electron oxidation proceeds



with tilting of the cyclopentadienyl rings. This process would become more difficult in the bridged macrocyclic structure and abnormal electrochemical properties might be expected for the ruthenocene cryptates.

### 3.3. THE DESIGN OF FERROCENE AND RUTHENOCENE MACROCYCLES CONTAINING ION-BINDING LIGANDS

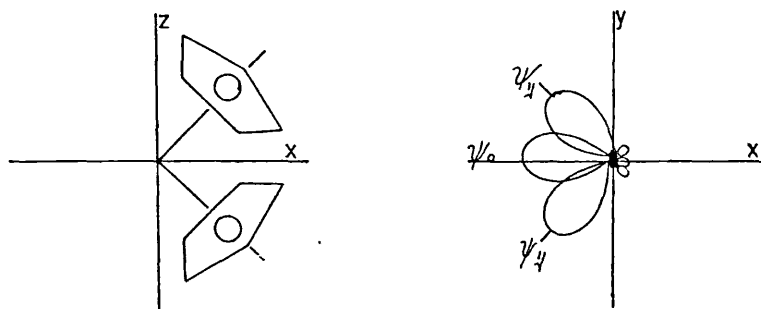
In attempting to design a useful synthetic target the following criteria were initially applied:

- i) The ion-binding complex should be a neutral crown ether, (monocyclic or bicyclic) or polyaromatic macrocyclic ligand.
  
- ii) The size of the binding cavity, the number and nature of the heteroatoms and hence the specificity towards different cations could be easily varied during the preparation of the macrocycle without major changes in the synthetic approach.
  
- iii) Ferrocene or ruthenocene should form one edge of the macrocycle which is therefore joined via functional groups on each cyclopentadienyl ring to the bonding ligand.

Any complexed metal ion would be expected to reside in the cavity in the plane of the ligand and benefit from any interaction due to its position adjacent to the central atom, Fe, Ru. It is known that ferrocene is protonated at the metal atom in strongly acidic media. It has been suggested that the cyclopentadienyl rings can splay without any significant loss in metal-cyclopentadienyl bond energy and that this alteration in geometry causes hybridisation of the non-bonding metal orbitals  $3dz$ ,  $3dxy$ ,  $3dx^2-y^2$  to give orthogonal orbitals orientated towards the

direction of the ring opening.<sup>33</sup> The proton can now make use of the  $\psi_0$  orbital where adverse repulsions are a minimum [Diagram 3.3].

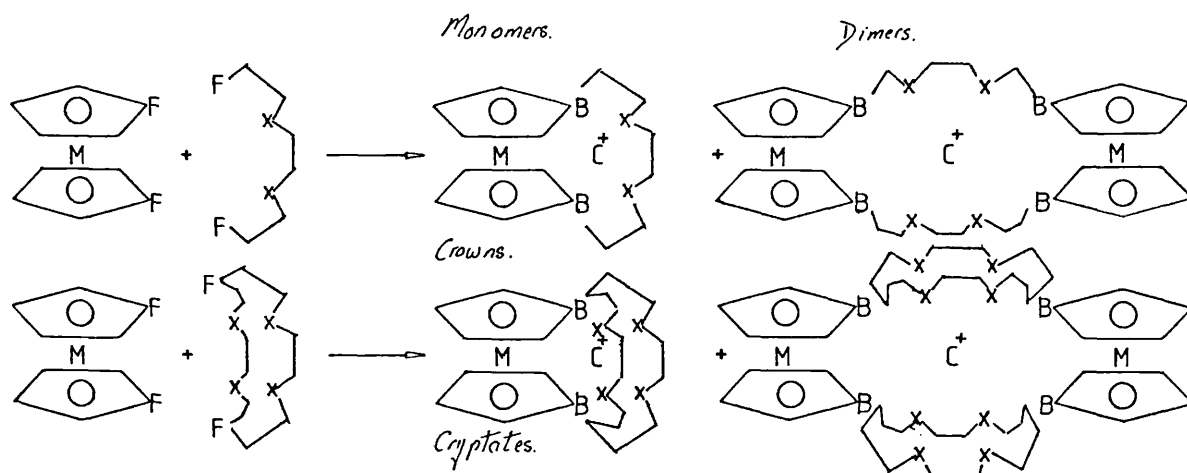
Diagram 3.3



It is not expected that a simple ferrocenyl, ruthenocenyl macrocycle would necessarily exhibit complex formation. Ligands of the type  $(\text{CH}_2\text{CH}_2\text{x})_n$   $\text{x}$  = heteroatom where complexation is by lone-pair interaction only show high affinity for specific cations when arranged in a symmetrical structure, but any disruption or increase in the aliphatic portion of the molecule, would cause a decrease in ion-binding ability.

The aim therefore is to couple as much ion-binding capacity to the metallocene as possible. The synthetic schemes which emerge from these considerations are [Scheme 3.1].

Scheme 3.1 . F = functional group, B = Bridge head atoms,  $\text{C}^+$  = Cation



The simplest form of this type of molecule would be the monocycle where the cyclopentadienyl rings are linked via a bridgehead atom B to a ligand chain  $(\text{CH}_2\text{CH}_2\text{x})_n$  ( x = heteroatom). The detailed manipulation of this reaction scheme will be dependent on the chemistry of the 1,1'-disubstituted metallocene and the type of bridgehead compound used.

CHAPTER 4: THE SYNTHESIS OF FERROCENE AND RUTHENOCENE  
DERIVATIVES AND CRYPTANDS

## CHAPTER 4

THE SYNTHESIS OF FERROCENE AND RUTHENOCENE DERIVATIVES  
AND CRYPTANDS

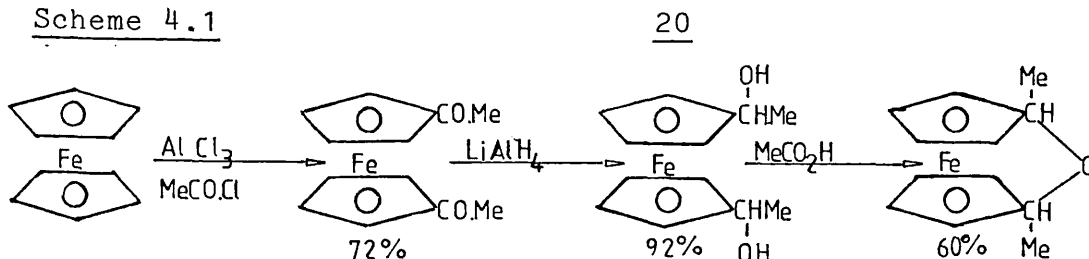
4.1. REACTIONS OF FERROCENE AND 1,1'-DISUBSTITUTED  
DERIVATIVES

There are only two efficient methods available for the preparation of symmetrical 1,1'-disubstituted ferrocenes:<sup>141,148</sup> i) Friedel-Crafts acylation and ii) lithiation. Both of these approaches have been investigated in the course of this project.

i) Friedel-Crafts acylation and subsequent reactions

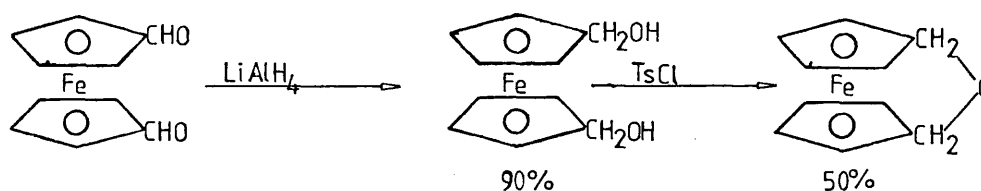
Ferrocene may be acylated by a number of Friedel-Crafts reagents to give mono or 1,1'-disubstituted products.<sup>141,148</sup> The yields of which are dependent on the reaction conditions and are generally in the region of 50%. A maximum yield of 72% may be obtained for the preparation of 1,1'-diacetyl ferrocene when excess acetyl chloride is used with a Lewis acid (aluminium chloride). The 1,1'-diacetyl ferrocene may be reduced by lithium aluminium hydride to give 1,1'-bis(1-hydroxy ethyl) ferrocene in 90% yields. This ferrocenediol

Scheme 4.1



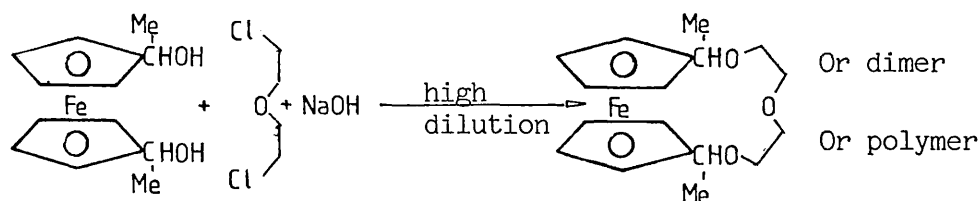
serves as a suitable starting point for the synthesis of a small ferrocene macrocycle [Scheme 4.1]. This general idea also follows for ferrocene-bisaldehyde [Scheme 4.2].

Scheme 4.2

21

This technique allows ferrocenophanes with bridges containing a single heteroatom to be prepared. However, these bridges are too small to allow a metal cation into the cavity. The preparation of larger ferrocene macrocycles may be carried out by esterification or anion displacement using the ferrocene alcohols (20) or (21).

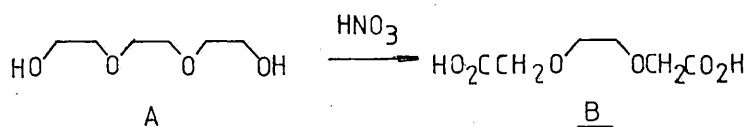
Reaction 4.1

Anion displacement

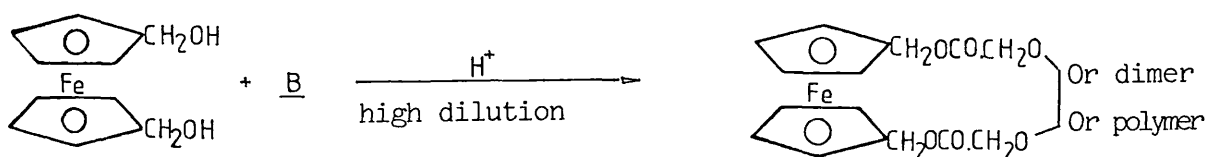
An anion displacement method [Reaction 4.1] was attempted following the general Pederson method. 1,1'-bis(1-hydroxyethyl) ferrocene was reacted with 2-chloroethyl ether under high dilution conditions.

The product from this preparation was a red/brown powder which was apparently insoluble in organic solvents. This material gave no satisfactory mass spectra as it seems to have a very high molecular weight. There was no clear melting point and only chaining was observed. From this it is believed that a polymer was formed. However, due to its insolubility in liquid media it proved difficult to characterize. This particular reaction could be improved in two ways: i) a better leaving group could be employed e.g. tosylate or bromine on the polyether chain; ii) the large methyl groups may impede the reaction and if this is replaced by a proton, the steric hindrance would be reduced.

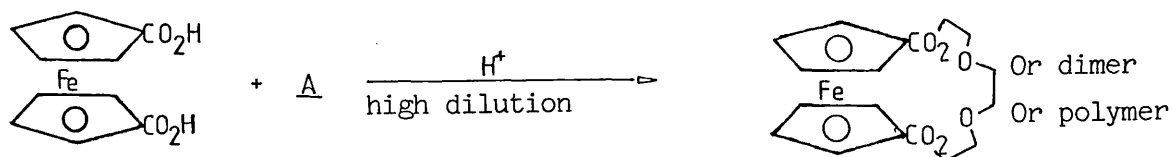
#### Esterification



#### Reaction 4.2



#### Reaction 4.3

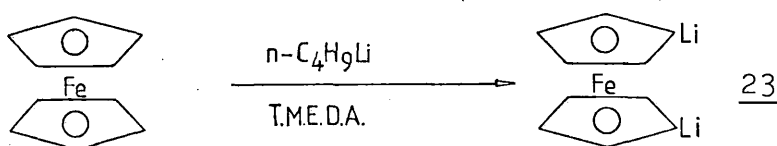
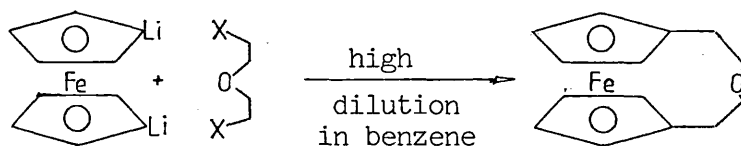




Reactions [4.2] and [4.3] which are esterifications have not been attempted. They may offer viable methods for synthesizing a monocyclic metallocene-crown which avoids the problems of anion leaving group in the anion displacement method. However, such an approach does have its own problems and limitations. 1,1'-ferrocene dicarboxylic acid (22) insoluble in most organic media except acetic acid and would therefore be unsuitable for the high dilution preparation which are used in the preparation of crown like compounds. This method is also limited to the preparation of monocyclic systems and cannot easily be generalized into bicyclic systems.

ii) Lithiation and subsequent reactions

Lithiation of ferrocene with excess n-butyllithium complexed with tetramethylethylene diamine in a 1:1 ratio proceeds to give 1,1'-dilithioferrocene (23) precipitates as a fine orange suspension and was used without any further purification due to its high reactivity [Reaction 4.4]. The high reactivity of 1,1'-dilithioferrocene could be exploited to great advantage in potential preparative routes to ferrocenyl macrocycles. But, the only reaction which has so far been attempted [Reaction 4.5] was not successful, ferrocene being recovered together with the bis chloro ether.

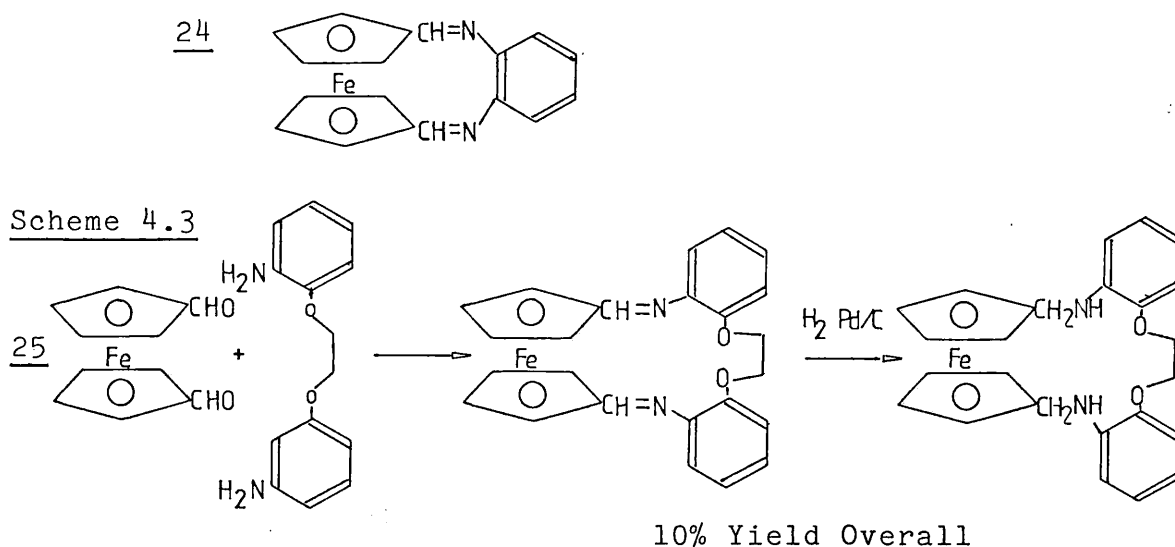
Reaction 4.4Reaction 4.5

X=Cl, Br or Ts.

A number of other leaving groups could be used in an attempt to overcome this problem e.g. bromide and tosylate but as yet these reactions have not been attempted.

However, the reactions of 1,1'-dilithioferrocene with carbon dioxide and N,N-dimethylformamide have provided the key steps in the synthesis of ferrocene-cryptates.

1,1'-dilithioferrocene reacts with dimethylformamide to give, after hydrolysis, 1,1'-ferrocenedicarboxaldehyde (25). This bisaldehyde was expected to be a suitable starting material for condensations with diamines to give macrocycles since the imine (24) is readily prepared<sup>150</sup> and other examples of bisaldehyde  $\alpha,\omega$ -diaminecondensations are known.

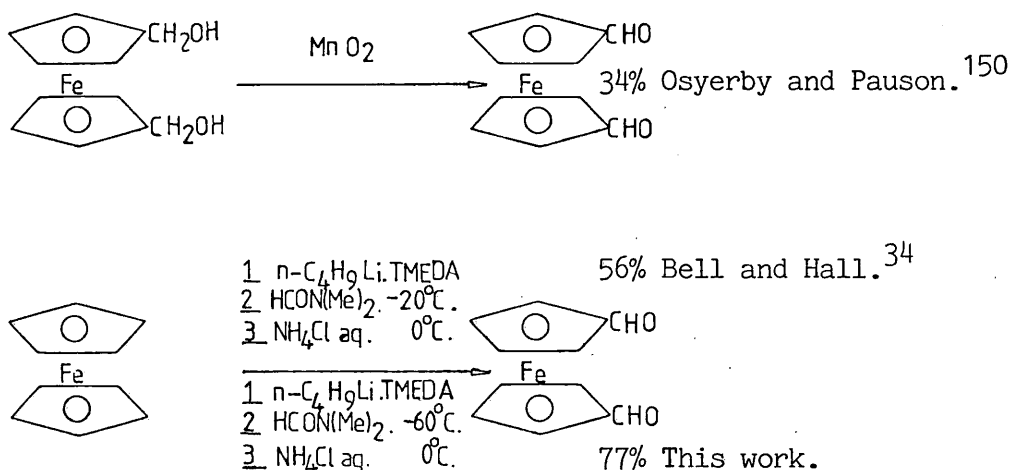


Bell and Hall<sup>34</sup> have developed a viable route [Scheme 4.3] to macrocyclic compounds but yields are low ( $\sim 10\%$ ). These preparations were limited by the difficulty in preparing large quantities of the bisaldehyde due to its tendency to polymerise in organic solutions giving a red oil, while in the solid state it is sensitive to oxygen and light. On further

investigation of the Bell and Hall method of preparing 1,1'-ferrocene dicarboxaldehyde, it was found that if the addition of 1,1'-dilithioferrocene is carried out at lower temperatures ( $-55^{\circ}$  -  $-60^{\circ}\text{C}$ ) a significantly higher yield of 1,1'-ferrocenedicarboxaldehyde is obtained. The above route could now be a viable method of preparing ferrocene macrocycles.

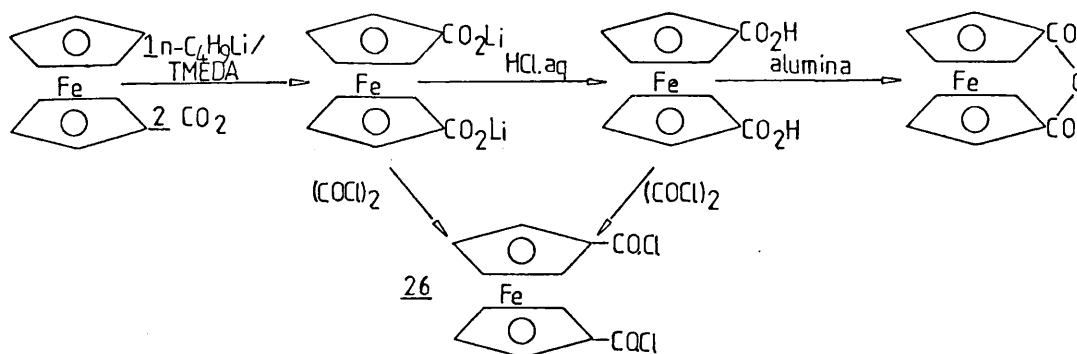
Scheme 4.4

Preparations of 1,1'-ferrocenedicarboxaldehyde



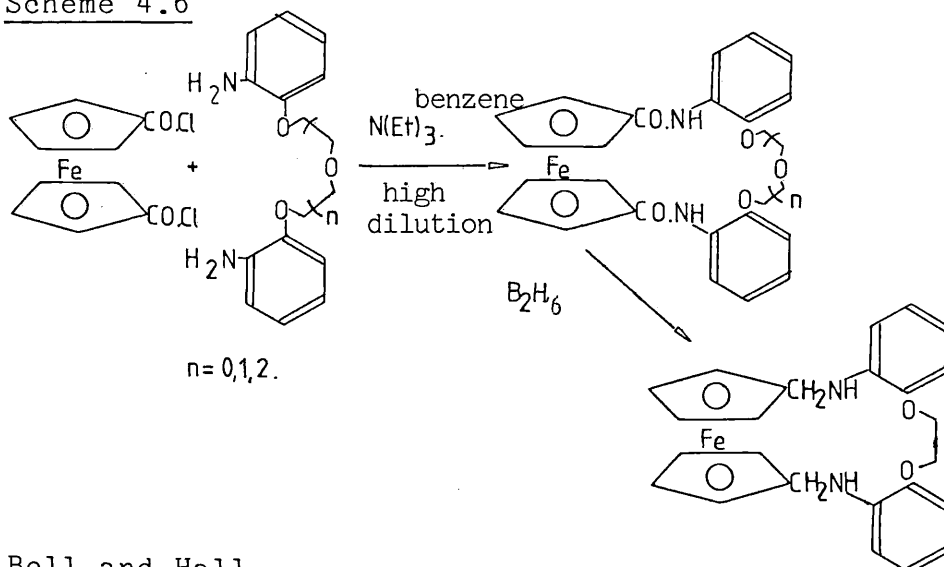
The carbonation of 1,1'-dilithioferrocene is achieved by injection of its ether/tetrahydrofuran suspension into a carbon dioxide ether slush to give lithium 1,1'-ferrocene dicarboxylate. This is easily converted into 1,1'-ferrocene dicarboxylic acid by acidification with dilute acid. This could be used to prepare ferrocene macrocycles (Chapter 3.3.i); however, as stated earlier it is insoluble in most organic media and therefore of limited use. Though it can be readily dehydrated to form the anhydride, which has no cation binding properties. Lithium 1,1'-ferrocene dicarboxylate

Scheme 4.5.



is readily converted into 1,1'-ferrocene dicarbonyl chloride<sup>151</sup> (26), by treatment with oxalyl chloride. This is a stable, easily purified, crystalline solid, which is soluble in benzene and more polar solvents [Scheme 4.5]. This has been found to react rapidly with amines to give amides and relatively slowly with alcohols and water. As the resultant amide is stable

Scheme 4.6



Bell and Hall

(via aldehyde route 10%)

Overall 60-70%<sup>34</sup>

and the reaction is rapid, it is clear that a high dilution reaction technique is required to prevent

polymer formation. The ferrocene bis acid chloride is therefore the ideal precursor for reactions with  $\alpha,\omega$ -diamines which may be primary [Scheme 4.6], e.g. diaminotetragol or secondary e.g. diaza crown ethers, and it is with this type of reaction that the synthesis of macrocyclic metallocenes has been achieved.

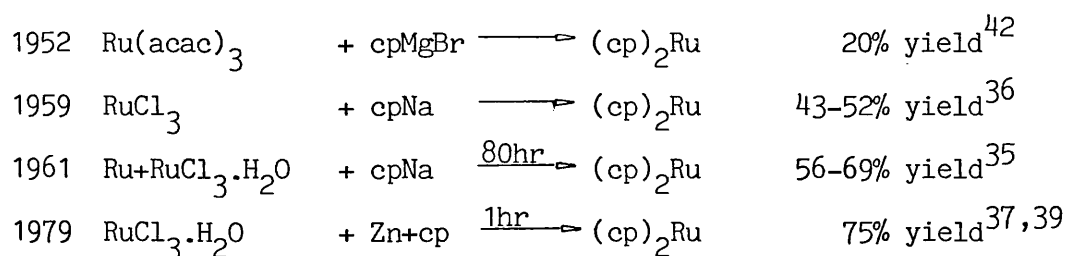
Whilst ferrocene is readily available commercially it was necessary to prepare ruthenocene prior to use.

#### 4.2.i. Preparation of ruthenocene

The first reported preparation of ruthenocene<sup>42</sup> was in 1952 a year after the discovery of ferrocene;<sup>43</sup> it was isolated from the reaction of ruthenium acetyl acetonate with a five-fold excess of cyclopentadienyl magnesium bromide in 20% yields. Substantially higher yields (43-52%) have been obtained by the reaction of ruthenium trichloride with cyclopentadienyl sodium in either tetrahydrofuran or ethyleneglycoldimethyl ether. Recent preparations have increased this method to (56-69%) however, the treatment of ruthenium trichloride in ethanol with cyclopentadiene in the presence of zinc dust results with a 75% yield. These latter

#### Scheme 4.7

##### Preparation of ruthenocene

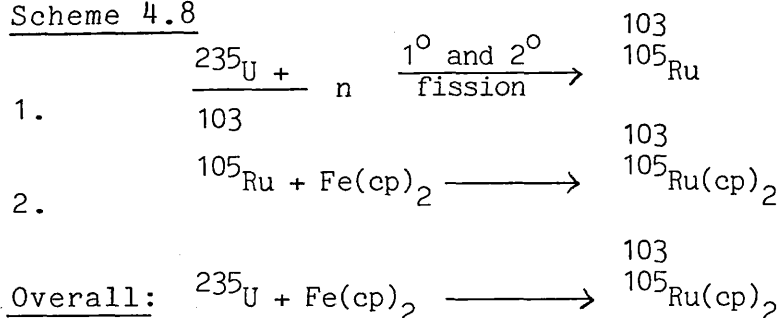


two methods seem to be the most favourable [Scheme 4.7], however, in each case there is a particular disadvantage. Obtaining the required activity for the zinc dust is always a problem and the direct sublimation from a pyrophoric residue can be hazardous.

An interesting alternative is the treatment of ruthenium trichloride with ferrocene which undergoes a ligand exchange reaction in a Carius tube at 250°.

This idea of a ligand exchange reaction has been used to prepare carrier-free radioactive ruthenocenes ( $^{103}_{105}\text{Ru}(\text{cp})_2$ ). The first preparations were from a nuclear fission reaction in which a powder-mixture of uranium oxide and ferrocene were heated together. The process is considered to be

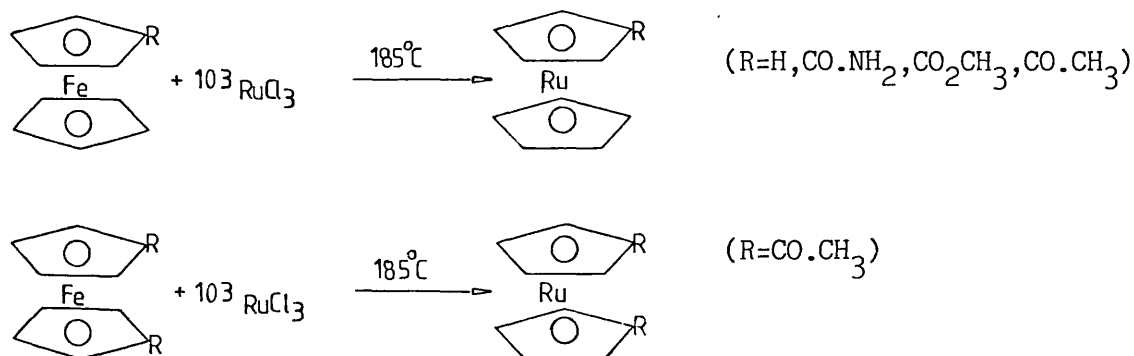
Scheme 4.8



a two step reaction where the key step of the mechanism is 'chemical'. The surprising feature of this reaction is that up to 50% of all the isotopes of the fission elements are found in the product<sup>44</sup> [Scheme 4.8].

More recently, the chemical exchange reaction has been developed to yield convenient starting materials ( $^{103}\text{RuCl}_3$ ). These reactions [4.7] occur

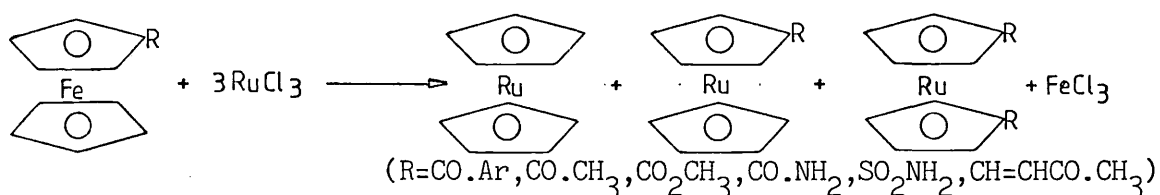
Reaction 4.7





with 5-70% yields, depending upon R. A detailed study of this reaction revealed that disproportionation occurs in these reactions. However, the major product

Reaction 4.8



is still the mono-substituted ruthenocene and the others are minor by-products<sup>44</sup> [Reaction 4.8].

Ruthenocene is readily purified by sublimation in vacuum at 120°C,<sup>35</sup> or by column chromatography with activated alumina. Ruthenocene may be recrystallized from a variety of organic solvents and forms pale yellow orthorombic crystals.

As with ferrocene, ruthenocene ring derivatives are easily prepared by two main routes [Table 4.1]. Friedel-Craft's reactions with a Lewis acid or a lithiation reaction with n-butyl lithium. Depending upon the reaction conditions, concentrations and strength of reactants, a variety of substituted products may be formed in both cases (mono-, di-, and trisubstituted ruthenocenes).<sup>38</sup> These reactions rarely proceed clearly to give 100% of a single product, instead there is usually obtained a mixture of products of which one will predominate. Further reactions to change the functional groups of the substituted derivatives are

possible and this leads to a large variety of compounds [Table 4.2].

The monosubstituted ruthenocenes have been extensively studied and characterised (54 known compounds). However this is not the case with the disubstituted ruthenocenes of which few are known. The disubstituted ruthenocenes may be subdivided into three groups [Table 4.3] and it is with the first class of compound that this research has been concerned.

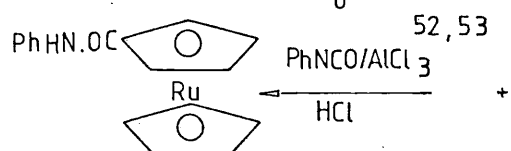
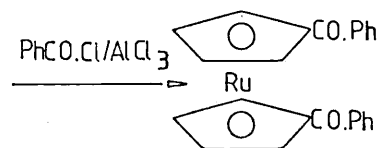
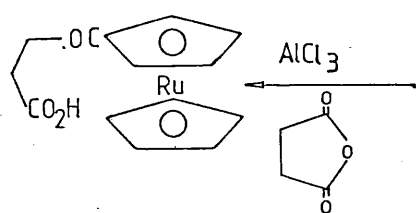
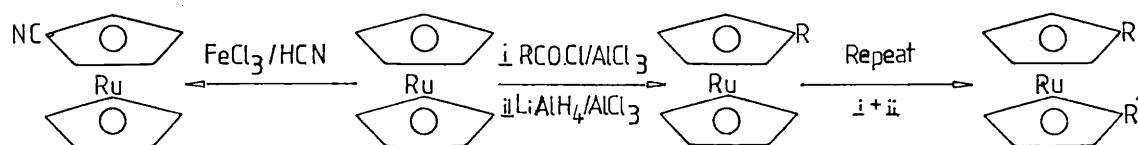
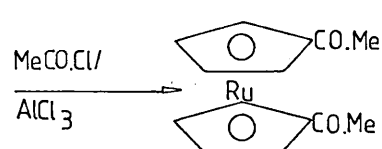
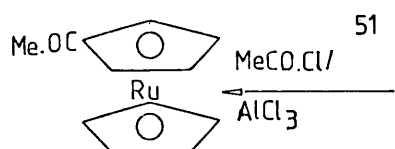
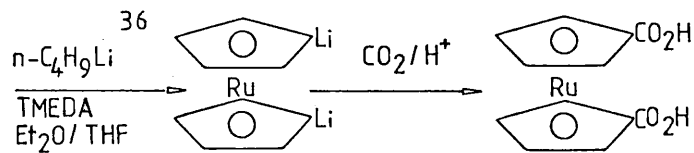
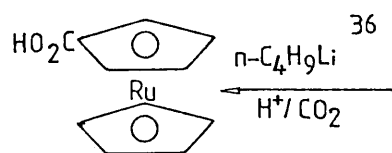
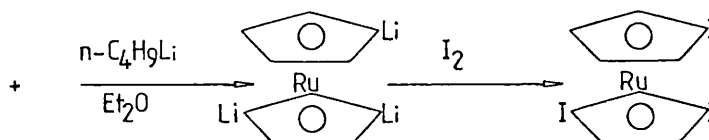
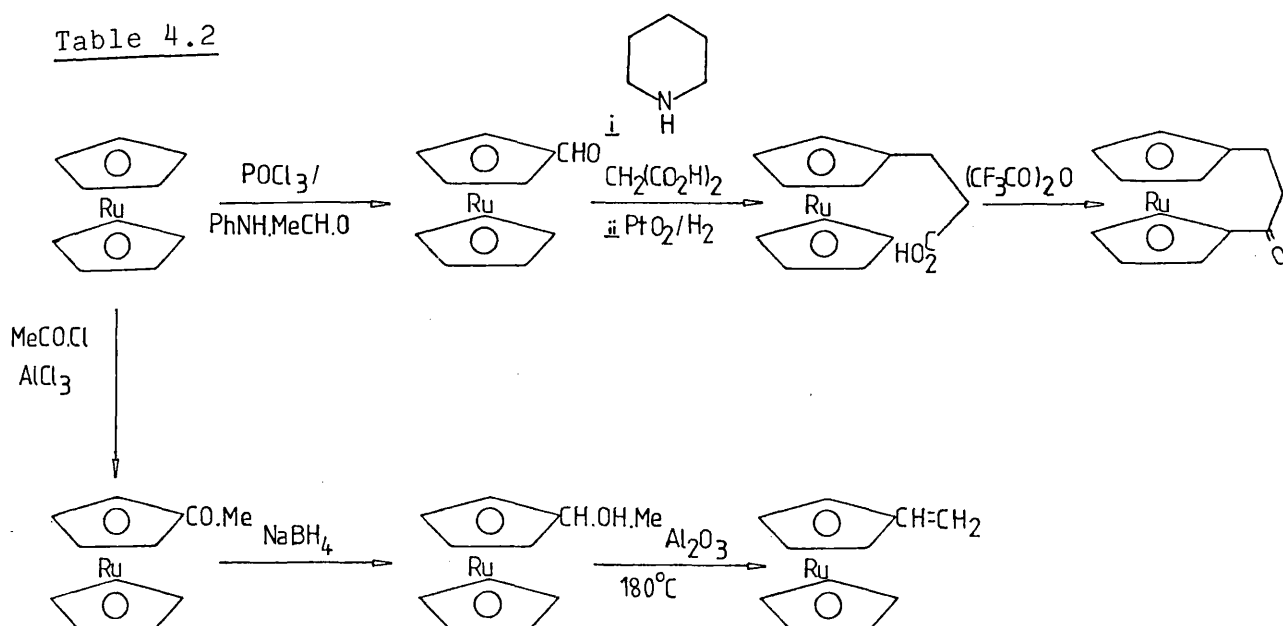
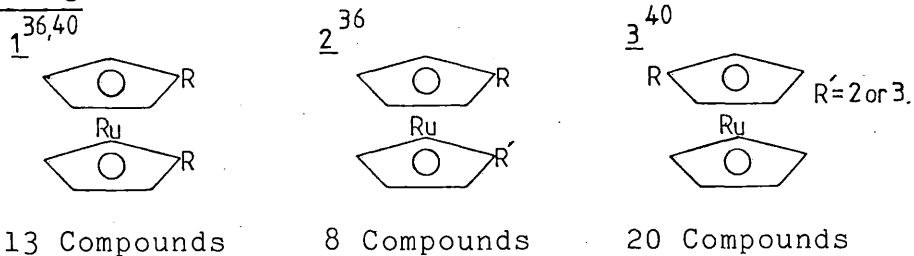
Table 4.1<sup>44</sup>Mono derivativesDisubstituted derivativesTrisubstituted derivatives

Table 4.2

Table 4.3<sup>44</sup>

1.  $\text{R} = \text{CH}_3, \text{C}_2\text{H}_5, \text{CH}=\text{CH}_2, \text{CH}(\text{OH})\text{CH}_3, \text{CO}_2\text{H}, \text{CO}\cdot\text{CH}_3, \text{CO}\cdot\text{Ph}, \text{Li}, \text{Br}, \text{I}, \text{Cl}, \text{CN}, \text{Ti}(\text{NET}_2)_3$

2.  $\text{R} = \text{CH}_3, \text{CH}_3, \text{CH}_3, \text{CH}_3, \text{CH}_3, \text{CH}_3, \text{CH}_2\text{OH}, \text{CO}\cdot\text{H}$   
 $\text{R}' = \text{CO}_2\text{H}, \text{CO}_2\text{CH}_3, \text{CO}\cdot\text{H}, \text{CO}\cdot\text{NPh}, \text{CH}=\text{N}(\text{OH}), \text{CN}, \text{CO}_2\text{CH}_3, \text{PO}_2\text{CH}_8$

3.  $\text{R} = \text{CH}_3, \text{CH}_3, \text{CH}_3, \text{CH}_3, \text{CH}_3, \text{CH}_3, \text{CH}_3, \text{CH}_3, \text{CH}_3, \text{CH}_3, \text{CH}_3$   
 $\text{R}' = 2\text{-CH}_3, 3\text{-CH}_3, 2\text{-CO}_2\text{H}, 3\text{-CO}_2\text{H}, 2\text{-CO}_2\text{CH}_3, 3\text{-CO}_2\text{CH}_3, 2\text{-CO}\cdot\text{H}, \text{CO}\cdot\text{NPh}_2, \text{CH}=\text{N}(\text{OH}), 2\text{-CN}$

$\text{R} = \text{CH}_3, \text{CH}_2\text{OH}, \text{CO}\cdot\text{H}, \text{CO}\cdot\text{Ph}, \text{CH}_2\text{N}(\text{CH}_3)_2, \text{CH}_2\text{N}(\text{CH}_3)_2, \text{CH}_2\text{N}(\text{CH}_3)_2,$   
 $\text{CH}_2\text{N}(\text{CH}_3)_2, \text{CH}_2\text{N}(\text{CH}_3)_2$

$\text{R}' = 3\text{-CN}, 2\text{-CO}_2\text{CH}_3, 2\text{-CO}_2\text{CH}_3, 2\text{-CO}\cdot\text{Ph}, \text{D}, 2\text{-CH}=\text{CH}(\text{CO}\cdot\text{CH}_3), 2\text{-CH}=\text{CH}(\text{CO}\cdot\text{Pb}),$   
 $2\text{-CH}=\text{CHPh}, 2\text{-CO}_2\text{Et}$

4.2.ii) The preparation of ruthenocene-1,1'-dicarboxylate and 1,1'-ruthenocene bis acid chloride

The lithiation and subsequent carbonation of ruthenocene was found to give predominantly a disubstituted product; however the subsequent hydrolysis and purification of the acid was difficult as the acid is only soluble in glacial acetic acid. To overcome this problem, the acid was left as the lithium salt and filtered, unreacted ruthenocene was removed by washing the solid with dry ether. The purity of the solid was determined by preparing the methyl esters via dimethylsulphate (a high yield method) [Scheme 4.9].

It has been reported that the metalation of ruthenocene is dependent upon: solvent conditions, temperature and the ratio of reactants [Table 4.4]. It was found that the use of a mixture of diethyl ether/tetrahydrofuran<sup>54,36</sup>

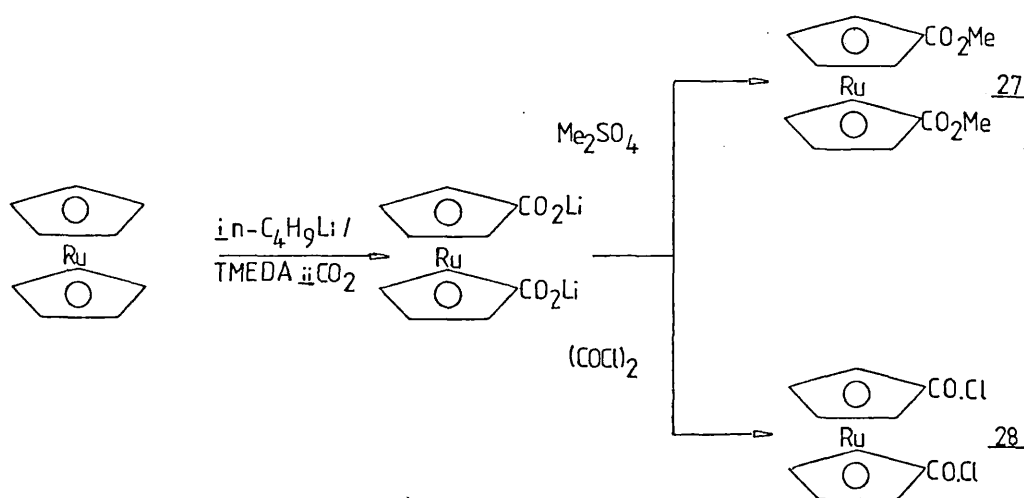
Table 4.4<sup>54,36,38</sup>

Ratio of n-C <sub>4</sub> H <sub>9</sub> Li:Ru(C <sub>5</sub> H <sub>5</sub> ) <sub>2</sub> TMEDA	Time hr	Temp. °C	Solvent System	% Yield			
				Mono.	Di.	Tri.	
3:1	24	25	Et <sub>2</sub> O	24	24	-	Determined as the acids
6:1	18	-50 to 25	Et <sub>2</sub> O/THF	1	86	-	
1.3:1	17	-50 to 25	Et <sub>2</sub> O/THF	10	10	-	
2:1:2	17	22 ± 3	Et <sub>2</sub> O/Hex.	11.8	56.8	35	Determined as the iodo derivatives
4:1:4	17	22 ± 3	Et <sub>2</sub> O/Hex.	-	72.4	8.4	
4:1:4	17	22 ± 3	Et <sub>2</sub> O	-	74.3	8.2	
6:1	17	-50 to 25	Et <sub>2</sub> O/THF	4* 2	40* 50	-	Acid determined
2.5:1:2.5	24	-50 to 25	Hexane 1.5/1	-	71	-	Determined as the methyl esters
6:1:6	24	-50 to 25	Et <sub>2</sub> O/THF	-	80	-	

\*The butyl lithium was found to be impure

as a solvent system for the metalation produces greatly enhanced yields of lithiated derivatives. A similar effect is seen when an equimolar amount of N,N,N',N'-tetramethylethylenediamine/n-butyl lithium<sup>38</sup> is added to the ruthenocene. In view of the earlier observations concerning the lithiation of ferrocene it was logical to assume that the optimum conditions for dilithiation would be found if a solvent mixture<sup>54</sup> (tetrahydrofuran/ether) and a n-butyllithium/T.M.E.D.A. adduct was used at low temperatures (-50°-25°). There seems to be no marked increase in the yield of disubstituted ruthenocene (80%). However, it should also be noted that no mono- or trisubstituted derivatives were isolated using this method and consequently this procedure was used for all further preparations of bis-ruthenocene compounds.

Scheme 4.9

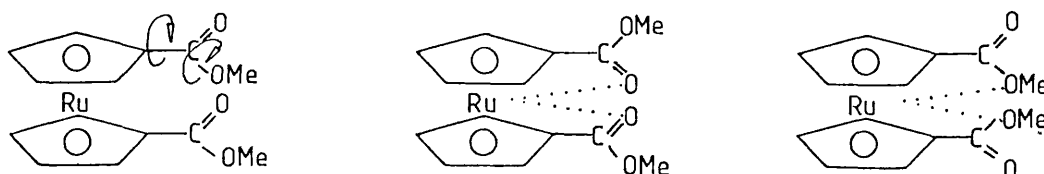


The bis methyl ester was prepared from the crude lithium salt of ruthenocene biscarboxylic acid by reaction

with dimethylsulphate in methanol. The product was purified on an alumina column and only one band was seen. The subsequent analysis and n.m.r. data confirmed the structure (27). The n.m.r. and i.r. data for dimethyl ruthenocene-1,1'-dicarboxylate was analogous to that for the ferrocene derivative [Table 4.5].

The  $^1\text{H}$  n.m.r. spectrum contains two sets of non-equivalent protons (the metallocene) and a singlet for the methyl groups in the correct ratio of 4:4:6. The  $^{13}\text{C}$  n.m.r. spectrum shows five different carbon signals, three ruthenocenyl, one methyl and one carbonyl. Since there are fourteen carbon atoms in the structure (27) there must be equivalence due to the free rotation of the carbonyl groups. This is confirmed from the  $^1\text{H}$  n.m.r. spectrum since H-2' is equivalent to H-5' and H-3' to H-4', thus eliminating the possibility of the carbonyl groups having a fixed configuration coplanar with the adjacent ruthenocene ring. There is an alternative explanation to the n.m.r. spectra: the carbonyl groups could have a perpendicular configuration. However, this is unfavourable since there are no available orbitals for bonding to occur between the ruthenium atom and the carbonyl group, thus keeping the perpendicular structure [Diag. 4.1] and conjugation with the cyclopentadienyl rings is minor. The carbonyl signals were weak in the  $^{13}\text{C}$  n.m.r., however they were confirmed as they were easily seen in the i.r. spectrum.

Diagram 4.1



Proposed free rotation structure.

Perpendicular type structures.

The crude lithium salt of ruthenocene bis carboxylic acid was converted into the acid chloride by reaction with oxalyl chloride following the general Prakt method. Ruthenocene bis acid chloride has been prepared before by Otloffer and Schlogel<sup>40</sup> but, they did not isolate the compound and only used it as an intermediate in a reaction sequence. Ruthenocene bis acid chloride (28) was best purified by a double recrystallization from hexane or benzene. The n.m.r. spectra were again similar to the ferrocene analogue [Table 4.6].

The <sup>1</sup>H n.m.r. spectrum contains two sets of non-equivalent protons (the metallocene). Again H-2' is equivalent to H-5' and H-3' to H-4', thus eliminating the coplanar structure and giving evidence to the free rotation of the carbonyl groups. The <sup>13</sup>C n.m.r. spectrum shows four different carbon signals, three ruthenocenyl and one carbonyl. Since there are twelve carbon atoms in the structure there must be equivalence again due to the free rotation of the carbonyl groups.



Table 4.5

1. Dimethyl ruthenocene-1,1'-dicarboxylate

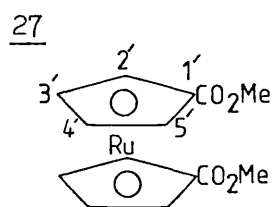
$$\text{CO. } \bar{\nu} = 1730 \text{ cm}^{-1}$$

1(b) Dimethyl ferrocene-1,1'-dicarboxylate

$$\text{C=O } \bar{\nu} = 1710 \text{ cm}^{-1}$$

 $^{13}\text{C}$  n.m.r. data in  $\text{CDCl}_3$  @ 22.6 MHz ambient

Assignment	1. ppm	1.(b) ppm
C=O	200.10	200.88
C <sub>1</sub> -	74.27	80.88
C <sub>2,5</sub>	74.01	73.57
C <sub>3,4</sub> -	73.29	71.02
CH <sub>3</sub>	51.70	27.63

 $^1\text{H}$  n.m.r. data in  $\text{CDCl}_3$  @ 90 MHz ambient

Assignment	1.ppm	inter	1.(b) ppm	inter
H <sub>2',5'</sub>	5.17t Hz 0.02	4	5.05t Hz 0.02	4
H <sub>3',4'</sub>	4.73t Hz 0.02	4	4.61t Hz 0.02	4
CH <sub>3</sub>	3.74s	6	3.62s	

t = triplet

s = singlet

$^1\text{H}$  n.m.r. of dimethyl ruthenocene-1,1'-dicarboxylate @ 90 MHz ( $\text{CDCl}_3$ ).

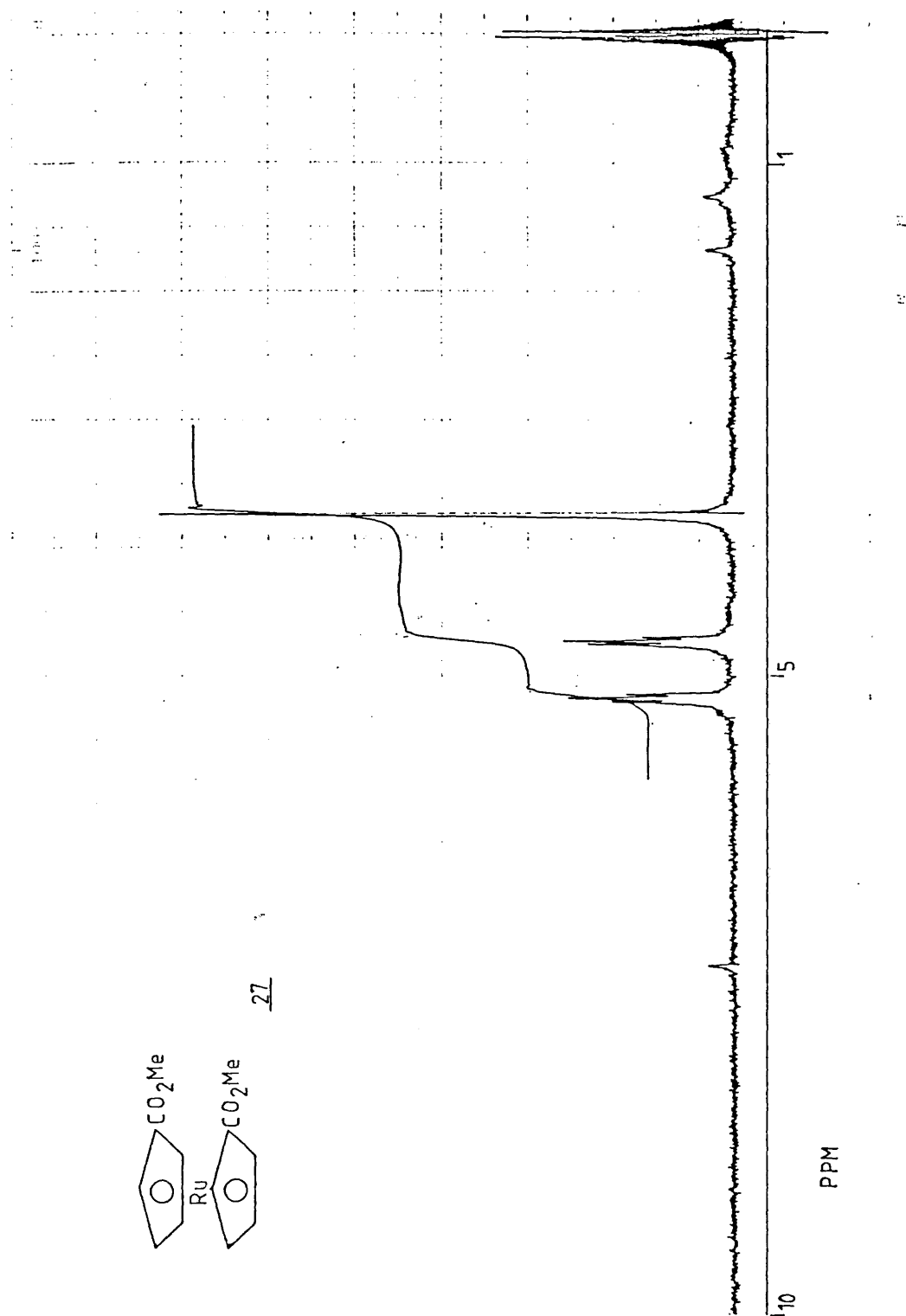
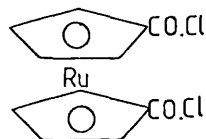


Table 4.6

2. Ruthenocene bis acid chloride 28

$$C=O \bar{\nu} = 1775 \text{ cm}^{-1}$$

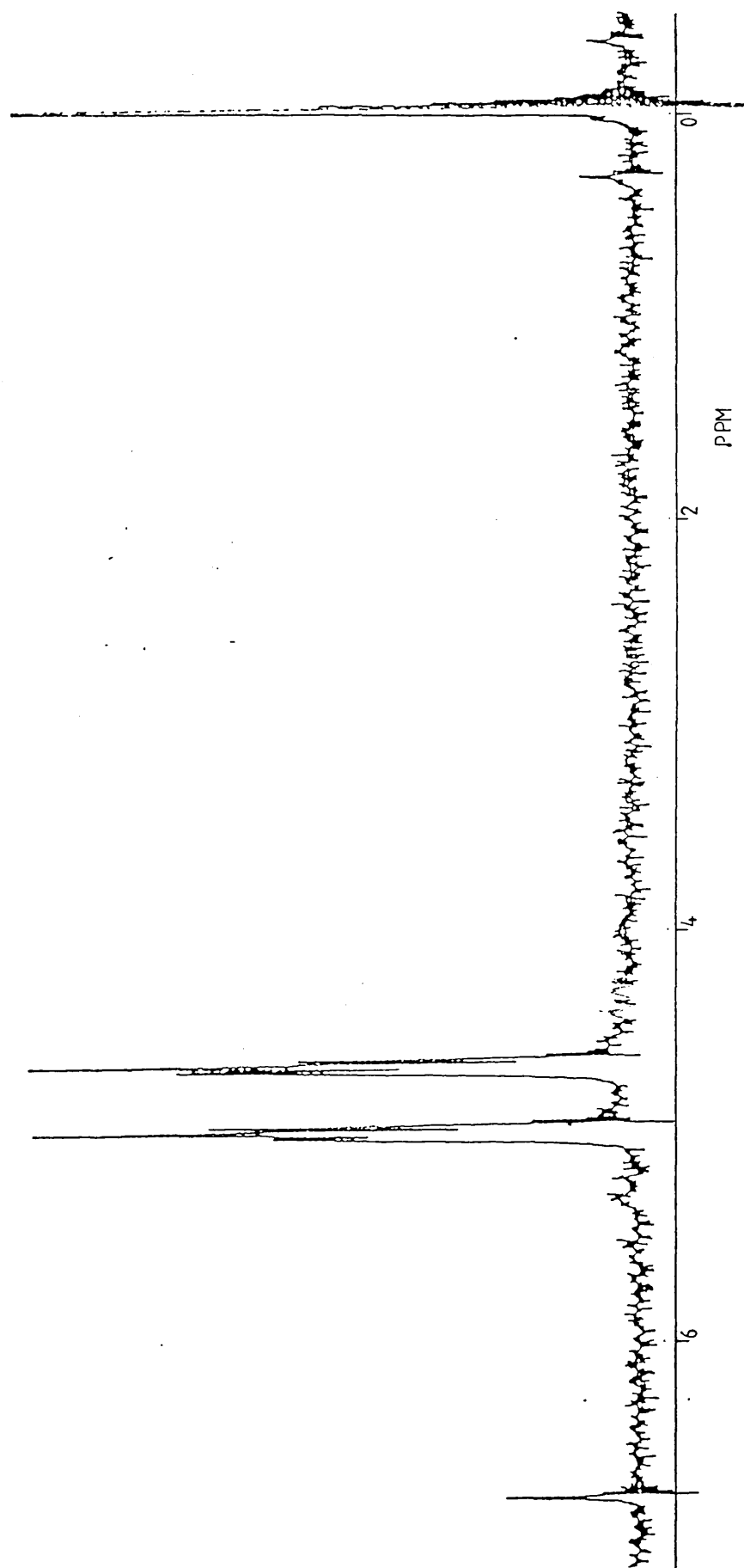
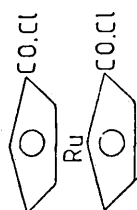
2.(b) Ferrocene bis acid chloride 2628 $^{13}\text{C}$  n.m.r. data in  $\text{CDCl}_3$  @ 22.6 MHz ambient

Assignment	2.ppm	2(b). ppm
CO	166.15	168.37
C <sub>1</sub>	77.32	77.45
C <sub>2,5</sub>	73.22	76.10
C <sub>3,4</sub>	72.18	74.14

 $^1\text{H}$  n.m.r. data in  $\text{CDCl}_3$  @ 90 MHz ambient

Assignment	2 ppm	inter	2b. ppm	inter
H <sub>2,5</sub>	5.16t $\frac{1}{2}$ 0.02	4	5.05t $\frac{1}{2}$ 0.02	4
H <sub>3,4</sub>	4.80t $\frac{1}{2}$ 0.02	4	4.75t $\frac{1}{2}$ 0.02	4

$^1\text{H}$  n.m.r. of 1,1'-ruthenocene bis acid chloride @ 90 MHz ( $\text{CDCl}_3$ )



### 4.3 PREPARATION OF BINDING LIGANDS

Having successfully prepared ruthenocene and ferrocene bis acid chloride it was decided to convert these into the desired crown ethers and cryptands by reaction with the appropriate primary and secondary diamines. Since few of these ligands are commercially available it was necessary to prepare them prior to use.

#### 4.3.i) Aliphatic $\alpha,\omega$ -diamines and diaza crown ethers

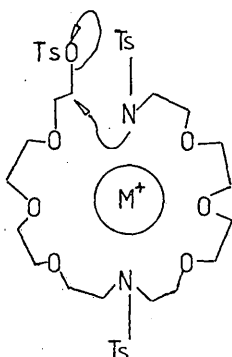
The aliphatic diamines; diaminodiethylene glycol, diaminotriethylene glycol and diaminotetraethylene glycol are readily prepared from the corresponding alcohols following the Lehn method.<sup>61</sup> Great care must be taken with the storage of the diaminoethylene glycols as they are very hygroscopic and must therefore be distilled from potassium hydroxide immediately prior to use. The solvents used in any subsequent reaction must be 'super dry' as any traces of water will cause hydrate formation and thus impede condensation reactions with bis-metallocene and chlorides to give macrocyclic products.

There are only two general routes by which diaza crown ethers may currently be prepared: i. the intramolecular nucleophilic displacement of tosyl or halide groups by an anion; and ii. the condensation of acid derivatives with diamines [Scheme 4.10]. The cyclisation stage for both routes gives approximately 20-30% yields. However, only route [1] was followed as this had the higher overall efficiency. This arises from the better

yields obtained from tosylation reactions against those found for the oxidation of ethylene glycols to ethylene dicarboxylic acid, route [2].

The overall yield for the preparation of diaza[24]crown-8 (3.3) was 7% and for diaza[21]crown-7 (3.2) was 10%. This three percent difference was thought to be due to a modification in the reaction procedure for the cyclisation step. It should be noted that both of these macrocycles have a large pore diameter; diaza[24]crown-8 (3.3) 4.5-5.2 Å and diaza[21]crown-7 (3.2) 3.4-4.3 Å, therefore a large cation should be used in the cyclisation

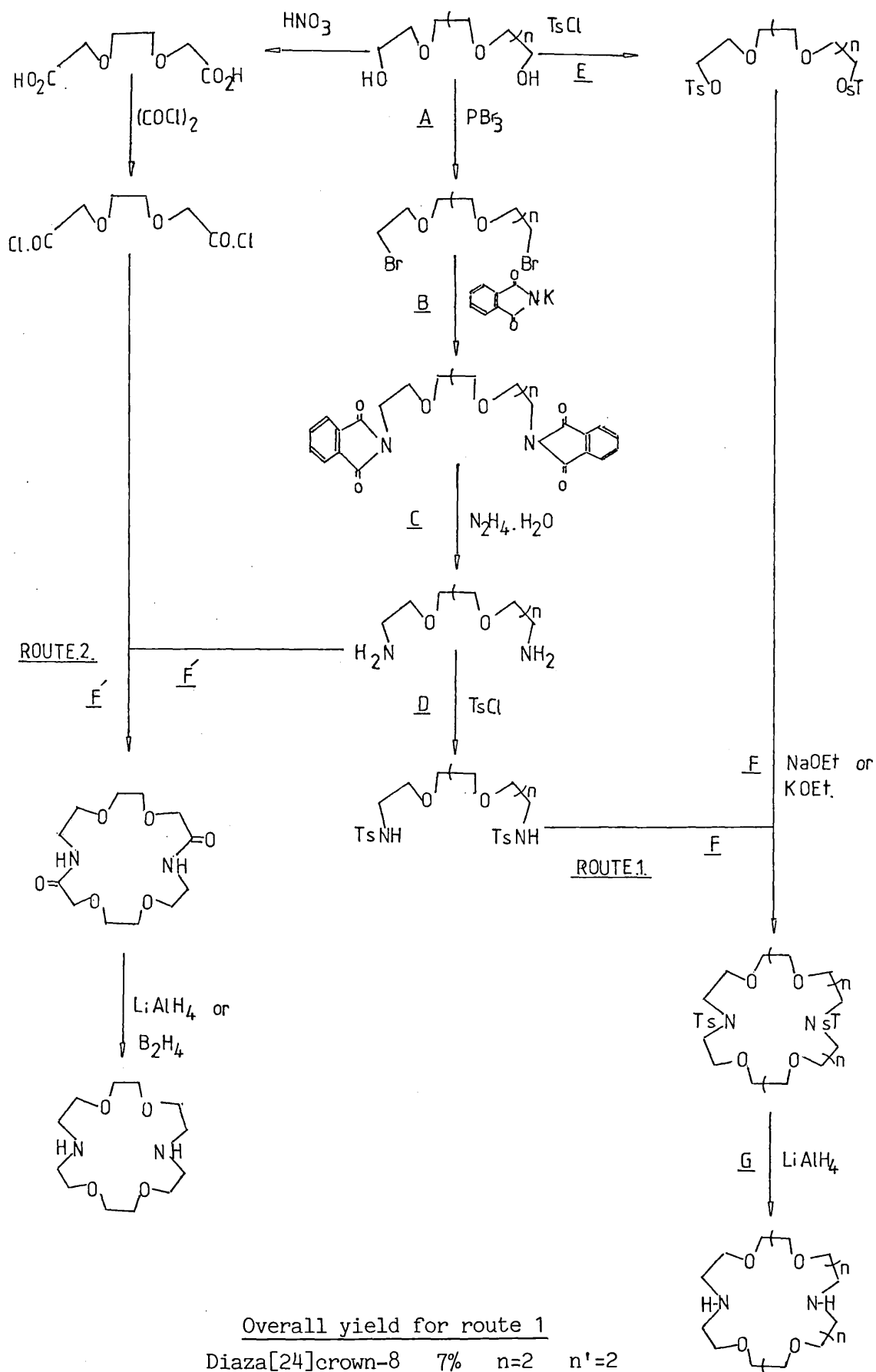
Diagram 4.2



stage, which would act as a template about which the glycol chain can coordinate themselves and thereby direct the reaction towards cyclisation. "The template effect".

Table 4.7. Percentage yields of ditosyl-diaza crown ether preparations using sodium and potassium cations as templates

Crown	CATION	Na <sup>+</sup> 1.36 Å	K <sup>+</sup> 2.66 Å
Ditosyldiaza[24]crown-8 (3.3) Pore diameter 4.5-5.2 Å		28%	Predict increase
Ditosyldiaza[21]crown-7 (3.2) Pore diameter 3.4-4.3 Å		54%	88%

Scheme 4.10  $n$  or  $n' = 0, 1, 2, \dots$ ; Ts = Me-C<sub>6</sub>H<sub>4</sub>-SO<sub>2</sub>

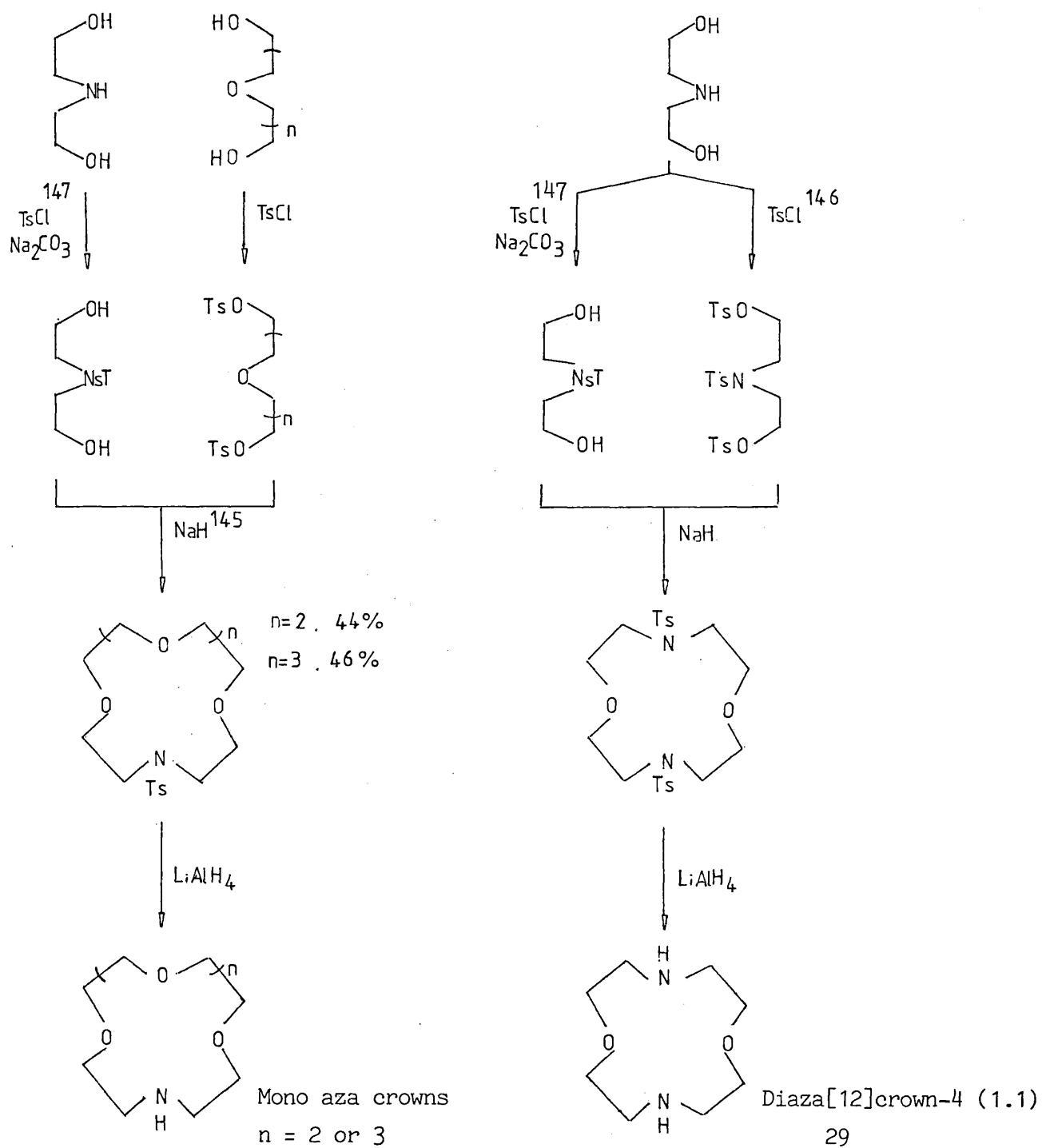
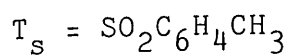
For the preparation of ditosyldiaza[21]crown-7 (3.2) two cations were used sodium and potassium. The increase in yield from 54% to 88% reflects the better correlation of pore diameter to cation diameter i.e. the maximum template effect for cyclisation can only be obtained when there is a good correlation of pore diameter to cation diameter. This therefore explains the poor yield of ditosyldiaza[24]crown-8 (3.3) when sodium was used as the cation was too small. One would predict a better yield if potassium or rubidium was used as the cation. However, for ditosyldiaza[21]crown-7 (3.2) the potassium cation seems to be the optimum size as there is a very good yield 88% and any further increase in cation size would most probably decrease the template effect as the glycol chains would not comfortably envelope the larger cation.

The literature routes to diaza[12]crown-4 (1.1) are outlined in [Scheme 4.10]. A new four stage synthesis of diaza[12]crown-4 (1.1) (29) analogous to the preparation of mono aza[12]crown-4<sup>145</sup> [Scheme 4.11] was attempted. Diethanolamine can be selectively tosylated (mono- or tri-)<sup>146</sup> by p-toluenesulphonyl chloride by protecting the alcohol groups in aqueous solution with sodium ions. It is therefore the ideal precursor for the preparation of diaza[12]crown-4 (1.1).

N-p-toluenesulphonyl diethanolamine has been used successfully for the synthesis of monoaza crowns via reactions with glycol ditosylates. This particular reaction

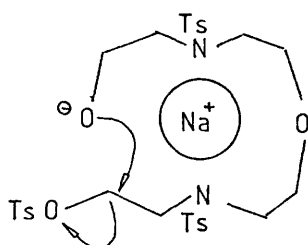


Scheme 4.11



is of interest in itself as reasonable yields are obtained without using a high-dilution procedure. A similar synthesis was envisaged for the reaction of N-p-tolylsulphonyldiethanolamine with tri-tolylsulphonyldiethanolamine in tetrahydrofuran using sodium hydride to synthesise the anion from N-p-tolylsulphonyldiethanolamine and act as the cation for the template [Diagram 4.3]. Unfortunately

Diagram 4.3



after three attempts no cyclic product was isolated. This was probably due to the cation being too large and thus preventing cyclisation via the template method [Diagram 4.3]. This experiment should be repeated using lithium as the cation as there is a better correlation of pore diameter to cation diameter and therefore has a better chance of success.

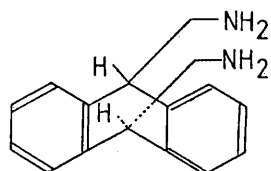
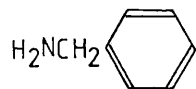
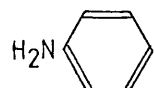
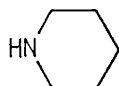
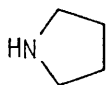
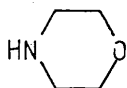
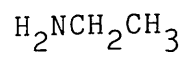
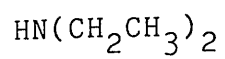
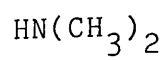
A number of diaza crowns were required to complete the series of compounds sought. Accordingly this labour was shared with collaborators at King's College. Diaza[24]crown-8 (3.3) and diaza[21]crown-7 (3.2) were prepared in the course of this work. Samples of diaza[18]crown-6 (3.1), diaza[18]crown[6] (2.2) and

diaza[15]crown-5 were prepared at King's College and subsequently the latter two compounds were obtained commercially.

#### 4.3.ii) Other amines

These amines are either commercially available or are readily synthesised from known procedures, [Table 4.8]. It was decided to prepare a series of amines for condensation reactions with ferrocene and ruthenocene bis and chloride to find the  $\Delta G^\ddagger$  values for rotation about the  $\text{CO} \begin{array}{c} \curvearrowright \\ \text{N} \end{array}$  bond for comparison with the macrocyclic metallocenes.

There was also the possibility of cation binding e.g.  $\text{Ag}^+$  with the aromatic amides metallocenes through the  $\pi$  clouds of the benzene rings. It was soon recognised that there may not be enough room for ion binding to take place between the aromatic groups except for  $\text{H}^+$ . However, with larger molecules this potential problem should not arise (30). This particular compound may be of interest since the aromatic rings will be at right angles to the cyclopentadienyl rings and thus may allow some interaction between the cation and the metal in the metallocene.

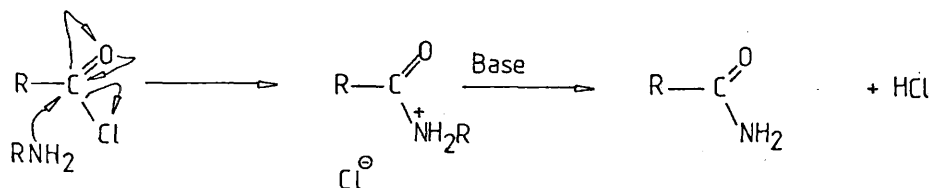
Table 4.8

CHAPTER 5: THE CONDENSATION OF METALLOCENE BIS ACID CHLORIDES  
WITH 'AMINES'

## CHAPTER 5

THE CONDENSATION OF METALLOCENE BIS ACID CHLORIDES WITH 'AMINES'5.1 PREPARATION5.1.i) Introduction

The condensation of acid chlorides with amines has been extensively studied and the mechanism is well understood. In these reactions the amine serves as a nucleophilic reagent, attacking the carbonyl and displacing chloride ion [Diagram 5.1]. In the process nitrogen

Diagram 5.1

loses a proton to a second molecule of amine or another base in the reaction. In a similar way secondary amines can be used to prepare other substituted amides. Tertiary amines, although basic, fail to yield amides, presumably because they cannot lose a proton (to stabilize the product) after attaching themselves to the carbonyl group.

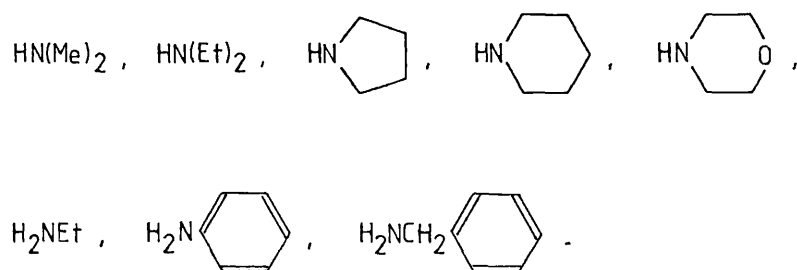
In this work aliphatic  $\alpha,\omega$ -diamines and diaza crown ethers were used in the presence of a tertiary amine (triethylamine). The tertiary amine acted as the base removing the proton in the complex and formed an insoluble hydrochloride salt (organic solvents). The tertiary

amine thus saved on the amount of  $\alpha,\omega$ -diamines or diaza crown ether required for any particular condensation.

### 5.1.ii) Simple 'amides'

The following amines [Table 5.1] were condensed with ferrocene and ruthenocene bis acid chloride, under anhydrous conditions in benzene. In all cases the

Table 5.1



reaction proceed quickly (5 minutes) and the yields were high (80-100%). The subsequent purification of the amides was easily achieved. The hydrochloride complex was filtered off and the amide was passed slowly down an alumina column, evaporation of the solvent yielded the amide.

### 5.1.iii) Macrocyclic amides

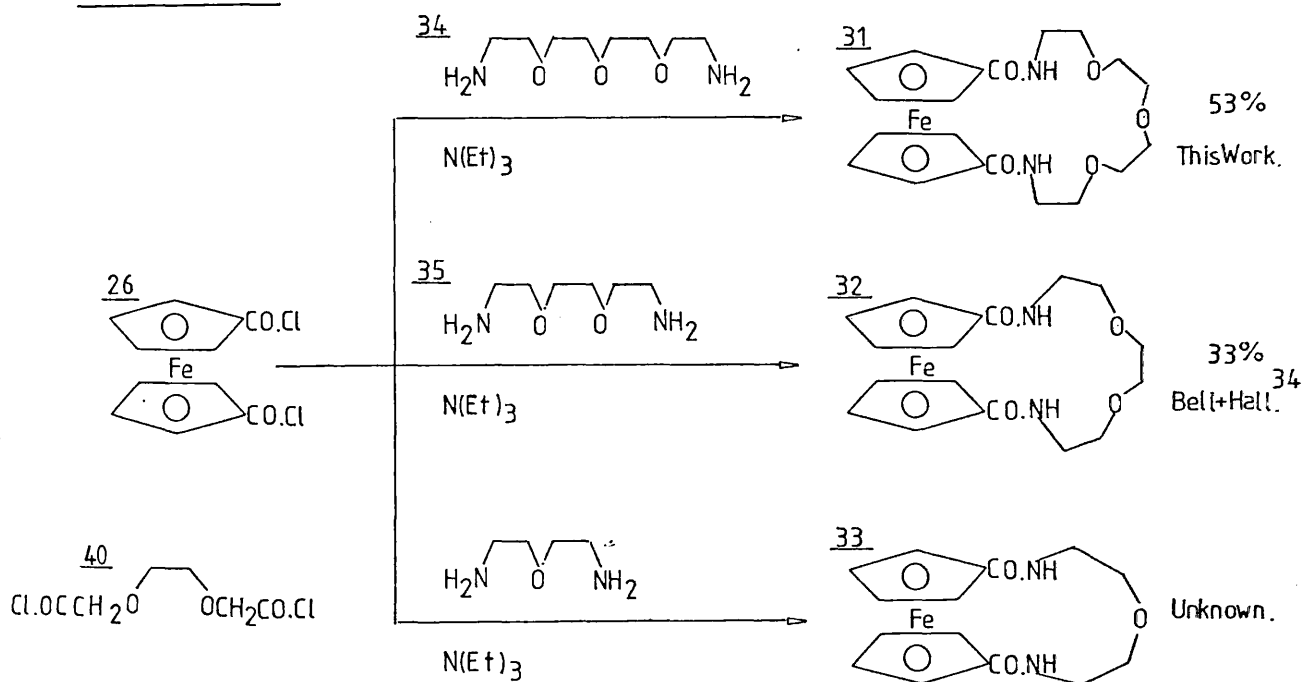
#### Ferrocene crown ether systems

As seen earlier amines and acid chlorides react rapidly to form amides; in order to prevent polymer formation a high dilution technique is required similar to that of B. Dietrich et al.<sup>14,15</sup> which would promote monomer and dimer formation. This involves the slow simultaneous

addition of dilute solutions of both  $\alpha,\omega$ -diamine and bis acid chloride over a period of hours to a bulk solvent, which is being stirred vigorously under dry conditions [Diagram 5.2].<sup>34</sup>

Three model ferrocene crown ethers were sought for this study but only two compounds have been properly characterised [Scheme 5.1]. 1,1'-ferrocenedicarbonyl chloride (26) reacted readily with 1,11-diamino-3,

Scheme 5.1

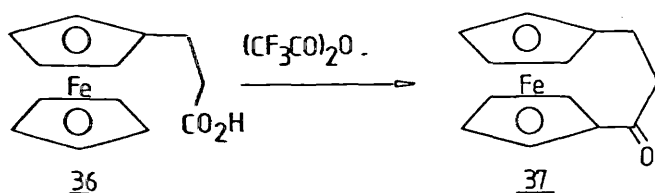


6,9,-trioxaunadecane (34) to give in 53% yield, a highly crystalline monocyclic amide 1,11-(1,1'-ferrocene diamido)-3,6,9-trioxaunadecane (31). Bell and Hall have shown that 1,8-(1,1'-ferrocene diamido)-3,6-dioxaoctane (32) is formed in poorer yield. This was probably due to micro-traces of water being present in the system causing hydrate formation and thus stopping cyclisation. Lehn<sup>61</sup>



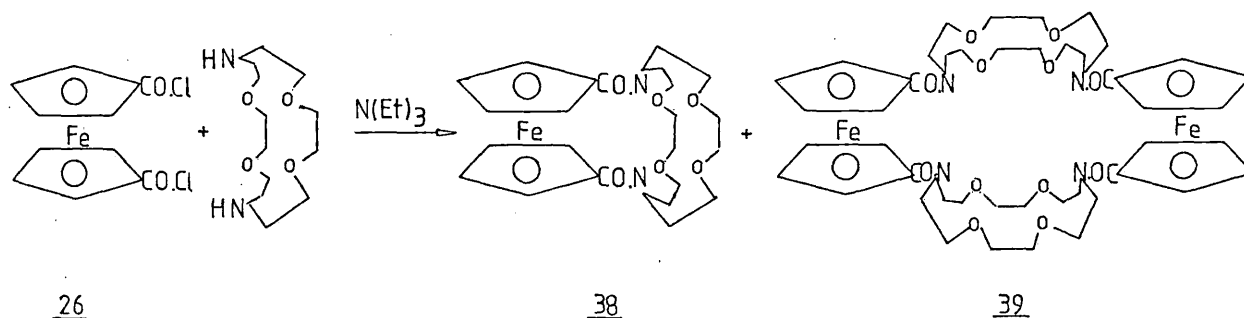
has reported the use of two mole-equivalents of bis amine (35) per acid chloride group in the condensation with triglycolyl chloride (40) instead of the more usual technique, one mole-equivalent of amine and excess tertiary base. This could be because the excess diamine effectively scavenged residual water in the system ((35) is a weaker base than triethylamine). The third compound (33) is now under investigation and it will be interesting to see if there is a further reduction in yield. If this is the case, the problem may not have been hydrate formation but a phenomenon of optimum cyclisation size. This however, is unlikely since  $\alpha$ -keto-1,1'-trimethylene ferrocene (37) can be readily prepared from ferrocenylpropionic acid (36) in 69% yields<sup>152</sup> where the linking bridge only contains three atoms [Reaction 5.1]. It is interesting to note that no dimer was detected in either of the reactions in [Scheme 5.1].

Reaction 5.1

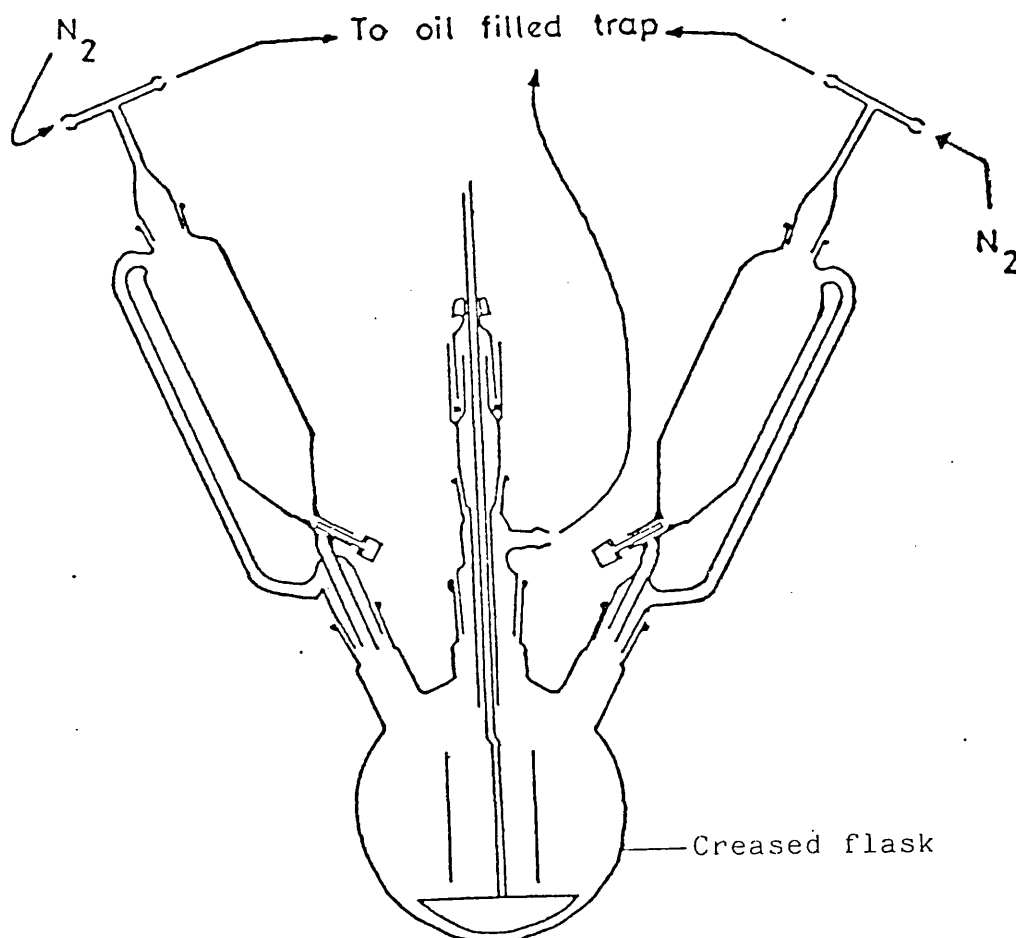


Mettalocene cryptands

Bell and Hall<sup>34</sup> have shown that the condensation of diaza[18]crown-6 (2.2) with 1,1'-ferrocene dicarbonyl chloride under high dilution conditions results with the formation of two main products, a monomer (38) (40%) and dimer (39) (26%) [Reaction 5.2]. More recently it has been found that the relative proportions of these

Reaction 5.2

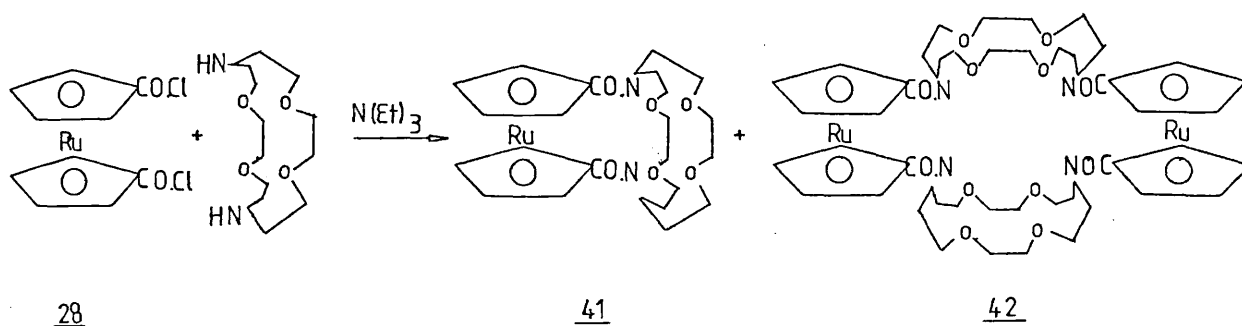
two products are somewhat temperature dependent.<sup>153</sup> The formation of the monomer being favoured at low temperatures and the dimer at higher temperatures. The monomer (38) was also reported by F. Vögtle (1979) but no detailed spectroscopic data were described and the dimer (39) was apparently not observed. Using a similar procedure the monomers and dimers have been obtained by reaction of ferrocene bis acid chloride with, diaza[12]crown-4 (1.1), diaza[15]crown-5 (2.1), diaza[21]crown-7 (3.2) and diaza[24]crown-8 (3.3).

Diagram 5.2

Apparatus for high dilution condensations

A series of ruthenocene macrocycles have been prepared by the general high dilution technique. The reaction of ruthenocene bis acid chloride with diaza[18]crown-6 (2.2) was also found to give two main products, a monomer (41) (38%) and a dimer (42) (26%) [Reaction 5.3]

Reaction 5.3



in proportions similar to those already found for the ferrocene analogues. The two compounds were readily separated by repeated column chromatography to give samples which were satisfactorily characterized by mass spectroscopy, micro-analysis and standard spectroscopic techniques. (The n.m.r. spectra of these compounds and others in this section will be discussed in detail in Section 5.2).

Table 5.2      Preparation of ruthenocene macrocycles from  
1,1'-ruthenocene bis acid chloride

Diaza[ ]crown-	% monomer	% dimer	Temp °C	Scale,g.	Solvent
Diaza[18]crown-6 (2.2)	38 ( <u>41</u> )	26 ( <u>42</u> )	ambient	1.0	Benzene
Diaza[21]crown-7 (3.2)	21 ( <u>76</u> )	56 ( <u>77</u> )	21°	1.0	Benzene
Diaza[18]crown-6 (3.1)	27 ( <u>78</u> )	48 ( <u>79</u> )	ambient	0.16	Benzene
Diaza[15]crown-5 (2.1)	15 ( <u>82</u> )	53 ( <u>83</u> )	60°	0.50	Toluene
Diaza[15]crown-5 (2.1)	5 ( <u>82</u> )	40 ( <u>83</u> )	1°	0.50	Toluene

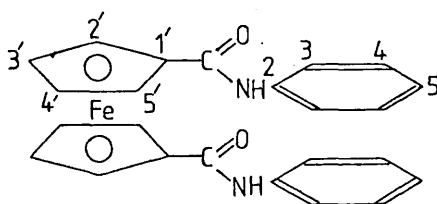
The effect of variation of the temperature of preparation of ruthenocene bis acid chloride with diaza[15]crown-5 (2.1) was investigated. Both reactions were carried out in toluene so that there could be a large temperature difference while all the other conditions were identical. Therefore, the ratio of products would be directly related to the temperature. It was found that toluene was a poor choice of solvent as reactants and products were not very soluble. It was found that the yield of the dimers decreased as the temperature was lowered which agrees with the results of Hall and co-workers. A sharp decrease in the yield of monomer however, resulted when the temperature was lowered. This was most probably due to a poor work up as the product was left on an alumina column overnight with dichloromethane where decomposition may have taken place. Further evidence for this has come from other metallocene cryptands in chlorinated solvents as decomposition is observed over a period of time.

5.2. n.m.r.

A detailed  $^1\text{H}$  and  $^{13}\text{C}$  n.m.r. study has been carried out on ferrocene and ruthenocene amides and cryptands. It was found that the spectra of these systems are temperature dependent and therefore dynamic phenomena were also investigated.

5.2.1.i) Ferrocene and ruthenocene amides

The condensation of 1,1'-ferrocene dicarbonyl chloride with aniline in the presence of triethylamine under dry conditions resulted with the formation of one product in 50% yield. Elemental analysis and mass spectra of this material were consistent with the molecular formulae ( $\text{C}_{24}\text{H}_{20}\text{N}_2\text{O}_2\text{Fe}$ ). The  $^{13}\text{C}$  and  $^1\text{H}$  n.m.r. data also supported the proposed general structure [Diagram 5.3] (43).

Diagram 5.343

The  $^{13}\text{C}$  n.m.r. spectrum of this compound shows seven different signals; two ferrocenyl, one carbonyl, and four aromatic resonances at room temperature. There is free rotation in the structure which contains twenty-

four carbon atoms: the signals must therefore represent groups of two, four or eight carbon atoms [Table 5.3]. There are two possible configurations for the planar amide group [Diagram 5.4]. Each configuration has its own particular characteristics which can be seen in the n.m.r. In order to determine a preferred configuration the following criteria must be considered: steric forces; dipolar repulsions between  $\pi$  systems; and, in substituted cases, hydrogen bonding may play an important role.

Diagram 5.4

Free rotating state of (43)

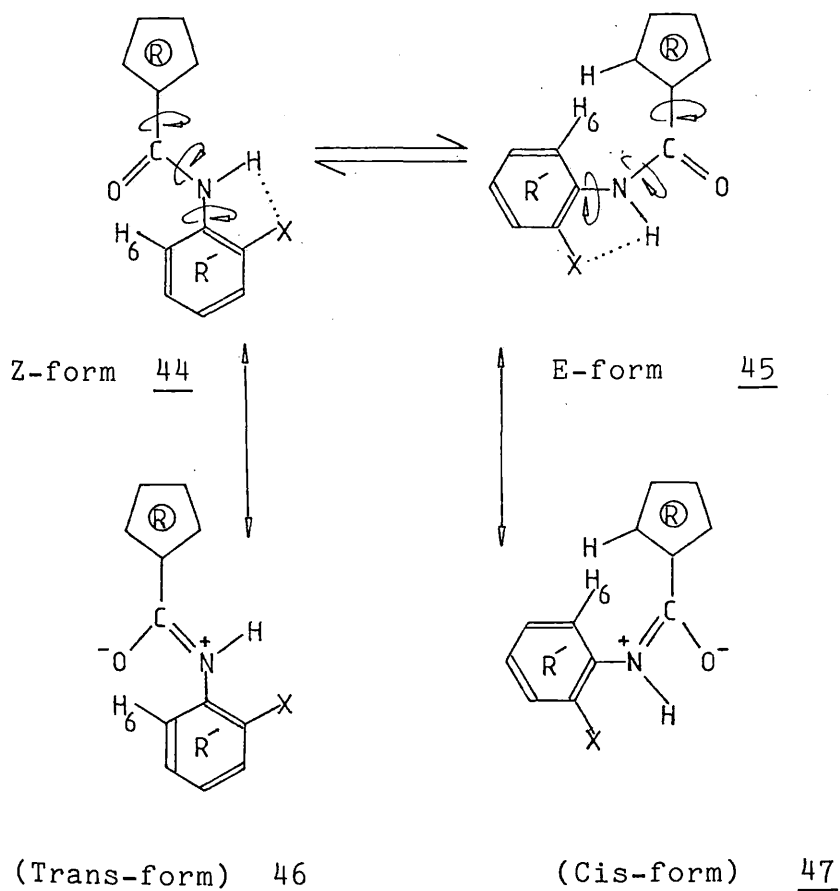


Table 5.3

1,1'-bis(N,phenylamido)-ferrocene (43)<sup>1</sup>H n.m.r. (CDCl<sub>3</sub>) ambient

(43) (250 MHz)			Aniline	
Assignment	ppm	Inter	Assignment	ppm
NH	8.69	2H	NH <sub>2</sub>	3.32
H <sub>3</sub>	7.80d Hz 0.03	4H	H <sub>3</sub>	6.44
H <sub>4</sub>	7.39t Hz 0.03	4H	H <sub>4</sub>	6.99
H <sub>5</sub>	7.15t Hz 0.03	2H	H <sub>5</sub>	6.52
H <sub>2,5</sub>	4.67t Hz 0.01	4H		
H <sub>3,4</sub>	4.49t Hz 0.01	4H		

t - triplet; d - doublet; c - complex; b - broad;

q - quartet; s - sharp

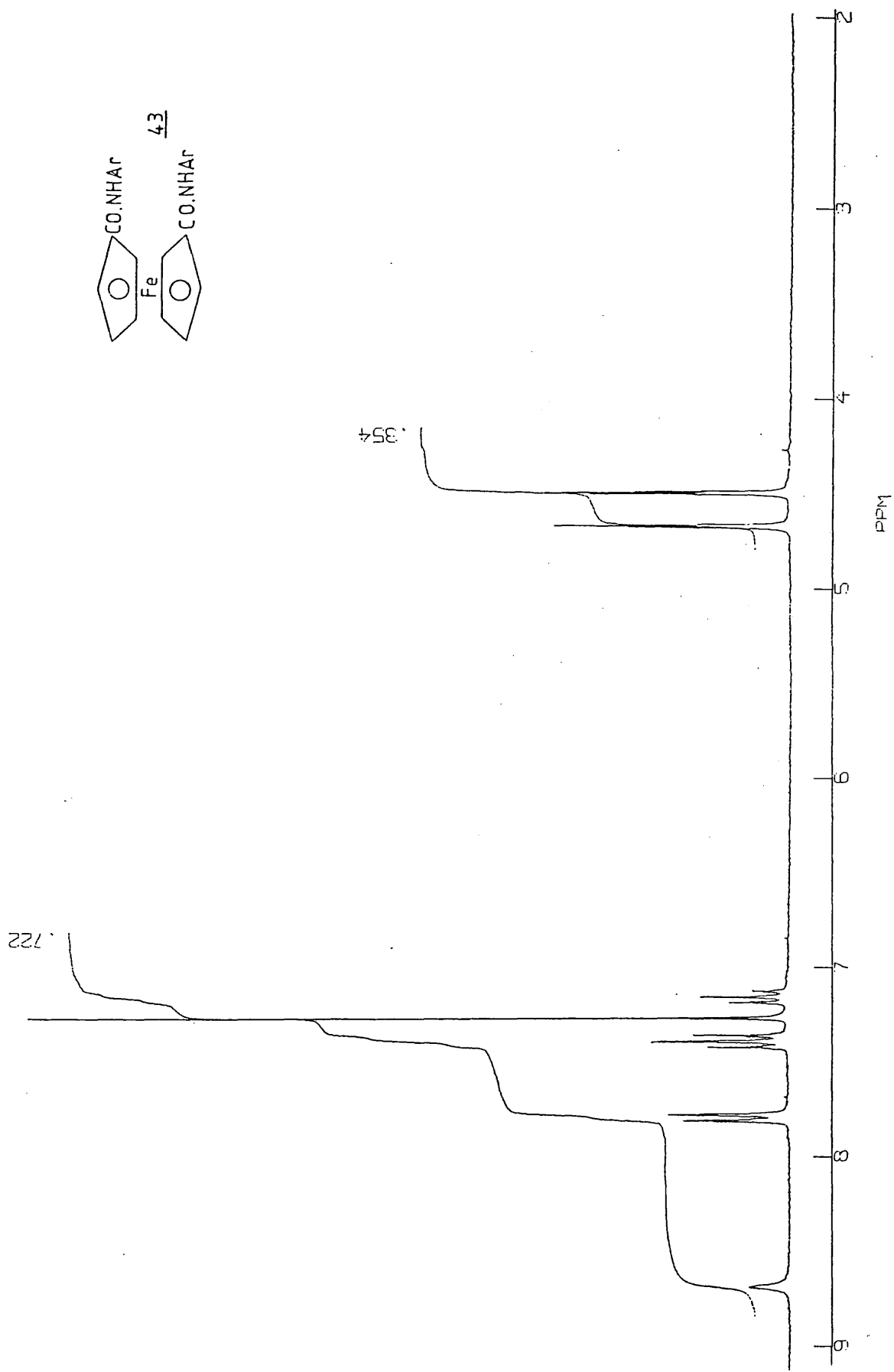
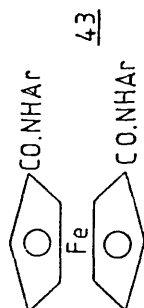
<sup>13</sup>C n.m.r. (CDCl<sub>3</sub>) ambient (43). 22.6MHz.

Assignment	ppm
Carbonyl C <sub>1</sub>	169.0
Ipsso benzene C <sub>2</sub>	138.5
o/m benzene C <sub>3,4</sub>	129.1
m/o benzene C <sub>4,3</sub>	124.2
p benzene C <sub>5</sub>	120.0
C <sub>1</sub>	74.2
C <sub>2,5</sub>	71.4
C <sub>3,4</sub>	

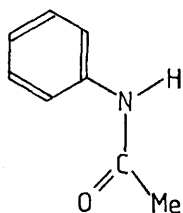
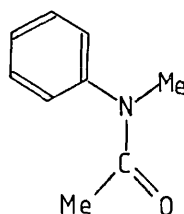


<sup>1</sup>H n.m.r. of 1,1'-bis(N-phenylamido)ferrocene @ 250 MHz (CDCl<sub>3</sub>)

WM 250 1H SPECTRUM NO. 7761  
JPK1 IN CDCL3 + TMS

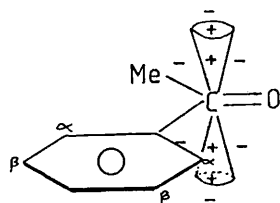
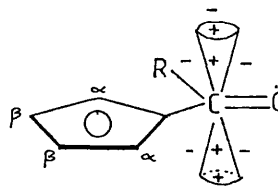


The hydrogen bonding interaction is typical of substituted anilides with a suitable hydrogen bond acceptor  $x$  [Z and E-form Diagram 5.4] and would cause a large deshielding effect on the amide proton which would be seen as a downfield shift. There would also be the favourable formation of a five or six membered ring. In (43) there is no hydrogen bond acceptor and repulsion occurs. However, a distinct downfield shift of the  $H_6$  protons can be seen in the  $^1H$  n.m.r. and must be explained. As the groups  $R$  and  $R'$  are large (cyclopentadienyl and benzene) the preferred configuration for steric reasons will be the  $z$ (trans)-forms (44) (46) as in the  $E$ (cis)-forms (45) (47), there is repulsion and hindrance between the protons in the two aromatic systems. There is also further repulsion due to the two  $\pi$  clouds in the two aromatic systems  $R$  and  $R'$ . Consequently, the proton  $H_6$  will be in a deshielding region of the carbonyl group which can account for the observed shift. The chemical shift for the  $H_6$ (ortho) proton has been reported for a large number of substituted anilides and is in the range 8.0-9.5 ppm. It is of interest to note that thioanilides have even larger  $H_6$ (ortho) shifts since thiocarbonyl groups have a greater magnetic anisotropy compared to the anilide carbonyl groups. As with most anilides, the steric effects determine the isomer populations  $E$  and  $Z$ . However, with acylanilides, a combination of steric and electronic factors must be considered. Acetanilide (48) exists almost completely in  $Z$ -form (48) where steric forces

Z-form 48E-form 49

a minimum and  $\pi$  dipolar interactions are a maximum, while N-methyl acetanilide (49), is completely in the E-form (49) where the  $\pi$  dipolar interactions are at a minimum.

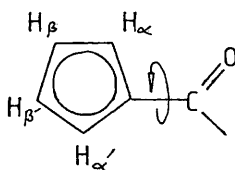
For 1,1' bis(N-phenylamido)-ferrocene (43) the  $\pi$  interaction will be a maximum in the sterically favoured Z-form (44) and a minimum in the sterically hindered E-form (45). This shows that steric forces dominate in controlling the configuration in (43). Further evidence for the favoured configuration of the amide group comes from the shift of the protons in the  $^1\text{H}$  n.m.r. of the cyclopentadienyl rings. The shift and splitting of these protons is partly due to the interaction with the deshielding zone of the carbonyl group and electron withdrawal from the  $\pi$  clouds of the cyclopentadienyl ring resulting with two pseudo-first order triplets [Table 5.3]. A similar deshielding phenomenon has been seen from benzene studies (acetophenone) (50) where the carbonyl group greatly deshields the ring protons adjacent to it; the  $\alpha$ -deshielding effect [Diagram 5.5].

Diagram 5.5Acetophenone (50)Cyclopentadienyl system

+ = shielding

- = deshielding

The preferred configuration of 1,1' bis(N-phenylamido)-ferrocene at room temperature in the n.m.r. time scale is neither the Z nor E-form [Diagram 5.4] but a time average, since there is rotation about the ipso cyclopentadienyl carbonyl bond [Diagram 5.6]. Consequently.

Diagram 5.6

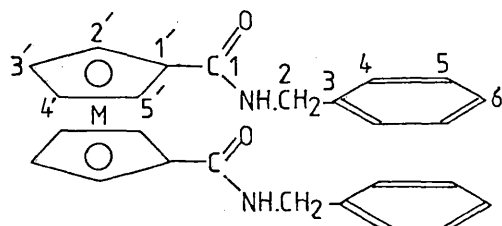
$H_{\alpha} = H_{\alpha'} \neq H_{\beta} = H_{\beta'}$ , which is seen as two pseudo-first order triplets in the  $^1\text{H}$  n.m.r. As the sample temperature is lowered one would expect all the signals to become non-equivalent  $H_{\alpha} \neq H_{\alpha'} \neq H_{\beta} \neq H_{\beta'}$ , and this has been seen in other ferrocene (38) and ruthenocene (41) amides.

1,1' bis(N-benzylamido)ferrocene (51) and 1,1'bis  
(N-benzylamido)ruthenocene (52)

The condensation of 1,1'-ferrocene dicarbonyl chloride or 1,1'-ruthenocene dicarbonyl chloride with benzylamine under dry conditions results with the formation of one product in 80% yield. This was purified by chromatography on alumina eluting with dichloromethane. Subsequent elemental analysis and mass spectra were consistent with the molecular formulae ( $C_{26}H_{24}O_2N_2M$ ). The  $^{13}C$  and  $^1H$  n.m.r. data also supports the proposed structure [Diagram 5.7].

Diagram 5.7

M = Fe 51, Ru 52



The  $^{13}C$  n.m.r. spectrum for each compound shows nine different signals; three cyclopentadienyl, one carbonyl, one methylene and four aromatics. There is therefore a degree of symmetry within the molecule as total asymmetry would lead to twenty six different carbon signals. In this case it appears that rotation about the carbonyl nitrogen bond and the ipso cyclopentadienyl carbonyl bond as well as rotation of the cyclopentadienyl

rings are all fast on the n.m.r. time scale at room temperature. Consequently  $H_2$ , is equivalent to  $H_5$ , and  $H_3$ , is equivalent to  $H_4$ , and these signals are seen as two pseudo first order triplets [Table 5.4].

Similar conformational arguments as for 1,1'-bis(N-phenylamido)ferrocene apply here and the favoured configuration should be the Z-form at low temperatures on the n.m.r.

Diagram 5.9

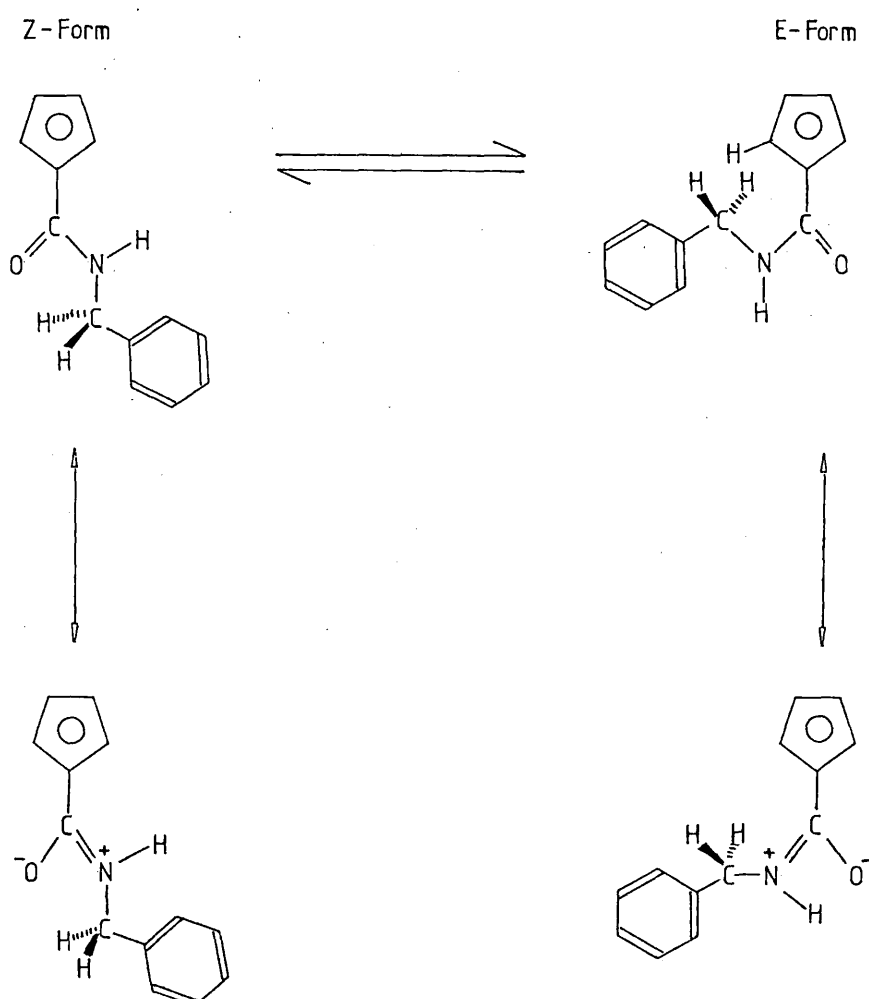


Table 5.4

1,1'-bis(N-benzylamido)ferrocene (51)    1,1'-bis(N-benzylamido) ruthenocene (52)

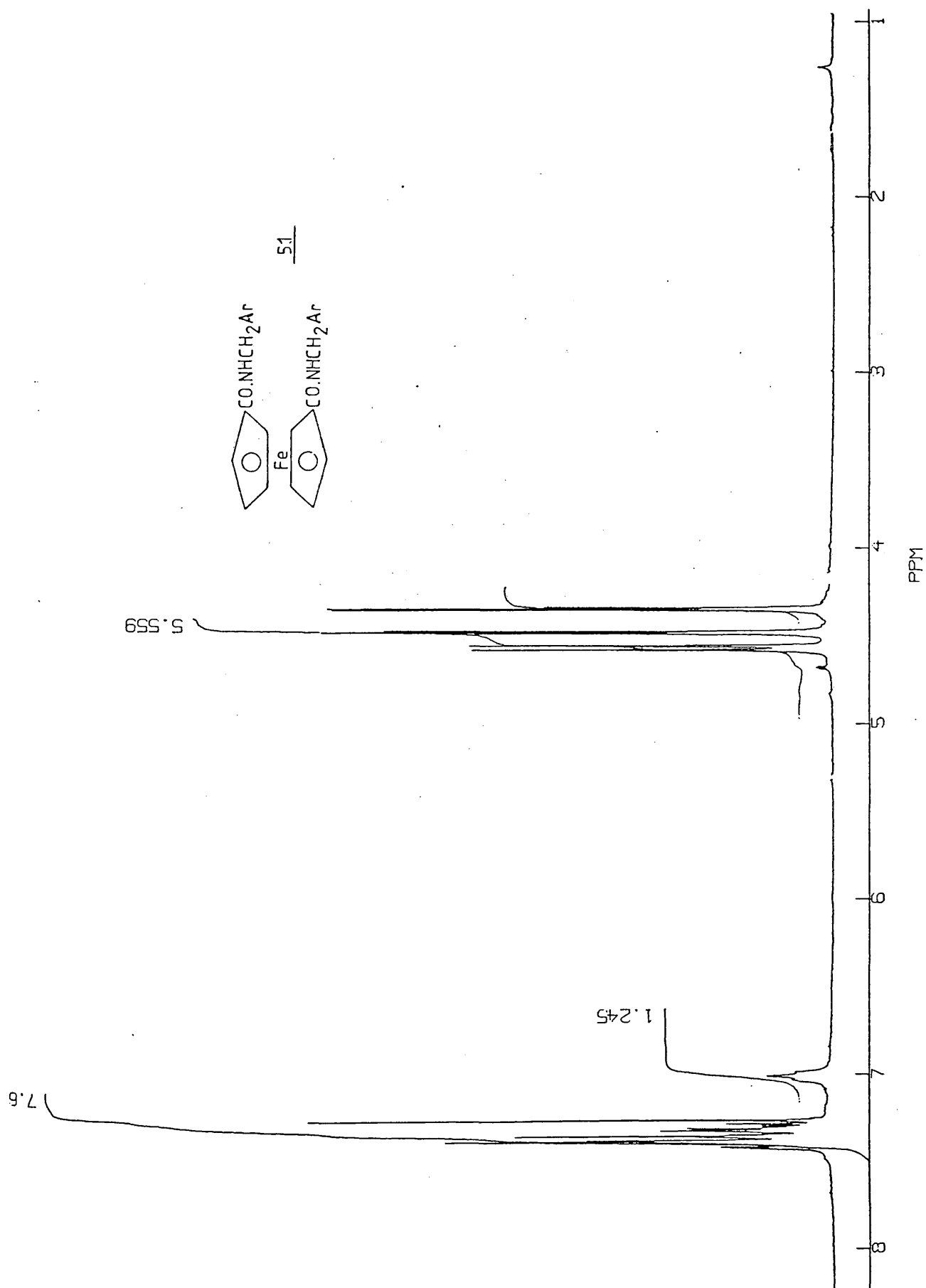
<sup>1</sup>H n.m.r. CDCl<sub>3</sub> ambient

Assignment	(51) (250 MHz)		(52) (90 MHz)		Benzylamine	
	ppm	inter	ppm	inter	ppm	inter
Aromatic	7.21c	10	7.32	10	7.29	5
NH	7.01t $\frac{1}{2}$ 0.02	2	6.79	2	1.52	2
CH <sub>2</sub>	4.57d. $\frac{1}{2}$ 0.03	2	5.09b	4	3.85	2
		2				
H <sub>2,5</sub>	4.48t $\frac{1}{2}$ 0.02	4	4.68b	4		
H <sub>3,4</sub>	4.34t $\frac{1}{2}$ 0.02	4	4.46b	4		

<sup>13</sup>C n.m.r. (CDCl<sub>3</sub>) ambient

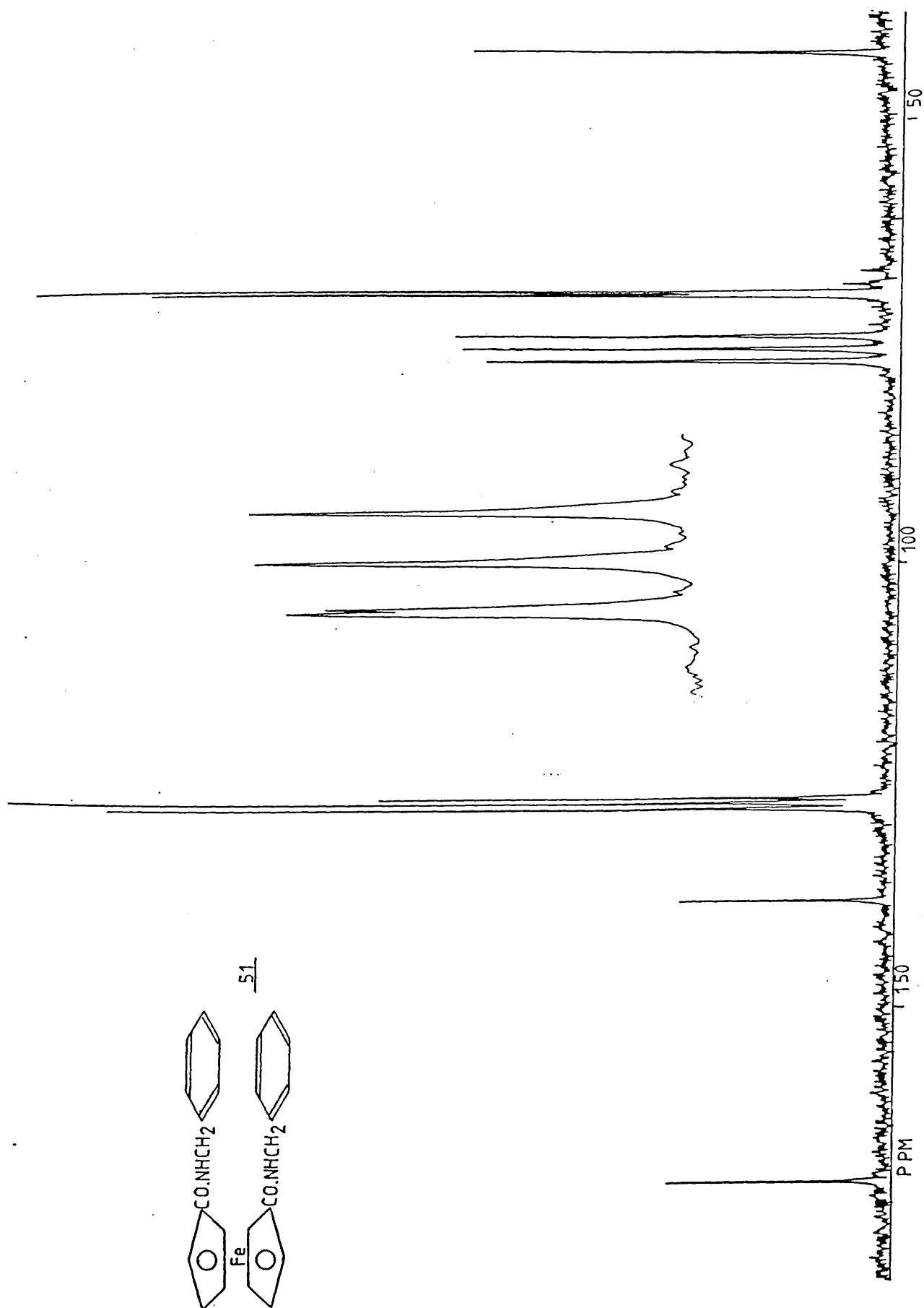
Assignment	(51) (22.63 MHz)	(52)
	ppm	ppm
C=O	170.2	168.8
ipso benzene C <sub>3</sub>	138.8	138.8
o/m benzene C <sub>4,5</sub>	128.6	128.7
m/o benzene C <sub>5,4</sub>	128.0	127.9
p benzene C <sub>6</sub>	127.4	127.5
C <sub>1'</sub>	78.3	73.1
C <sub>2,5</sub>	71.1	72.2
C <sub>3,4</sub>	70.7	72.1
N-CH <sub>2</sub>	43.7	43.4

$^1\text{H}$  n.m.r. of 1,1'-bis(N-benzylamido)ferrocene @ 250 MHz ( $\text{CDCl}_3$ )





$^{13}\text{C}$  n.m.r. of 1,1'-bis(N-benzylamido)ferrocene @ 22.63 MHz ( $\text{CDCl}_3$ )

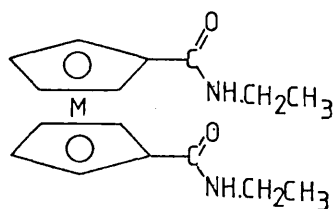


time scale. The deshielding region about the carbonyl function and  $\pi$  withdrawal [Diagram 5.9] no longer effects the  $H_4$  ortho protons to any great degree as there is no noticeable shift of the signals when compared with benzylamine (7.21 ppm Fe; 7.32 ppm Ru; 7.29 ppm benzylamine). However, there is a large shift of the methylene protons when compared with benzylamine (4.58, 4.55 ppm Fe; 5.0% Ru; 3.85 ppm benzylamine). This downfield shift may be due to the methylene protons residing near the deshielding region of the carbonyl function. It is of interest to note that the prochiral methylene protons are clearly split in the ferrocene derivative and are diastereotopic.

1,1'-bis(N-ethylamido)ferrocene (53) and 1,1'-bis(N-ethylamido)ruthenocene (54)

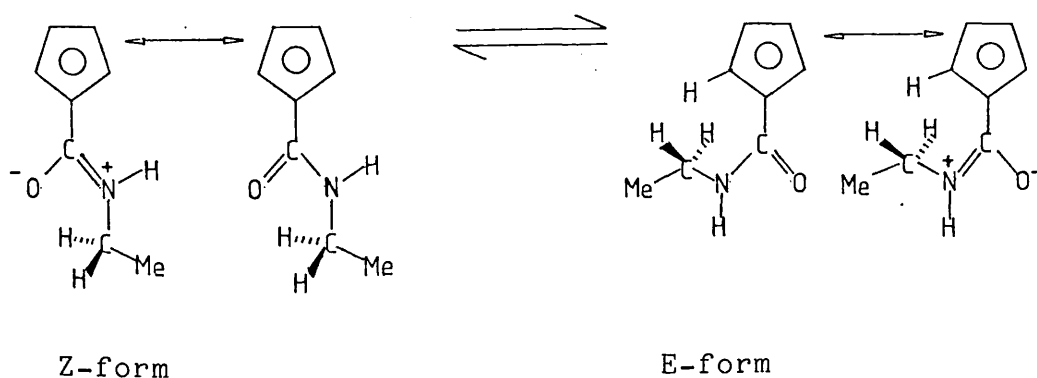
The condensation of 1,1'-ferrocene dicarbonyl chloride or 1,1'-ruthenocene dicarbonyl chloride with ethylamine under dry conditions results in the formation of one product in 70% yield. This was purified by passing the compound down an alumina column with dichloromethane and 1% methanol. Subsequent analysis was consistent with the molecular formula ( $C_{16}H_{20}O_2N_2M$ ). The  $^{13}C$  and  $^1H$  n.m.r. data also supports the proposed structure [Diagram 5.10].

Diagram 5.10

M = Fe 53 or Ru 54

The  $^{13}\text{C}$  n.m.r. spectrum for each compound shows six different signals; three cyclopentadienyl, one carbonyl, one methylene and one methyl. As there is free rotation about the ipso cyclopentadienyl carbonyl bond which is fast on the n.m.r. time scale  $\text{C}_2$  is equivalent to  $\text{C}_6$  and  $\text{C}_3$  is equivalent to  $\text{C}_4$ . This is supported from the  $^1\text{H}$  n.m.r. as two pseudo first order triplets are seen,  $\text{H}_2$  equivalent to  $\text{H}_5$  and  $\text{H}_3$  equivalent to  $\text{H}_4$  ( $J$ . 0.02 ppm Fe;  $J$  0.02 ppm Ru) [Table 5.5]. Due to the poor solubility of (53) in chloroform a little methanol was added to the n.m.r. sample. This must be taken into account

Diagram 5.11



since the solvent can effect the conformation of an amide at low temperatures on the n.m.r. time scale.

Table 5.5

1,1'-bis(N-ethylamido)ferrocene (53)      1,1'-bis(N-ethylamido)ruthenocene (54)

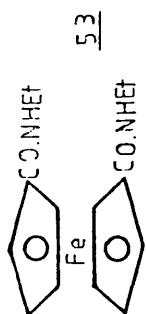
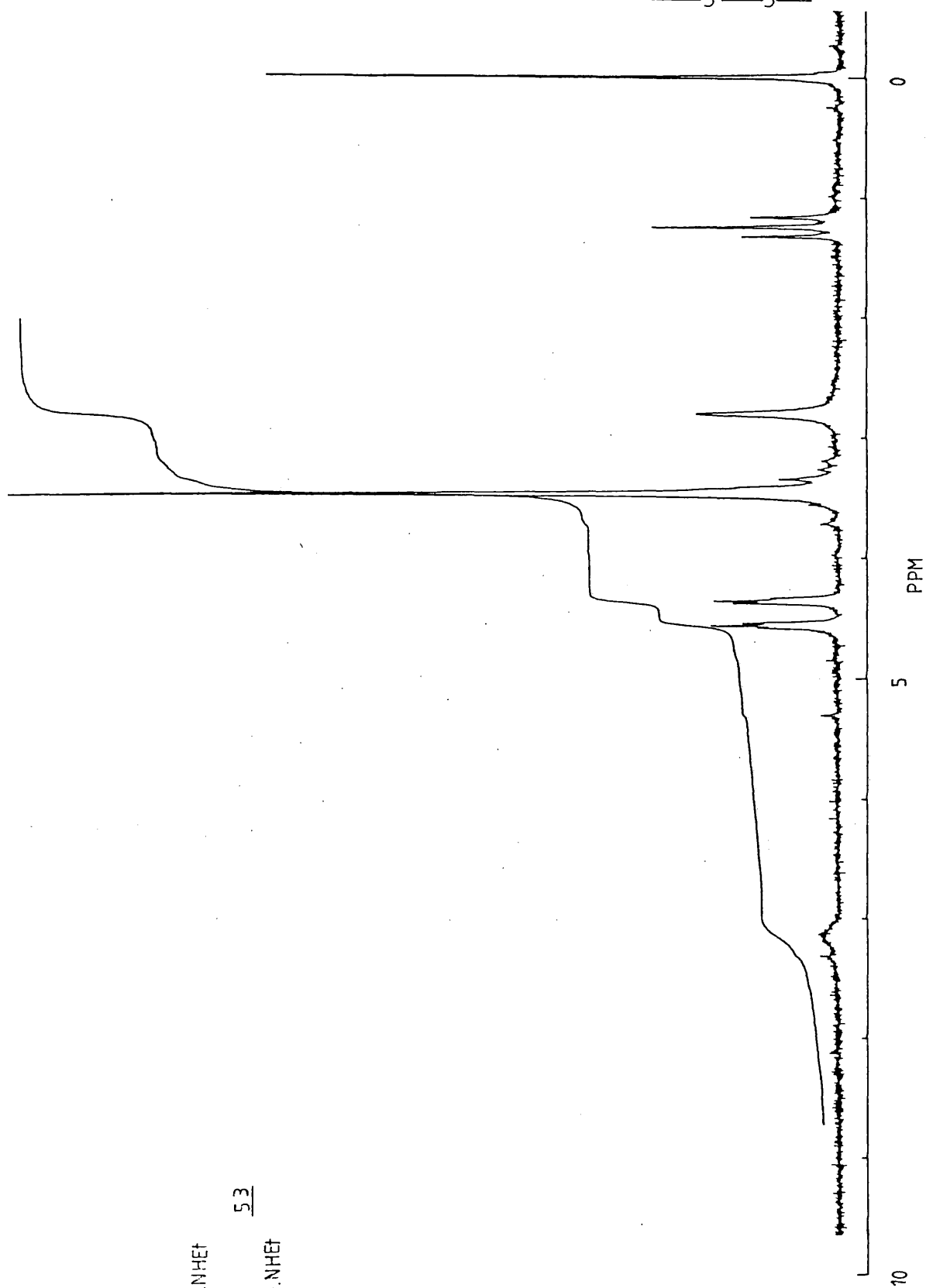
$^1\text{H}$  n.m.r. 90 MHz ambient,  $\text{CDCl}_3$ .

Assignment	<u>(53)</u> ( $+\text{CD}_3\text{OD}$ )		<u>(54)</u>		Ethylamine
	ppm	inter	ppm	inter	ppm
NH	7.2b	2	7.2b	2	4.58s
$\text{H}_{2,5}$	4.55t $\frac{1}{2}$ 0.02	4	4.96t $\frac{1}{2}$ 0.02	4	
$\text{H}_{3,4}$	4.35t $\frac{1}{2}$ 0.02	4	4.60t $\frac{1}{2}$ 0.02	4	
$\text{CH}_2$	2.80b	4	3.25q $\frac{1}{2}$ 0.14	4	2.68q
$\text{CH}_3$	1.25t $\frac{1}{2}$ 0.08	6	1.12t $\frac{1}{2}$ 0.12	6	1.14t

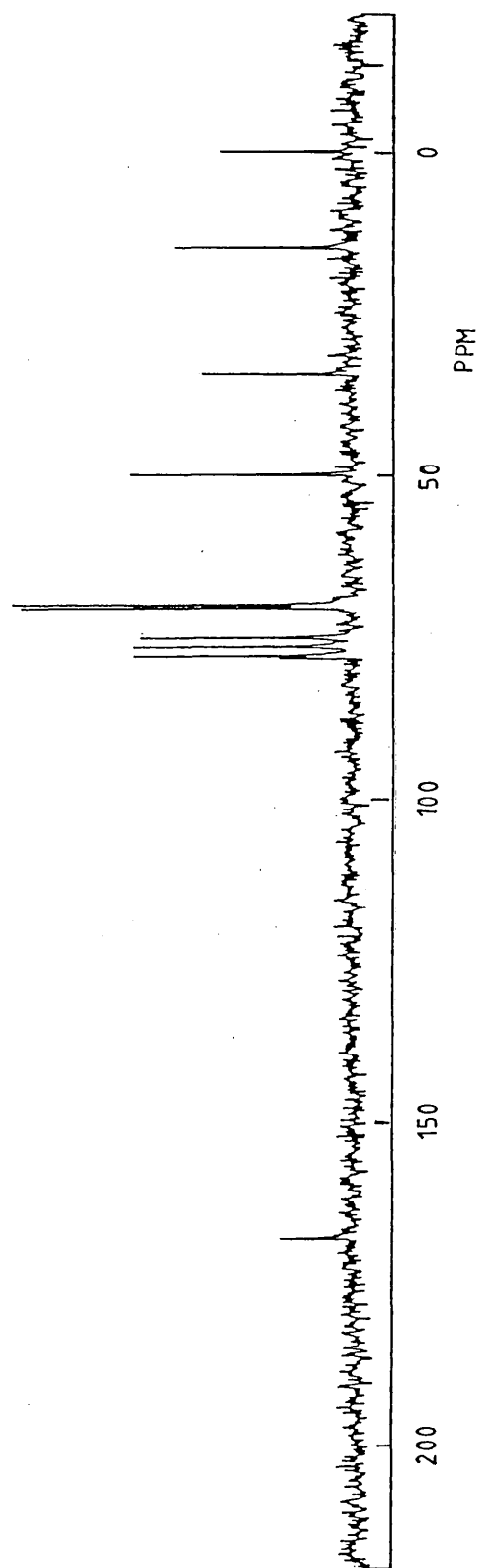
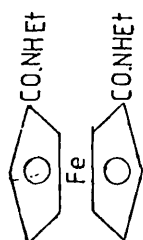
$^{13}\text{C}$  n.m.r.  $\text{CDCl}_3$  ambient 22.6MHz.

Assignment	<u>(53)</u> ( $+\text{CD}_3\text{OD}$ )	<u>(54)</u>
	ppm	ppm
C=O	170.3	176.7
$\text{C}_1$	79.1	80.2
$\text{C}_{2,5}$	71.2	72.6
$\text{C}_{3,4}$	70.6	70.8
$\text{CH}_2$	50.5	37.8
$\text{CH}_3$	15.0	19.9

$^1\text{H}$  n.m.r. of 1,1'-bis(N-ethylamido)ferrocene @ 90 MHz ( $\text{CDCl}_3$ ,  $\text{CD}_3\text{OD}$ )



$^{13}\text{C}$  n.m.r. of 1,1'-bis(N-ethylamido)ferrocene @ 22.6 MHz ( $\text{CDCl}_3, \text{CD}_3\text{OD}$ )



5.2.1.ii). Other ferrocene and ruthenocene amides

The n.m.r. of all these 'simple' metallocene amides [Tables 5.6, 5.7] give the expected  $^1\text{H}$  and  $^{13}\text{C}$  spectra at ambient temperature and can be seen in [Tables 5.8, 5.9].

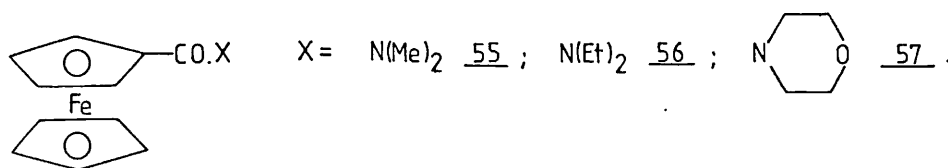
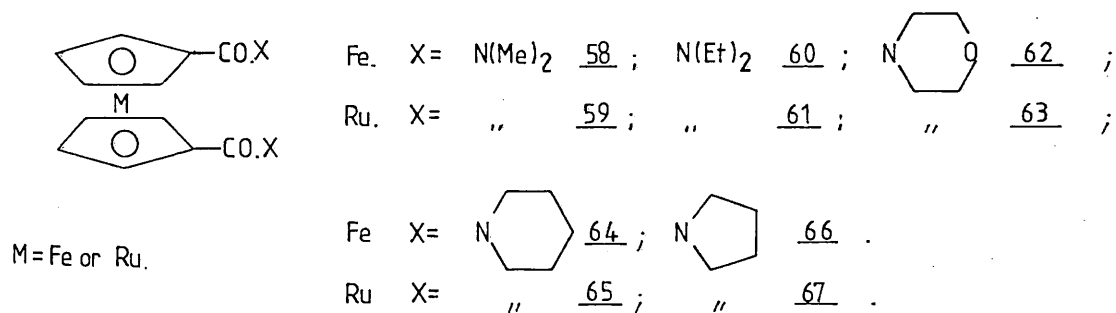
Table 5.6. Monosubstituted ferrocene amidesTable 5.7 1,1'-Disubstituted metallocene amides

Table 5.8

$^{13}\text{C}$  n.m.r.  $\text{CDCl}_3$  of monosubstituted ferrocene amides ambient  
@ 22.6 MHz

Assignment	C=O	C <sub>1</sub>	C <sub>2,5</sub>	Ring 2	C <sub>3,4</sub>	C <sub>1'</sub>	C <sub>1''</sub>	C <sub>2'</sub>	C <sub>2''</sub>
Derivative									
(55)	170.7	78.4	70.5	69.7	69.2	37.3			
(56)	170.2	79.6	70.3	69.8	69.2	41.7		13.7	
(57)	170.0	77.1	70.2	69.8	69.2	67.9	66.9	46.4	

$^1\text{H}$  n.m.r.  $\text{CDCl}_3$  of monosubstituted ferrocene amides ambient

Assignment	H <sub>2,5</sub>	H <sub>3,4</sub>	Ring 2	H <sub>1</sub>	H <sub>1</sub>	H <sub>2</sub>	H <sub>2</sub>
Derivative							
(55)	4.62t	4.29t	4.22s	3.10s			
(56)	4.64t	4.32b	4.22s	3.54q		1.22t	
(57)	4.70t	4.45t	4.39b		3.86s		

@ 90 MHz

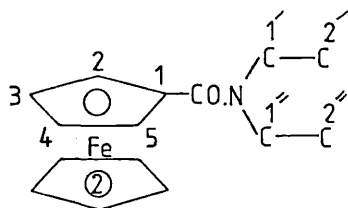




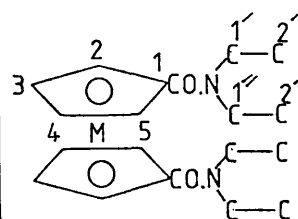
TABLE 5.9

$^{13}\text{C}$  n.m.r.  $\text{CDCl}_3$  of disubstituted metallocene amides ambient  
@ 22.6 MHz

Assignment	C=O	C <sub>1</sub>	C <sub>2,5</sub>	C <sub>2,5</sub>	C <sub>3,4</sub>	C <sub>3,4</sub>	C <sub>1'</sub>	C <sub>1''</sub>	C <sub>2'</sub>	C <sub>2''</sub>	
Derivative											
(58)	170.1	80.6	72.3	71.3	37.7						
(59)	168.5	83.6	74.3	73.2	37.8						
(60)	169.1	81.3	71.8	71.4	41.8	13.9					
(61)	159.3	81.3	71.9	70.1	34.6	14.5					
(62)	169.1	80.9	72.2	71.3	45.7	67.1					
(63)	167.5	78.9	74.0	73.2	72.5	71.6	45.7	66.9			
(64)	108.5	81.4	71.9	71.1	46.1	26.3					-CH <sub>2</sub> - 24.8
(65)	ir	84.2	74.0	73.1	72.6	71.4	46.3	45.9	26.3		-CH <sub>2</sub> - 24.7
(66)	167.9	79.5	71.6	71.2	47.4	25.3					
(67)	166.7	82.0	73.7	73.1	72.4	71.9	47.99	47.40	26.9		

$^1\text{H}$  n.m.r.  $\text{CDCl}_3$  of disubstituted metallocene amides ambient  
@ 90 MHz

Assignment	H <sub>2,5</sub>	H <sub>3,4</sub>	H <sub>1'</sub>	H <sub>1''</sub>	H <sub>2'</sub>	H <sub>2''</sub>
Derivative						
(58)	4.19t	3.95t	2.77			
(59)	5.00t	4.70t	3.02			
(60)	4.64t	4.36t	3.45q		1.20t	
(61)	5.00t	4.72t	3.55q		1.20t	
(62)	4.60t	4.40t		3.66		
(63)	4.96t	4.76t		3.74		
(64)	4.58t	4.38t	3.65		-CH <sub>2</sub> CH <sub>2</sub> CH <sub>2</sub> - 1.62	
(65)	4.85b	4.62b	3.58		-CH <sub>2</sub> CH <sub>2</sub> CH <sub>2</sub> - 1.60	
(66)	4.76t	4.36t	3.59		1.99	
(67)	4.96t	4.58t	3.52		1.82	



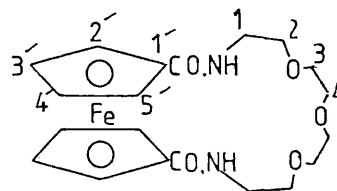
5.2.2. Ferrocene crown-ethers (31), (32)

It is clear from the n.m.r. data that the macrocyclic amides (31) and (32) permit some flexibility of the bridging crown and this is not found in the ferrocene [2.2]cryptand (monomer) (38) or the ruthenocene[2.2]cryptand

Table 5.10

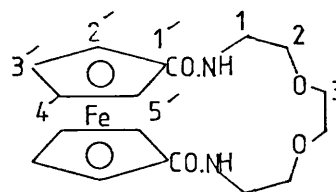
$^{13}\text{C}$  n.m.r.  $\text{CDCl}_3$  22.6 MHz ambient ppm.

Assignment	(31)	(32)
C=O	169.9	169.8
C <sub>1'</sub>	77.5	77.4
C <sub>2;5'</sub>	72.0	71.3
C <sub>3;4'</sub>	70.4	70.3
OCH <sub>2</sub>	70.0b	C <sub>3</sub> 69.9 C <sub>2</sub> 69.8
NCH <sub>2</sub>	39.7	C <sub>1</sub> 39.3

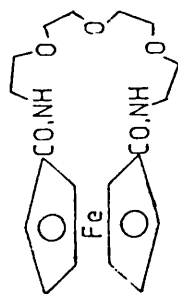
31

$^1\text{H}$  n.m.r.  $\text{CDCl}_3$  250 MHz ppm ambient.

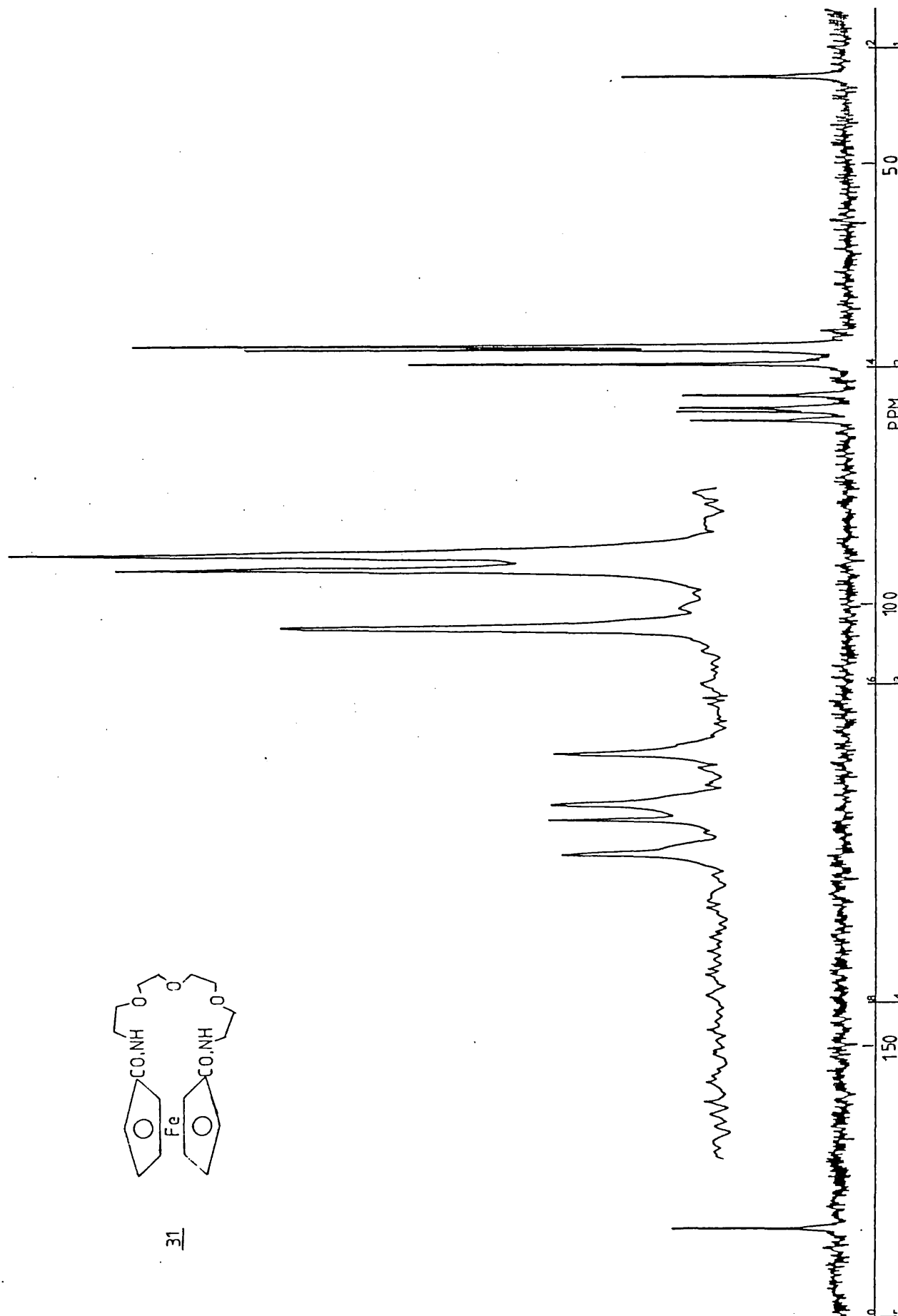
Assignment	(-50 -70°C) (31)	(32)
NH	7.04t 2H	6.54t 2H
H <sub>2;5'</sub>	4.66t 4H	4.53t 4H
H <sub>3;4'</sub>	4.40t 4H	4.46t 4H
OCH <sub>2</sub>	3.71b 12H	3.71b 12H
NCH <sub>2</sub>	3.63b 4H	

32

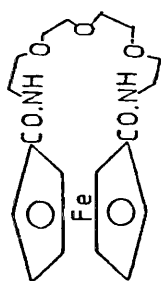
$^{13}\text{C}$  n.m.r. of (31) @ 22.6 MHz ( $\text{CDCl}_3$ )



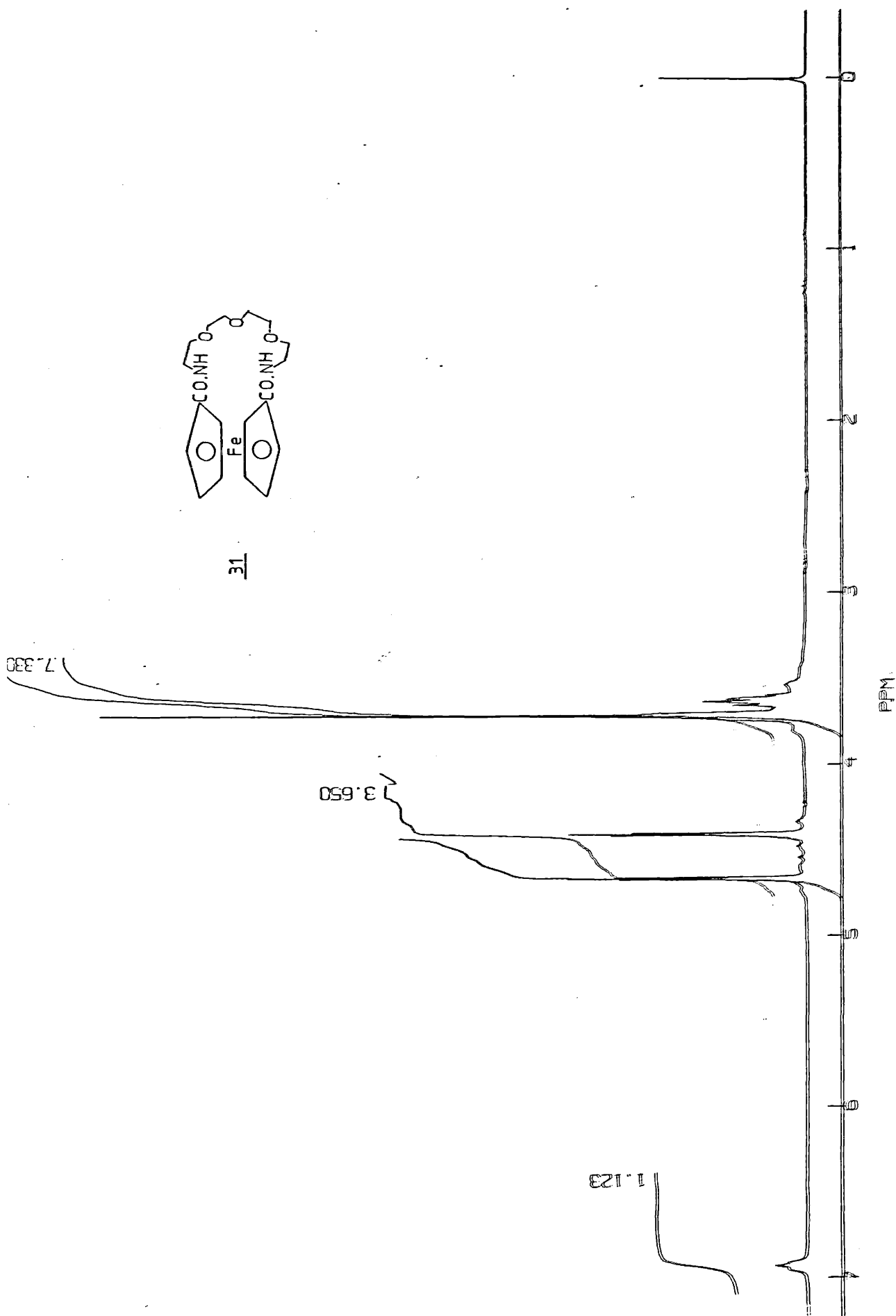
31



$^1\text{H}$  n.m.r. of (31) @ 250 MHz ( $\text{CDCl}_3$ )



31



(monomer) (41). This is evident since, on contrast to (38) and (41) only two sets of non-equivalent protons are seen in the cyclopentadienyl rings. The fact that  $H_2$  is equivalent to  $H_5$ , and  $H_3$  to  $H_4$ , eliminates the possibility of each carbonyl group having a fixed configuration coplanar with the adjacent cyclopentadienyl ring. A perpendicular configuration of the carbonyl groups cannot be ruled out since the size of the bridging group will allow such a configuration. However, this static form is unlikely since there is no  $\pi$  conjugation between the carbonyl and the cyclopentadienyl ring and therefore, a favoured static form would be with the carbonyl and cyclopentadienyl ring coplanar where  $\pi$  conjugation could take place. It appears that in the metallocene[2.2]cryptands (monomer) (38)(41) the crown bridge locks the carbonyl groups and in the dimers (39)(42) the carbonyl groups are able to rotate with respect to the cyclopentadienyl rings. A variable temperature  $^1H$  n.m.r. study of (31) at  $-70^\circ C$  shows that there is no change in the cyclopentadienyl ring protons and therefore there must be rotation about the ipso cyclopentadienyl carbonyl bond.

5.2.3 Metallocene cryptands monomers5.2.3.i) Ruthenocene[2.2]cryptand (monomer) (41) and ferrocene[2.2]cryptand (monomer) (38)

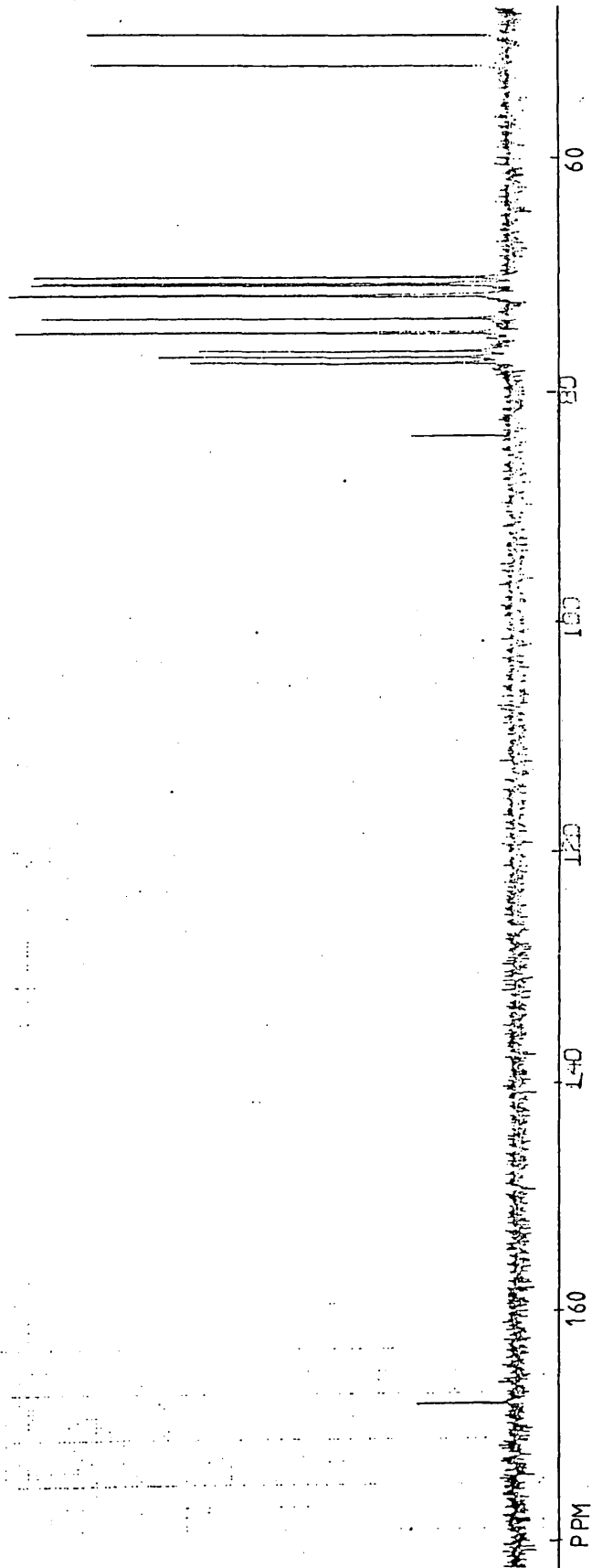
The  $^{13}\text{C}$  and  $^1\text{H}$  n.m.r. of the ruthenocene[2.2]cryptand (41) is very similar to the analogous ferrocene[2.2]cryptand (38). [Tables 5.11, 5.12]. Since the ferrocene [2.2]cryptand (38) has been fully characterised by Hall and Hammond it has been possible to carry out a similar analysis for (41).

Table 5.11

$^{13}\text{C}$  n.m.r. and  $^1\text{H}$  ( $\delta$ -values) of (38) and (41) in  $\text{CDCl}_3$   
@ 62.5 MHz ambient

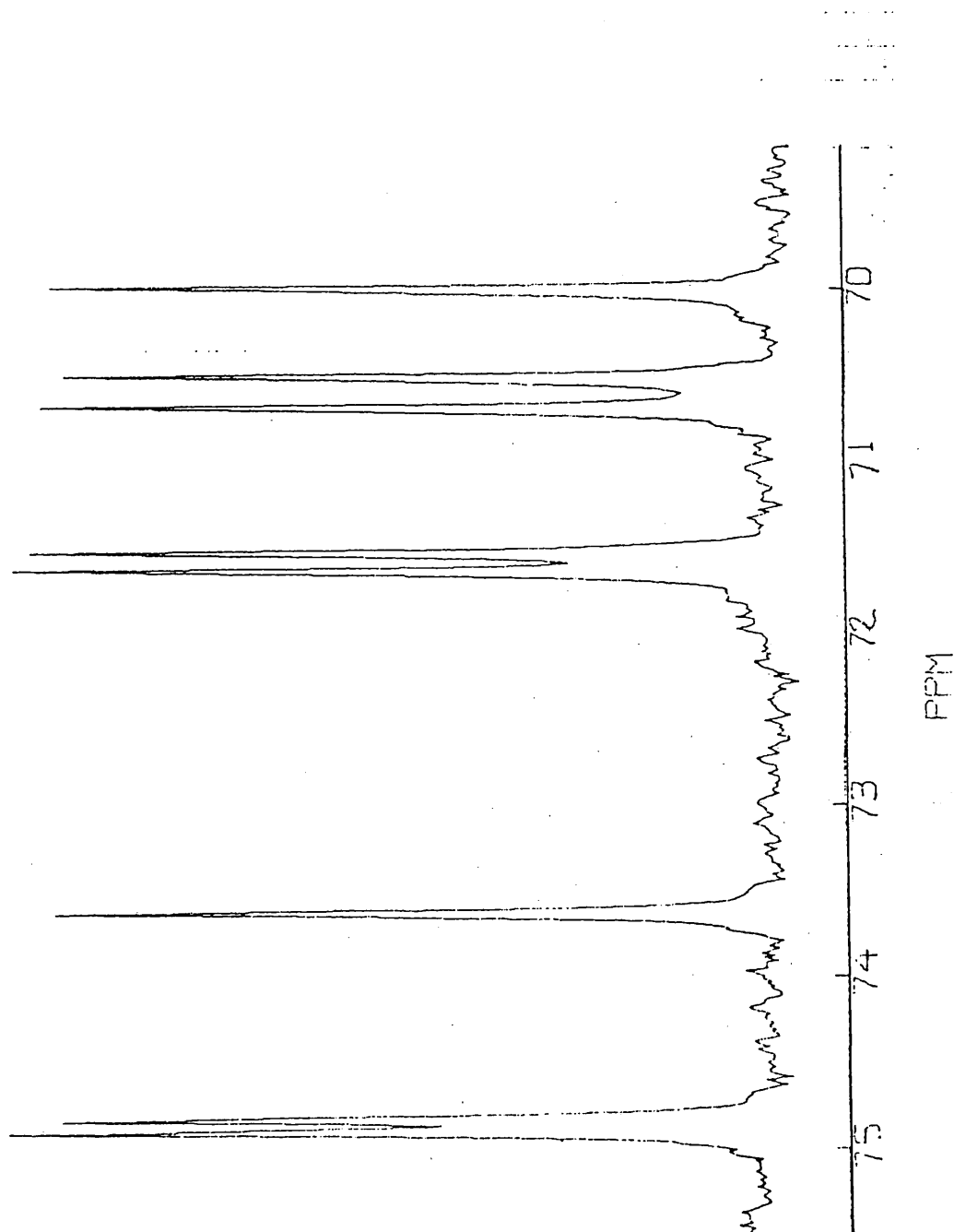
Ferrocene[2.2]cryptand(38)			Ruthenocene[2.2]cryptand (41)		
$\delta^{13}\text{C}$ ppm	Assignment	$\delta^1\text{H}$ shifts of attached protons	$\delta^{13}\text{C}$ ppm	Assignment	$\delta^1\text{H}$ shifts of attached protons
170.7	C=O		169.4	C=O	
78.5	C <sub>1'</sub>		83.8	C <sub>1'</sub>	
73.3	C <sub>2'</sub>	4.80	74.9	C <sub>2'</sub>	5.17
72.9	C <sub>3',C<sub>4'</sub></sub>	4.47/4.48	74.8	C <sub>5'</sub>	4.88
72.9	C <sub>4',C<sub>3'</sub></sub>	3.70	73.6	C <sub>4'</sub>	4.79
71.5	C <sub>4',C<sub>3'</sub></sub>	4.47/4.48	71.6	C <sub>3'</sub>	4.68
71.0	C <sub>5'</sub>	4.57	71.5	C <sub>4'/C<sub>3'</sub></sub>	3.56,3.68
70.5	C <sub>3',C<sub>4'</sub></sub>	3.70	70.7	C <sub>4'/C<sub>3'</sub></sub>	3.68
70.1	C <sub>5'</sub>	3.81,4.06	70.5	C <sub>2'</sub>	3.52,3.92
69.4	C <sub>2'</sub>	3.51,4.12	70.0	C <sub>5'</sub>	3.72,3.79
51.5	C <sub>6'</sub>	3.25,4.15	51.4	C <sub>6'</sub>	3.50,4.17
50.1	C <sub>1'</sub>	2.92,4.27	48.8	C <sub>1'</sub>	2.95,4.26

$^{13}\text{C}$  n.m.r. of ruthenocene[2.2]cryptand (monomer) @ 62.5 MHz ( $\text{CDCl}_3$ )



$^{13}\text{C}$  n.m.r. expansion of ruthenocene[2.2]cryptand (monomer) @ 62.5 MHz ( $\text{CDCl}_3$ )

EXPANSION AT 25 HZ/CM





$^{13}\text{C}$  n.m.r. of ferrocene[2.2]cryptand (monomer) @ 62.5 MHz ( $\text{CDCl}_3$ )

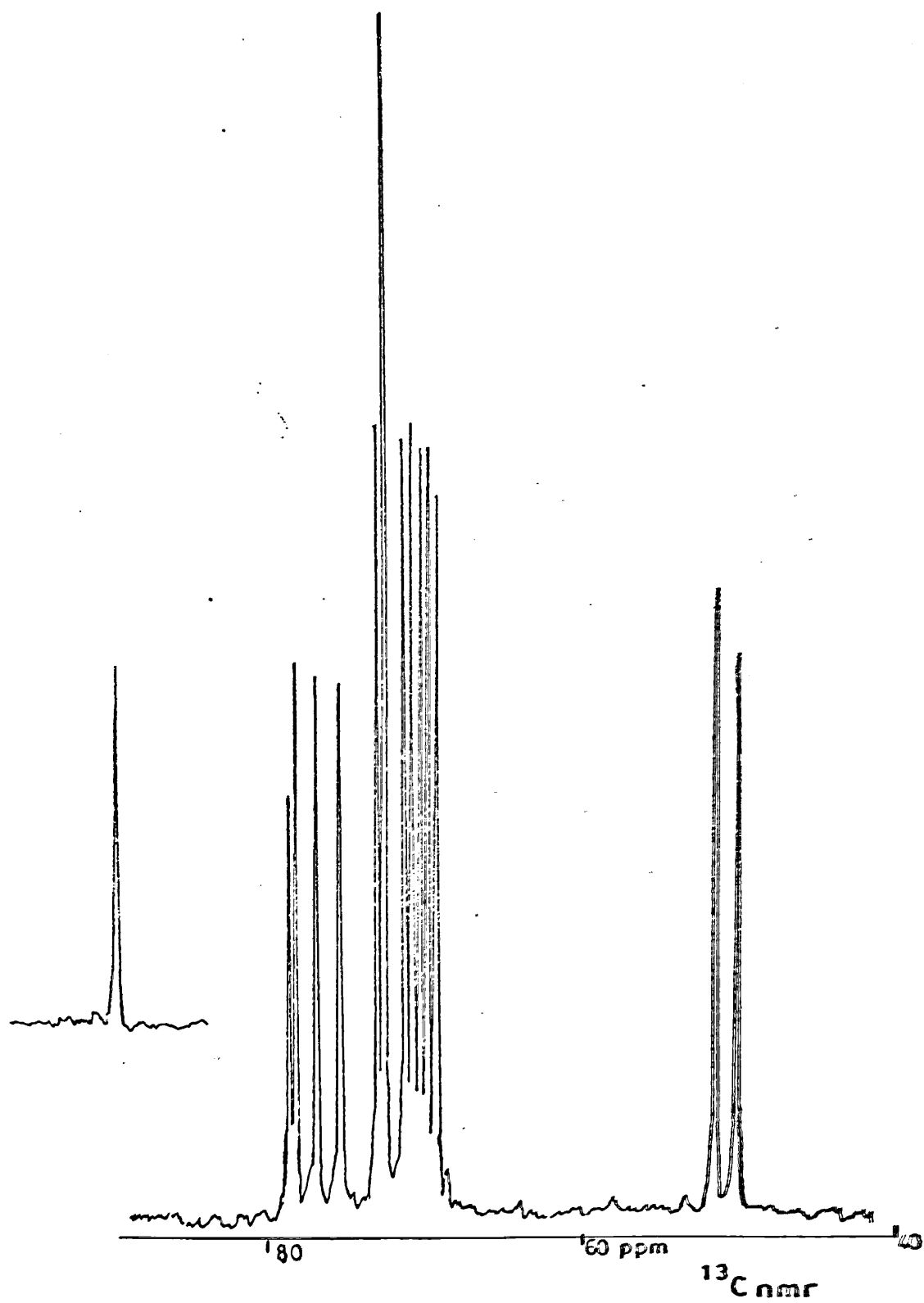
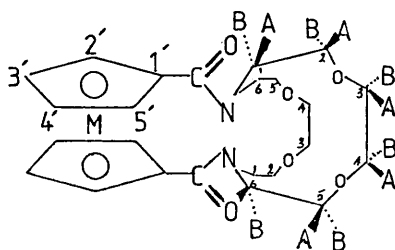


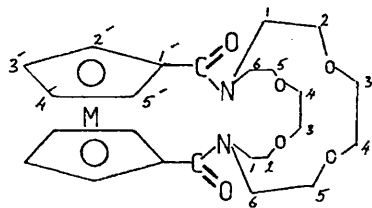
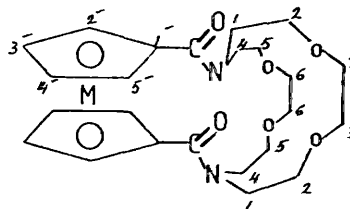
Diagram 5.12

M = Fe 38 or Ru 41

The  $^{13}\text{C}$  n.m.r. spectra of (38) and (41) each show twelve different signals; five cyclopentadienyl, one carbonyl, four different carbons attached to oxygen and two different carbons attached to nitrogen. As there are twenty-four carbon atoms in the structure each signal must represent two equivalent carbon atoms. From this it can be seen that there is some rigidity in the structure since free rotation about the two carbonyl groups, as observed in amidoferrocenes [Section 5.2.1.] would mean equivalence of signals and therefore fewer than twelve non-equivalent carbons. There must be an element of symmetry with the molecules since total assymetry would lead to twenty-four non-equivalent carbons. There are two possible configurations of (38) and (41) which are consistent with the n.m.r. data [Diagram 5.13].

Diagram 5.13

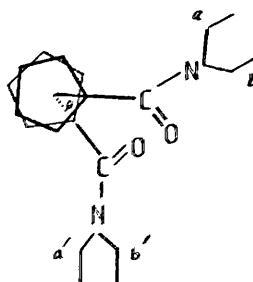
M = Fe or Ru

6869

Both have carbonyl groups coplanar with the cyclopentadienyl rings since this conformation allows maximum conjugation. However, in (68) the carbonyls are cis and in (69) they are trans. In (68) the two bridges of the diaza-crown ether unit each contain the same six, non-equivalent carbons and, as shown in (70), the  $C_{2v}$  symmetry and hence the carbon and proton equivalences are retained whatever the angle of twist between the two rings. In (69) the  $^{13}C$  and  $^1H$  n.m.r. are only satisfied when the cyclopentadienyl rings and the amide groups are eclipsed and the two bridges of the diaza-crown ether unit contain six different pairs of equivalent carbons.

Diagram 5.14

( $\theta$  = Twist angle)

70

The eclipsed configurations (69) is energetically unfavourable due to the parallel dipoles of the carbonyl groups. This interaction can be decreased by twisting the cyclopentadienyl rings but, the plane of symmetry in the molecule is lost. Therefore 1 is not equivalent to 1' and 6 to 6'. The carbon equivalences are lost and would therefore give a more complex spectra than is observed for (41) and (38)\* This does not preclude (41) and (38) from having cis carbonyl groups specifically in an eclipsed conformation, but the configuration of (41) and (38) with trans carbonyls and an indeterminate angle of twist offers a better description. Further support for this conclusion comes from theoretical calculations<sup>154</sup> and other studies<sup>155</sup> of acylferrocenes which have shown that the trans configuration of the carbonyl groups is preferred.

The <sup>1</sup>H n.m.r. spectrum of (41) and (38) has been recorded at 90 and 250 MHz. The assignments of the protons could not be made by chemical shifts alone, so they were established by using <sup>13</sup>C and <sup>1</sup>H heteronuclear and homonuclear decoupling techniques [Table 5.12]. Further evidence for the trans configuration of the carbonyl group comes from the fact that the eight cyclopentadienyl protons, eight protons  $\alpha$  to nitrogen and eight protons  $\beta$  to nitrogen are each found as four pairs of equivalent protons.

---

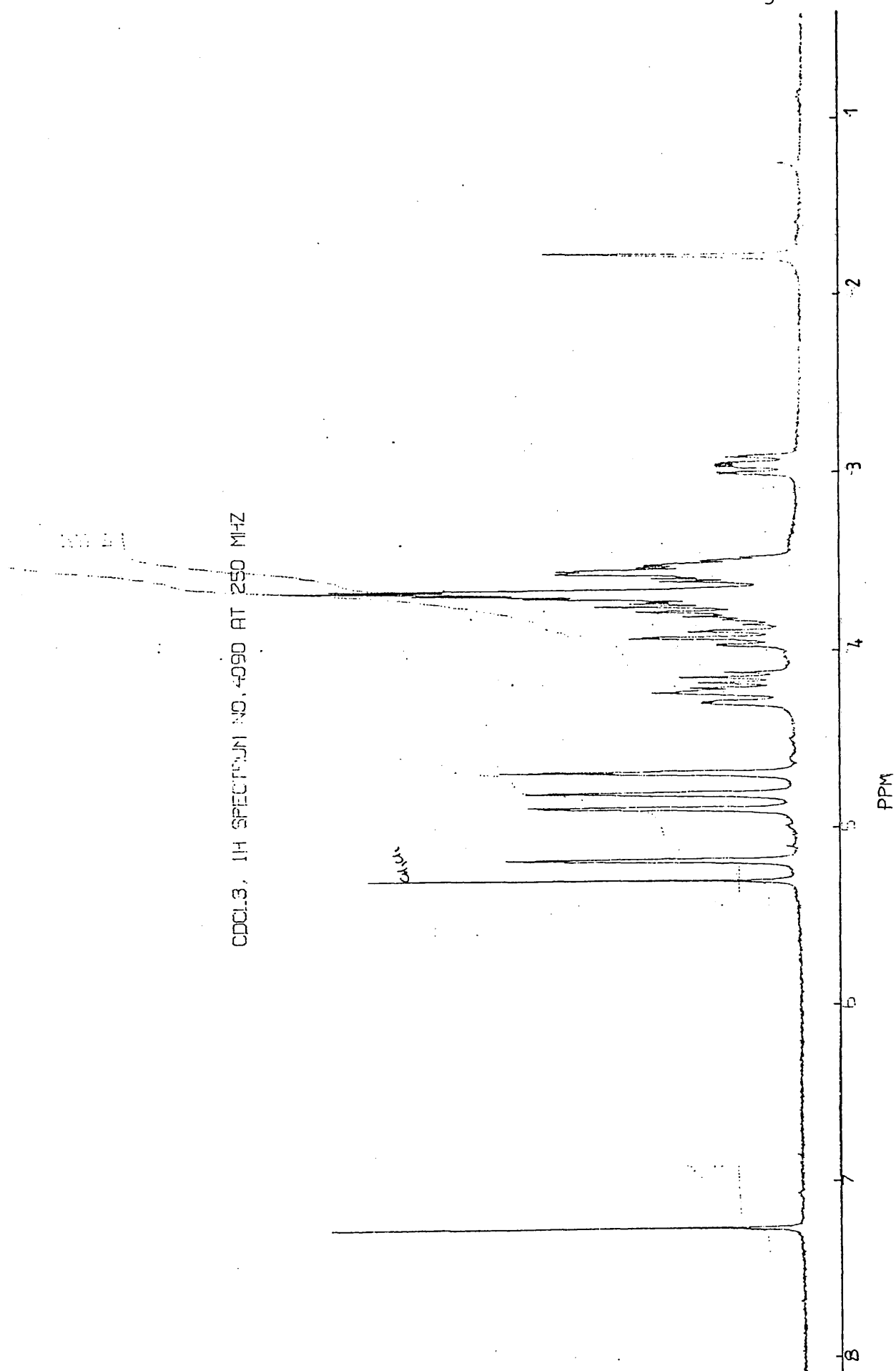
\*However, of course, rapid oscillation between two staggered forms through the eclipsed form would lead to a "time-averaged" spectrum of the eclipsed form.

Table 5.12

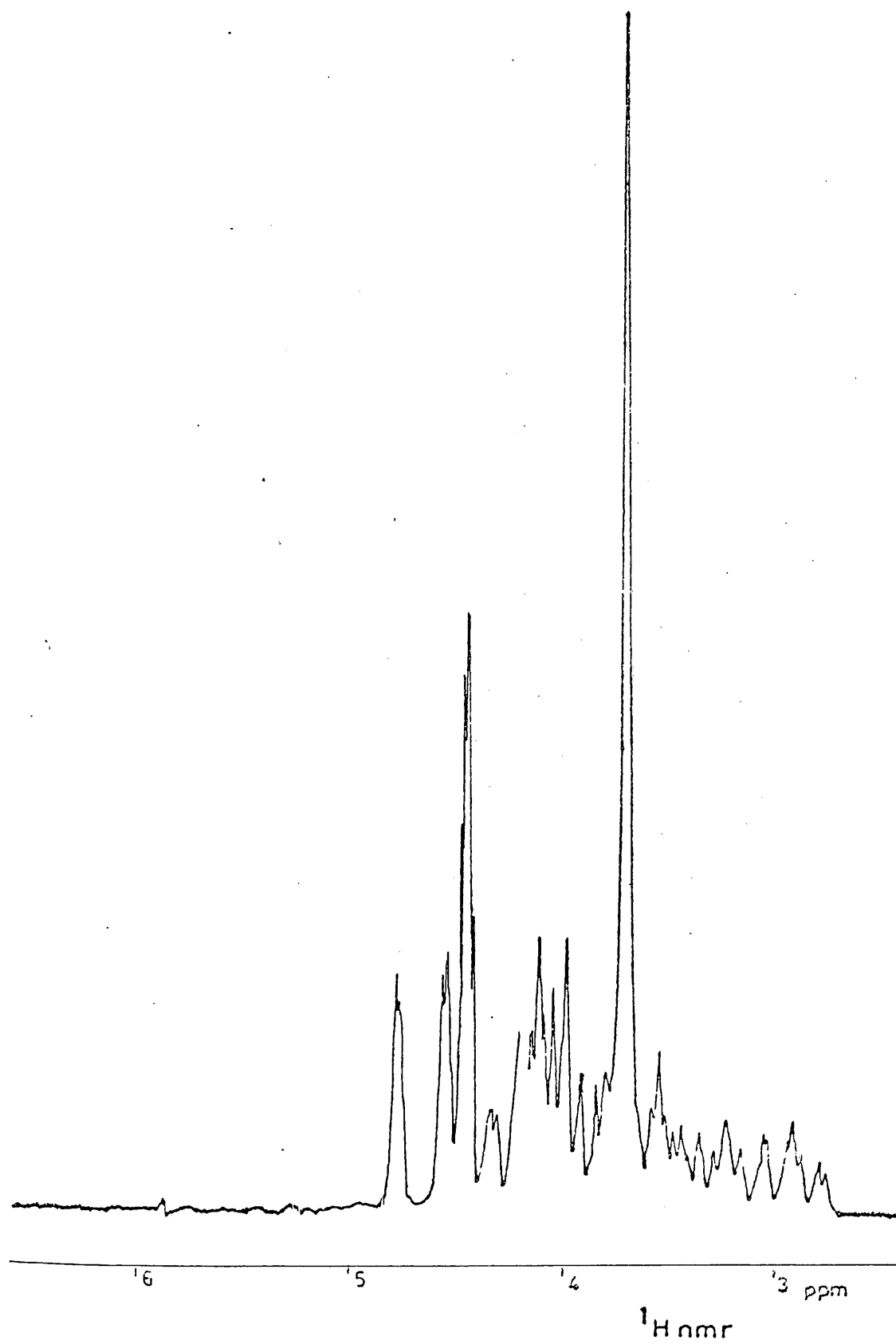
 $^1\text{H}$  n.m.r. of (38) and (41) in  $\text{CDCl}_3$  @ 250 MHz ambient. [Diagram 5.12]

Ferrocene[2.2]cryptand (38)				Ruthenocene[2.2]cryptand (41)			
ppm	Inter	Assignment	J.Hz	ppm	Inter	Assignment	J.Hz
2.92	2	1A	1B 14.1,2A 2.9,2B 10.3	2.95	2	1A	1B 14.3,2A 2.2,2B 9.6
3.25	2	6A	6B 14.7,5A 5.0,5B 8.2	3.50	2	6A	6B 15.1,5A 5.0,5B 4.4
3.51	2	2A	2B 10.0,1B 3.2	3.53	2	2A	2B 2.2,1B 4.0,2B 9.5
3.70	8	3A 3B 4A 4B		3.68	8	3A 3B,4A 4B	
3.81	2	5A	5B 9.7,6B 8.2	3.72	2	5A	6A 5.9,6B 7.7,5B 10.7
4.06	2	5B	6B 6.5,	3.79	2	5B	6A 4.4,6B 6.6,5A 10.7
4.12	2	2B	1A 10.3	3.92	2	2B	1A 9.6,2B 1.8,2A 9.6
4.15	2	6B		4.17	2	6B	6A 15.1,5A 7.7,5B 6.6
4.27	2	1B		4.26	2	1B	1A 14.3,2A 4.0,2B 1.8
4.47t	2	4'		4.68t	2	4'	
4.48T	2	3'		4.79t	2	3'	
4.57t	2	5'		4.88t	2	5'	
4.80t	2	2'		5.17t	2	2'	

$^1\text{H}$  n.m.r. of ruthenocene[2.2]cryptand (monomer) @ 250 MHz ( $\text{CDCl}_3$ )



$^1\text{H}$  n.m.r. of ferrocene[2.2]cryptand (monomer) @ 250 MHz ( $\text{CDCl}_3$ )



Selective heteronuclear decoupling experiments were performed on the methylene protons adjacent to nitrogen to see which were geminal, e.g. (41). Heteronuclear decoupling at either 2.95 ppm or 4.26 ppm causes collapse of the  $^{13}\text{C}$  n.m.r. spectrum at 48.8 ppm  $\text{C}_1$  from a triplet to a doublet thus identifying a geminal pair of protons and its associated carbon atom. Similar effects were seen for the protons which are attached to the carbons which resonate at 51.4 ppm  $\text{C}_6$ . It was not clear from the chemical shifts which of the pair  $\text{C}_1$  or  $\text{C}_6$  is adjacent to the group and only by reference to earlier reports on dialkylamides<sup>156</sup> (di-isopropylamides)<sup>157</sup> was an assignment possible. From these studies it would seem that the methylene carbon cis to the carbonyl group has the higher field  $^{13}\text{C}$  n.m.r. absorption i.e. ( $\text{C}_1$  48.8 ppm) and the greater disparity between the shifts of the geminal protons (1A 2.95 ppm; 1B 4.26 ppm). Thus the  $\text{C}_6$  (51.4 ppm) is trans to the carbonyl group with its protons at 3.50 ppm and 4.17 ppm. Given the shielding cone of the carbonyl group it would be expected that the most deshielded proton of each geminal pair will be that which lies closest to the plane of the carbonyl group. The methylene groups  $\beta$ - to nitrogen also show a similar phenomenon in their  $^{13}\text{C}$  and  $^1\text{H}$  n.m.r. spectra. It is assumed that the carbon which is cis to the carbonyl  $\text{C}_2$  resonates upfield of  $\text{C}_5$  and that proton 2B resonates downfield of 5A whereas 2A resonates upfield of 5A. No definite assignment can be made for  $\text{C}_3$  and  $\text{C}_4$  however, it seems likely that a similar trend will follow and thus



the resonance of  $C_3$  should be up-field with respect to that of  $C_4$ .

Of the four cyclopentadienyl protons  $H_2$ , and  $H_5$ , are known to be deshielded with respect to  $H_3$ , and  $H_4$ , from earlier studies on metallocenes (acetylferrocene).<sup>158</sup> In (38) and (41) where the configuration of the carbonyl is fixed with respect to the cyclopentadienyl ring,  $H_2$ , is expected to resonate downfield from  $H_5$ , due to the closer spatial proximity of the carbonyl group.<sup>159</sup> Selective irradiation of  $H_2$ , collapses  $H_4$ , to a triplet and  $H_3$ , to a doublet of doublets and hence allows assignment of  $H_3$ , and  $H_4$ .

A crystal structure analysis by X-ray diffraction was attempted to determine the absolute structure of (41). Crystals of (41) were grown by solute diffusion using n-pentane and dichloromethane. The initial rotation photographs were taken using a Weissenberg camera. These gave a clear diffraction pattern which suggested that a suitable crystal had been selected and space-group determinations were made [Table 5.13]. A data profile

Table 5.13

<u>Cell Parameters</u>			
$\text{\AA}$	9.6998	20.7284	26.4535
Degree	89.90°	89.96°	90.07°
Niggli values	94.0871	429.666	699.7861
Volume	5318.7930 $\text{\AA}^3$ - 8 molecules per unit cell		
Orthorombic crystal			

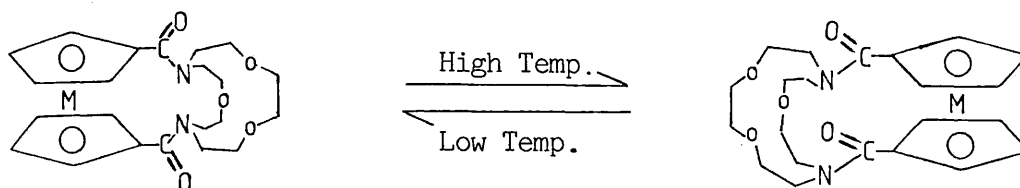
using the Precession method for heavy-atoms was collected over a period of twenty-four hours, however due to a fault in the computer program the data profile had no access and was therefore useless. It was also noticed that the crystals changed colour from pale clear yellow to an opaque yellow/white. This was probably due to the loss of solvent from the cryptand. It is hoped that further attempts at data collection will be carried out on (41) and (38) in sealed capillary tubes.

5.2.3.ii) Metallocene cryptands (monomers)

The  $^1\text{H}$  and  $^{13}\text{C}$  n.m.r. spectra of the other metallocene cryptands (monomers) [Scheme 5.2] are unlike those of the rigid ruthenocene and ferrocene[2.2]cryptand [(41) and (38)]. The  $^1\text{H}$  and  $^{13}\text{C}$  n.m.r. spectra [Tables 5.14 and 5.15] are broadened and complex at room temperature and many resonances overlap. In Section 5.2.4. some dynamic phenomenon associated with these spectra are discussed and rotational energy barriers have been determined by variable temperature n.m.r. The assignments of the spectra at room temperature have been made on the basis of the earlier analysis of (41) and (38) and on the results of the variable temperature n.m.r. investigation.

In the case of unsymmetrical metallocene cryptands one would expect a more complex spectrum to result from the unsymmetrical cryptand bridge. This is best seen in the ruthenocene and ferrocene[2.1]cryptands [(82) and (80)] as there is little overlap of  $^{13}\text{C}$  resonances and little broadening due to dynamic effects of the  $^{13}\text{C}$  n.m.r. spectra at room temperature. On investigation, the structure of (80) and (82) offers two time-averaged forms, [Diagram 5.15] cis and trans, which have sharply contrasting n.m.r. spectra. Thus the preferred structure is easily determined at room temperature. From Table 5.15 it can be seen that there are 22 non-equivalent  $^{13}\text{C}$  resonances for (80), (two carbonyls, ten cyclopentadienyls, six carbons attached to oxygen and four carbons attached

Diagram 5.15

M = Fe (80) or Ru (82)Trans.22 non-equivalent  $^{13}\text{C}$  resonances28 non-equivalent  $^1\text{H}$  resonancesCis11 non-equivalent  $^{13}\text{C}$  resonances14 non-equivalent  $^1\text{H}$  resonances

to nitrogen) and 20 non-equivalent  $^{13}\text{C}$  resonances for (82), two of which have not been observed due to overlap, (two carbonyls, a total of 14 cyclopentadienyls and carbons attached to oxygen, four carbons attached to nitrogen). The  $^1\text{H}$  n.m.r. spectra of (80) and (82) [Table 5.14] are broad and there is much equivalence and only four resonances are seen. (Two cyclopentadienyl and two methylene peaks). From the  $^{13}\text{C}$  n.m.r. it can be concluded that (80) and (82) are in a trans configuration at room temperature. It should be noted that this is in agreement with the proposed structure of (41) and (38) and gives further evidence for the favourable trans configuration. In the other unsymmetrical cryptands there is considerable overlap and broadening in the n.m.r. spectra at room temperature thus a general assignment has been made as in the symmetrical cases.

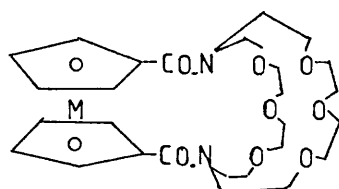
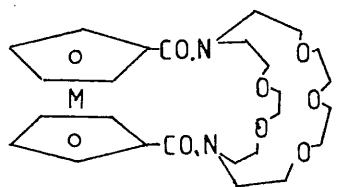
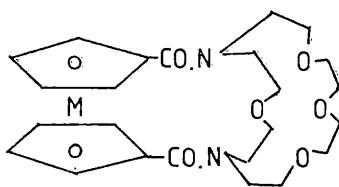
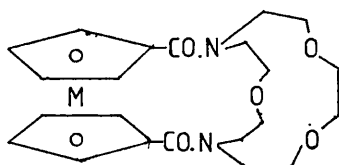
Scheme 5.2. Metallocene cryptands (monomers)M = Ru (72)M = Fe (70)M = Ru (76)M = Fe (74)M = Ru (78)M = Ru (82)M = Fe (80)

Table 5.14

<sup>1</sup>H n.m.r. of metallocene cryptands (monomers), CDCl<sub>3</sub>, ambient 250 MHz

Assignment	Fe.3.3(70)		Ru.3.3(72)		Fe.3.2(74)		Ru.3.2.(76)		Ru.2.1(82)		Ru.3.1(78)	
	δ	int	δ	int	δ	int	δ	int	δ*	int	δ*	int
cyclopentadienyl	4.92tb	4	5.34 b 5.24b 5.12t	1 1 2	4.89b 4.78b 4.68b	1 1 2	5.24b 5.18b 5.14b 5.08b	1 1 1 1	5.10b	4	5.01b	4
cyclopentadienyl	4.58tb	2	5.78t	2	4.39b 4.32b	3	4.76b	4	4.70b	4	4.73b	4
	4.24tb	2	5.70t	2	4.09b	1						
OCH <sub>2</sub>	4.14-4.02c	32	4.30-4.06c 3.80-3.50c 3.16-3.06c	32 32 32	4.2-3.9b	28	4.24-4.14b 3.8-3.46b	28 28	3.64b 3.08b	20	3.81b 3.63b	24
N.CH <sub>2</sub>	3.88-3.62c											
Total		40		40		36		36		28		32

\*90 MHz

Table 5.15

 $^{13}\text{C}$  n.m.r. of metallocene cryptands (monomers)  $\text{CDCl}_3$  ambient 62.5 MHz

	Fe 3.3(70)	Fe 3.2(74)	Ru 3.2(76)	Ru 3.1(78)	Ru 2.1(82)	Fe 2.1(80)
Assignment	$\delta$	$\delta$	$\delta^*$	$\delta$	$\delta$	$\delta$
C=O	170.5	170.9 170.1	168.69	i.r.	169.2 168.4	173.7 171.3
C <sub>1'</sub>	77.8	83.7 75.8	38.1		83.6b	78.9 78.8 78.1 73.8
C <sub>2',5'</sub>	74.9	72.9	74.5	74.7b	74.7 73.6	73.5 72.7
C <sub>3',4'</sub>	72.9	72.1 71.8 71.2	73.7	74.0b		72.3 71.0 70.6 70.4
OCH <sub>2</sub>	71.3b 71.0b 70.1b	OCH <sub>2</sub> and cyclopentadienyl.c. 70.7 70.3 70.1 69.8 69.0 68.6 68.4	72.9b 71.8b 70.9b 70.6b 69.8b	71.1b 70.8b 70.0b	OCH <sub>2</sub> and cyclopentadienyl.c. 71.8 70.9 70.8 70.6 69.9 69.6 69.4 69.2 68.4 67.6 64.0	70.2 70.1 69.8 69.5 68.9 68.2
NCH <sub>2</sub>	50.4 48.9	51.5s 49.7s 48.3s 47.1s	49.9b	50.8c 49.7c	51.6 49.6 48.8 48.0	52.3 51.3 50.9 45.4

\*22.5 MHz

5.2.3.iii) Metallocene cryptands (dimers)

The  $^1\text{H}$  and  $^{13}\text{C}$  n.m.r. spectra [Table 5.16, 5.17] of the metallocene cryptands (dimers) [Scheme 5.3] are very broad and complex at room temperature and again many resonances are rendered equivalent by the rotational phenomena associated with the two amide groups. In most cases a general assignment has been made at room temperature, as the cryptands are nearing the coalescence temperature point ( $T_c$ ). A more detailed explanation of the n.m.r. spectra can be seen in Section 5.2.4. on dynamic n.m.r. as at low temperatures where the rotational process is slow the spectra become clearer.



Scheme 5.3. Metallocene cryptands (dimers)

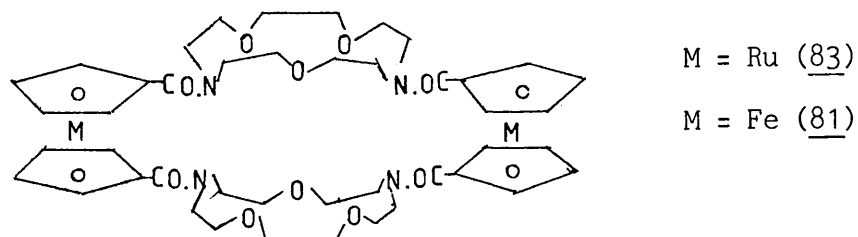
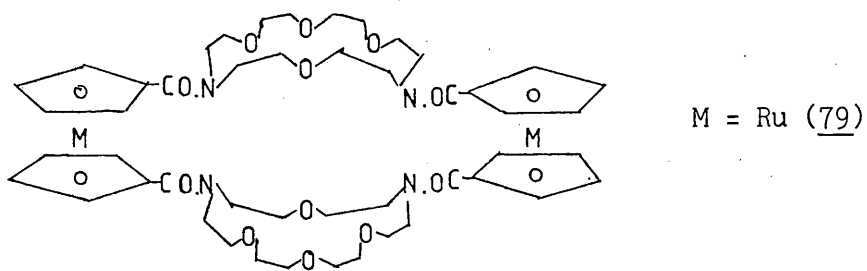
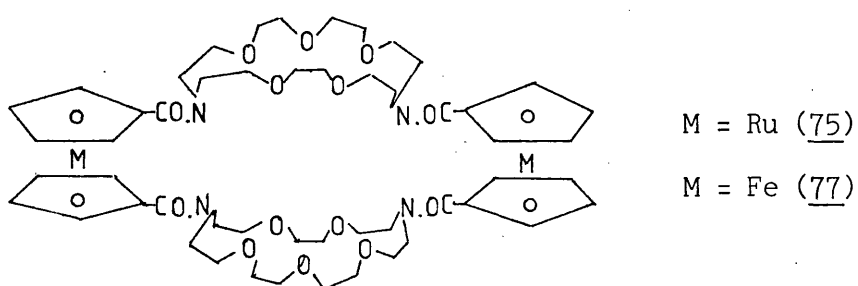
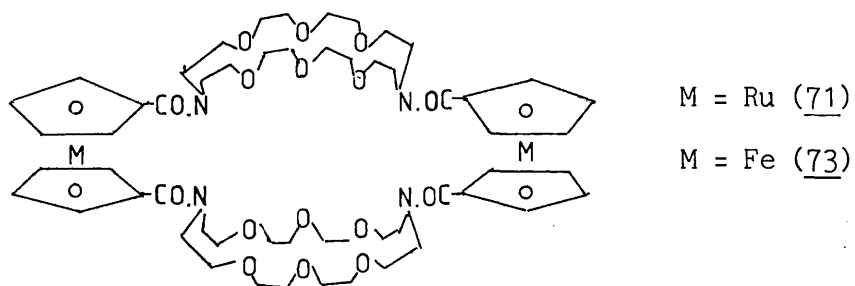


Table 5.16

<sup>1</sup>H n.m.r. of metallocene cryptands (dimers). CDCl<sub>3</sub> 250 MHz ambient

Assignment	Fe 2.2.(39)		Ru 2.2.(42)		Fe 3.3.(71)		Ru 3.3.(73)		Fe 3.2.(75)		Ru 3.2.(77)		Ru 2.1(83)		Ru 3.1(79)	
	δ*	int	δ	int	δ	int	δ	int	δ	int	δ	int	δ*	int	δ	int
cyclopentadienyl	4.63t	8	4.95t	8	4.72t	8	5.16b	4	4.69t	8	5.28b 5.24b 5.08b 5.04b 4.98b 4.70b 4.66b 4.55b	1 1 1 1 1 1 1 1	5.1b	8	5.07b	8
cyclopentadienyl	4.35t	8	4.66t	8	4.38t	8	4.76b	4	4.39t	8	4.70b	4	4.7b	8	4.73b	8
OCH <sub>2</sub>							4.18b		3.72b							
NCH <sub>2</sub>	3.4-4.0b	48	3.6-3.8 <sup>b</sup>	48	3.85b 3.66b 3.65b 3.62b	64	3.8-3.5c	64	3.66b	56	3.62b	56	4.0-3.7b	40	3.63b	48
Total		68		68		80		80		72		72		56		68

\*90 MHz

Table 5.17

 $^{13}\text{C}$  n.m.r. of metallocene cryptands (dimers)  $\text{CDCl}_3$  ambient 62.5 MHz

	Fe 2.2(39)	Ru 2.2(42)	Fe 3.3(71)	Fe 3.2(75)	Ru 3.2(77)	Ru 2.1(83)	Ru 3.1(79)
Assignment	$\delta$	$\delta$	$\delta$	$\delta$	$\delta^+$	$\delta$	$\delta$
C=O	170.0	169.6	170.0	170.0	169.7	169.5 169.0	169.0
C <sub>1'</sub>	79.6	81.5	79.8	79.9 <sup>b</sup> 79.4 <sup>b</sup>	88.1b	82.9 81.4 82.9 <sup>b</sup>	88.3 <sup>b</sup> 82.9 <sup>b</sup>
C <sub>2'5'</sub>	73.9	74.3	72.3	72.4b	74.7 <sup>b</sup>	74.7 74.2	74.6 <sup>b</sup>
C <sub>3'4'</sub>	70.3	73.8	71.9		74.4 <sup>b</sup>	73.6 72.9	73.9 <sup>b</sup>
OCH <sub>2</sub>	72.1		70.8	71.6	70.9b	72.0 <sup>b</sup> 71.3 <sup>b</sup>	73.0 72.7 71.9 71.8
	70.0	70.8b	70.7	70.6	70.7b	70.5b	71.2 71.0
	69.9	70.0b	70.0	70.2	69.8b	69.1b	70.7 70.0b
	67.0	69.8b	69.7	69.4		51.5 50.2 48.6	50.9 <sup>b</sup> 49.6 <sup>b</sup>
NCH <sub>2</sub>	49.1	49.9	49.7	49.6	CD <sub>3</sub> OD		
	47.0	48.0	47.7	47.6	region	47.1	48.7b

\*22.5 MHz

+ (plus CD<sub>3</sub>OD)

5.2.4 Dynamic n.m.r.5.2.4.i) Introduction

The temperature dependence of n.m.r. spectra can be used to obtain information about energy barriers for certain rearrangement processes.<sup>55,56,57,58</sup> From a study of the temperature dependence of the n.m.r. spectrum of the compound the rate constant  $K_c$  for the rearrangement can be obtained at a temperature  $T_c$ .

Consider, for example, the spectrum of an N,N-dimethylamide in which the two methyl groups are not in identical environments. When rotation about the CO-N bond is slow there will be two sharp singlets in the p.m.r. spectrum (each of relative area equal to three protons) and two sharp singlets in the c.m.r. spectrum consistent with the non-equivalence of the two methyl groups. As the temperature at which the spectrum is being recorded is raised the rate of rotation will increase until at higher temperatures only one sharp singlet will be seen at a frequency half way between those of the two original signals. Here both methyl groups will be rapidly interchanging on the p.m.r. or c.m.r. time scale and will thus appear to be in identical environments. If the sample temperature is slowly raised from the "frozen" condition the peak will initially broaden and then merge into one broad signal which eventually sharpens up. The point at which merging occurs is known as the coalescence temperature ( $T_c$ ) and here equation 5.1 holds.

Equation 5.1

$$K_c = \pi \cdot \Delta\nu \cdot \sqrt{2}$$

$\Delta\nu$  = the frequency of separation of the two exchanging signals in the "frozen" condition Hz.

From transition-state theory equation 5.2 also holds and combining these two expressions leads to equation 5.3 for which the free energy of activation ( $G^\ddagger$ ) for the rearrangement process can be calculated.

Equation 5.2

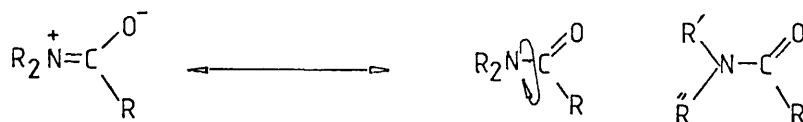
$$K_c = (K \cdot T_c / h) \exp(-\Delta G^\ddagger / R \cdot T_c)$$

Equation 5.3

$$\Delta G^\ddagger = R \cdot T_c \log_e (K \cdot T_c \cdot \sqrt{2} / \pi \cdot h \cdot \Delta\nu)$$

$h$  = Plank's constant     $K$  = Boltzmann's constant     $T_c$  = °K.

Restricted rotation about the carbon-nitrogen bond in amides is the classical example<sup>160,56</sup> of a rate process that can be studied by dynamic n.m.r. Resonance theory describes the electronic structure of amides by a hybrid [Diagram 5.16] suggesting a certain amount of double bond character for the carbon nitrogen bond and therefore an increase of the rotational barrier over than in simple single bonds, e.g. amines ( $\Delta G^\ddagger$  for  $\text{Me}_3\text{N}$  7.5 kcal mol<sup>-1</sup>).<sup>161</sup>

Diagram 5.16

Since  $R'$  and  $R''$  reside in different magnetic environments ( $R'$  being more shielded than  $R''$ ) in the "frozen" structure and become time-averaged on rapid rotation it is possible to calculate the free energy of activation ( $\Delta G^\ddagger$ ) for the rotation if the coalescence temperature;  $T_c = ^\circ K$ , and the frequency of separation of the two exchanging signals in the "frozen" condition; ( $\Delta\nu = H_3$ ) are known.

In the case of the metallocene amide derivatives there is another rotation barrier which can be investigated by n.m.r. spectroscopy. The rotation barrier between the cyclopentadienyl ring and the carbonyl group. When this process is slow on the n.m.r. time scale, the ortho protons and carbons on the metallocene ring become non-equivalent. It has sometimes proved possible to measure both rotational barriers. It would be expected that these two energy barriers for the rotational processes should be dependent on each other. For, increased interaction between the nitrogen lone pairs and the carbonyl group should reduce the electron donation of the carbonyl carbon atom and hence lower the degree of conjugation with the cyclopentadienyl ring.

5.2.4.ii) Discussion(a) 'Simple' metallocene amides

A series of simple ferrocene and ruthenocene amides were prepared and variable temperature n.m.r. [Tables 5.20-5.30] were run in order to investigate the dynamic processes about the bonds of the carbonyl group and thus calculate  $\Delta G^\ddagger$  the free energy of activation for these rotational processes [Table 5.18]. The second objective was to see if these values would be of the same order of magnitude as the macrocyclic metallocene amides and thus show that they have a similar dynamic phenomena.

There are a number of factors which may influence the free energy of rotation, some of which may be discounted on close examination of Table 5.18:-

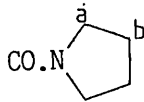
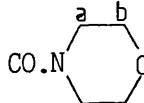
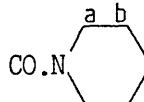
(i) In disubstituted metallocenes the substituent on the upper cyclopentadienyl ring may sterically hinder the rotation of the amide on the lower ring since the cyclopentadienyl rings are separated by approximately 3.32 Å (ferrocene) or 3.68 Å (ruthenocene). This is easily discounted by comparing the values of N,N-dimethylamido-ferrocene and 1,1' bis(N,N-dimethylamido) ferrocene since both  $\Delta G^\ddagger$  values are 14.3 kcal mol<sup>-1</sup>, also N,N-diethylamido ferrocene and 1,1' bis (N,N-diethylamido)ferrocene since both values are again the same ( $\Delta G^\ddagger = 14.5$  kcal mol<sup>-1</sup>). Such a result is not surprising since the cyclopentadienyl rings can freely rotate with respect to each other (ferrocene  $\Delta G^\ddagger \sim 0.9$  kcal mol<sup>-1</sup>, ruthenocene  $\Delta G^\ddagger \sim 1.8-4.5$  kcal mol<sup>-1</sup>).

(ii) Other factors which may influence the free energy of rotation for these are, the size and charge density of the transition metal ions. The size and charge density seem to be minor factors as a rotation barrier in ferrocene disubstituted amides and ruthenocene disubstituted amides seem to be similar (though ruthenocene derivatives are slightly higher).



Table 5.18

 $\Delta G^\ddagger$  values for simple metallocene amides

Amide derivative	Ferrocene		Ruthenocene
	Monosubstituted	Disubstituted	Disubstituted
$\text{CO.N}(\text{CH}_3)_2$ a 3 b	*14.34	*14.31	*14.55
$\text{CO.N}(\text{CH}_2\text{CH}_3)_2$	a. 14.50 b. 14.40	a. 14.50 b. 14.20	No splitting of signals
		a. 14.70 b. 14.80	a. 15.41
	No splitting of signals	a. 13.28	a. 13.45
		a. 13.70 b. 13.70	a. 14.29 b. 13.72

Values are kcal mol<sup>-1</sup> from <sup>13</sup>C n.m.r. - \*from <sup>1</sup>H n.m.r.

*It should be noted that these results (a,b) are not intended to imply two different coalescence processes in this case but, rather refer to different estimates to the same coalescence energy.*

Table 5.19.

 $\Delta G^\ddagger$  values for other amides

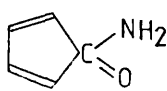
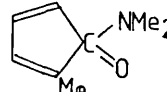
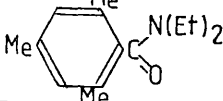
Amide	$\Delta G^\ddagger$ kcal mol <sup>-1</sup>
$\text{H.CO.N}(\text{CH}_3)_2$	20.6
$\text{CH}_3\text{CO.N}(\text{CH}_3)_2$	18-20
$\text{ArCO.N}(\text{CH}_3)_2$	16.45
	14.1
	12.2
	22.5

Table 5.20

1-N,N-dimethylamido-ferrocene (55)Variable temperature  $^1\text{H}$  n.m.r.  $\text{CDCl}_3$  ppm @ 90 MHz

Assignment	Temperature $^{\circ}\text{C}$			
	$-13^{\circ}$	$2^{\circ}$	$8^{\circ}$	$27^{\circ}$
H <sub>2,5</sub>	4.62t	4.62t	4.62t	4.62t
H <sub>3,4</sub>	4.31t	4.31t	4.30t	4.29t
Ring 2	4.23s	4.22s	4.22s	4.22s
Methyl	3.24s	3.19b	3.11b	3.10s
Methyl	3.03s	3.04b		
$T_c = 281^{\circ}\text{K}$ $\Delta\nu = 18.31 \text{ Hz}$				

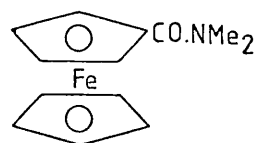
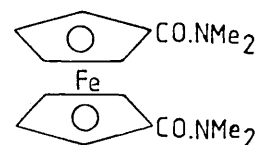


Table 5.21

1,1'-bis(N,N-dimethylamido)-ferrocene (58)Variable temperature  $^1\text{H}$  n.m.r. ( $\text{CDCl}_3$ ) 90 MHz in ppm

Assignment	Temperature $^{\circ}\text{C}$						
	$-35^{\circ}$	$-15^{\circ}$	$-8^{\circ}$	$5^{\circ}$	$28^{\circ}$	$40^{\circ}$	$60^{\circ}$
H <sub>2,5</sub>	6.95t	6.95t	6.95t	6.95t	6.95t	6.95t	6.95t
H <sub>3,4</sub>	6.58t	6.58t	6.58t	6.58t	6.58t	6.58t	6.58t
Methyl	4.76s	4.76s	4.76b	4.61bs	4.61s	4.61s	4.61s
Methyl	4.50s	4.50s	4.50b	"	"	"	"
$T_c = 278^{\circ}\text{K}$ $\Delta\nu = 14.6 \text{ Hz}$							



V.T. H n.m.r. of (55) @ 90 MHz (CDCl<sub>3</sub>)

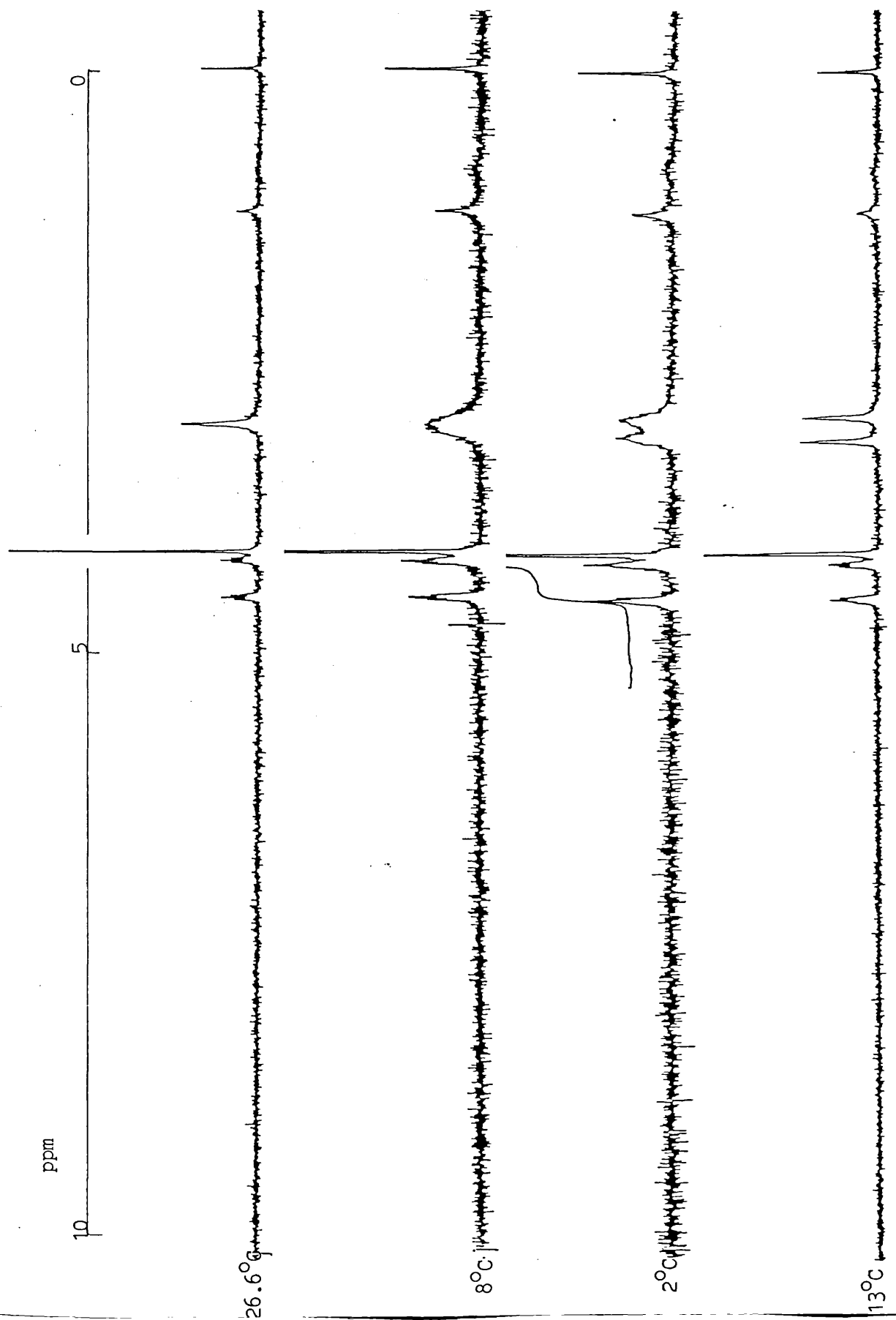


Table 5.22

1,1'-bis(N,N-dimethylamido)-ruthenocene (59)Variable temperature  $^1\text{H}$  n.m.r. ( $\text{CDCl}_3$ ) ppm @ 90 MHz

Assignment	Temperature $^{\circ}\text{C}$				
	$-145^{\circ}$	$7.5^{\circ}$	$12^{\circ}$	$13.5^{\circ}$	ambient
$\text{H}_{2,5}$	5.02t	5.02t	5.02t	5.02t	5.0t
$\text{H}_{3,4}$	4.75t	4.71t	4.69t	4.72t	4.7t
Methyl	3.22s	3.28b	3.14b	3.06b	3.02s
Methyl	2.99s	2.99b	2.99b	"	"
$T_c = 286.5^{\circ}\text{K}$ $\Delta\nu = 21 \text{ Hz}$					

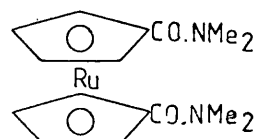
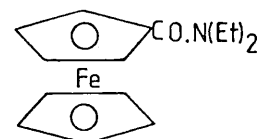


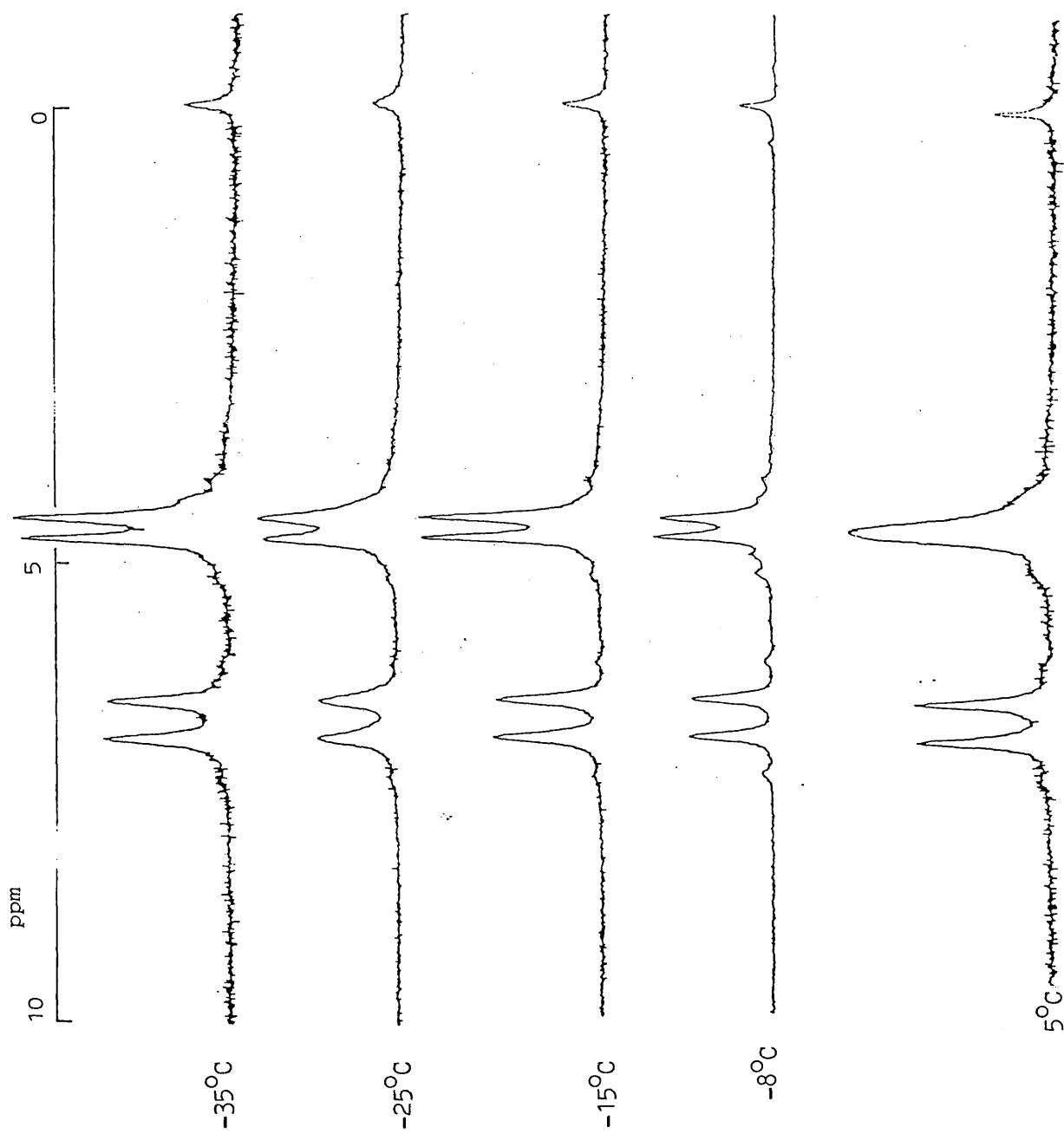
Table 5.23

1-N,N-diethylamido ferrocene (56) $^{13}\text{C}$  n.m.r. Variable Temperature  $\text{CDCl}_3$  ppm @ 22.6 MHz

Assignment	Temperature $^{\circ}\text{C}$				
	$-41^{\circ}$	$-10^{\circ}$	$-6^{\circ}$	$25^{\circ}$	$26.6^{\circ}$
$\text{C}=\text{O}$	109.6	-	-	-	170.2
ipso $\text{C}_1$	77.5	77.5	77.5		79.0
$\text{C}_{2,5}$	70.3	70.2	70.2	70.2	70.3
Ring 2	69.6B	69.6B	69.6B	69.7	69.8
$\text{C}_{3,4}$	-	-	-	69.2	69.2
$\text{NCH}_2$ a.	42.3	42.4B	42.4	41.6B	41.7B
	40.7	40.7B	40.7	"	"
$\text{CH}_3$ b.	14.8	14.8B	14.7	13.8B	13.7B
	12.6	12.7B	12.6	"	"
(a)	$T_c = 293^{\circ}\text{K}$ $\Delta\nu = 36.6 \text{ Hz}$				
(b)	$T_c = 293^{\circ}\text{K}$ $\Delta\nu = 51.3 \text{ Hz}$				



V.T.  $^1\text{H}$  n.m.r. of (58) @ 90 MHz ( $\text{CDCl}_3$ )



V.T.  $^1\text{H}$  n.m.r. of (59) @ 90 MHz ( $\text{CDCl}_3$ )

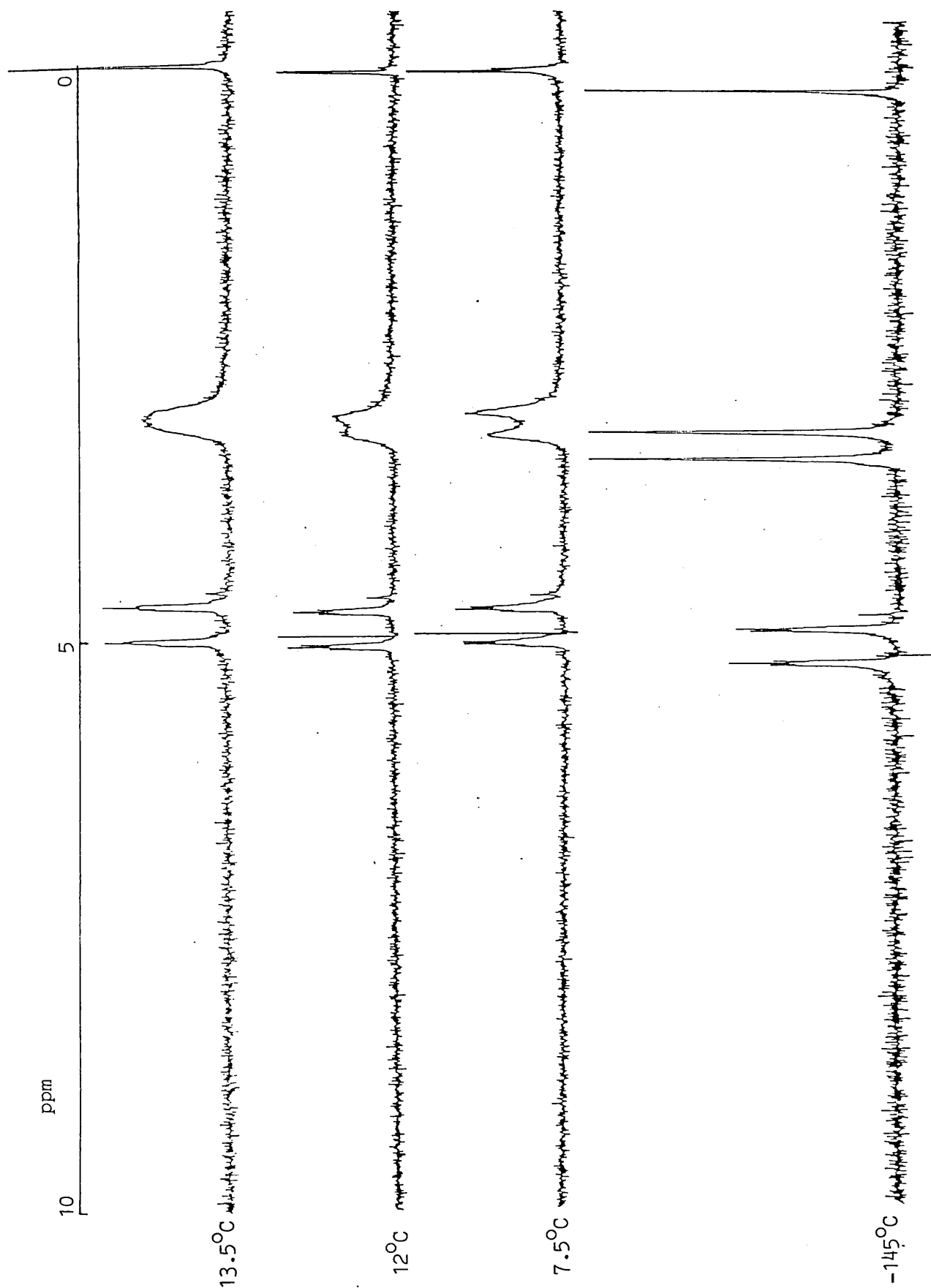
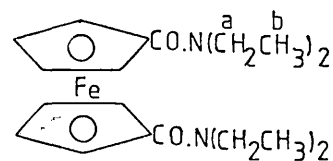


Table 5.24

1,1'-bis(N,N-diethylamido) ferrocene (60)Variable Temperature  $^{13}\text{C}$  n.m.r.  $\text{CDCl}_3$  ppm @ 22.6 MHz

Assignment	Temperature $^{\circ}\text{C}$					
	$-18^{\circ}$	$-10^{\circ}$	$7^{\circ}$	$15^{\circ}$	$20^{\circ}$	$28^{\circ}$ ambient
Carbonyl C=O	168.8	168.9	168.9	168.9	169.1	169.1
$\text{C}_1$	79.8	79.8	80.2	80.2	81.3	81.3
$\text{C}_{2,5}$	71.7	71.7	71.7	71.7	71.8	71.8
$\text{C}_{3,4}$	71.4	71.4	71.4	71.4	71.4	71.4
$\text{CH}_2$ a.	42.5s	42.5s	42.6s	42.6b	41.9b	41.8s
( $\text{CH}_2$ )	40.8s	40.8s	40.6s	40.6b		
$\text{CH}_3$ b.	14.7s	14.7s	14.7s	14.7b	13.9b	13.9s
( $\text{CH}_3$ )	12.6s	12.6s	12.7s	12.7b		
(a)	$T_c = 293^{\circ}\text{K}$	$\Delta\nu = 42.68 \text{ Hz}$				
(b)	$T_c = 293^{\circ}\text{K}$	$\Delta\nu = 47.56 \text{ Hz}$				



V.T.  $^{13}\text{C}$  n.m.r. of (60) @ 22.6 MHz ( $\text{CDCl}_3$ )

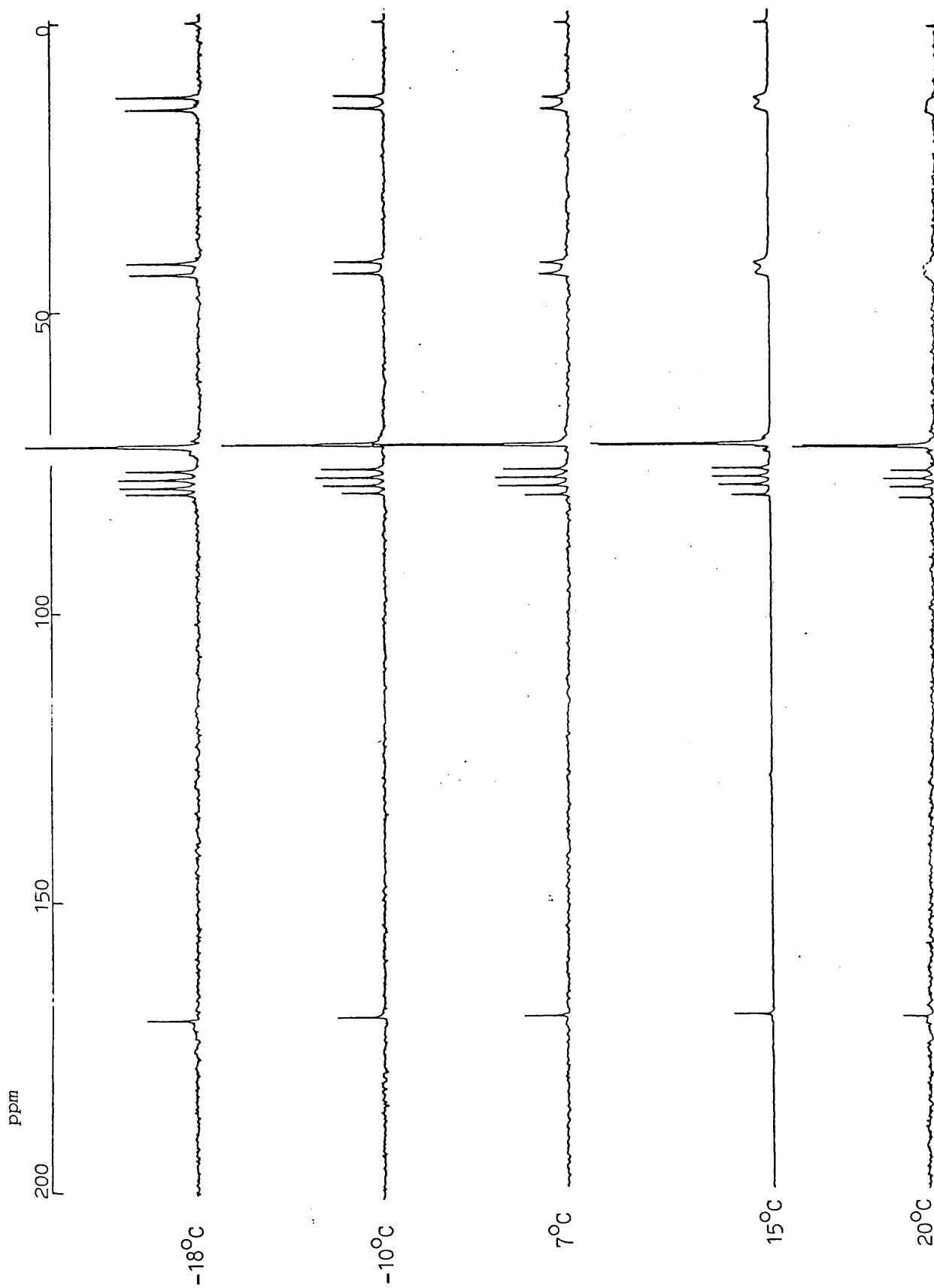


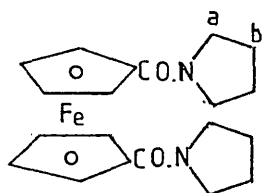


TABLE 5.25

1,1'-bis(N,N-pyrrolidine amido)ferrocene (66)

 $^{13}\text{C}$  nmr. Variable Temperature  $\text{CDCl}_3$  ppm @ 22.6 MHz

Assignment	Temperature $^{\circ}\text{C}$				
	$-18^{\circ}$	$-10^{\circ}$	$+7^{\circ}$	$20^{\circ}$	$30^{\circ}$
Carbonyl C=O	168.1	168.1	167.9	168.1	167.9
$\text{C}_1$	78.7	78.7	78.7	79.0	79.5
$\text{C}_{2,5}$			71.5b	71.7s	71.6s
$\text{C}_{3,4}$	71.5s	71.5s	71.4	71.5s	71.2s
$\text{NCH}_2$ a	48.0	48.0	48.0	48.0s	47.4s
	47.1	47.1	47.1	47.2s	
$\text{CH}_2$ b	26.5	26.5	26.5	26.8s	25.3b
	23.8	23.8	23.8	24.0s	
(a) $297^{\circ}\text{K}$	$\Delta\nu = 43.95\text{Hz}$				
(b) $301^{\circ}\text{K}$	$\Delta\nu = 46.39\text{Hz}$				



V.T.  $^{13}\text{C}$  n.m.r. of (66) @ 22.6 MHz ( $\text{CDCl}_3$ )

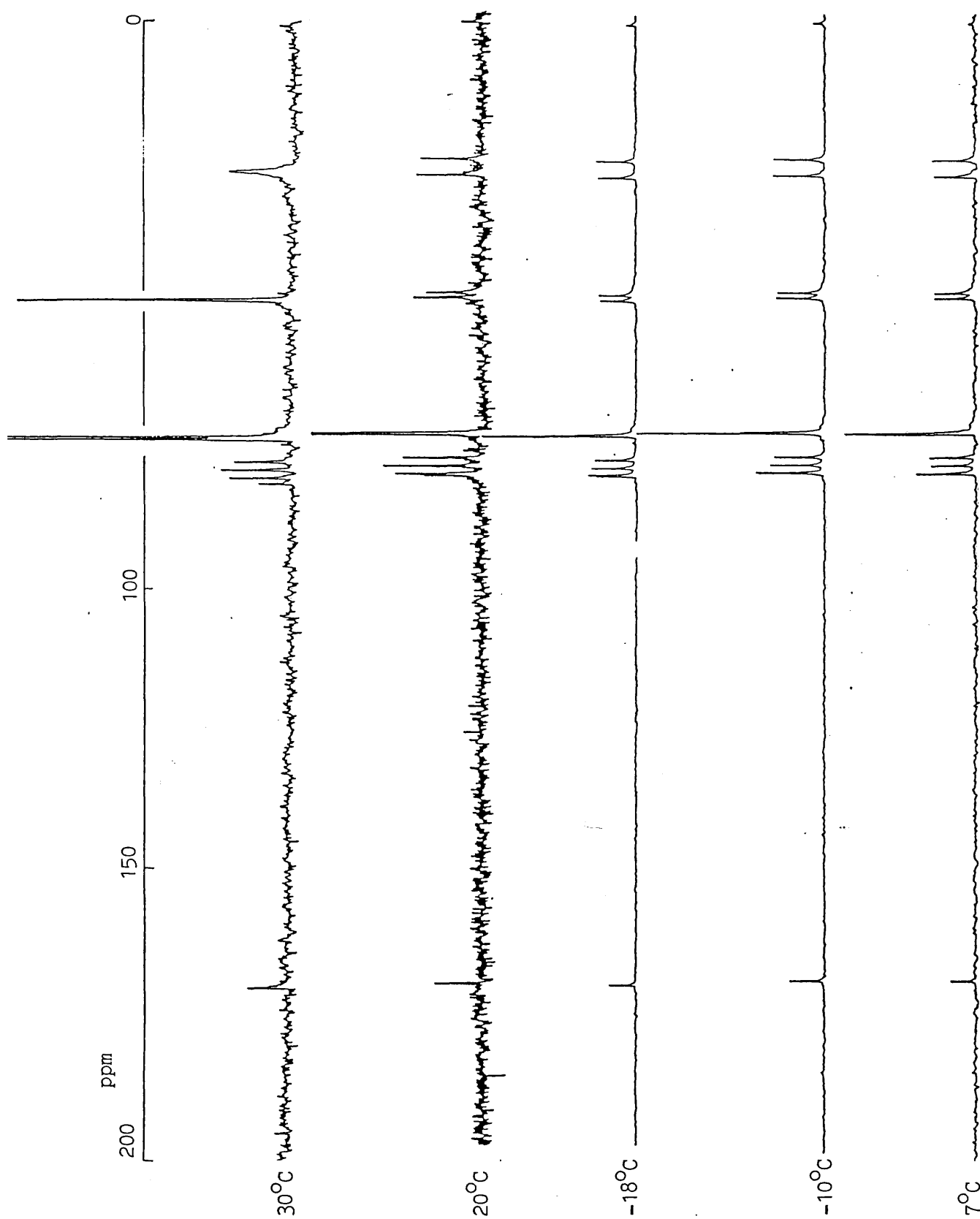


TABLE 5.26

1,1'-bis(N,N-pyrolidine amido)ruthenocene (67) $^{13}\text{C}$  nmr Variable Temperature  $\text{CDCl}_3$  ppm @ 22.6 MHz

Assignment	Temperature $^{\circ}\text{C}$				
	$-41^{\circ}$	$-7^{\circ}$	$26.6^{\circ}$	$29^{\circ}$	$60^{\circ}$
C=O	166.37	166.40	166.64	166.7	
ipso.1	82.56	82.51	81.96	83.3	83.4
2,5	73.46	73.35	73.67	73.6	73.7
2,5	73.19	72.97	73.08	73.0	73.0
3,4	72.27	72.11	72.38	72.4	72.4
3,4	72.11	71.72	71.89	71.9	71.7
$\text{NCH}_2^{\text{a}}$	48.16	47.78	(47.99)	47.5b	47.6s
$\text{NCH}_2^{\text{a}}$	47.29	46.92	(47.40)		
$\text{CH}_2^{\text{b}}$	26.99	26.53	26.92B	24.1	25.5
$\text{CH}_2^{\text{b}}$					
$T_c$ 302 $^{\circ}\text{K}$ $\Delta\nu = 20\text{Hz}$					

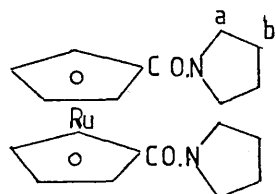
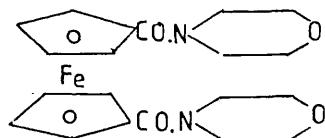


TABLE 5.27

1,1'-bis(N,N-morpholine amido)ferrocene (62) $^{13}\text{C}$  nmr. Variable Temperature  $\text{CDCl}_3$  ppm @ 22.6 MHz

Assignment	Temperature $^{\circ}\text{C}$				
	$-22^{\circ}$	$-18^{\circ}$	$-10^{\circ}$	$+7$	ambient( $26^{\circ}$ )
Carbonyl	168.7	168.7	168.7	168.8	169.1
$\text{C}_1$	79.9	79.9	79.9	80.1	80.9
$\text{C}_{2,5}$	72.0	72.0	72.0	72.1	72.2
$\text{C}_{3,4}$	71.2	71.2	71.2	71.2	71.3
$\text{OCH}_2$	66.8	66.8	66.8	66.9	67.1
$\text{NCH}_2$	47.6 <sub>s</sub>	47.6 <sub>s</sub>	47.6 <sub>b</sub>	45.1 <sub>b</sub>	45.7 <sub>s</sub>
$\text{NCH}_2$	42.7 <sub>s</sub>	42.7 <sub>b</sub>	42.7 <sub>b</sub>		
$T_c = 280^{\circ}\text{K}$ $\Delta\nu = 112 \text{ Hz}$					



V.T.  $^{13}\text{C}$  n.m.r. of (62) @ 22.6 MHz ( $\text{CDCl}_3$ )

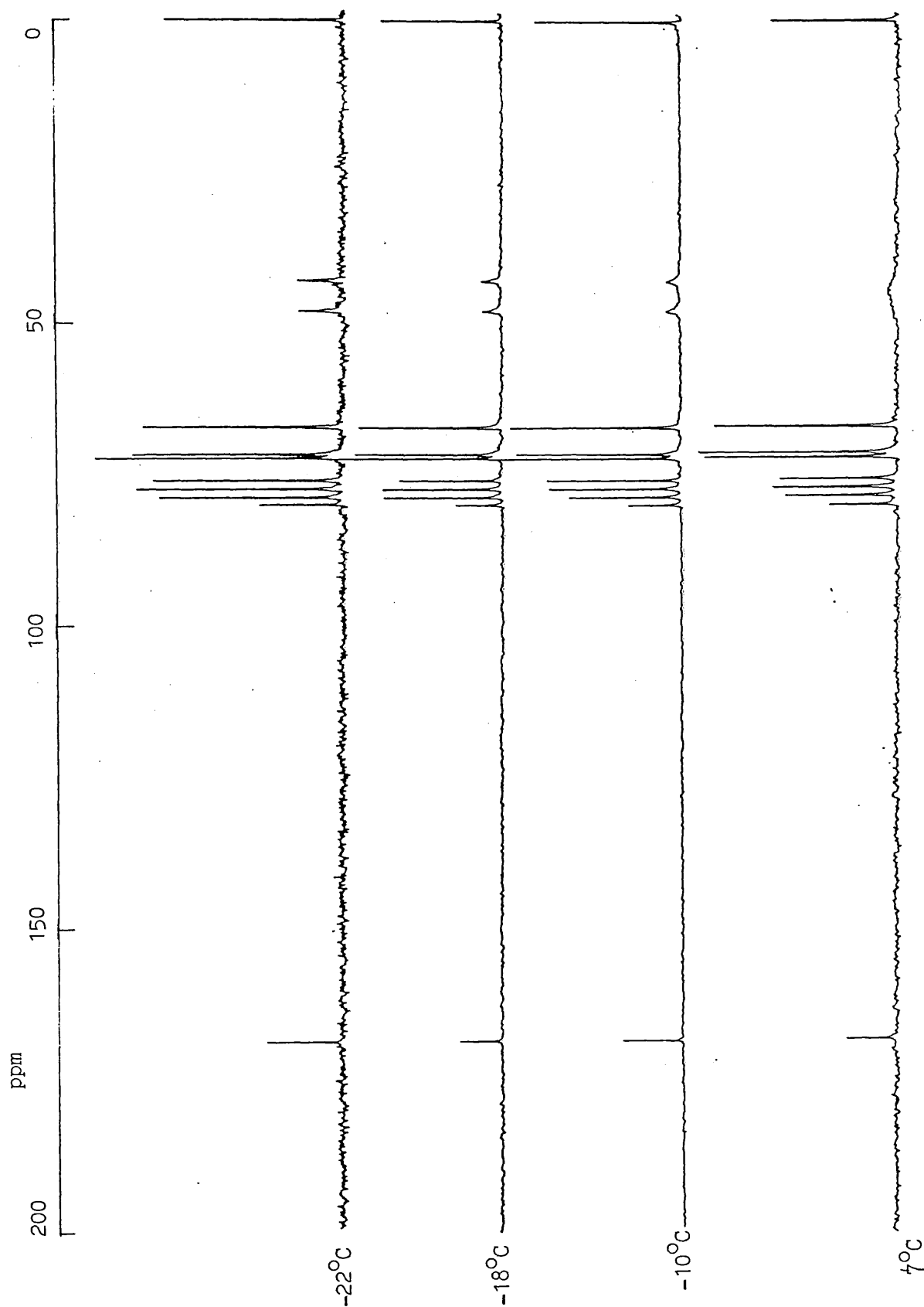


TABLE 5.28

1,1'-bis(N,N-piperidine amido)ruthenocene (63) $^{13}\text{C}$  nmr Variable Temperature  $\text{CDCl}_3$  ppm @ 22.6 MHz

Assignment	Temperature $^{\circ}\text{C}$				
	$-15^{\circ}$	$11^{\circ}$	$20^{\circ}$	$26.6^{\circ}$	$60^{\circ}$
C=O	167.3	167.3	167.4	167.45	167.5
ipso $\text{C}_1$	82.7	83.2	83.4	83.48	(78.9)
$\text{C}_{2,5}$	73.9	74.0	74.0	74.00	74.0
$\text{C}_{2,5}$	73.4	73.3	73.3	73.30	73.2
$\text{C}_{3,4}$	72.5	72.5	72.5	72.49	72.5
$\text{C}_{3,4}$	71.7	71.8	71.8	71.78	71.6
$\text{OCH}_2$	66.8	66.9	66.9	66.96	66.9
$\text{NCH}_2$	47.9	45.7	45.6b	45.67b	45.7
$\text{NCH}_2$	42.6				

$T_c = 234^{\circ}\text{K}$        $\Delta\nu = 118 \text{ Hz}$

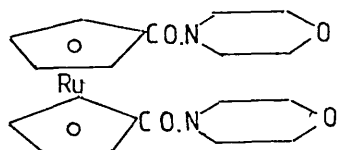


TABLE 5.29

1,1'-bis(N,N-piperidine amido)ferrocene (64)

 $^{13}\text{C}$  nmr. Variable Temperature  $\text{CDCl}_3$  ppm @ 22.6 MHz

Assignment	Temperature $^{\circ}\text{C}$							
	$-33^{\circ}$	$-22^{\circ}$	$-18^{\circ}$	$-10^{\circ}$	0	$7^{\circ}$	$15^{\circ}$	Ambient
Carbonyl CO	168.3	168.3	168.3	168.4	168.4	168.4	168.4	168.5
$\text{C}_1$	80.3	80.3	80.3	80.7	80.7	80.6	80.7	81.4
$\text{C}_{2,5}$	71.7	71.7	71.7	71.8	71.8	71.8	71.8	71.9
$\text{C}_{3,4}$	71.1	71.1	71.1	71.1	71.1	71.1	71.1	71.1
$\text{NCH}_2$ (a)	48.1	48.1	48.1s	48.2s	48.0b	48.0b	46.2b	46.1s
	43.5	43.5	43.5s	43.6s	44.0b	44.0b		
$\text{CH}_2$ (b)	26.6	26.6	26.6s	26.6b		26.1b	26.1s	26.3s
	25.5	25.5	25.5s	25.5b	26.1b			
$\text{CH}_2$	24.5	24.5	24.5	24.6	24.7	24.7	24.7	24.8
(a)	$T_c = 288^{\circ}\text{K}$		$\Delta\nu = 103.8 \text{ Hz}$					
(b)	$T_c = 273^{\circ}\text{K}$		$\Delta\nu = 24.41 \text{ Hz}$					

V.T.  $^{13}\text{C}$  n.m.r. of (64) @ 22.6 MHz ( $\text{CDCl}_3$ )

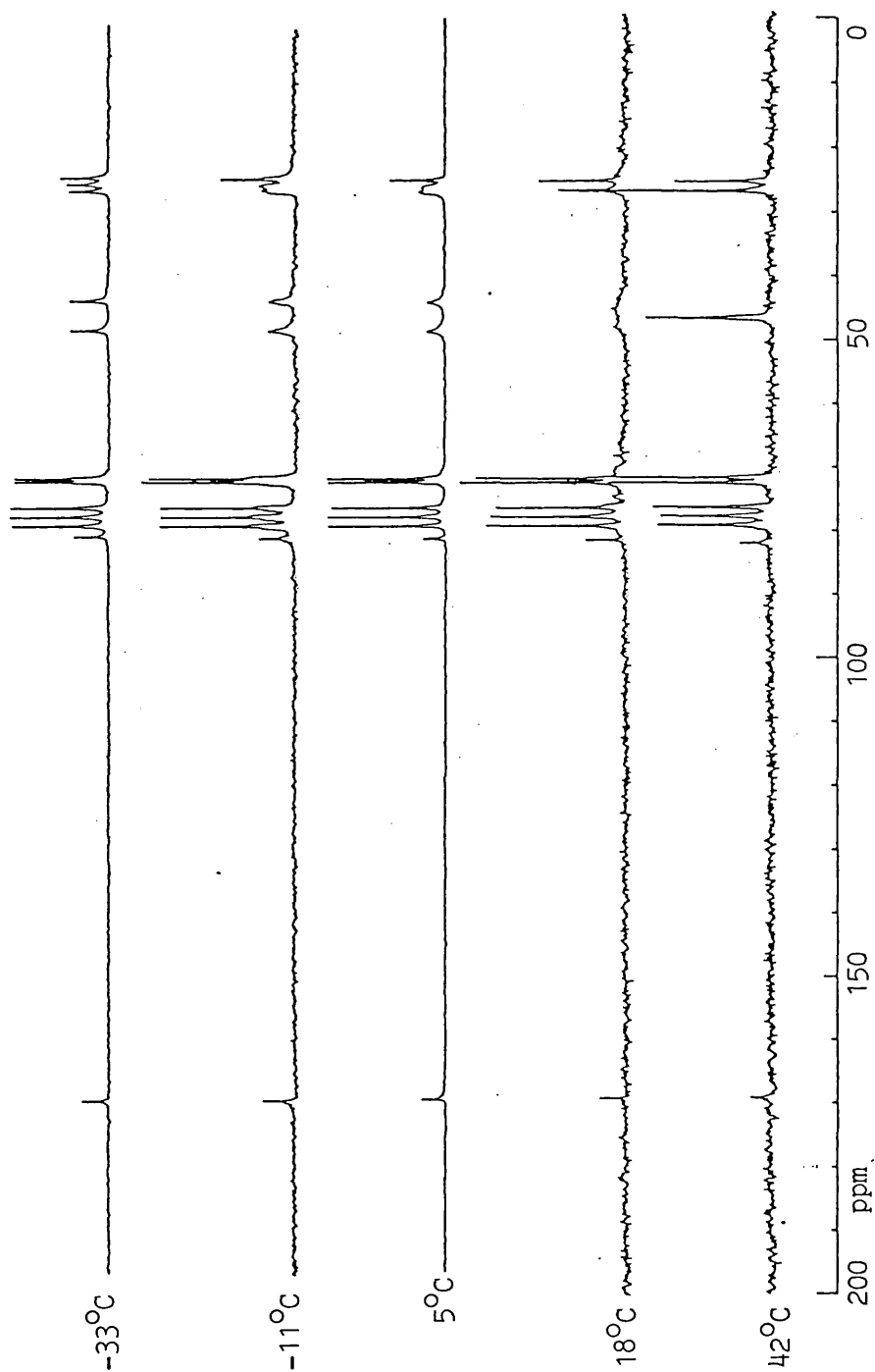




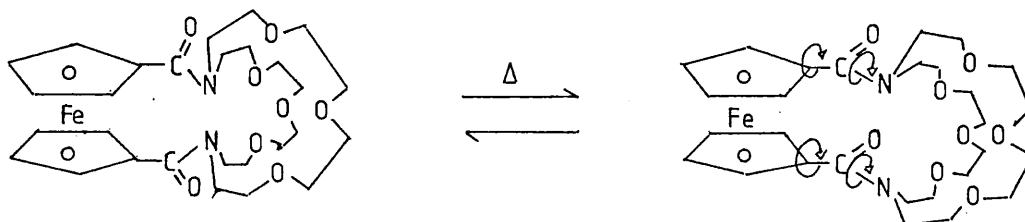
TABLE 5.30

1,1'-bis(N,N-piperidine amido)ruthenocene (65) $^{13}\text{C}$  nmr. Variable Temperature  $\text{CDCl}_3$  ppm @ 22.6 MHz

Assignment	Temperature $^{\circ}\text{C}$						
	$-25^{\circ}$	$5^{\circ}$	$10^{\circ}$	$15^{\circ}$	$26.6^{\circ}$	$46^{\circ}$	$56^{\circ}$
Carbonyl	167.1	-	167.0	167.0	-	-	-
$\text{C}_1$	83.4	-	84.2	-	-	84.4	84.6
$\text{C}_{2,5}$	74.0	74.0	74.0	73.9	74.0	74.0	74.0
$\text{C}_{2,5}$	73.2	73.1	73.0	73.1	73.1	73.1	73.0
$\text{C}_{3,4}$	72.7	72.5	72.6	72.5	72.5	72.6	72.5
$\text{C}_{3,4}$	71.7	71.5	71.4	71.4	71.4	71.4	71.3
$\text{NCH}_2$	48.4	46.3	47.2	47.1	46.5 <sub>b</sub>	46.3 <sub>s</sub>	46.3
	43.7	42.9	45.8	45.3			
$\text{CH}_2$	26.8	26.4	26.3	26.3	26.4	26.4	26.4
	25.6						
$\text{CH}_2$	24.5	24.8	24.7	24.7	24.7	24.8	24.8
$T_c = 273^{\circ}\text{K}$ $\Delta\nu = 107.4 \text{ Hz}$							

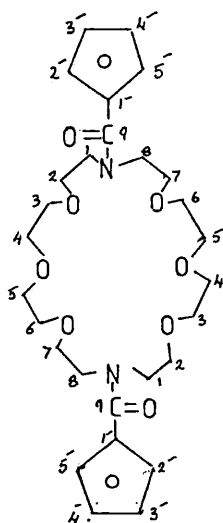
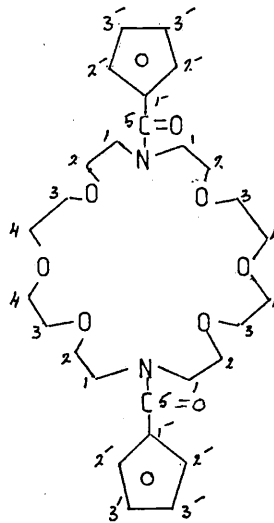
(b) Cryptands (monomers)

The metallocene cryptands have a similar dynamic phenomena to the 'simple' metallocene amides. However, in these larger molecules the molecular motion associated with the amide groups leads to much more complex spectra as a result of the larger number of methylene groups.

DIAGRAM 5.17

Low temperature structure

High temperature structure

TRANS14 non-equivalent  $^{13}\text{C}$  resonancesCIS8 non-equivalent  $^{13}\text{C}$  resonances

The ferrocene[3.3]monomer(70) has  $^{13}\text{C}$  and  $^1\text{H}$  nmr spectra which are temperature dependent and are best explained by the following equilibrium [Diagram 5.17]. On investigation of the structure of (70) and the implications of the suggested molecular motion on the  $^{13}\text{C}$  and  $^1\text{H}$  nmr spectra, it can be seen that at low temperatures when the carbonyls are fixed relative to each other on the nmr time scale, there are only two possible stereo isomers, a cis and trans form. As explained for the (38) and (41) (Section 5.2.3), the trans form should be more favourable since in the cis, the eclipsed conformation is energetically unfavourable due to the parallel dipoles of the carbonyl groups repelling each other. Therefore one would expect to see fourteen non-equivalent resonances [Diagram 5.17] in the  $^{13}\text{C}$  spectra and four ferrocenyl triplets and the appropriate other resonances in the  $^1\text{H}$  nmr spectra [Tables 5.31, 5.32]. As the temperature is raised from  $-50^\circ\text{C}$  one would expect to see a simplification of the  $^{13}\text{C}$  nmr spectra as there is now rapid rotation of the carbonyls (fast on the nmr time scale) which causes coalescence of the same non-equivalent resonances. At  $90^\circ\text{C}$  in the rapidly exchanging state one would expect to see eight non-equivalent resonances. One can make a case for this due to the superimposition of signals as only six  $^{13}\text{C}$  signals are seen at  $90^\circ\text{C}$ . From the coalescence temperature of the  $-\text{N}(\text{CH}_2)$  signals  $\Delta G^\ddagger$  can be found for the rotation barrier

about the amide bond. CO-N  $\Delta\nu = 51.6$  Hz,  $T_c \sim 45^\circ\text{C}$   
 $\Delta G^\ddagger = 15.66$  k.cal mol<sup>-1</sup>  $\pm 0.5$ .

The second dynamic process can be in the variable temperature <sup>1</sup>H nmr. At  $-50^\circ\text{C}$  the rotation of the ipsoferrocene-carbonyl bond is slow on the nmr time scale and four ferrocenyl triplets can be seen each with an integral of two protons. The typical downfield shift of these protons H<sub>2'</sub>,<sub>3'</sub>,<sub>4'</sub>,<sub>5'</sub> is due to deshielding effect and  $\pi$  withdrawal of the carbonyl function and the  $\alpha$ - and  $\beta$ -deshielding effects can be found:  $\alpha_{2'} = -1113$ ,  
 $\alpha_{5'} = -0.993$ ,  $\beta_{3'} = -0.253$ ,  $\beta_{4'} = -0.173$ .  
 It is easily seen and expected that the  $\alpha$ -positions are deshielded to a greater degree than the  $\beta$ -positions since they have a nearer spacial proximity to the carbonyl function. As the temperature is raised to  $0^\circ\text{C}$  the four triplets broaden into humps and at ambient temperature the H<sub>2'</sub> and H<sub>5'</sub> resonances have coalesced into a broad singlet with an integral of four. The H<sub>3'</sub> and H<sub>4'</sub> protons are now seen as two broad humps which eventually coalesce at a higher temperature. At  $100^\circ\text{C}$  where the ipso-carbonyl bond rotation is fast on the nmr time scale two sharp triplets are seen each with an integral of four protons. The  $\alpha$ - and  $\beta$ -deshielding effect values can be found for these two triplets:  $\alpha = -0.783$ ,  $\beta = -0.133$  which again shows that the  $\alpha$  positions are deshielded to a greater degree than the  $\beta$  positions.

TABLE 5.31

Variable temperature  $^{13}\text{C}$  nmr of (70) ferrocene[3.3]monomer  
@ 62.5 MHz ppm

Assignment	Temperature $^{\circ}\text{C}$		
	$-60^{\circ}\text{C}$	Ambient( $30^{\circ}$ )	$90^{\circ}$
C=O	169.37	170.49	absent due to long $\pi$
ipso $\text{C}_{1'}$	77.31	77.84	80.10
$\text{C}_{2',5'}$	76.37	74.94	] 72.75
$\text{C}_{3',4'}$	74.01	72.90	
$\text{OCH}_2$ C	71.64	71.27	] 71.52 <sup>+</sup>
$\text{OCH}_2$ C	71.30	] 70.96	
$\text{OCH}_2$ C	71.08		] 71.35 <sup>+</sup>
$\text{OCH}_2$ C	70.88		
$\text{OCH}_2$ $\text{C}_{4,5}$	70.50*	70.09	70.79
$\text{NCH}_2$ $\text{C}_8$	50.08s	50.43B	] 50.14s
$\text{NCH}_2$ $\text{C}_1$	49.27s	48.86B	
Total signals	14		(8)

\*four superimposed signals

<sup>+</sup>superimposed signals

$T_c = 45^{\circ}\text{C}$        $\Delta\nu = 51.6 \text{ Hz}$

TABLE 5.32

Variable temperature  $^1\text{H}$  nmr of (70) ferrocene[3.3]monomer ppm

@ 250 MHz

Assignment	Temperature $^{\circ}\text{C}$																																																																			
	$-50^{\circ}\text{C}$		$0^{\circ}\text{C}$		ambient		$100^{\circ}\text{C}$																																																													
	$\delta\text{ppm}$	inter.	$\delta\text{ppm}$	inter	$\delta\text{ppm}$	inter	$\delta\text{ppm}$	inter																																																												
ferrocenyl H	5.27T	2.	5.18B	2.	4.92TB	4	4.94T	4																																																												
	5.15T	2.	5.08B	2.					ferrocenyl H	4.41T	2.	4.41B	2.	4.58TB	2	4.29T	4	4.33T	2.	4.30B	2.	4.24TB	2	$\text{OCH}_2$	4.28		4.17		4.14		4.17T	4	4.26C	4.10C	4.02	4.11T	3.79T	3.83T	32	32	3.72C	4	3.47	32	3.6	3.88	3.64C	4	3.10C	3.2C	3.62	4.45C	16	$\text{NCH}_2$	3.06		2.66				3.22B	4	2.53C		Total no. of protons		40	
ferrocenyl H	4.41T	2.	4.41B	2.	4.58TB	2	4.29T	4																																																												
	4.33T	2.	4.30B	2.	4.24TB	2			$\text{OCH}_2$	4.28		4.17		4.14		4.17T	4	4.26C	4.10C	4.02	4.11T	3.79T	3.83T		32		32		3.72C		4		3.47	32	3.6	3.88	3.64C	4	3.10C	3.2C	3.62	4.45C	16	$\text{NCH}_2$	3.06		2.66				3.22B	4	2.53C		Total no. of protons		40		40		40		40					
$\text{OCH}_2$	4.28		4.17		4.14		4.17T	4																																																												
	4.26C		4.10C		4.02		4.11T																																																													
	3.79T		3.83T		32		32			3.72C		4																																																								
	3.47		32		3.6		3.88			3.64C		4																																																								
	3.10C		3.2C		3.62		4.45C		16																																																											
$\text{NCH}_2$	3.06		2.66				3.22B	4																																																												
	2.53C																																																																			
Total no. of protons		40		40		40		40																																																												

From the coalescence temperatures of the  $H_{2'}$ ,  $H_{5'}$  signals and the  $H_{3'}$ ,  $H_{4'}$  signals  $G^\ddagger$  can be found for the rotation barrier about the ipso ferrocene carbonyl band C=CO.

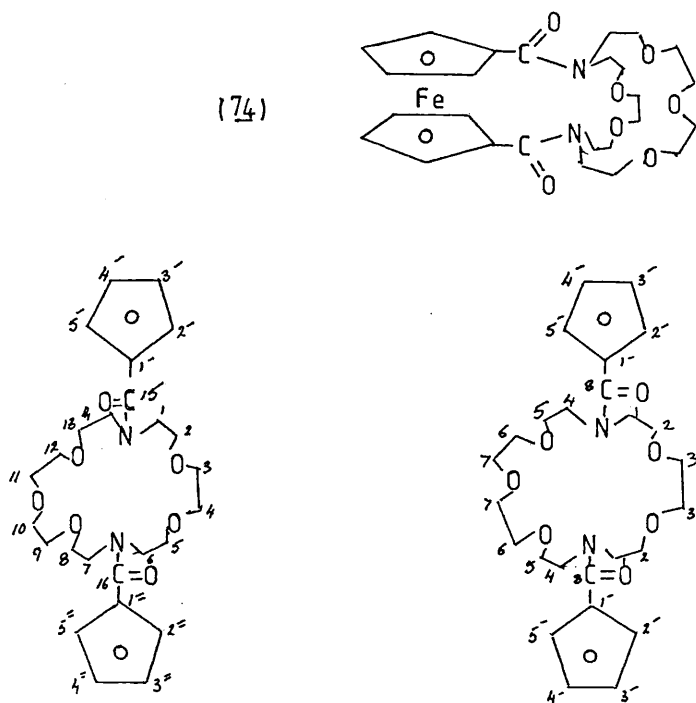
$$H_{2'}, H_{5'}, \Delta\nu = 7.2 \text{ Hz} \quad T_c \sim 15^\circ \quad \Delta G^\ddagger = 15.3 \text{ kcal mol}^{-1} \pm 0.5$$

$$H_{3'}, H_{4'}, \Delta\nu = 4.8 \text{ Hz} \quad T_c \sim 40^\circ \quad \Delta G^\ddagger = 16.8 \text{ kcal mol}^{-1} \pm 0.5$$

The alternative explanation of the nmr spectra is that the molecule has static carbonyl groups and that the two polyether chains interchange. Thus at low temperatures the chains are static on the nmr time scale and at high temperatures they are seen to be interchanging due to the coalescence now present in the spectra. This molecular motion is complex and will be hindered due to the protons on the bridging chains and is therefore unlikely. Further evidence comes from variable temperature studies of the 'simple' metallocene amides where similar dynamic processes can be seen.

The nmr spectra of (74) are consistent with the molecular formulae and has a similar temperature dependence to the other metallocene macrocycles (70). Due to the non-symmetry of the systems the  $^{13}\text{C}$  and  $^1\text{H}$  spectra are necessarily more complex. There will remain a large portion of the spectroscopic data - that of the central glycolic linkages - that will remain unresolved due to its complexity and the proximity of the chemical shifts.

DIAGRAM 5.18



26 non-equivalent  $^{13}\text{C}$   
resonances

13 non-equivalent  $^{13}\text{C}$   
resonances

Again, considering the two structures of the monomer [Diagram 5.18] (Trans or Cis) and the implications of the suggested molecular structure on the  $^{13}\text{C}$  nmr spectra, it can be seen that the Trans-form should have 26 non-equivalent  $^{13}\text{C}$  resonances, (two carbonyls, ten ferrocenyls, four carbons bonded to nitrogen and ten carbons bonded to oxygen) as there is no symmetry in the molecule. The Cis-form requires 13 non-equivalent  $^{13}\text{C}$  resonances (one carbonyl, five ferrocenyls, two carbons bonded to nitrogen, and five carbons bonded to oxygen) as there is a plane of symmetry



through the molecule. From the  $^{13}\text{C}$  nmr spectra at ambient temperature [Table 5.15], twenty clear  $^{13}\text{C}$  signals are seen, of which there are two obvious carbonyl signals and four carbons bound to nitrogen. There are six signals which are superimposed thus representing twelve carbon atoms (these signals are over twice the intensity of any other signal), thus making a total of 26  $^{13}\text{C}$  resonances. These factors in the spectrum therefore suggest the molecule has a trans-configuration [Diagram 5.18].

The  $^1\text{H}$  nmr spectrum at ambient temperature [Table 5.14] is consistent with the general structure [Diagram 5.18] and as expected, it is complex due to the rotation of amide bonds, the lack of symmetry and close proximity of the chemical shifts in the aliphatic region thus making methylene assignments difficult.

At  $100^\circ\text{C}$  the  $^1\text{H}$  nmr is broad and simplified relative to that at ambient and low temperatures. There are four ferrocenyl resonances with an integral ratio of 1:1:1:1 representing the four pairs of equivalent protons in the freely rotating form [Diagram 5.19]. As the temperature is lowered [Table 5.33] the rotation about the ipso ferrocene-carbonyl bond becomes slower on the nmr time scale the number of ferrocenyl resonances increases ( $100^\circ\text{C}$  4 signals,  $23^\circ\text{C}$  6 signals,  $0^\circ\text{C}$  8 signals). At  $0^\circ\text{C}$  the molecule appears 'frozen' on the nmr time scale and eight non-equivalent

TABLE 5.33

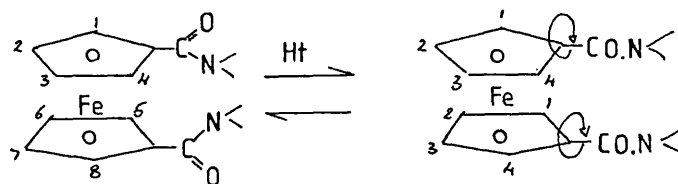
Variable temperature  $^1\text{H}$  nmr of (74) ferrocene[3.2]monomer  
 @ 250 MHz TOL. d6/DMSO.d.6

Assignment ppm ferrocene region only	Temperature $^{\circ}\text{C}$				
	$0^{\circ}$	$23^{\circ}$	$55^{\circ}$	$80^{\circ}$	$100^{\circ}$
Ferrocenyl	4.99shm	4.84b			
	4.78shm	4.65b	4.72b	4.71b	4.69b
	4.65shm				
	4.61shm				
	4.33shm	4.41b	4.31b	4.32b	4.33b
	4.27shm	4.38b			
	4.16shm	4.16b	3.89b	4.06b	4.06b
	4.02shm	3.99b		3.98b	3.99b

DIAGRAM 5.19

Trans 'frozen state'

Freely rotating

Low Temp.  $0^{\circ}\text{C}$ High Temp.  $100^{\circ}\text{C}$

resonances are seen each representing one proton from the ferrocenyl ring. This is consistent with the previously outlined ipso ferrocenyl-carbonyl rotation (70). It is of interest to compare this molecule with the similar motion of the ferrocene[3.3]cryptand monomer (70) where, due to the symmetry of the cryptand part of the molecule there are at high temperatures only two non-equivalent ferrocenyl  $^1\text{H}$  resonances and four at low temperatures. Whereas, in (74), the different chain lengths of the cryptand confer four non-equivalent ferrocenyl  $^1\text{H}$  resonances at high temperatures and eight at low temperatures.

The ruthenocene[2.1]cryptand (82) has similar structural and spectroscopic properties to the ferrocene analogue (80) [Diagram 5.15]. The low temperature  $^{13}\text{C}$  n.m.r. supports the case of a molecule with a trans configuration with respect to the carbonyl groups as twenty-one of the expected twenty-two non-equivalent  $^{13}\text{C}$  resonances are seen [Table 5.34]. (One resonance not observed due to overlap). While in the cis-form only eleven non-equivalent  $^{13}\text{C}$  resonances are seen and as the temperature is raised from  $-45^\circ\text{C}$  the  $\text{N}(\text{CH}_2)$  resonances broaden and coalescence is seen. From the coalescence temperature of the  $-\text{N}(\text{CH}_2)_2$  signals  $G^\ddagger$  was found for the rotation barrier about the amide bond  $\text{CO-N}$ .

$$\Delta\nu = 168 \text{ Hz}, \quad \text{TC} \sim 28^\circ\text{C}, \quad \Delta G^\ddagger \sim 14.1 \text{ Kcal.mol}^{-1} \pm 0.5.$$

TABLE 5.34

V.T.  $^{13}\text{C}$  n.m.r. of (82)  $\text{CDCl}_3$  ppm @ 22.5 MHz

Assignment	Temperature $^{\circ}\text{C}$	
	$-40^{\circ}$	ambient
C.O	170.0 s.	169.2 b.
C.O	169.0 s.	168.4 b.
ipso $\text{C}_1$	82.8	82.7
ipso $\text{C}_1$	82.0	
	76.4	74.7
	76.0	73.6
Cyclopentadienyl	75.2	71.8
and	74.8	70.9
$\text{OCH}_2$	74.4	70.8
resonances	73.8	70.6
	73.6	70.0
	72.0	69.6
	70.6	69.4
	70.2	69.2
	68.8	68.4
	68.2	67.6
	66.8	64.0
$\text{NCH}_2$	52.0 s.	51.6 vb.
$\text{NCH}_2$	50.0 s.	49.6 vb.
$\text{NCH}_2$	49.2 s.	48.8 vb.
$\text{NCH}_2$	46.8 s.	48.0 vb.

The ruthenocene[3.1]cryptand (78) has a similar dynamic phenomena which can be seen in the variable temperature  $^{13}\text{C}$  n.m.r. [Table 5.35]. A general assignment

TABLE 5.35

V.T.  $^{13}\text{C}$  n.m.r. of (78)  $\text{CDCl}_3$  ppm @ 22.6 MHz

Assignment	Temperature $^{\circ}\text{C}$	
	ambient <sup>(i)</sup>	+45 <sup>o(ii)</sup>
CO	confirmed	by i.r.
cyclopentadienyl ( $\text{C}_{1'}$ )	74.7 b.	74.5 b.
cyclopentadienyl ( $\text{C}_{2',5'}$ )	74.0 b.	73.5 b.
cyclopentadienyl ( $\text{C}_{3',4'}$ )	71.9 b.	71.8 b.
	71.1 b.	70.9 b.
$\text{OCH}_2$	70.8 b.	70.7 b.
		70.2 b.
	70.0 c.	70.0 b.
$\text{NCH}_2$	50.8 c.	
$\text{NCH}_2$	49.7 c.	49.7 b.

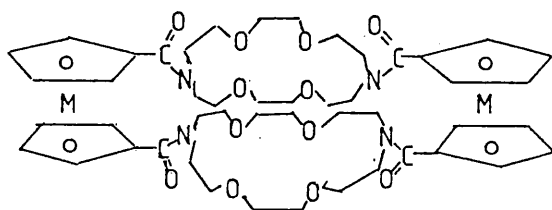
was made based on the other metallocene cryptands. However, in this case, the spectra are broad due to the highly unsymmetrical nature of the cryptand. No detailed thermodynamic data was obtained since it was not possible to give a definite assignment to the  $\text{N-CH}_2$  signals. Theoretically there should be four  $\text{N-CH}_2$   $^{13}\text{C}$  resonances at low temperatures and two at high temperatures and this clearly has not been seen. Further n.m.r. studies were not possible as the cryptand (78) decomposed before data could be collected.

(c) Cryptands (dimers)

The ferrocene and ruthenocene[2.2]cryptand dimers (39) and (42) [Diagram 5.20] unlike the monomers (38) and (41) do not have a fixed configuration and are able to rotate the cryptand about its horizontal axis. This is seen in the nmr spectra which are more complex and temperature dependent.

DIAGRAM 5.20

M = Fe(39)<sup>153</sup> or Ru(42) (This work)



The  $^{13}\text{C}$  nmr spectrum of (39) at  $-50^\circ\text{C}$  looks similar to its monomer (38) and has twelve resonances, five ferrocenyl, one carbonyl, four different carbons bonded to oxygen and two different carbons bound to nitrogen.

TABLE 5.36

V.T.  $^{13}\text{C}$  nmr data of (39)<sup>153</sup> and (42)<sup>(This work)</sup>  $\text{CDCl}_3$  ppm

@ 62.5 MHz. Ferrocene[2.2]cryptand(39)					@ 22.5 MHz. Ruthenocene[2.2]cryptand(42)				
Assignment	Temperature $^\circ\text{C}$				Assignment	Temperature $^\circ\text{C}$			
	$-50^\circ$	$0^\circ$	$23^\circ$	$55^\circ$		$-30^\circ$	$-1^\circ$	$5^\circ$	$56^\circ$
C=O	168.7	170.0	170.1	170.0	C=O	168.4	168.4	168.5	-
C <sub>1'</sub>	78.0	79.1	79.6	80.0	C <sub>1'</sub>	83.9	83.8	84.0	84.0
C <sub>2',5'</sub>	75.5	73.9b	73.9b	73.3b	C <sub>2',5'</sub>	74.3b	74.6b	74.2c	74.3
C <sub>2',5'</sub>	72.2				C <sub>2',5'</sub>				
OCH <sub>2</sub>	72.1	72.1	72.0		OCH <sub>2</sub>				
C <sub>3',4'</sub>	72.0	70.0			C <sub>3',4'</sub>	73.6b	73.7c	73.6c	73.6b
OCH <sub>2</sub>	69.7	70.3b	70.4b	70.6b	OCH <sub>2</sub>	71.8b	71.8b	71.8b	71.8b
OCH <sub>2</sub>	69.3	69.9			OCH <sub>2</sub>	70.4b	70.4c	70.5c	70.3b
C <sub>3',4'</sub>	69.1				C <sub>3',4'</sub>				
OCH <sub>2</sub>	65.8	67.0	67.7b		OCH <sub>2</sub>				
NCH <sub>2</sub>	48.5	49.1	49.3b	48.0b	NCH <sub>2</sub>	51.3	51.4	51.3	51.0b
NCH <sub>2</sub>	46.8	47.0	47.3b		NCH <sub>2</sub>	49.7	50.1	50.5	
N-CH <sub>2</sub> : T <sub>c</sub> = $60^\circ\text{C}$ : $\Delta\nu = 158\text{Hz}$ : $\Delta G^\ddagger = 15.7\text{kcalmol}^{-1}$					NCH <sub>2</sub> : T <sub>c</sub> = $56^\circ$ : $\Delta\nu = 95\text{Hz}$ : $\Delta G^\ddagger = 15.8\text{kcalmol}^{-1}$				
C <sub>1'</sub> -CO: T <sub>c</sub> = $-10^\circ$ : $\Delta\nu = 200\text{Hz}$ : $\Delta G^\ddagger = 12.1\text{kcalmol}^{-1}$									

A similar case can be made for (42) since the oxygen-methylene signals and the cyclopentadienyl signals are broad and therefore must represent more than one  $^{13}\text{C}$  signal.

The conventional rotation of the carbonyl nitrogen bond can be seen in both molecules. At low temperatures the spectra shows two non-equivalent carbons  $\alpha$  to the nitrogen and in (39) four non-equivalent carbons bonded to oxygen. This indicates that the macrocyclic rings in (39) are in a non-fluxional, co-planar environment relative to the carbonyl groups on the nmr time scale. As the temperature is raised the  $\text{N-CH}_2$  signals coalesce and from the coalescence temperature the free energy of rotation was found [Table 5.36].

A second dynamic process can clearly be seen in the variable temperature  $^{13}\text{C}$  nmr of (39). The rotation of the macrocyclic amide groups about the ferrocene-carbonyl bond is slow on the nmr time scale at  $-50^\circ$  and four cyclopentadienyl carbons are seen. As the temperature is raised the signals coalesce and two cyclopentadienyl signals are seen (excluding the ipso). Again from the coalescence temperature the free energy of rotation was found [Table 5.36]. A second value of  $\Delta G^\ddagger$  was obtained from the variable temperature  $^1\text{H}$  nmr of (39) [Table 5.37]. The cyclopentadienyl protons are clearly seen to be split into two pairs of well-resolved absorptions at low temperatures which coalesce



TABLE 5.37

Variable temperature  $^1\text{H}$  nmr data of (39)<sup>153</sup> @ 250 MHz  
in  $\text{CDCl}_3$ .

Assignment	-80°C ppm $\text{CD}_2\text{Cl}_2/\text{CFCl}_3$	23°C ppm	50°C ppm
$\text{OCH}_2$	3.3-4.2b	3.4-4.0b	3.68
$\text{NCH}_2$			3.75b
$\text{H}_3, \text{H}_4'$	4.21	4.35b	4.36
$\text{H}_4, \text{H}_3'$	4.49		
$\text{H}_5'$	4.30	4.63b	4.64
$\text{H}_2'$	4.90		

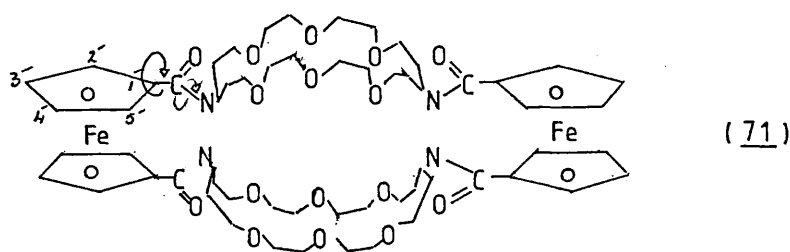
$$T_c = -10^\circ\text{C}; \quad \Delta G^\ddagger \approx 12 \text{ kcal.mol}^{-1}$$

into two absorption bands at higher temperatures. The two values for the free energy of rotation for the ferrocenyl carbonyl bond were in good agreement:

$$^{13}\text{C} \quad \Delta G^\ddagger = 12.1 \text{ kcal mol}^{-1}, \quad ^1\text{H} \quad \Delta G^\ddagger = 12 \text{ kcal mol}^{-1}.$$

The nmr spectra of the ferrocene[3.3]dimer (71) supports the contention of two independent rotational phenomenon as outlined earlier for the ferrocene[2.2]dimer (39).

DIAGRAM 5.21



The  $^{13}\text{C}$  nmr spectrum [Table 5.38] at  $52^\circ\text{C}$  shows seven sharp non-equivalent resonance signals which represent: three ferrocenyl, three different carbon atoms bound to oxygen and one carbonyl. There is also a broad resonance which represents the carbons bound to nitrogen at just above coalescence, if the temperature were raised further this signal would become a sharp singlet. As the temperature is lowered from  $52^\circ\text{C}$  one would expect to see the spectrum become more complex as the rotation about the amide bonds become slow on the nmr time scale. At  $31^\circ\text{C}$  the rotation about the CO-N bond has become slow on the nmr time scale and two clear resonances can be seen. This slow rotation also affects the carbon atoms bound to oxygen at 69.91 ppm as splitting now occurs because the signals are no longer equivalent. At  $-30^\circ\text{C}$  the spectrum

is even more complex as the molecule appears frozen on the nmr time scale. As expected from Diagram 5.21 fourteen non-equivalent  $^{13}\text{C}$  resonances can be explained: one carbonyl, two carbon atoms bound to nitrogen, one ipso ferrocene, two superimposed ferrocenyl signals representing four carbon signals, four sharp carbon bound to oxygen signals and two superimposed carbon bound to oxygen signals representing two carbon signals. From the coalescence temperature of the  $-\text{N}(\text{CH}_2-)_2$  signals  $\Delta G^\ddagger$  can be found for rotation barrier about the amide bond CO-N.

$$T_c = 55^\circ\text{C}; \quad \Delta\nu = 126 \text{ Hz}; \quad \Delta G^\ddagger = 15.6 \text{ kcal mol}^{-1}$$

The  $^1\text{H}$  nmr spectra of the ferrocene[3.3]dimer (71) [Table 5.39] has very broad regions due to the close proximity of the central glycolic linkages and thus the only factors worth monitoring are the integrations and change in the cyclopentadienyl resonance patterns. At  $-30^\circ\text{C}$  four ferrocenyl triplets are seen each with an integration of four protons. As the temperature is raised to  $55^\circ\text{C}$  the four signals coalesce into two sharp triplets with an integral of eight protons each. The complexity of the rest of the spectrum decreases as the temperature is raised due to equivalence caused by the increased speed of rotation of the amide bonds. From the ferrocenyl proton signals  $\Delta G^\ddagger$  can be found for the free rotation of the ipso ferrocene-carbonyl bond.

$$T_c \approx 248^\circ\text{K}; \quad \Delta\nu = 2 \text{ Hz}; \quad \Delta G^\ddagger \approx 13.7 \text{ kcal.mol}^{-1}.$$

TABLE 5.38

Variable temperature  $^{13}\text{C}$  nmr of (71) ferrocene[3.3]dimer  
 @ 62.5 MHz

Assignment	Temperature $^{\circ}\text{C}$		
	$-30^{\circ}$	$31^{\circ}\text{C}$	$52^{\circ}\text{C}$
C=O	169.94	170.02	170.07
ipso $\text{C}_{1'}$	78.73	79.83	80.23
$\text{C}_{2',5'}$	72.30B*	72.29	72.36
$\text{C}_{3',4'}$		71.87	71.82
$\text{OCH}_2$	70.49*	70.78	70.88
$\text{OCH}_2$	70.21	70.69	70.78
$\text{OCH}_2$	69.73	69.96	
$\text{OCH}_2$	69.49		69.91
$\text{OCH}_2$	69.29	69.69	
$\text{NCH}_2$	49.28s	49.73	48.5B
$\text{NCH}_2$	47.66s	47.72	
non-equivalent C	(14)*		8

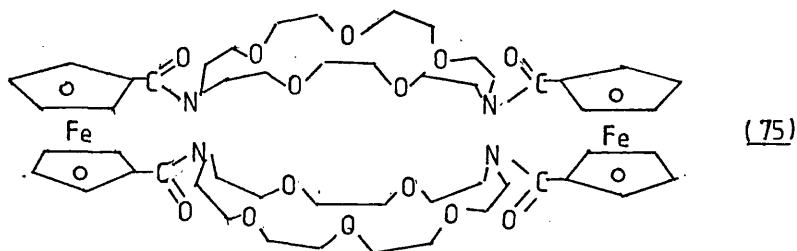
\*Less than 14 due to superimposed signals.

TABLE 5.39

Variable temperature  $^1\text{H}$  nmr of (71) ferrocene[3.3]dimer  
 @ 250 MHz

Assignment	Temperature $^{\circ}\text{C}$							
	$-30^{\circ}\text{C}$		$0^{\circ}$		ambient		$55^{\circ}$	
	ppm	inter	ppm	inter	ppm	inter	ppm	inter
ferrocenyl	4.75T	4	4.72B	8	4.72T	8	4.72T	8
	4.72T	4						
ferrocenyl	4.44T	4	4.41B	8	4.38T	8	4.38T	8
	4.42T	4						
$\text{OCH}_2$	3.94BT	16	3.88BT	16	3.85B			
$\text{OCH}_2$	3.68B	48	3.67B	48	3.66B	64	3.71	64
$\text{OCH}_2$	3.62B		3.63B		3.65B		3.64	
$\text{NCH}_2$	3.61B				3.62B			
Total no. of protons		80		80		80		80

The nmr spectra of the ferrocene[3.2]dimer (75) also supports the contention of two rotational phenomena as outlined earlier.



The  $^1\text{H}$  nmr [Table 5.40] shows the expected simplified spectrum at high temperatures ( $55^\circ\text{C}$ ) and one of increased complexity at low temperatures ( $-20^\circ\text{C}$ ). The only region where distinguishable resonance patterns can be seen are in the ferrocenyl region as in the aliphatic region only two broad signals are seen, due to the close proximity of the chemical shifts. Unlike the ferrocene[2.3]monomer (74) only two sharp ferrocenyl triplets are seen at high temperatures. These two triplets represent the  $\text{H}_{2,5}$  and  $\text{H}_{3,4}$  protons and are in the ratio of 1:1. As the temperature is lowered and the ipso ferrocenyl-carbonyl bond rotation becomes slow on the nmr time scale, the two triplets broaden at ambient temperature into singlets. As the temperature is lowered further to  $-20^\circ\text{C}$  these signals collapse into two sets of four broad singlets each representing two ferrocenyl protons. This is expected since the macrocyclic cross-linkage is unsymmetrical and will cause all the ferrocenyl protons to be non-equivalent.

TABLE 5.40

Variable temperature  $^1\text{H}$  nmr of ferrocene[3.2]dimer (75) $\text{CDCl}_3$  250 MHz

Assignment	Temperature $^{\circ}\text{C}$					
	$-20^{\circ}\text{C}$		ambient		$+55^{\circ}\text{C}$	
	$\delta\text{ppm}$	inter	$\delta\text{ppm}$	inter	$\delta\text{ppm}$	inter
ferrocenyl 2'5'	4.76B	2				
	4.73B	2	4.69BT	8	4.70T	8
	4.69B	2				
	4.66B	2				
ferrocenyl 3'4'	4.42B	2				
	4.38B	2	4.39BT	8	4.38T	8
	4.36B	2				
	4.28B	2				
$\text{OCH}_2$	3.72B		3.72B	56	3.74s	56
	3.68B	56	3.66B		3.63s	
$\text{NCH}_2$	3.66B				3.62s	
TOTAL		72		72		72

TABLE 5.41

Variable temperature  $^{13}\text{C}$  nmr of ferrocene[2.3]dimer (75)

@ 62.5 MHz

Assignment	Temperature $^{\circ}\text{C}$		
	$-30^{\circ}\text{C}$	ambient	$52^{\circ}\text{C}$
Carbonyl	169.94	169.95	170.04
ipso ferrocenyl	79.36	79.87B	
ipso ferrocenyl	78.58	79.47B	-80.08s
$\begin{array}{c}   \\   \\   \\   \\   \\   \\   \\   \\   \\   \\ \text{ferrocenyl and OCH}_2 \end{array}$	72.25B	72.41	72.52
	71.88		
	71.62	-71.64B	71.62
	71.38		
	70.31	70.64	
	70.13	70.47	70.78
	69.77	70.17	
	69.59		
	68.95	69.4B	69.89B
	N-CH <sub>2</sub>	49.01	49.56
N-CH <sub>2</sub>	47.14	47.58	



The  $^{13}\text{C}$  nmr spectra, [Table 5.41] is temperature dependent and two dynamic phenomena again can be seen. The first dynamic phenomena, the rotation about the carbonyl nitrogen bond ( $\text{CO} \begin{array}{c} \curvearrowright \\ \downarrow \end{array} \text{N}$ ) is easily seen and explained. At  $-30^\circ\text{C}$ , two sharp signals appear in the N-C region and these signals represent two pairs of resonances. As the temperature is raised to ambient these signals broaden and eventually converge into one broad hump at  $52^\circ\text{C}$ . This broad signal should represent the coalescence of two pairs of resonances into a single pair of resonances.

$$T_c = 325^\circ\text{K}; \quad \Delta\nu = 118 \text{ Hz}; \quad \Delta G^\ddagger = 15.48 \text{ kcal.mol}^{-1}$$

From this coalescence temperature and the maximum splitting of the N- $\text{CH}_2$  signals at  $-30^\circ\text{C}$   $\Delta G^\ddagger$  can be calculated for the carbonyl nitrogen rotation barrier. There is no reason why these N- $\text{CH}_2$  resonances should ever reduce to a sharp singlet as the two chains of this cryptand are different in this molecule and should thus give at higher temperatures e.g. ( $110^\circ\text{C}$ ) two sharp singlets again each representing two pairs of resonances.

The second dynamic process, is seen by the splitting of the ipso ferrocenyl signal and it is not clear what causes this dynamic phenomena. At  $52^\circ\text{C}$  one sharp ipso ferrocenyl peak is seen. This must represent all four ferrocenyl signals. At ambient temperature this signal becomes broad and is possibly the coalescence of two non-

equivalent ipso signals. At  $-30^{\circ}\text{C}$  two sharp signals are seen and each must represent two pairs of non-equivalent resonances. A  $\Delta G^{\ddagger}$  value can be calculated but what this value refers to is uncertain.

$$T_c = 303^{\circ}\text{K}; \quad \Delta\nu = 49.5 \text{ Hz}; \quad \Delta G^{\ddagger} = 14.92 \text{ kcal.mol}^{-1}$$

### 5.3 Ion binding

The cation binding properties of (38) were tested by C.D. Hall et al. at King's College using the Pedersen\* method. The results were in the following unusual sequence:  $\text{Ca}^{2+} \gg \text{Li}^+ > \text{Na}^+ \approx \text{Mg}^{2+} \gg \text{K}^+ \approx 0$ . The order of alkali metal binding suggests a small cavity similar in size to [12]crown-4 which prefers small alkali metal cations. However, the very strong binding of  $\text{Ca}^{2+}$  which is similar in ionic size to  $\text{K}^+$  which is bound  $\approx 0$  does not follow the observation of [12]crown-4. This may be due to the fact that calcium picrate is not very stable in aqueous solutions and may have formed calcium hydroxide and picric acid. Thus it will be the  $\text{H}^+$  from picric acid that will have been measured in the macrocycle giving the sequence:  $\text{H}^+ > \text{Li}^+ > \text{Na}^+ \approx \text{Mg}^{2+} \gg \text{K}^+, \text{Ca}^{2+} \approx 0$  which is more understandable. Also in solvents of low dielectric constant, ligands with a large portion of lyophilic character favour complex formation with ions of lower charge (Section 1.5). The relatively strong binding of  $\text{Mg}^{2+}$  is unusual because of the small size and high charge density of  $\text{Mg}^{2+}$  and usually

---

\*The Pedersen method for testing cation binding properties with picrates:- A methylene chloride solution of the macrocycle and aqueous metal picrate are mixed. Electrical neutrality is preserved, so on transfer of a cation from the aqueous to the organic phase a picrate ion will follow. This is now detected as it has a  $\lambda_{\text{max}}$  378 nm in  $\text{CH}_2\text{Cl}_2$ . It is of interest to note that no picrate is transferred without a  $\text{CH}_2\text{Cl}_2$  soluble binding ligand present.

forms much less stable complexes than  $\text{Na}^+$ , ( $\log K_s.\text{Na}^+ > 4$ ,  $\log K_s \text{Mg}^{2+} < 2$  for small cryptands). Again this may be a phenomenon of the stability of the picrate and not the binding properties of the macrocycle. The binding sequence would be more informative if a run had been made against picric acid itself. No conclusions can be made from these observations however a  $\pi$  interaction may be important and the iron atom has the potential to contribute to the degree of binding via a similar mechanism by which it is protonated in ferrocene to the ferricenium ion.

In this work the binding properties of (39) were tested with ammonium benzoate via  $^1\text{H}$  nmr. This has one major advantage over the Pedersen method as both the anion and cation can be detected and the ratios in the complex found. 50 mg of (39) was dissolved in 50 ml of dry chloroform and to this a 4 molar excess of ammonium benzoate was added. The mixture was then stirred for four hours, after which it was filtered and evaporated. The  $^1\text{H}$  nmr was then run [Table 5.42]. This experiment was also repeated without (39) to test the solubility of ammonium benzoate in chloroform. No ammonium benzoate was detected in the  $^1\text{H}$  nmr. The  $^1\text{H}$  nmr of the complex clearly shows ammonium benzoate is present in a 1:1 ratio with the macrocycle. This suggests that the ammonium cation is in the centre of the macrocyclic rings hydrogen bonded to the ether linkages and associated with the now positive

TABLE 5.42

 $^1\text{H}$  nmr of (39)  $\text{CDCl}_3$  @ 60 MHz

Assignment	(39)		(39) + ammonium benzoate	
	ppm	inter	ppm	inter
$\text{NH}_4^+$			8.28b	4
$\text{ArCO}_2^-$			7.69b	5
$\text{H}_{2,5}$	4.64t	8	4.68t	8
$\text{H}_{3,4}$	4.38t	8	4.42t	8
$\text{NCH}_2 + \text{OCH}_2$	3.7b	48	3.7b	48

molecule is the benzoate anion. It is not unreasonable to consider the ammonium cation (diam. 2.68 Å) between two macrocyclic rings each with a diameter of 2.6-3.2 Å separated by 4.08 Å, the distance between the upper and lower cyclopentadienyl rings, since [18]crown-6, with a diameter of 2.6-3.2 Å binds strongly with the potassium cation (diameter 2.66 Å) - Chapter 1.

CHAPTER 6: CYCLIC VOLTAMMETRIC STUDIES OF SOME FERROCENE  
DERIVATIVES

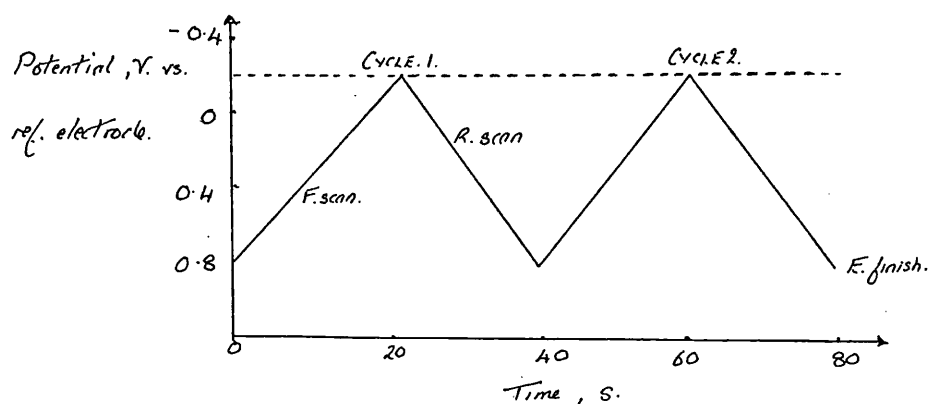
CHAPTER 6  
CYCLIC VOLTAMMETRIC STUDIES OF SOME  
FERROCENE DERIVATIVES

6.1 INTRODUCTION

Cyclic voltammetry<sup>175,176,177</sup> is a simple and direct method for measuring the formal potential of a half reaction when both oxidized and reduced forms are stable during the time required to obtain the voltammogram (a current potential curve).

The current measured is that between the working and auxillary electrodes. The potential of the working electrode is adjusted relative to the reference electrode so that no current passes between them and there is negligible potential drop. The potential read from the voltammogram now corresponds to that between the working and auxillary electrodes.

In cyclic voltammetry, the potential of a small, stationary working electrode in an unstirred solution is changed linearly with time between two limits [Diagram 6.1]. This triangular potential waveform (a sawtooth) sweeps the potential of the working electrodes between two values. These are called the switching potentials and must be within the voltammetric stability range for the particular solvent being used.

Diagram 6.1

The potential of the working electrode as a function of time

The time scale of the experiment is controlled by the scan (or sweep) rate. The total potential traversed can be varied over the range of  $10^2$ - $10^{-5}$ s though quantitative experiments are usually restricted to  $10$ - $10^3$ s.

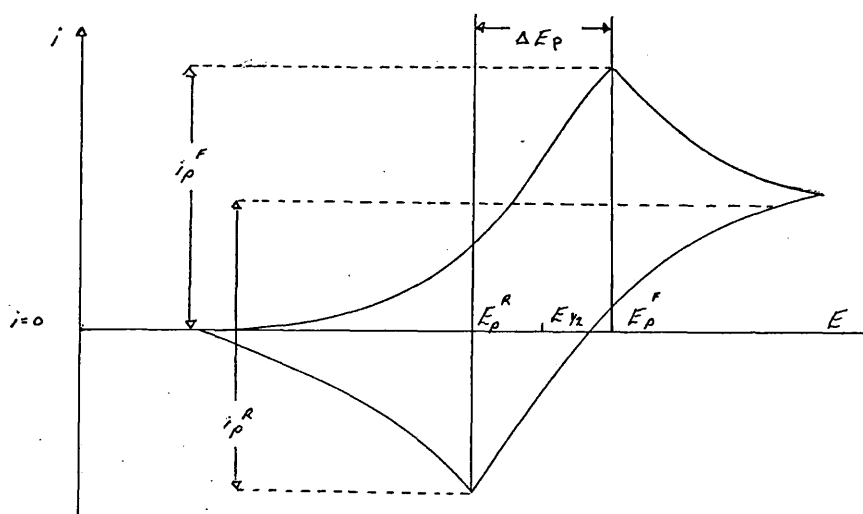
A supporting electrolyte is required to keep the cell resistance low and to reduce the migration of charged reactants and products. The concentration of the base electrolyte should be at least fifty times that of the electroactive species under study.

In work with both aqueous and non-aqueous media, the solvents must be deoxygenated and anaerobic conditions must be maintained because at potentials negative with respect to the saturated calomel electrode, oxygen is reduced and such reductions would interfere with other



processes under investigation. A simple cyclic voltammogram is shown in diagram [6.2]. It is

Diagram 6.2. A simple cyclic voltammogram



characterized by several important parameters; ( $E_p^F$ ) the peak potential of the forward reaction; ( $E_p^R$ ) the peak potential of the reverse reaction; ( $i_p^R$ ) the peak current of the reverse reaction; ( $E_{1/2}$ ) the half-wave potential and ( $E_p^{1/2}$ ) the half-peak potential. One method for measuring  $i_p$  involves the extrapolation of a baseline current as shown in diagram [6.2]. The establishment of a correct baseline is essential for the accurate measurement of peak currents. This is not always easy, particularly for more complicated systems.

The shapes of the curves are determined by the ratio of the ions in solution. At potentials more positive than the formal electrode potential, the

concentration of the neutral species at the working electrode is zero but, the concentration of the oxidised species is high. As the potential approaches the formal electrode potential, some of the oxidised ions are reduced and a current flows, increasing rapidly. At a potential equal to the formal electrode potential, the two concentrations are equal and at negative potentials, there is more neutral species than oxidised, the current again increases rapidly until there is no oxidised species present.

When two electroactive species are in the solution or when the electroactive species is oxidised or reduced in two steps, two peaks are produced on the reduction and oxidation half cycles.

The definition of  $E_{\frac{1}{2}}$  has been borrowed from classical polarography [Equation 6.1], ( $E^{\circ}$  is the formal potential relating to the ionic strength of the solution,  $D_O$  and  $D_R$  are the diffusion coefficients and  $n$  is the number of electrons in the half reaction.)

Equation 6.1

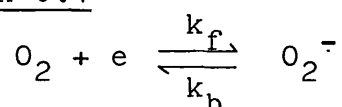
$$E_{\frac{1}{2}} = E^{\circ} + (RT/nF) \ln(D_R/D_O)^{\frac{1}{2}}$$

N.B. Because  $D_O \sim D_R$ ,  $E_{\frac{1}{2}}$  is usually within a few mV of  $E^{\circ}$ .

Taking the reduction of oxygen as an example of a reversible reaction [Reaction 6.1], the ratio of

the surface concentrations of oxidised ( $O_2$ ) and reduced ( $O_2^-$ ) constituents as calculated from the Nerst equation for a given potential differs insignificantly from the actual ratio. In other words the electron transfer at the electrode surface is so rapid that equilibrium

Reaction 6.1



conditions are maintained even with a substantial net current and a rapidly changing potential. The criteria of reversibility over a given range of conditions can be seen in equation [6.2] and the values must be

Equation 6.2

$$\Delta E_p = E_{pa} - E_{pc} \approx 57/n \text{ mV}$$

$$E_{p\frac{1}{2}} - E_{pc} = 57/n \text{ mV}$$

independent of scan rate and concentration. The  $E_{\frac{1}{2}}$  is situated exactly (within  $57/n$  mV) midway between  $E_{pa}$  and  $E_{pc}$ . Slow electron transfer at the electrode surface ("irreversibility") causes the peak separation to increase. The reduction of oxygen is also diffusion-controlled (no other process limits the current). The criterion for diffusion is that  $ip_c/v^{\frac{1}{2}}$  must be constant ( $v$ , sweep rate). This is true for planar electrodes.

However, spherical electrodes will show significant positive deviations (10%) when  $(D_0 RT/nFv r^2)^{1/2} \geq 0.1$  ( $r$ , electrode radius). If the reaction is also reversible, the dimensionless group  $ip_c \ln FAC_0 (D_0 nFv/RT)^{1/2}$  will equal 0.446 ( $A$ , electrode area,  $C_0$ , concentration of the reactant). An irreversible reaction will give as much as a 50% reduction in the magnitudes of the current function.

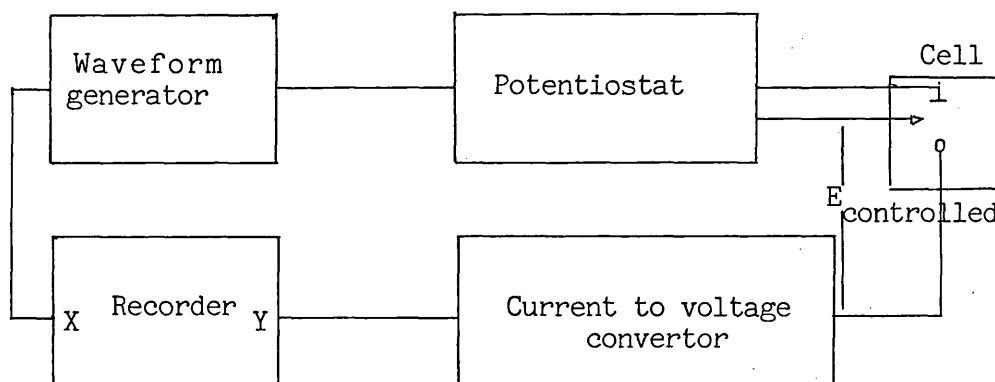
The electron transfer processes are fast for a thermodynamically reversible system and have no influence on the shape of the voltammogram. If the electron transfer processes are slow, the shape of the voltammogram is affected when the voltammogram is less steep and the system is said to be irreversible. The reason for this could be that the electroactive species diffusing to the working electrode from the solution are not being reduced or oxidised fast enough at the electrode surface. Alternatively the oxidised species may be reacting to form other products, which are not reducible.

If a voltammogram is irreversible, its half wave potential is not equal to the formal electrode potential.

6.2 INSTRUMENTATION

Cyclic voltammetry requires (i) a waveform generator to produce the excitation signal, (ii) a potentiostat to apply this signal to the electrochemical cell, (iii) a current-to-voltage convertor to measure the resulting current and (iv) an x,y recorder to display the voltammogram [Diagram 6.3]. The potentiostat ensures

Diagram 6.3



○ working

+ auxiliary

- reference

that the working electrode potential will not be influenced by the reaction which takes place.

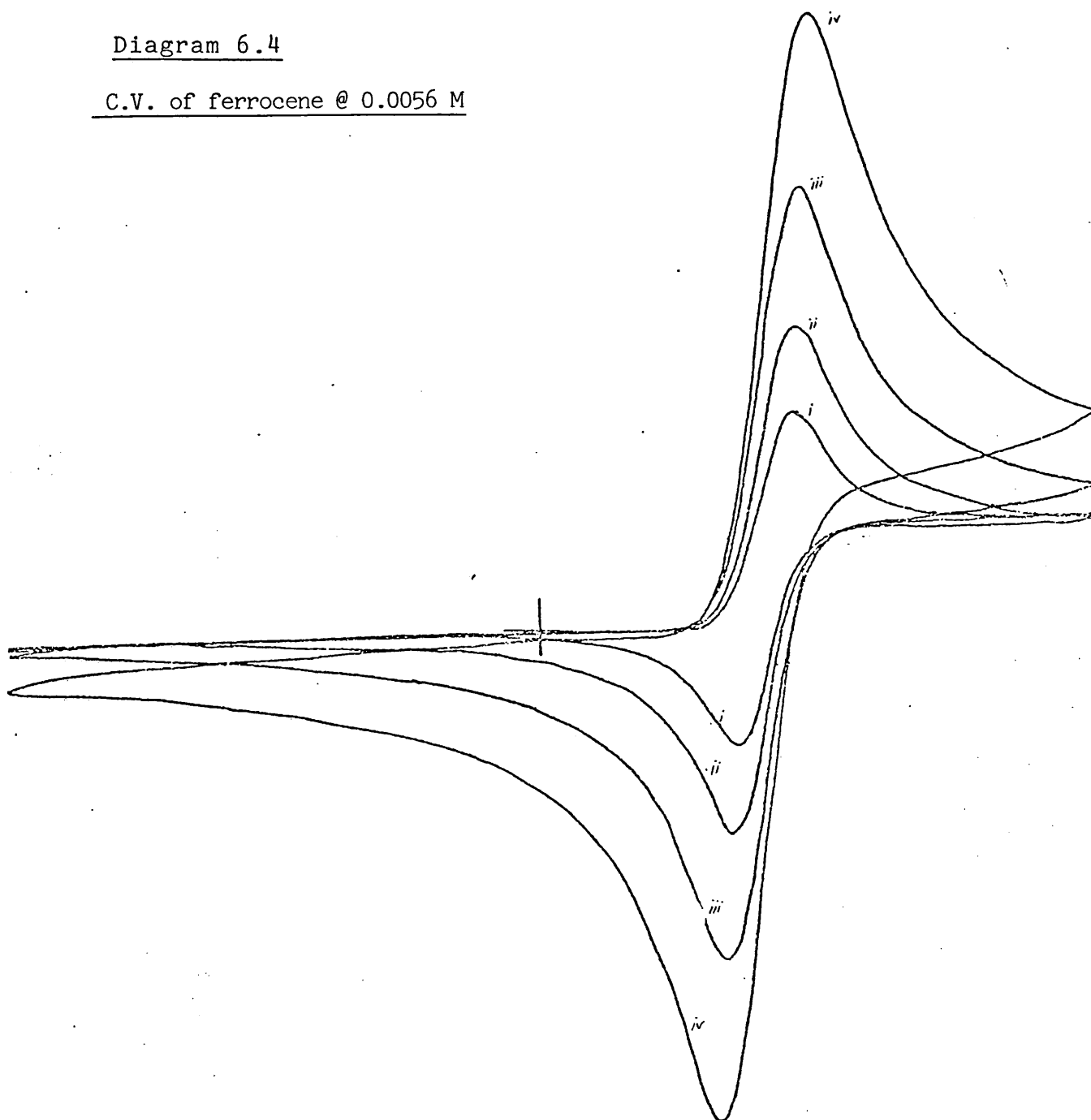
The reference electrode used in the following voltammograms was the saturated calomel electrode S.C.E. (+0.244V). All measurements were made at room temperature ( $22 \pm 2^\circ\text{C}$ ) and no correction was made for temperature variation. (The S.C.E. varies linearly by 0.5 mV per  $^\circ\text{C}$  from  $20^\circ\text{C}$  to  $30^\circ\text{C}$ ). Dry, HPLC grade acetonitrile was used as the solvent for all samples and this was periodically checked for purity.

Tetrabutylammonium perchlorate and tetraethylammonium perchlorate (0.1 M solutions in acetonitrile) were used as the base electrolytes. The sample solution was deoxygenated with dry nitrogen before each sample was run and 1 cm<sup>3</sup> platinum working and auxiliary electrodes were used. After each run the S.C.E. was washed and the working and auxiliary electrodes were cleaned by immersion in concentrated nitric acid and then washed and dried.

### 6.3 RESULTS AND DISCUSSION

The concentration dependence of the cyclic voltammetry of ferrocene was initially investigated by Dr. E.A. Seddon et al., University of Sussex in order to establish the optimum conditions of the concentration and scan speed. (Samples of metallocenes prepared in this thesis were also sent to Dr. E.A. Seddon who ran cyclic voltammograms as a blind, to check that the results obtained on our basic equipment were reasonable). Solutions of ferrocene at 0.1400, 0.0280, 0.0056 and 0.0011 mols l<sup>-1</sup> were run at scan speeds of 250, 100, 50 and 25 mVs<sup>-1</sup> [Table 6.1].

Diagram 6.4

C.V. of ferrocene @ 0.0056 M

Sweep Rate

i	$250 \text{ mV}^{-1}$
ii	$100 \text{ mV}^{-1}$
iii	$50 \text{ mV}^{-1}$
iv	$25 \text{ mV}^{-1}$

Table 6.1

Molarity mols s l <sup>-1</sup>	Scan Speed mVs <sup>-1</sup>	Peak to peak separation mV	Halfwave potential* mV
0.1400	250	490	435
	100	330	435
	50	270	435
	25	216	438
0.0280	250	170	390
	100	144	392
	50	120	395
	25	100	395
0.0056	250	100	400
	100	80	400
	50	70	400
	25	60	400
0.0011	250	74	397
	100	54	397
	50	50	395
	25	46	395

\*versus the standard calomel electrode.

From these results it was seen that the peak-to-peak separation and current (i.e. height of the peaks), varied with the concentration of the ferrocene and with the scan speed. The ferrocene solution of concentration 0.0056 M run at 50 mVs<sup>-1</sup> produced the optimum cyclic voltammogram [Diagram 6.4]. This represented a compromise between a reasonable scan speed and acceptable peak-to-peak separation, (found 70 mV, theoretical value for a one-electron change 57 mV). Subsequent voltammograms run on the rather basic apparatus at Bedford College never produced such an accurate result with regard to



the peak-to-peak separation. However, voltammograms were run with a scan speed of  $20 \text{ mVs}^{-1}$  and the best peak-to-peak separation was found to be 100 mV.

All voltammograms were run against a reference which was either ferrocene or tris(2,4-Pentanedionato) ruthenium(III)  $[\text{Ru}(\text{acac})_3]$ . The disubstituted ferrocene complexes were found to have their peaks too close to those of  $[\text{Ru}(\text{acac})_3]$  for the peaks to be resolved, hence ferrocene was used as the reference for these compounds.

The oxidation potentials of some metallocenes were investigated by cyclic voltammetry and the results may be seen in Table [6.2].

The redox potentials of the substituted ferrocenes appear to correlate with the electron withdrawing and releasing properties of the substituents. This can clearly be seen in the series: ferrocene,  $\beta$ -ferroceneacrylic acid and ferrocene propionic acid. One would expect ferrocene propionic acid to be more difficult to oxidise than ferrocene due to presence of the electron withdrawing carboxyl group. However, since this functional group is two saturated carbons away from the cyclopentadienyl ring the effect is greatly reduced and only a difference of 0.01V is seen. The difference between ferrocene and  $\beta$ -ferroceneacrylic acid is much larger, 0.13V. This is due to the presence of the double bond which provides a conjugative pathway between the ferrocene

moiety and the carboxyl group and therefore gives a much larger electron withdrawing effect.

The difference between the monocyclic (N-phenyl-amides) and bicyclic amides 38, 39 0.16V and 0.17V reflects the sensitivity of the ferrocene oxidation potential to the nature and orientation of the amide substituent. It follows that a change in the redox potential of the metallocene in a metallocene macrocycle may be expected upon formation of a complex with a metal ion due to the withdrawal of charge from the host ligand by the guest cation and any conformational change involving the amide group.

A series of chlorinated ferrocenes and decamethyl ferrocene was also prepared as part of this project in order to examine the effects of extreme cases of electron withdrawing and *don*-ating groups. Samples of each of these compounds were sent to the University of Sussex but as yet no results have been obtained.

In Chapter 7.4 there is a further discussion of the electrochemical data so far obtained with a view to their possible correlation with the photoelectron spectroscopy and  $\sigma$  Hammett values for these compounds.

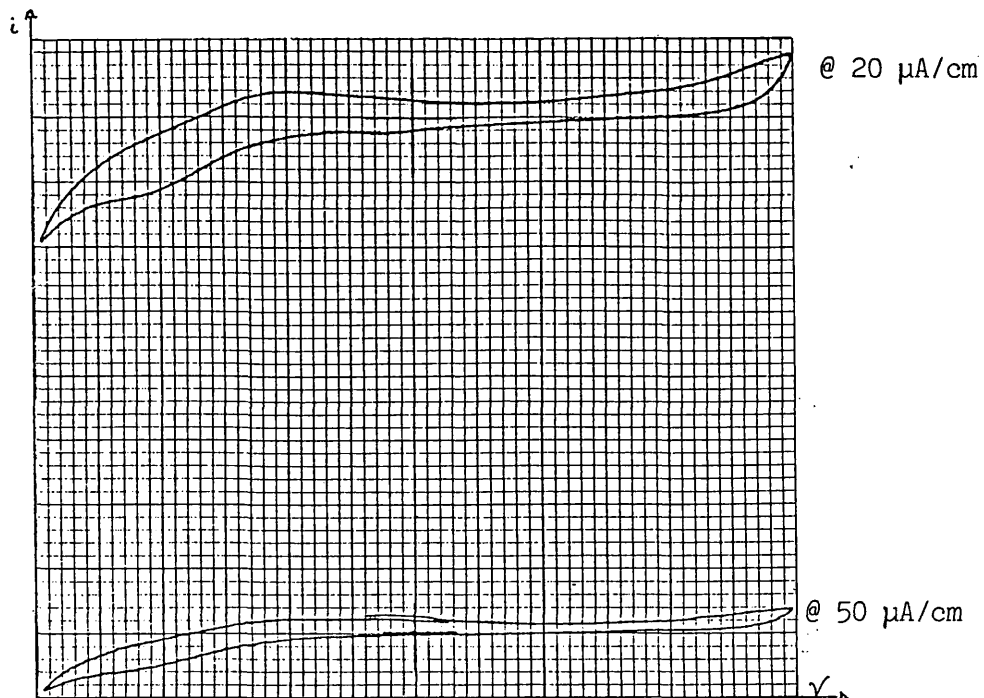
Table 6.2

COMPOUND	$E_{1/2}/V(\text{vs. S.H.E.})$
Ferrocene	0.39
1-Acetyl ferrocene	0.64 <sup>b</sup>
1,1'-Diacetyl ferrocene	0.87 <sup>a</sup>
1,-Methyl ferrocene carboxylate	0.64 <sup>b</sup>
1,1'-Dimethyl ferrocene dicarboxylate	0.79 <sup>a</sup>
Ferrocene[2.2]cryptand monomer (38)	0.64 <sup>a</sup>
Ferrocene[2.2]cryptand dimer (39)	0.63 <sup>a</sup>
Formyl ferrocene	0.68 <sup>b</sup>
$\beta$ -Ferrocene acrylic acid	0.52 <sup>b</sup>
Ferrocene propionic acid (36)	0.40 <sup>b</sup>
cp. Fe cp. CO.CH <sub>2</sub> CH <sub>2</sub> CO <sub>2</sub> H	0.62 <sup>b</sup>
1,1'-Ferrocene dicarboxylic acid, morpholide (62)	0.66 <sup>a</sup>
0,0'-(1,1'-ferrocenediamido)1,5-diphenoxy-3-oxapentane <sup>34</sup>	(0.8) <sup>a</sup>
0,0'-(1,1'-ferrocenediamido)-1,8-diphenoxy-3,6-dioxaoctane <sup>34</sup>	(0.8) <sup>a</sup>
Ruthenocene	0.84

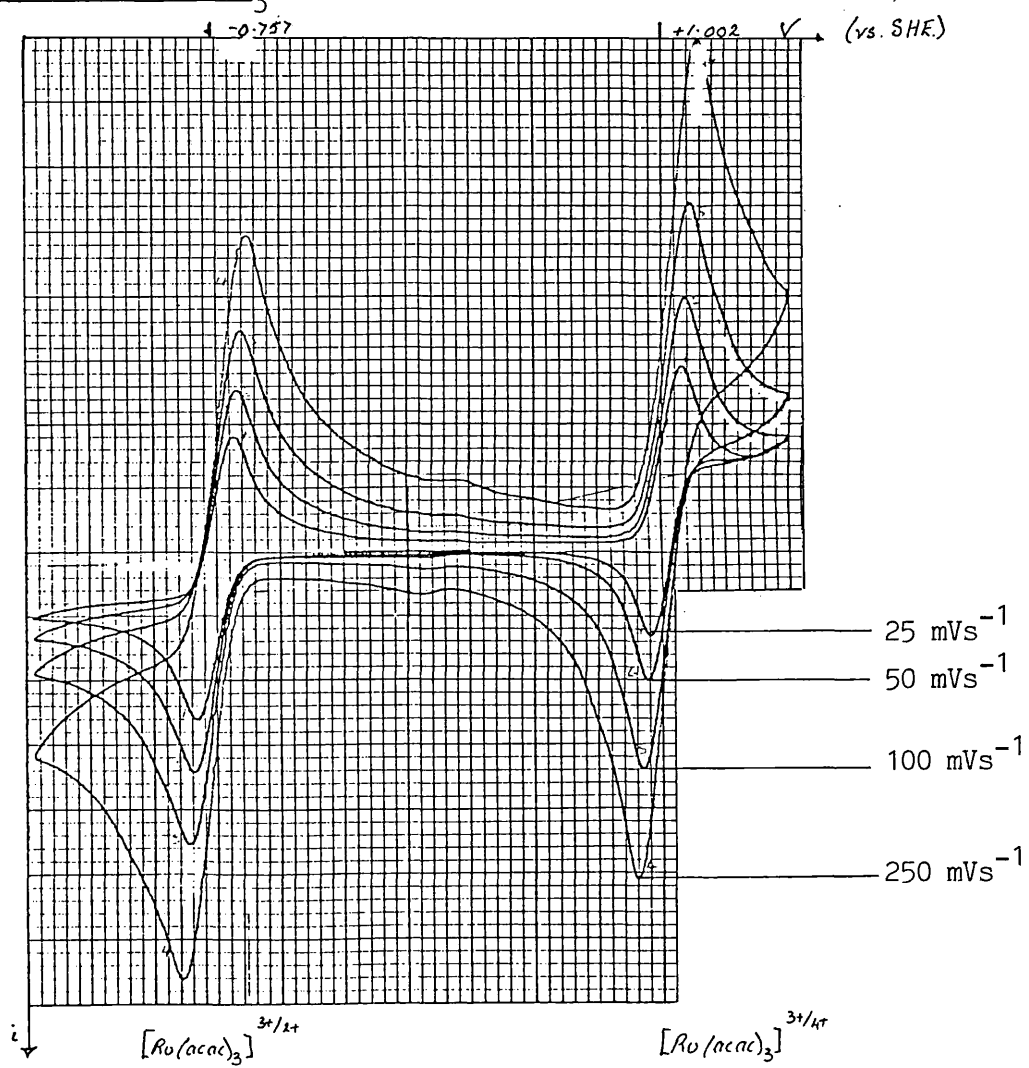
<sup>a</sup>Corrected using ferrocene

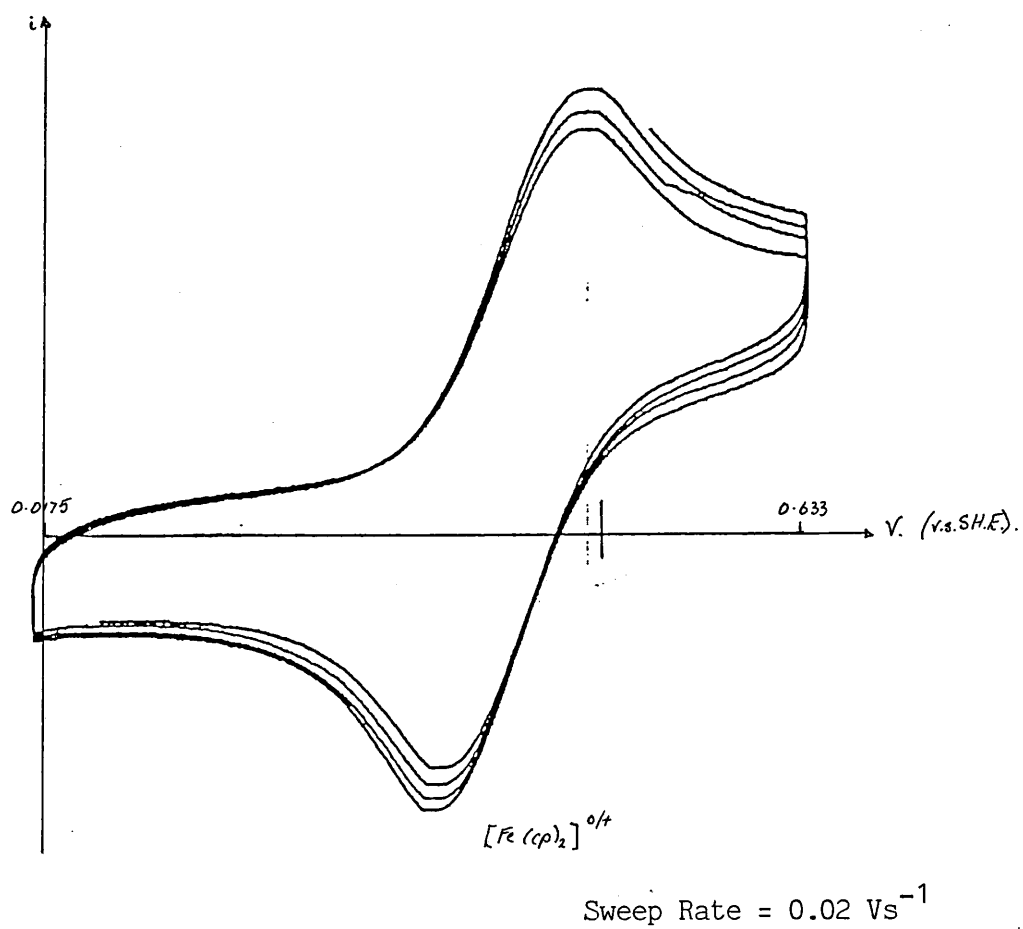
<sup>b</sup>Corrected using Ru(acac)<sub>3</sub>

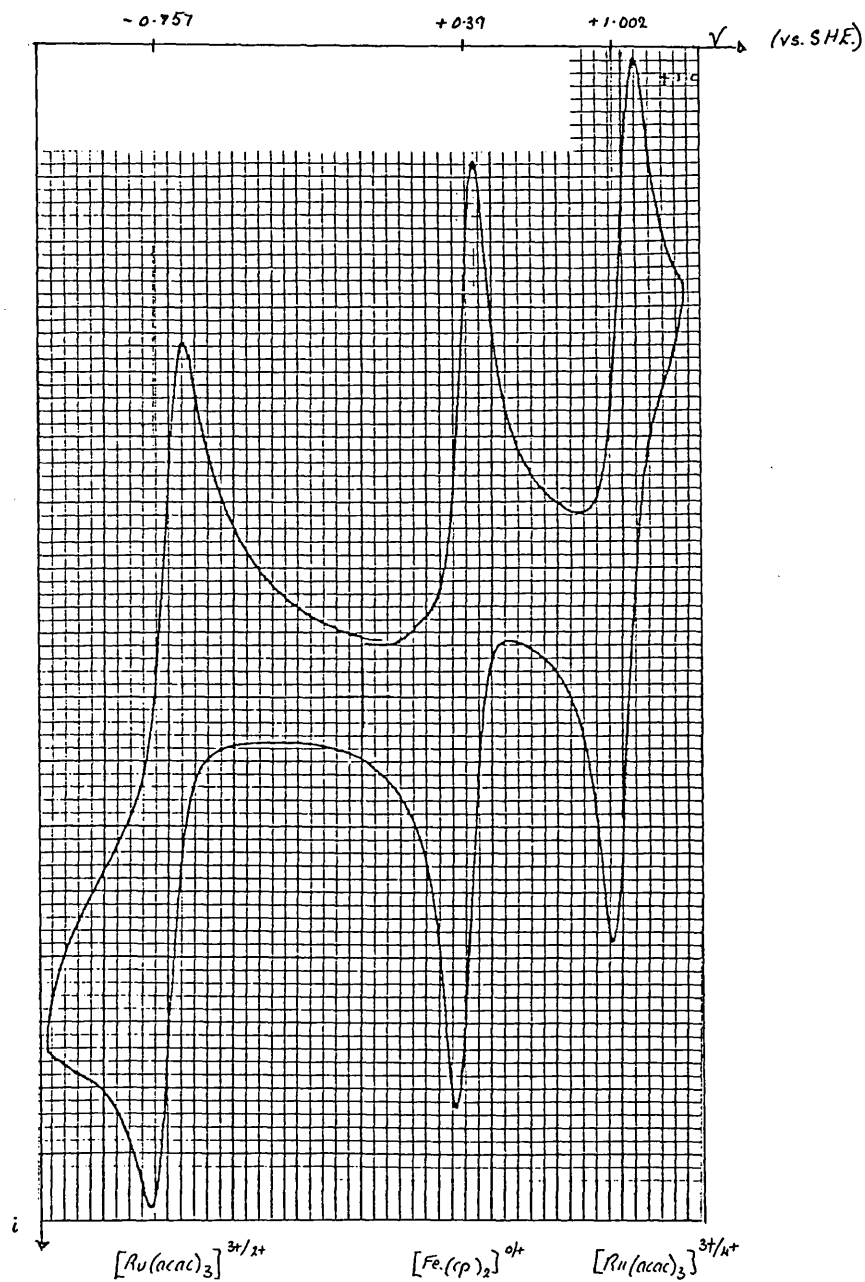
C.V. of solvent/o.1 M  $\text{Et}_4\text{NClO}_4$  in acetonitrile

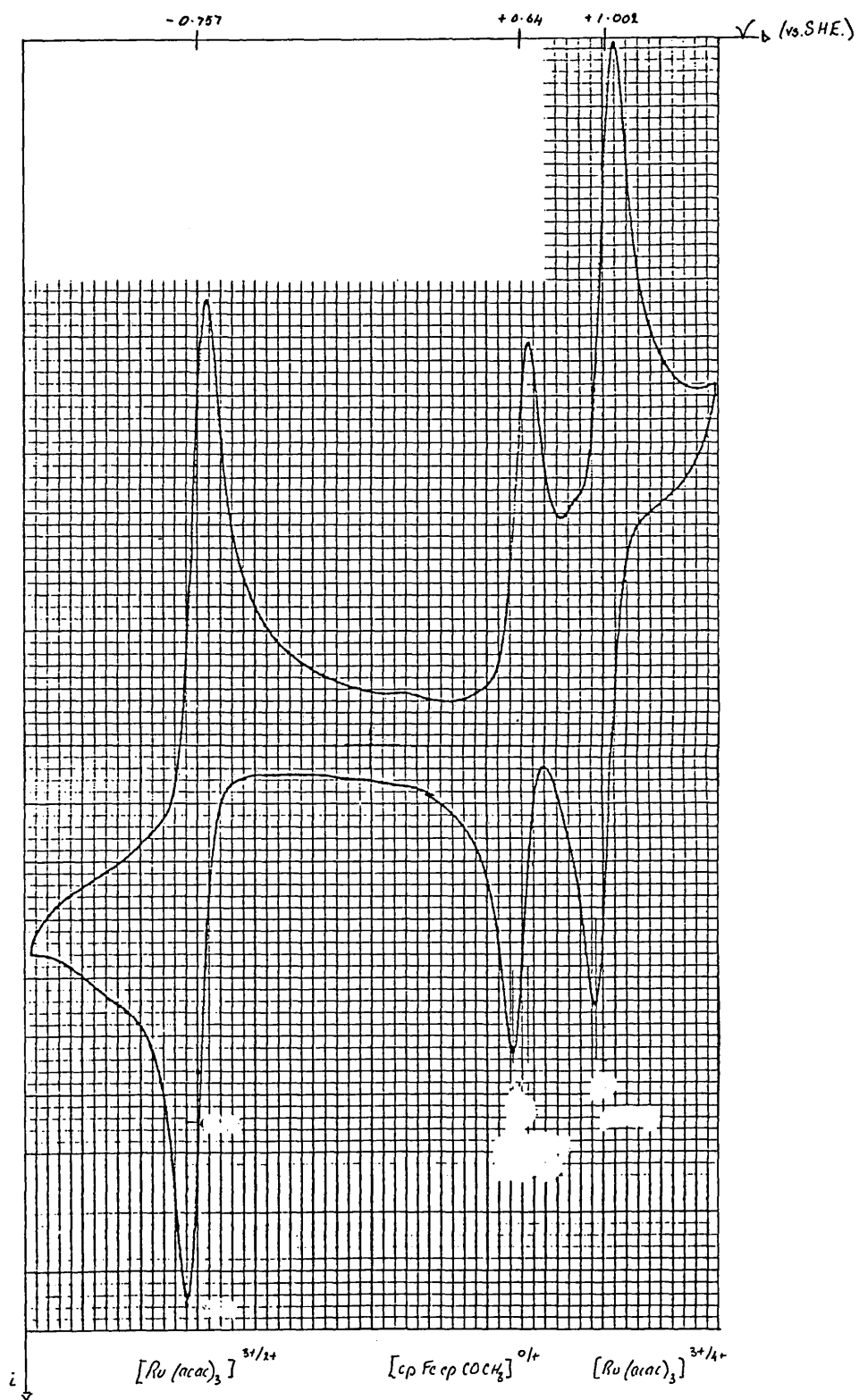


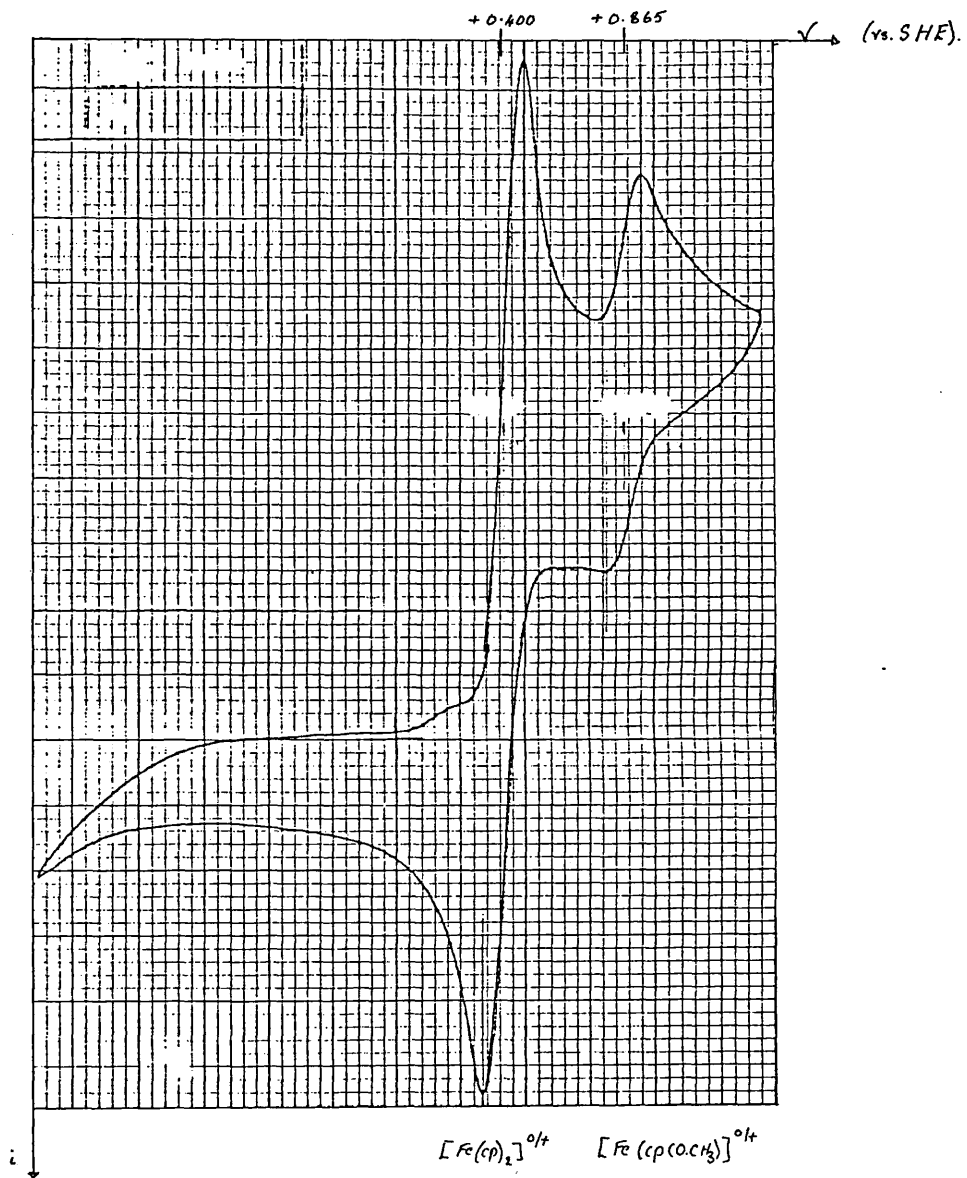
C.V. of  $\text{Ru}(\text{acac})_3$



C.V. of ferrocene

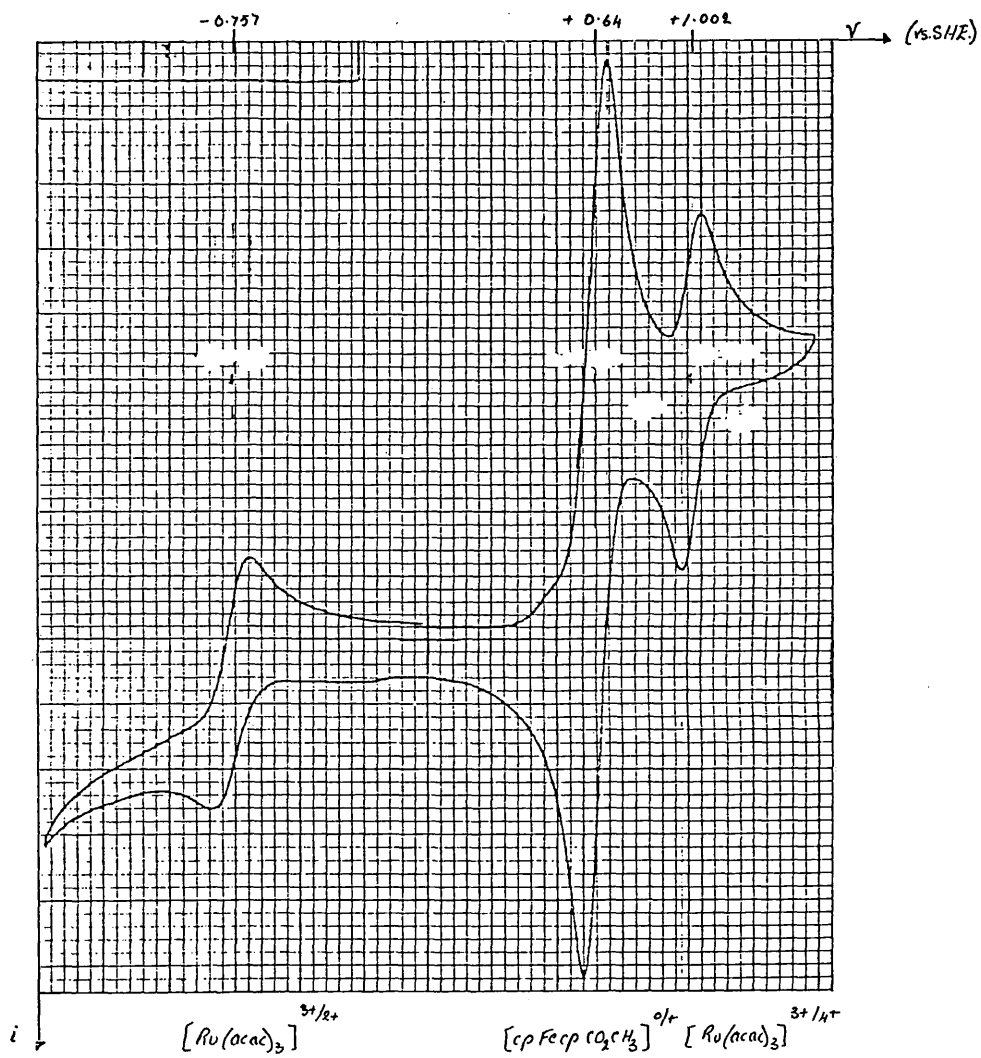
C.V. of ferrocene

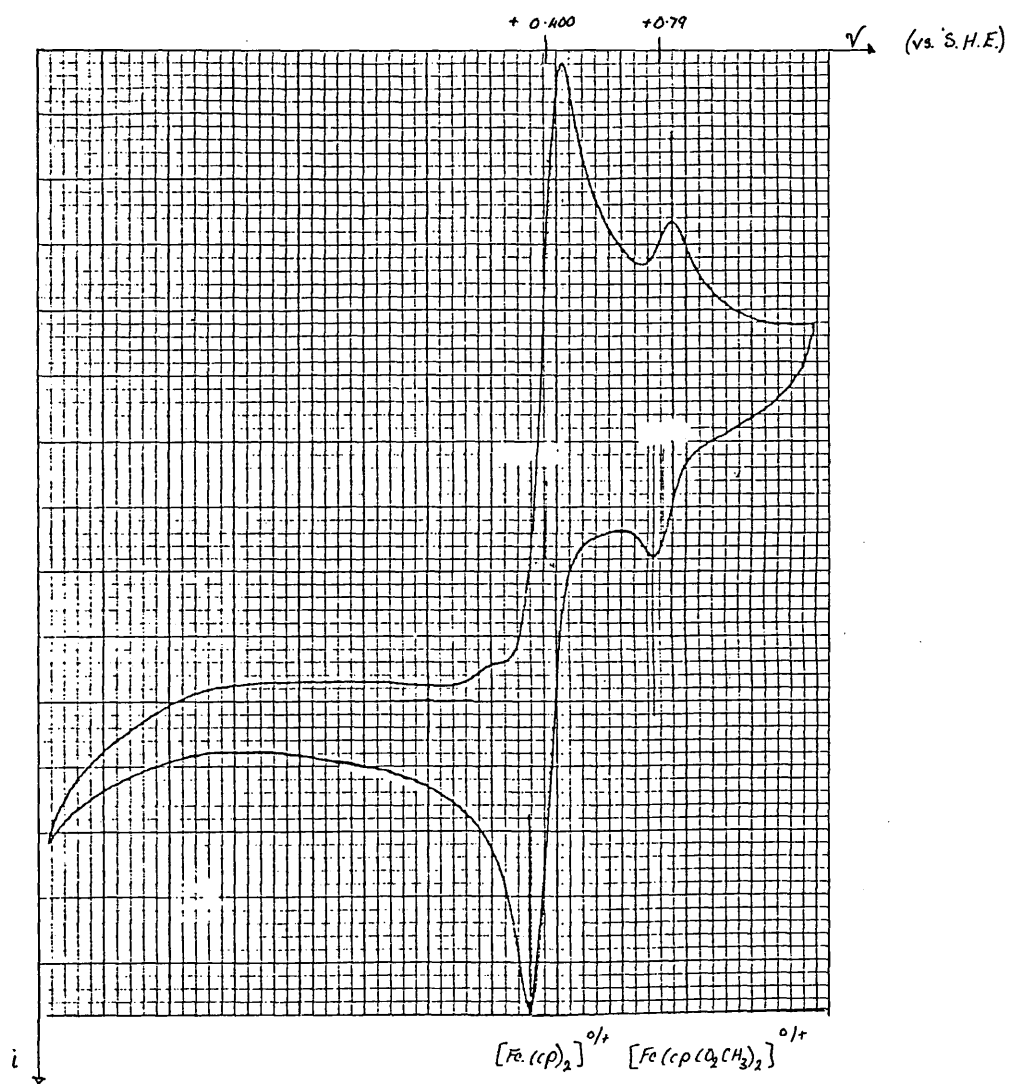
C.V. of 1-acetylferrocene

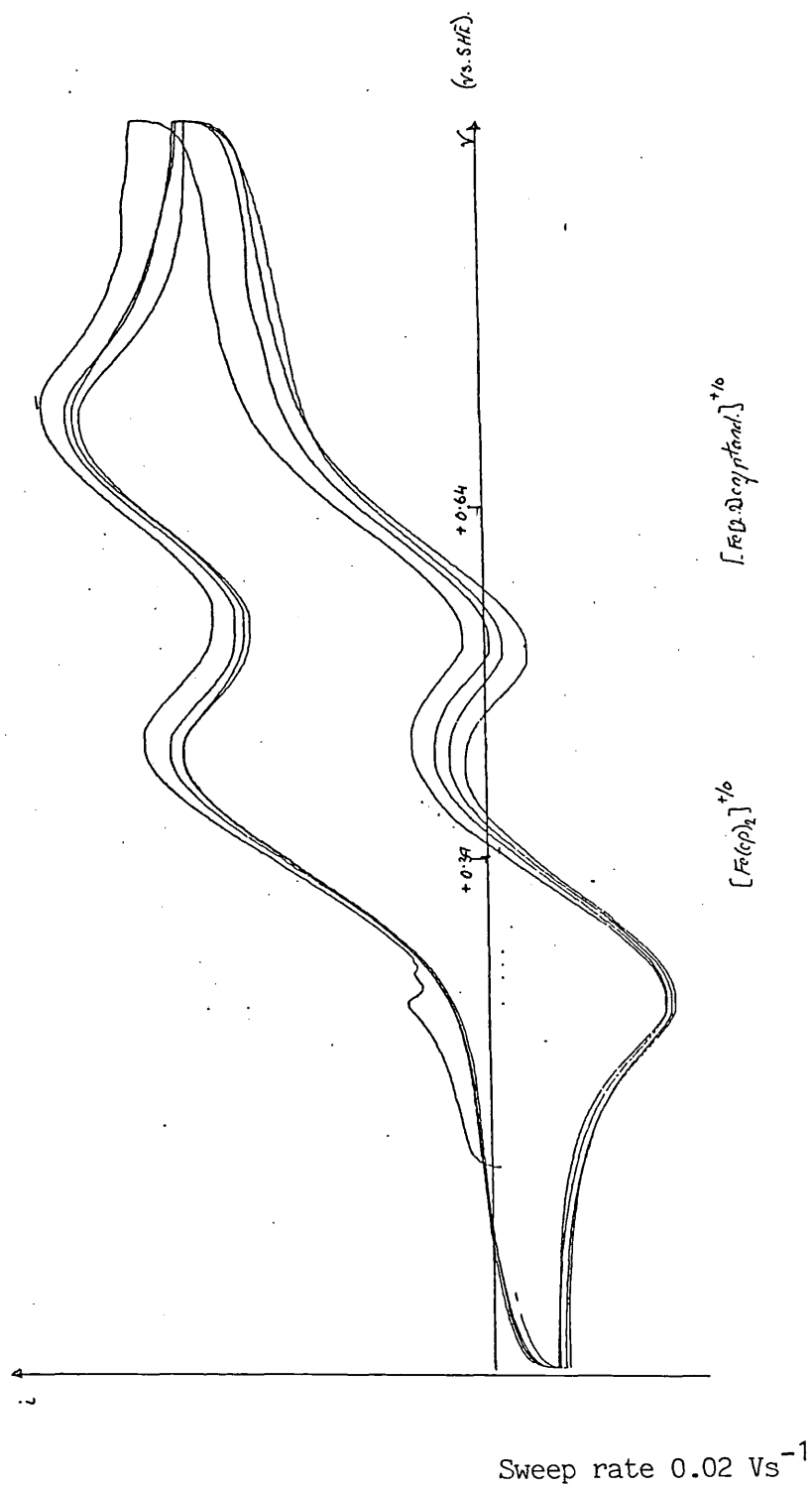
C.V. of 1,1'-diacetylferrocene

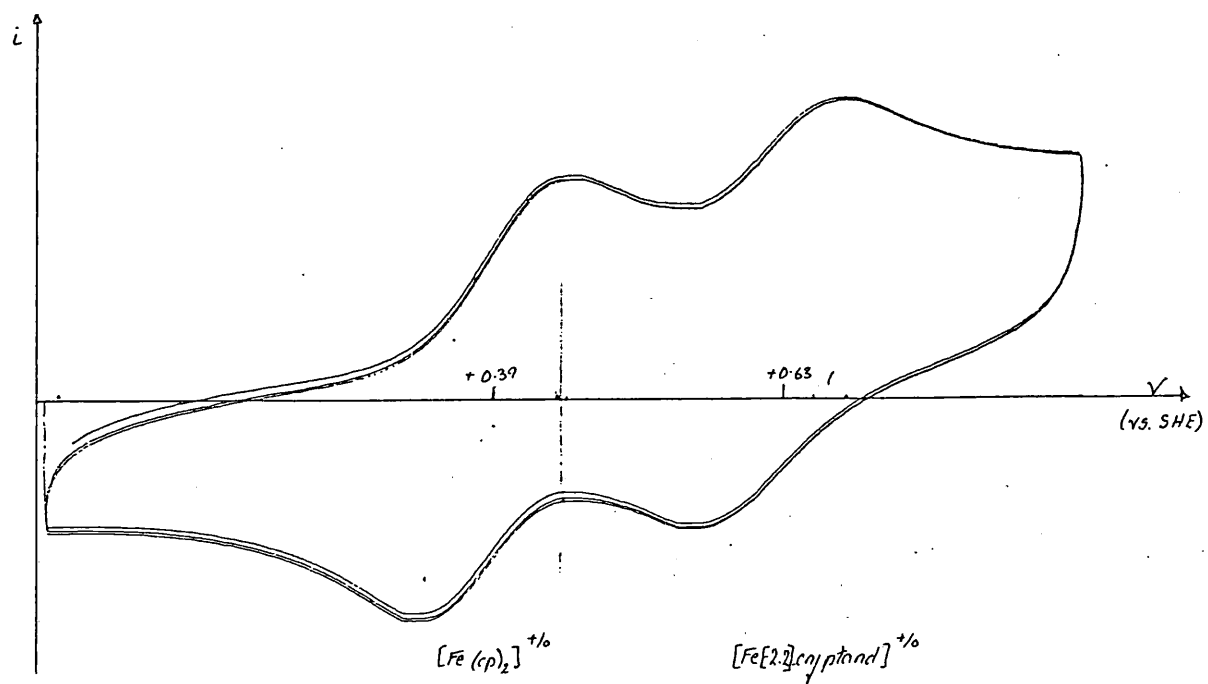


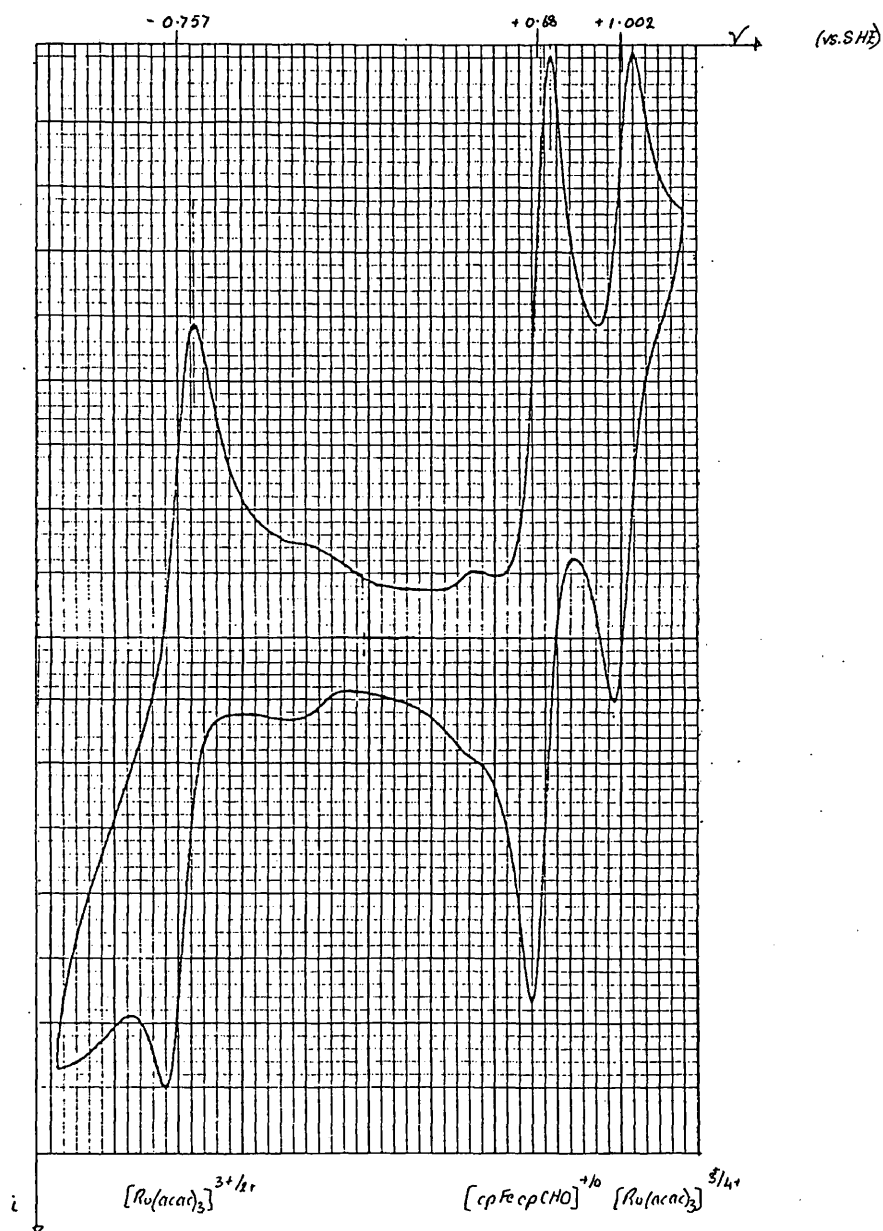
## C.V. of 1-methylferrocene carboxylate

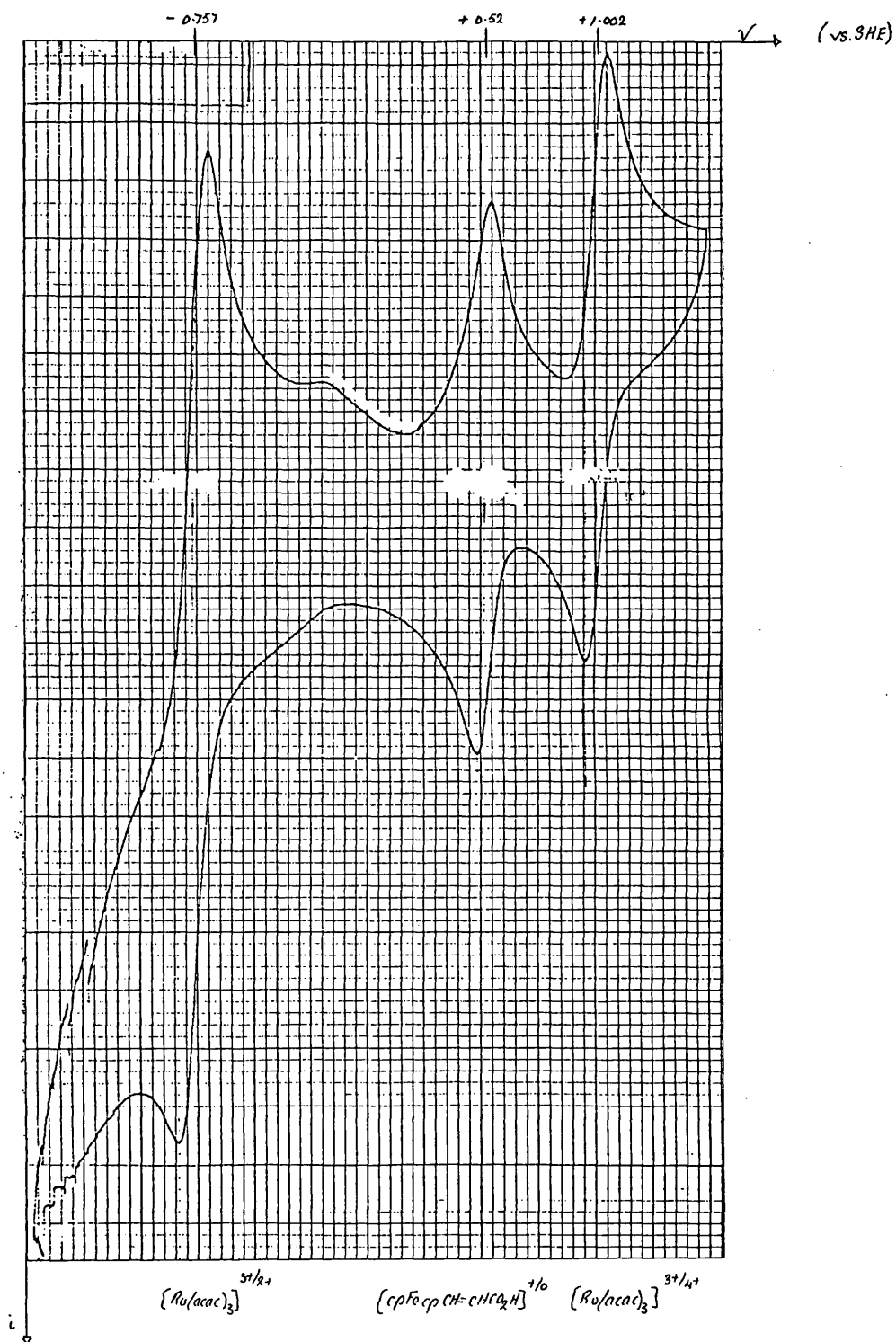


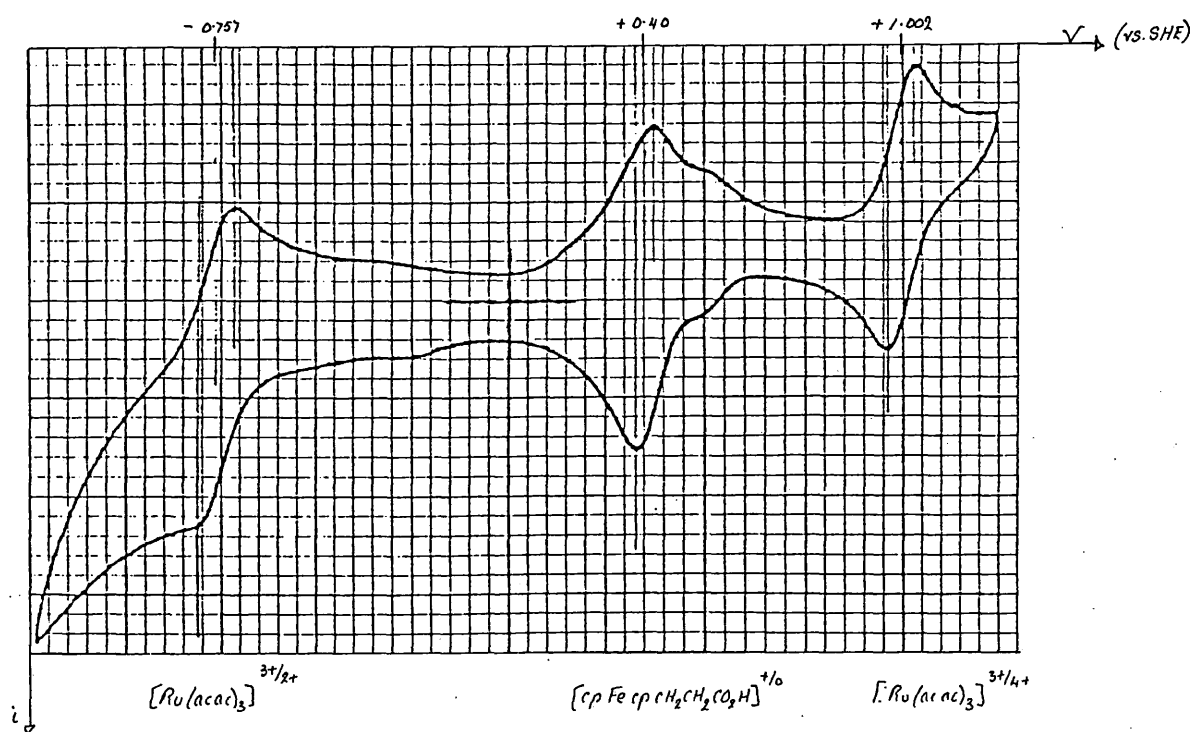
C.V. of 1,1'-Dimethylferrocene dicarboxylate

C.V. of ferrocene[2.2]cryptand (monomer) (38)

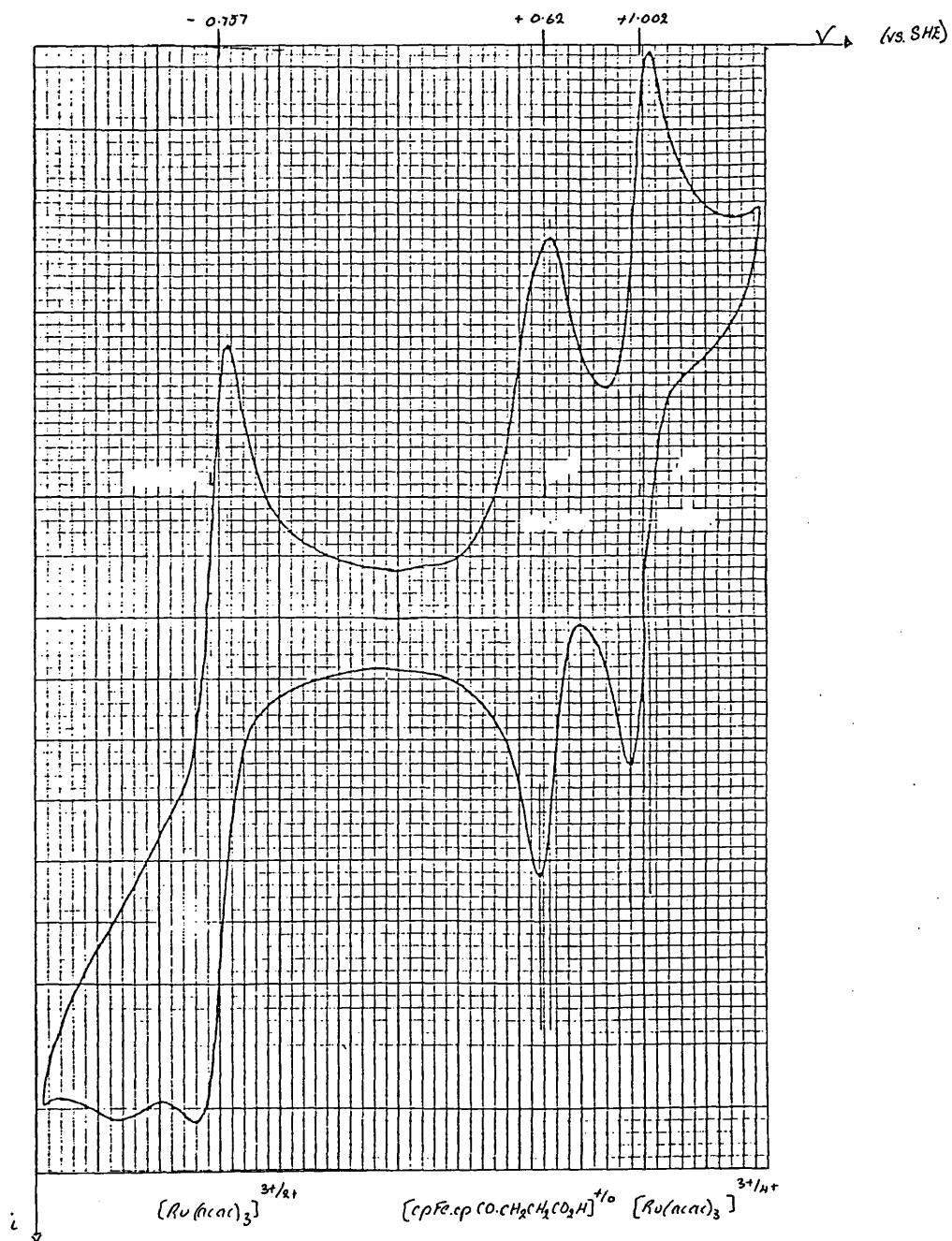
C.V. of ferrocene[2.2]cryptand (dimer) (39)Sweep rate  $0.02 \text{ Vs}^{-1}$

C.V. of formylferrocene

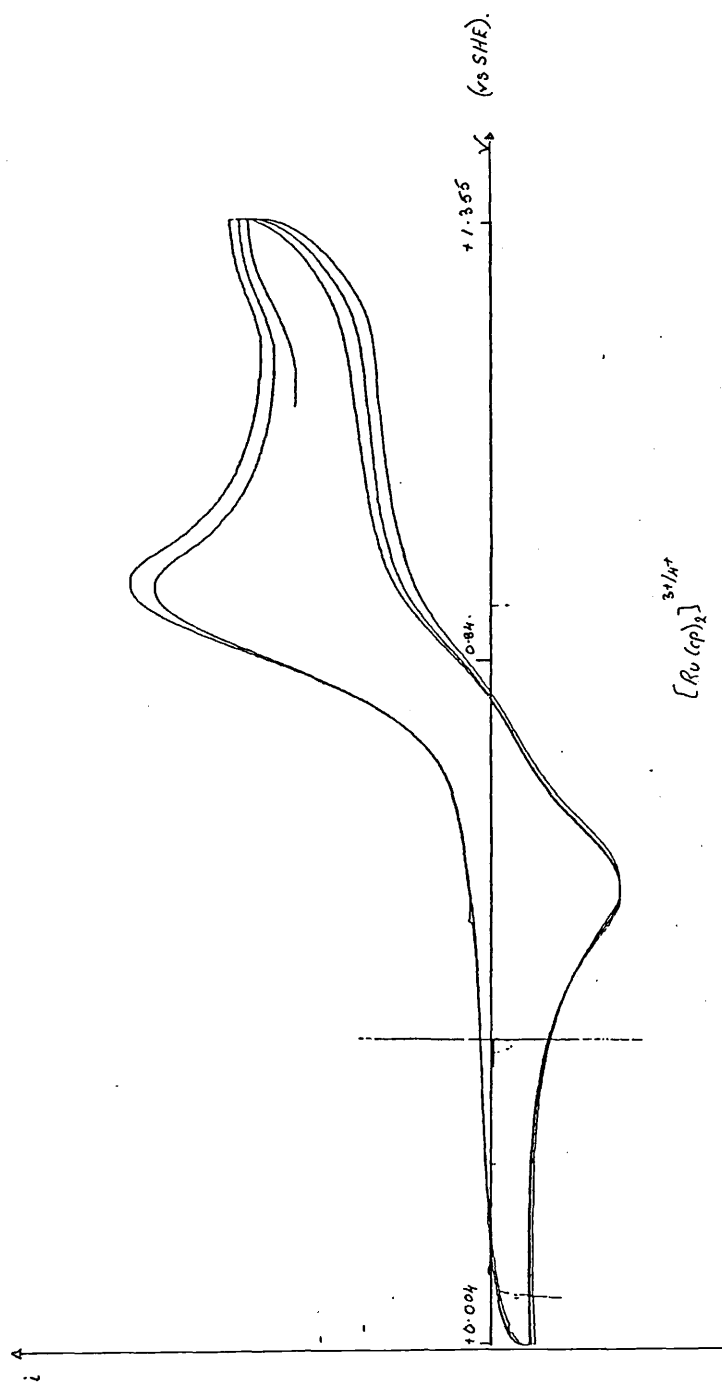
C.V. of  $\beta$ -ferroceneacrylic acid

C.V. of ferrocene propionic acid (36)

C.V. of  $\text{cp.Fe.cpCO.CH}_2\text{CH}_2\text{CO}_2\text{H}$





C.V. of ruthenoceneSweep rate  $0.01 \text{ Vs}^{-1}$

CHAPTER 7: PHOTOELECTRON SPECTROSCOPIC STUDIES OF SOME  
SUBSTITUTED FERROCENES

CHAPTER 7  
PHOTOELECTRON SPECTROSCOPIC STUDIES  
OF SOME SUBSTITUTED FERROCENES

7.1. INTRODUCTION

It is observed experimentally, that electrons are emitted by materials when they absorb high frequency electromagnetic radiation.<sup>178</sup> The photoionisation that occurs is usually a one photon to one electron event which obeys equation 7.1.

Equation 7.1

$$h\nu = \text{I.E.} + \text{K.E.}$$

$h\nu$  : energy of the photon  
 I.E. : ionisation energy of the electron  
 K.E. : kinetic energy of the electron

For any material, there is a minimum energy required to remove an electron. This is known as the threshold energy,  $h\nu_0$  and is equal to the first ionisation energy level.

Molecular orbital energy diagrams have a number of discrete features:

- i) a series of occupied energy levels where  $\epsilon < 0$  (0 refers to the vacuum level) i.e. energy of an electron an  $\alpha$  distance from ion.

- ii) empty levels having energy  $\epsilon < 0$
- iii) continuum energy levels with energy  $\epsilon \geq 0$ .

If an orbital is fully occupied, the orbital energy can be defined by equation 7.2.

Equation 7.2

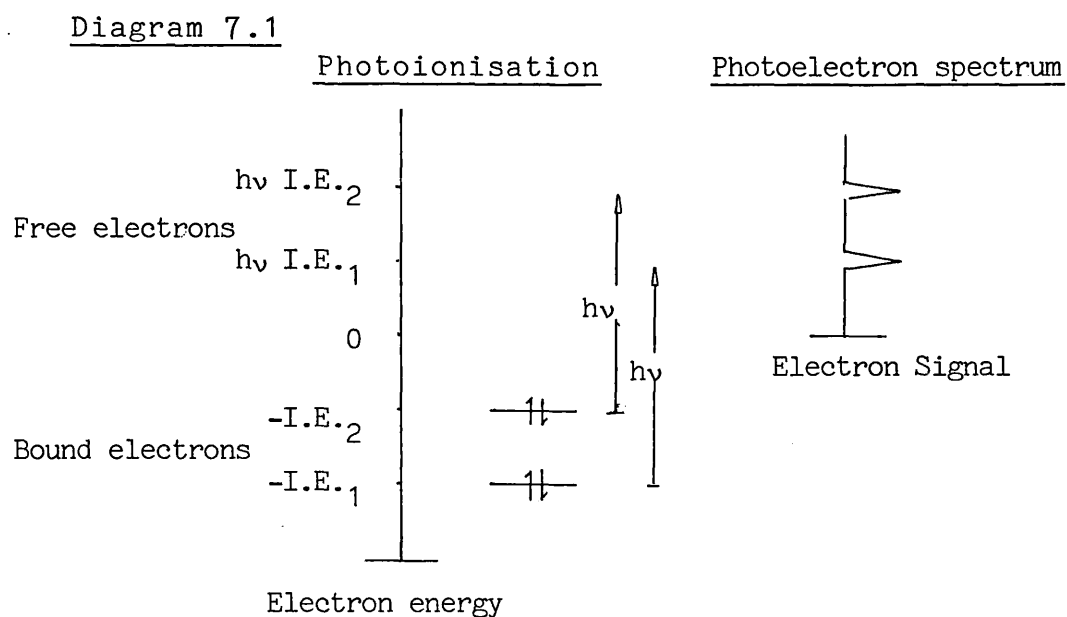
$$\epsilon_a = T_a + V_a + R_a$$

- $T_a$  : The kinetic energy of an electron in orbital a.
- $V_a$  : The potential energy of an electron in orbital a.
- $R_a$  : The repulsive energy of the other electrons in the system.

If it is assumed that photoionisation occurs without affecting the other orbitals in the system, then Koopmans has shown that:

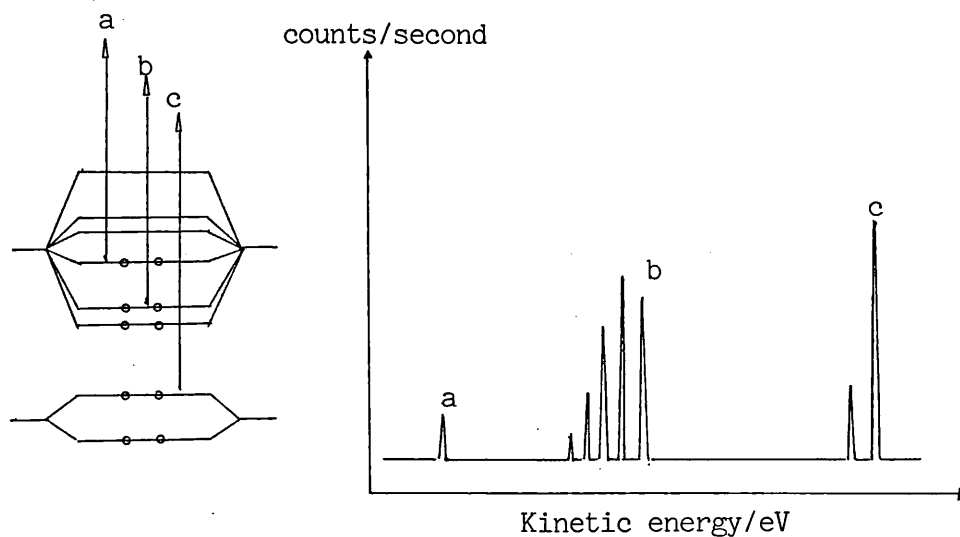
$$I.E_a = -\epsilon_a$$

If electromagnetic radiation of higher energy than  $h\nu_0$  is used, then the electrons that are emitted will have various kinetic energies, depending on the orbitals they occupied [Diagram 7.1]. Photoionisation thus gives electrons with a range of kinetic energies. As the allowed energy levels for a molecule are quantised, the allowed kinetic energies of the photoelectrons are discrete. Therefore the kinetic energy distribution mirrors the electronic energy levels.

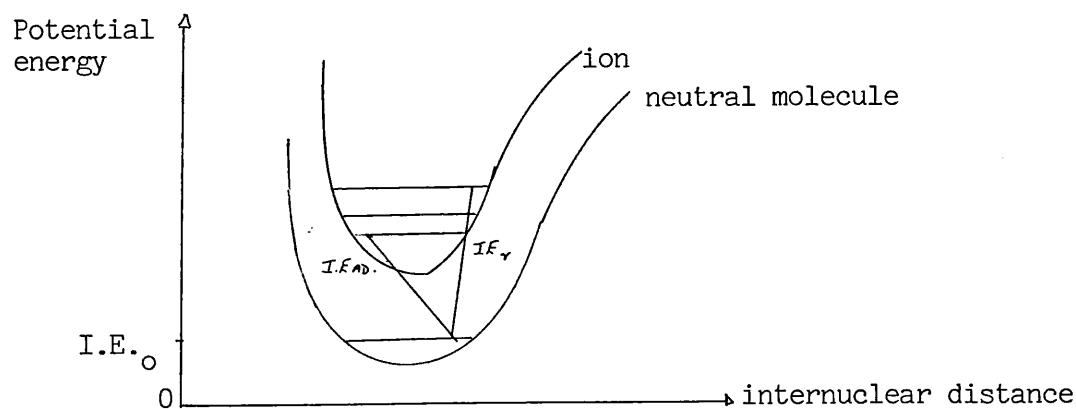


Photoelectron spectroscopy is the determination of the kinetic energy distribution of the photoelectrons, using a monochromatic source of radiation. In gas-phase studies, this is usually He-I (21.2 eV) or He-II (40.8 eV) radiation.

After ionisation, the photoelectrons are passed through an electrostatic analyser and deflected at angles dependent on their velocities and then recorded. Thus a photoelectron spectrum is a plot of the number of photoelectrons in a given time period against the ionisation energy or the kinetic energy. The main features of the spectrum can thus be interpreted in terms of molecular orbital theory [Diagram 7.2]. It should be noted that there are two types of ionisation energy that can be seen from a photoelectron spectrum. The adiabatic ionisation energy,  $I.E._{AD}$  is the difference in energy between the neutral molecule in its lowest electronic,

Diagram 7.2Photoelectron spectrum of  $N_2$  and its interpretation in terms of molecular orbital diagram

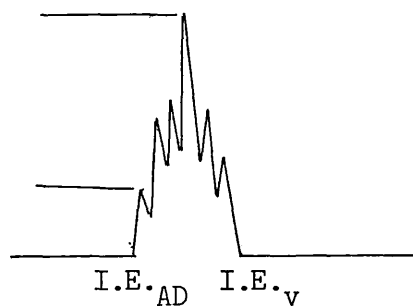
vibrational and rotational state and the ion in its equivalent state. The vertical ionisation energy, I.E., is the difference in energy between the neutral molecule in its ground state and the ion in a state where the nuclei are in the same positions as in the neutral molecule [Diagram 7.3].

Diagram 7.3Vertical and adiabatic ionisation energy changes

The vertical ionisation energy is the peak of maximum intensity in a photoelectron spectrum, while the adiabatic ionisation energy is represented by the peak of lowest intensity [Diagram 7.4].

Diagram 7.4

The vertical and adiabatic ionisation energies of a photoelectron spectrum



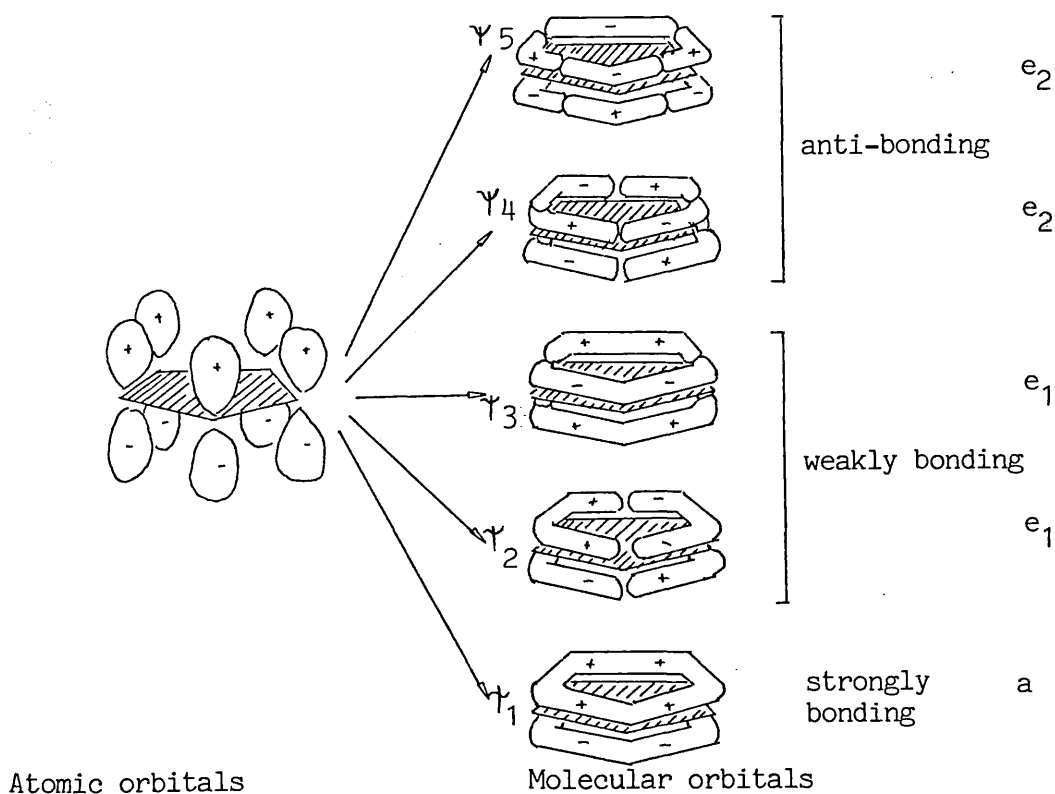
7.2 THE MOLECULAR ORBITAL BOND SYSTEM FOR FERROCENE

In the solid state, the cyclopentadienyl rings of ferrocene are staggered [Chapter 3.2] and the molecule has  $D_{5d}$  symmetry. However, in the solution and in the gas phase, the rings are free to rotate.

The p orbitals (the  $\pi$  molecular orbitals) of the rings are used for bonding of the cyclopentadienyl rings to the iron atom. Since there are five p orbitals on the ring, there are five molecular orbitals. The five molecular orbitals for the cyclopentadienyl ring are of three types, a (no nodes), e (one node) and  $e_2$  (two nodes) with the  $e_1$  and  $e_2$  orbitals being doubly degenerate. These five  $\pi$  molecular orbitals [Diagram 7.5] may be combined in a limited number of combinations

Diagram 7.5

The five molecular orbitals of the cyclopentadienyl ring. 179

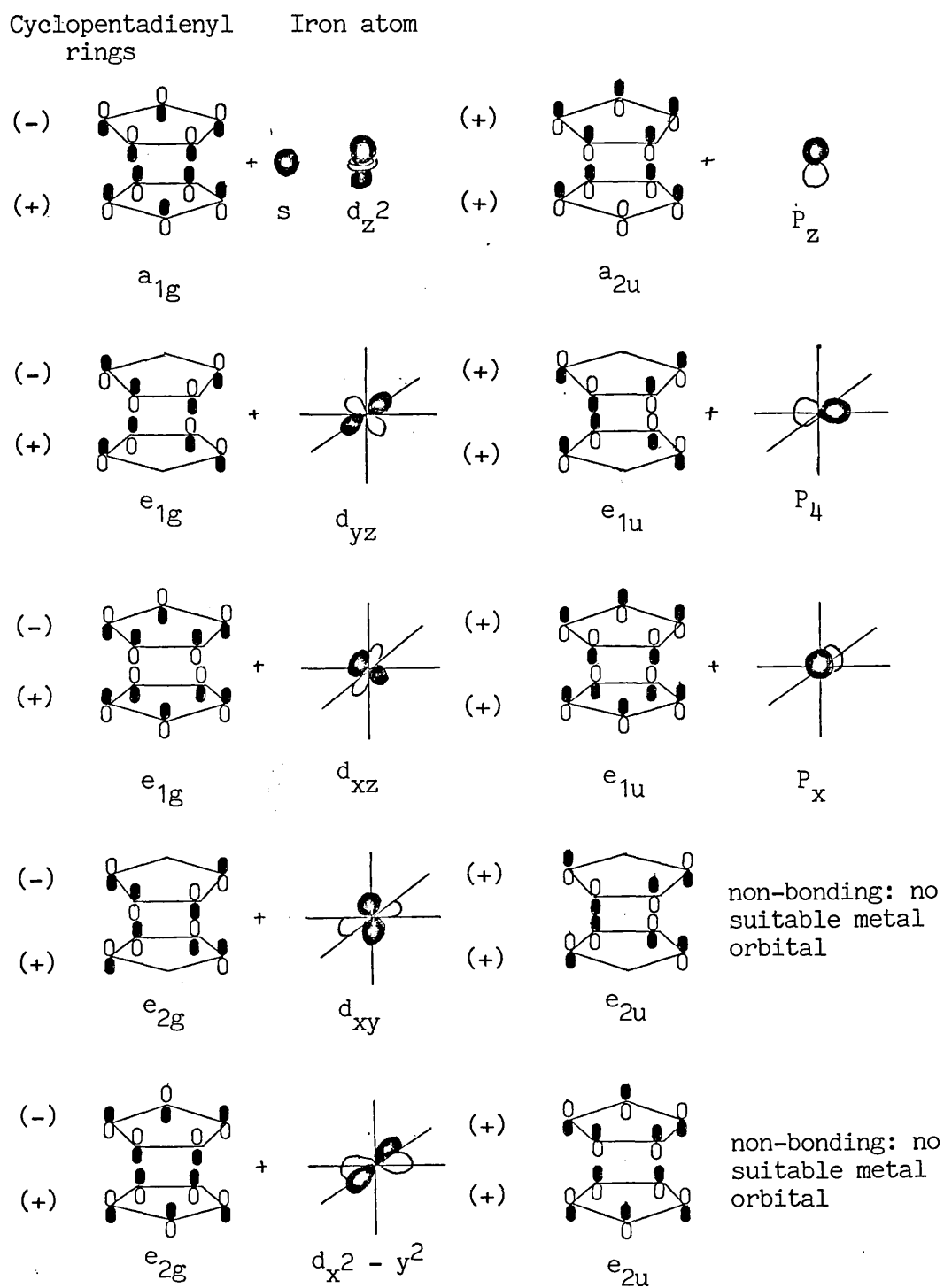




so that there is symmetry on inversion (g, gerade) or antisymmetry on inversion (u, ungerade). Thus ten molecular orbitals are produced [Diagram 7.6].

Diagram 7.6

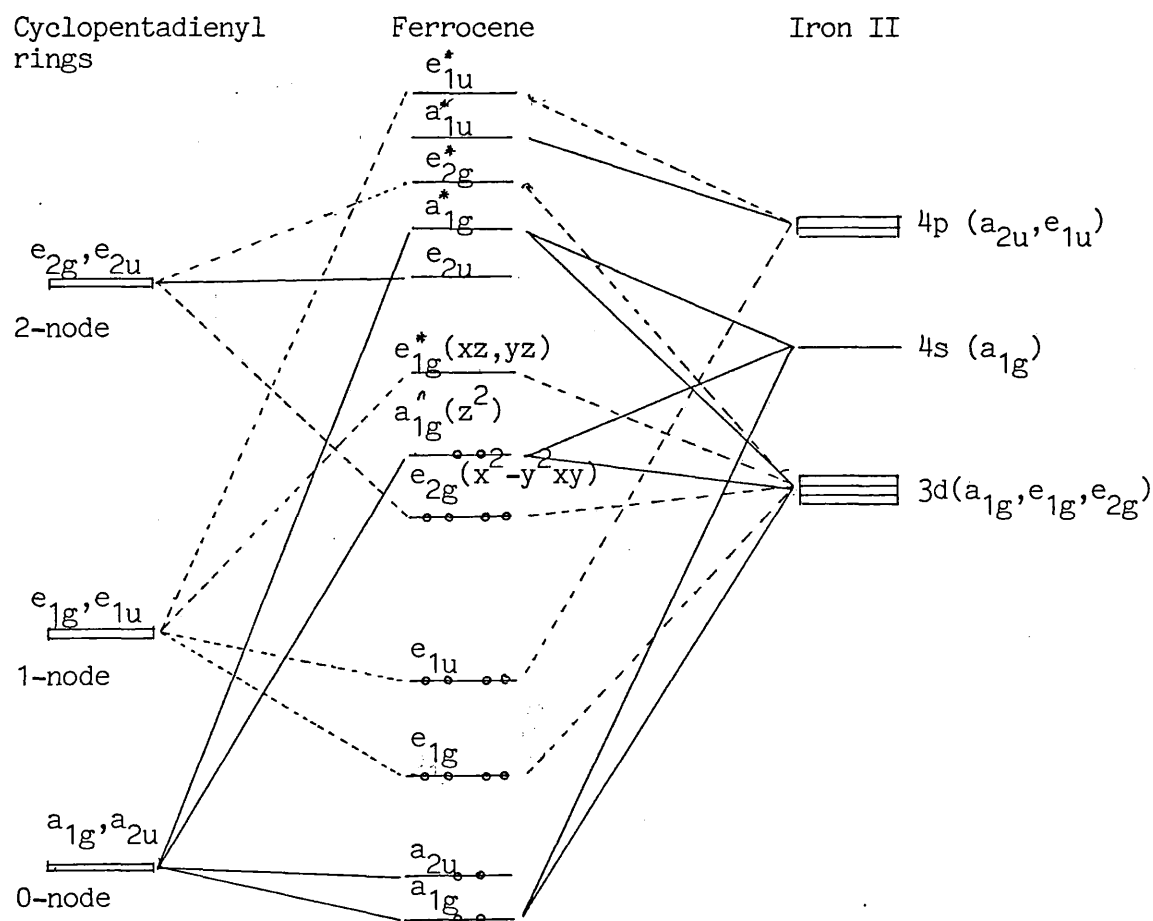
Ten symmetry orbitals of ferrocene



The molecular orbitals of the iron atom must now be considered to see which of them combines with the orbitals of the cyclopentadienyl rings [Diagram 7.6]. From this a qualitative molecular orbital diagram for ferrocene can be deduced [Diagram 7.7].

Diagram 7.7

The qualitative molecular orbital diagram for ferrocene<sup>180,181</sup>



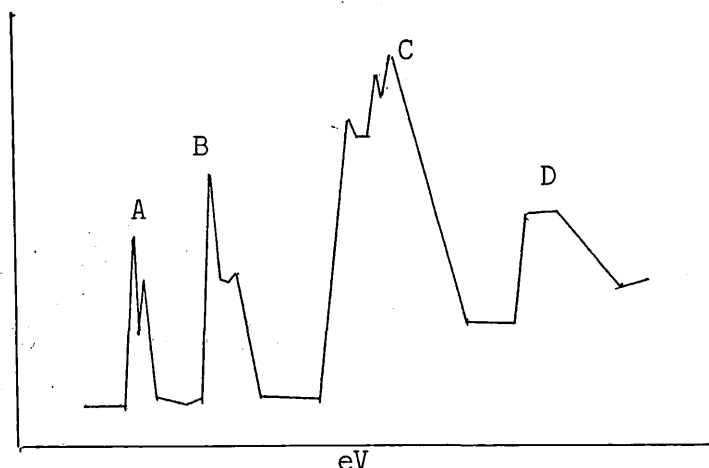
Ferrocene has eighteen valence electrons, six from each cyclopentadienyl ring and six from the iron II atom. When these eighteen electrons are placed in the

molecular orbital diagram, they fill the bonding and non-bonding orbitals while the antibonding orbitals are left empty.

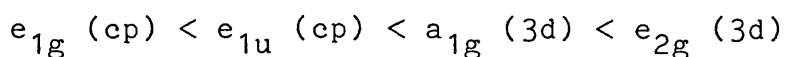
The photoelectron spectrum of ferrocene can be seen in Diagram 7.8. This spectrum has been interpreted

Diagram 7.8

The He(I) photoelectron spectrum of ferrocene



as follows: band A is due to the ionisation of the metal-localised  $e_{2g}$  orbital, band B is attributed to the ionisation of the essentially non-bonding  $a_{1g}$  metal orbital, bands C and D are due to the ionisation of the cyclopentadienyl orbitals  $e_{1u}$  and  $e_{1g}$ . These assignments imply that the molecular orbitals for ferrocene may be ordered in the molecular ground state as follows:



The discrepancies between the spectroscopically deduced energy level ordering and those predicted by Hartree-Fock calculations are thought to arise from relaxation effects. Whilst little electronic rearrangement occurs upon ionisation of the delocalised ligand  $\pi$ -type molecular orbitals, the localised metal molecular orbitals are thought to undergo much reorganisation.

A third set of energy level orderings has been obtained by electron spin resonance studies of the ferricenium cations.<sup>182,183</sup>

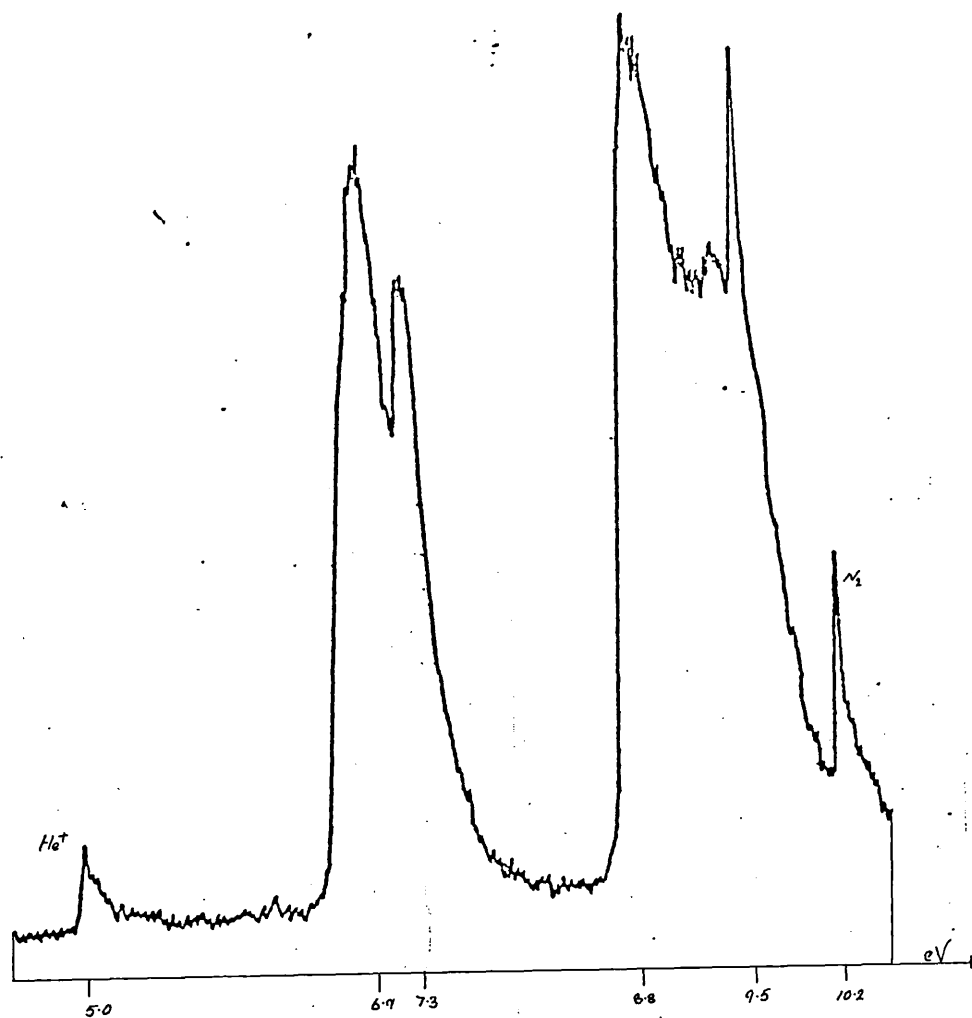
### 7.3 RESULTS AND DISCUSSION

Photoelectron spectra of a number of ferrocene derivatives [Table 7.1] were recorded by E.A. Seddon (University of Sussex) using a modified Perkin-Elmer PS16 spectrometer fitted with a Helectros lamp which could provide both He(I) and He(II) radiation. The first ionisation energies were deduced from the He(I) spectra, which were calibrated using the helium self-ionisation line (I.E. = 4.991 eV) and methyl iodide (I.E. = 9.538 and 10.165 eV). A low pressure of calibrant gas was mixed with the sample so that a spectrum of both species was recorded at the same time. Since all samples were air stable they were loaded into small phials and then inserted into the spectrometer. The resolution of the probe was checked periodically using Argon. Experimental conditions and results are summarised in Table 7.1.

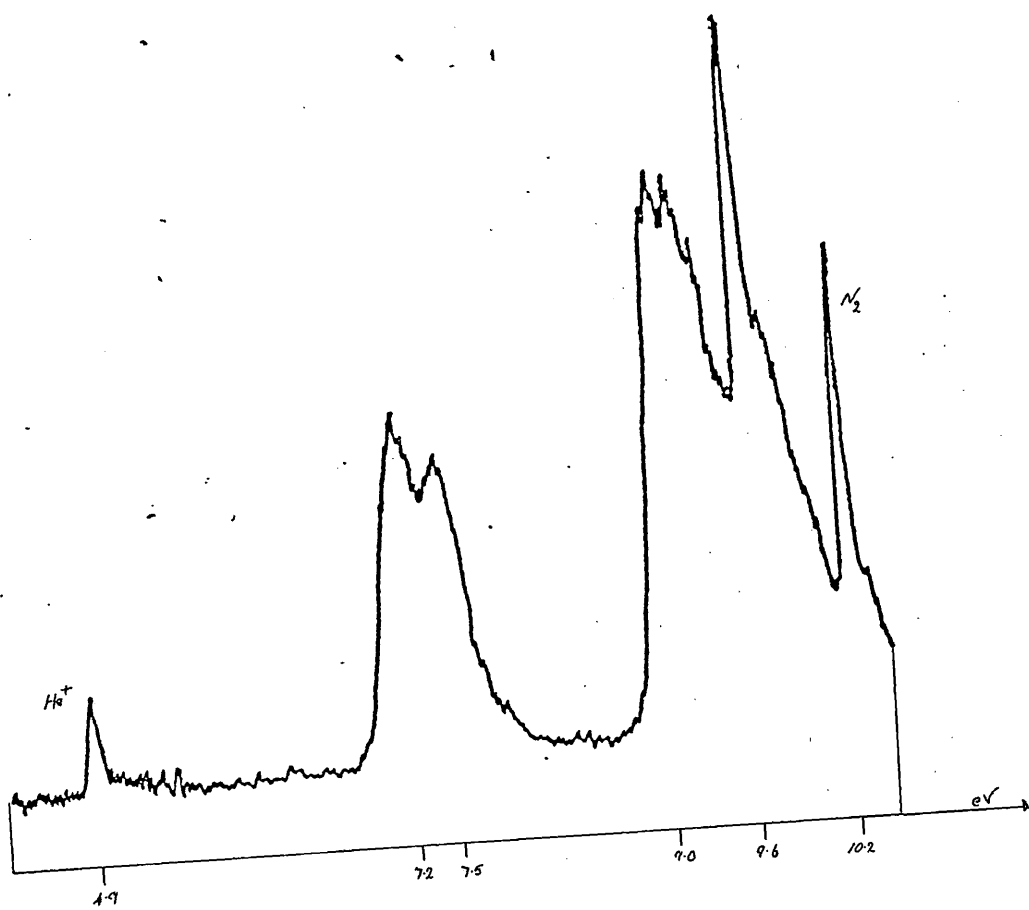
It can be seen from the data that as the cyclic voltammograms (Chapter 6.3), ionisation potentials are determined by the inductive effects of the substituents on the cyclopentadienyl rings. One would therefore expect that in the series: decamethyl ferrocene, ferrocene and decachloroferrocene, the decamethyl ferrocene should have the lowest ionisation potential since the electron donating ability of the methyl groups should destabilize the ring electrons whereas the electron withdrawing substituents should stabilize the system. These trends are reflected in the experimental data [Table 7.1].

Table 7.1.

Compound	Probe Temp. °C	Lamp Temp. °C	Counts	Time Constant	Scan Speed mms <sup>-1</sup>	I.E./eV eV
Ferrocene	59	80	10 <sup>3</sup>	1	0.2	6.95
1-Acetylferrocene	78	102	10 <sup>3</sup>	2	0.2	7.18
1,1'-Diacylferrocene	113	-	400	2	0.2	7.47
1-Methylferrocene carboxylate	101	121	800	2	0.1	7.10
1,1'-Dimethylferrocene dicarboxylate	143	169	10 <sup>3</sup>	1	0.2	7.27
Formylferrocene	89	109	400	2	0.1	7.31
Ferrocene propionic acid	-	-	900	1	0.2	6.93
β-Ferroceneacrylic acid	-	-	10 <sup>3</sup>	1	0.2	7.00
cp Fe cp CO.CH <sub>2</sub> CO <sub>2</sub> H	-	-	800	1	0.2	7.11
1,1'-Dichloroferrocene	-	-	800	2	0.1	7.20
1,1',2,2'-Tetrachloroferrocene	-	-	10 <sup>3</sup>	1	0.2	7.51
Decachloroferrocene	-	-	-	-	-	7.97
Decamethylferrocene	-	-	10 <sup>3</sup>	2	0.1	5.99
1,1'-Bis(N,N-Dimethylamido)-ferrocene	-	-	-	-	-	7.00

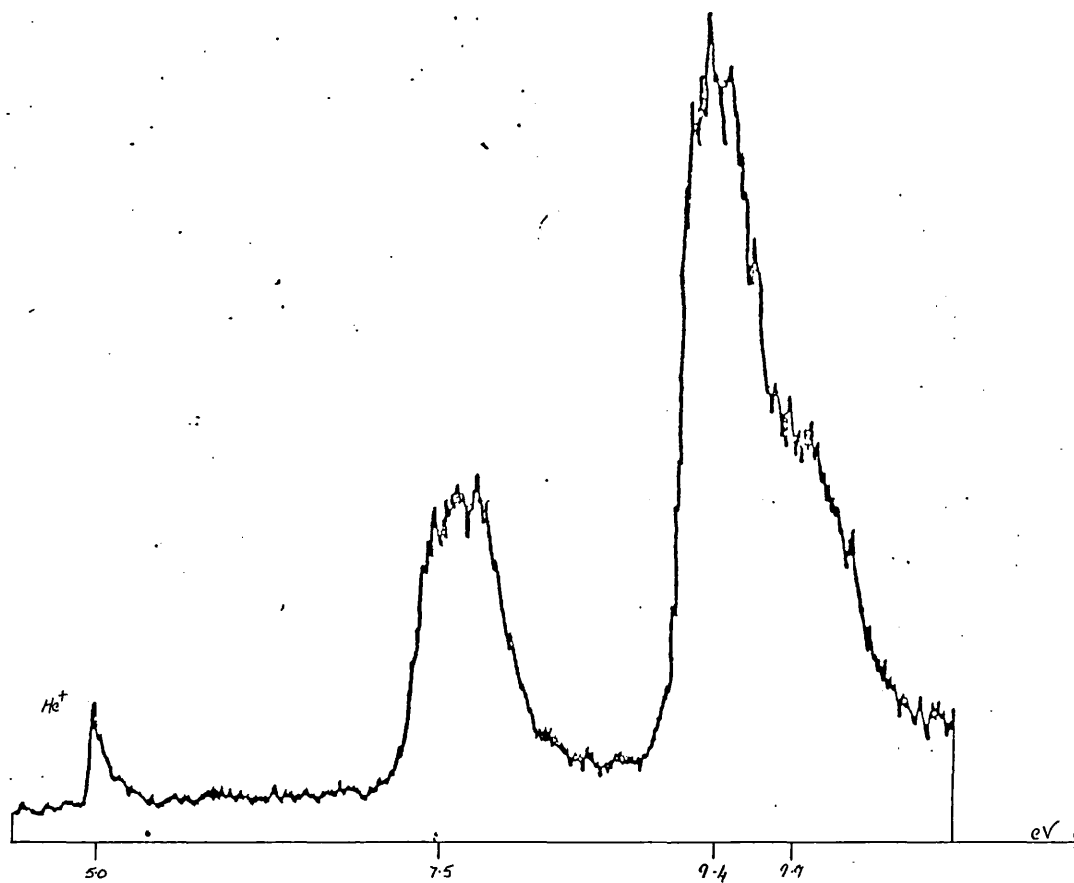
The He(I) P.E.S. of ferrocene

The He(I) P.E.S. of 1-acetylferrocene

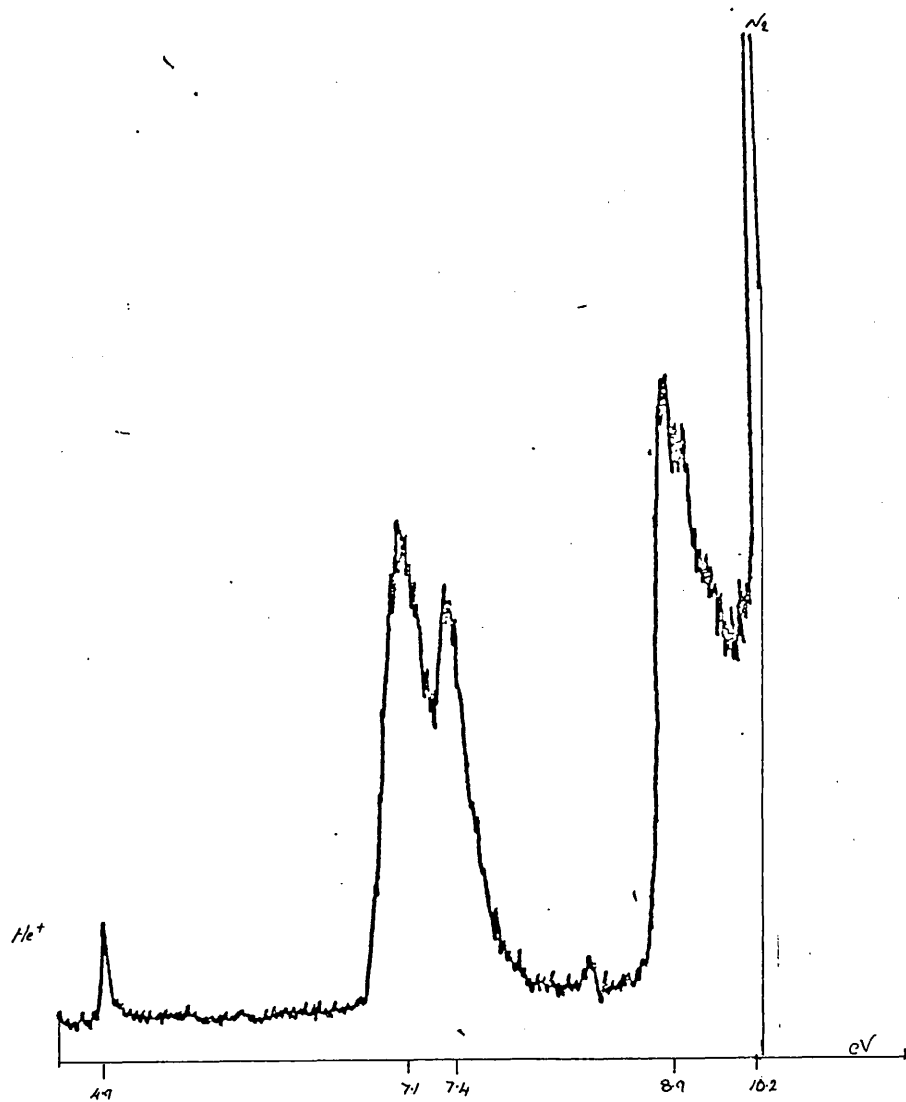




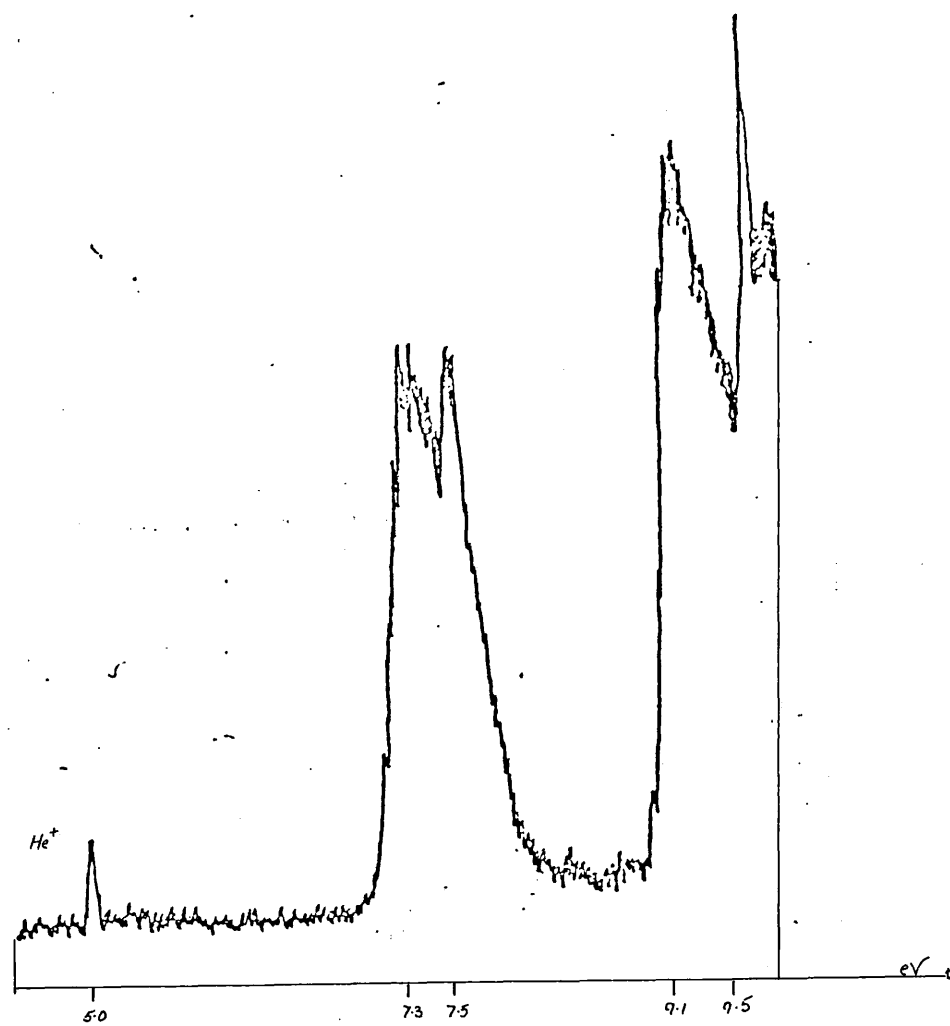
The He(I) P.E.S. of 1,1'-diacetylferrocene

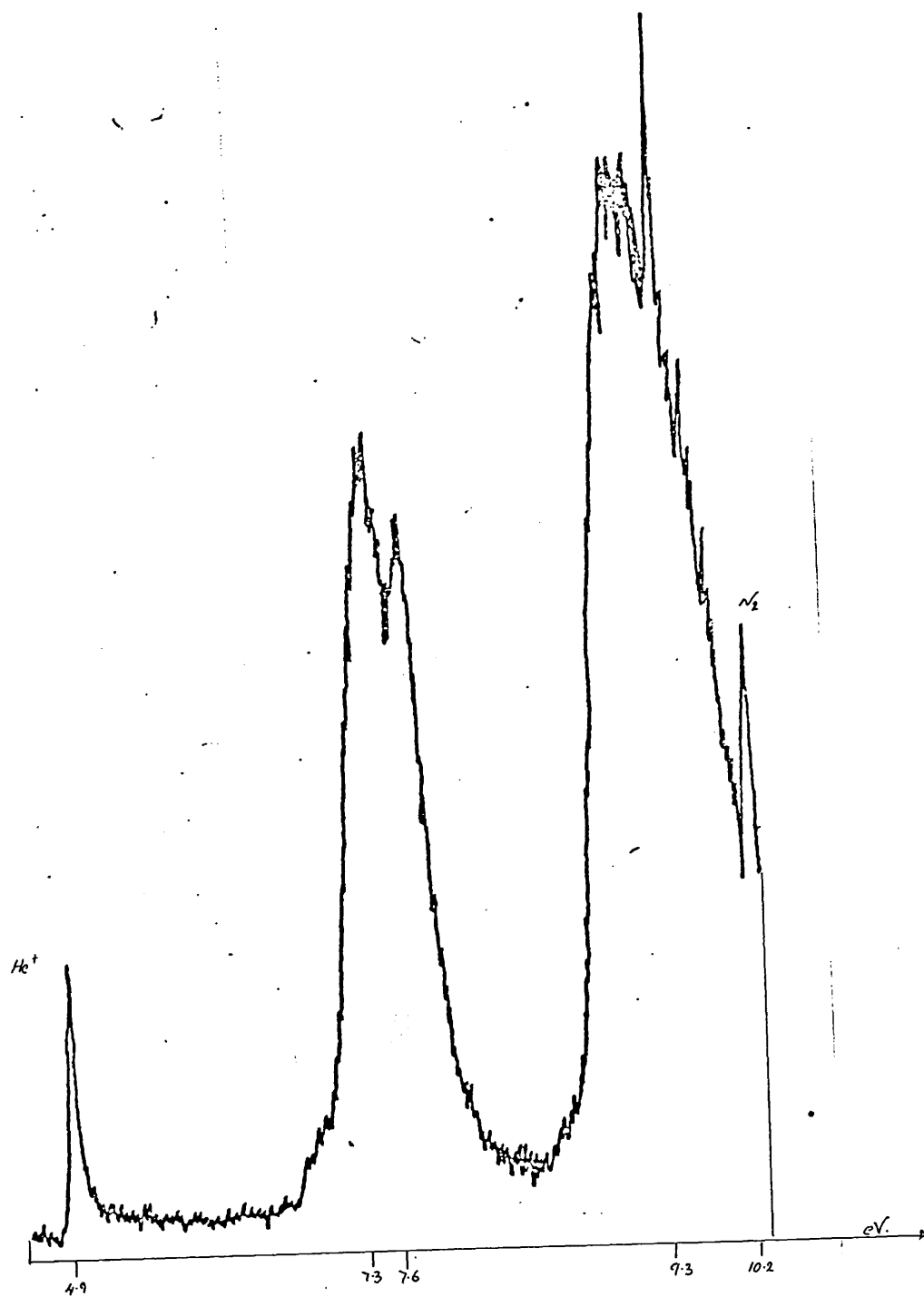


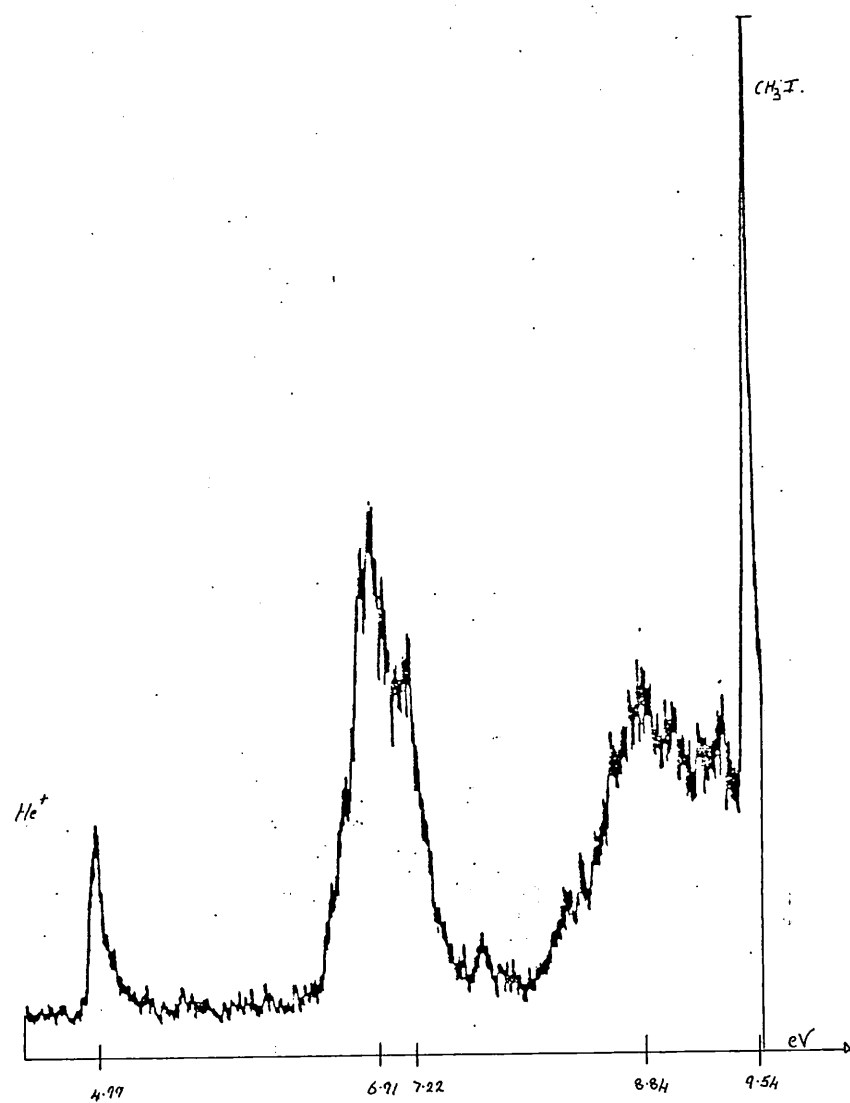
The He(I) P.E.S. of 1-methylferrocene carboxylate



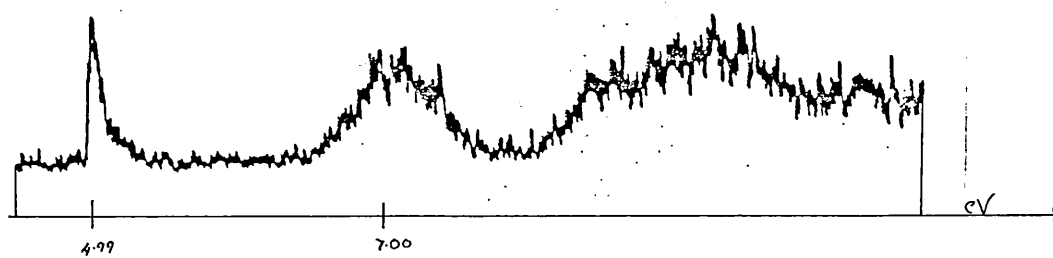
The He(I) P.E.S. of 1,1'-dimethylferrocene dicarboxylate



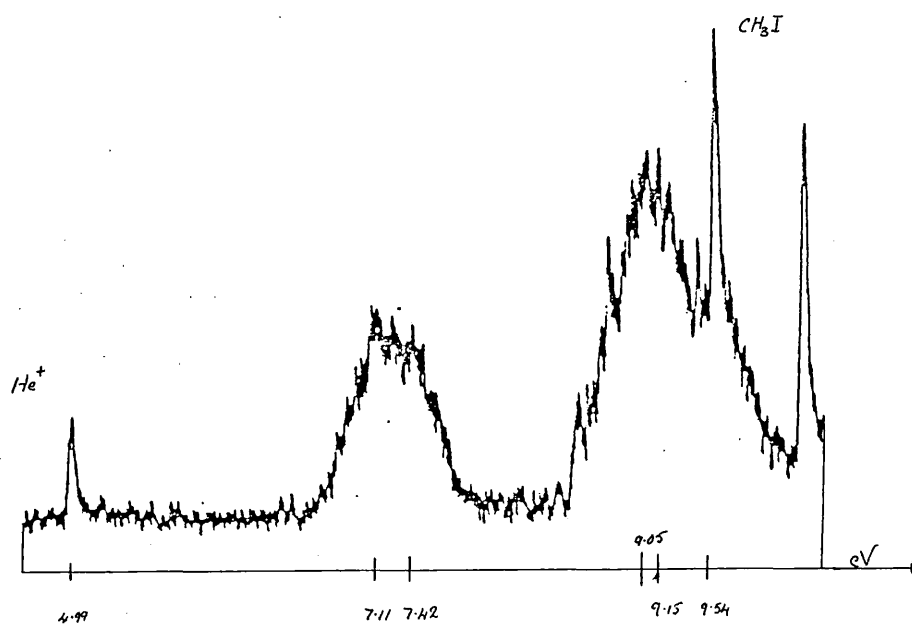
The He(I) P.E.S. of formylferrocene

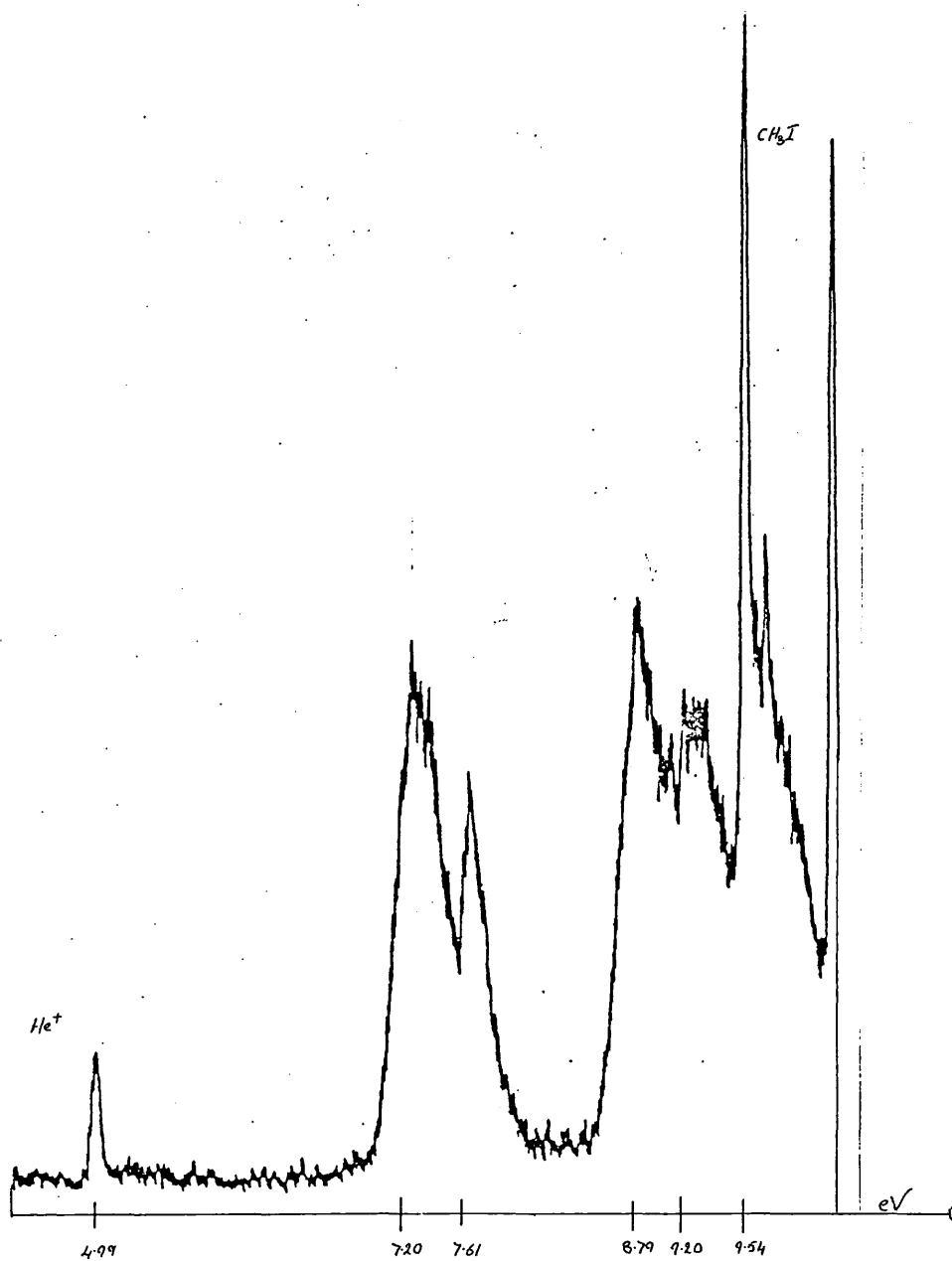
The P.E.S. of ferrocene propionic acid

The P.E.S. of  $\beta$ -ferrocene acrylic acid



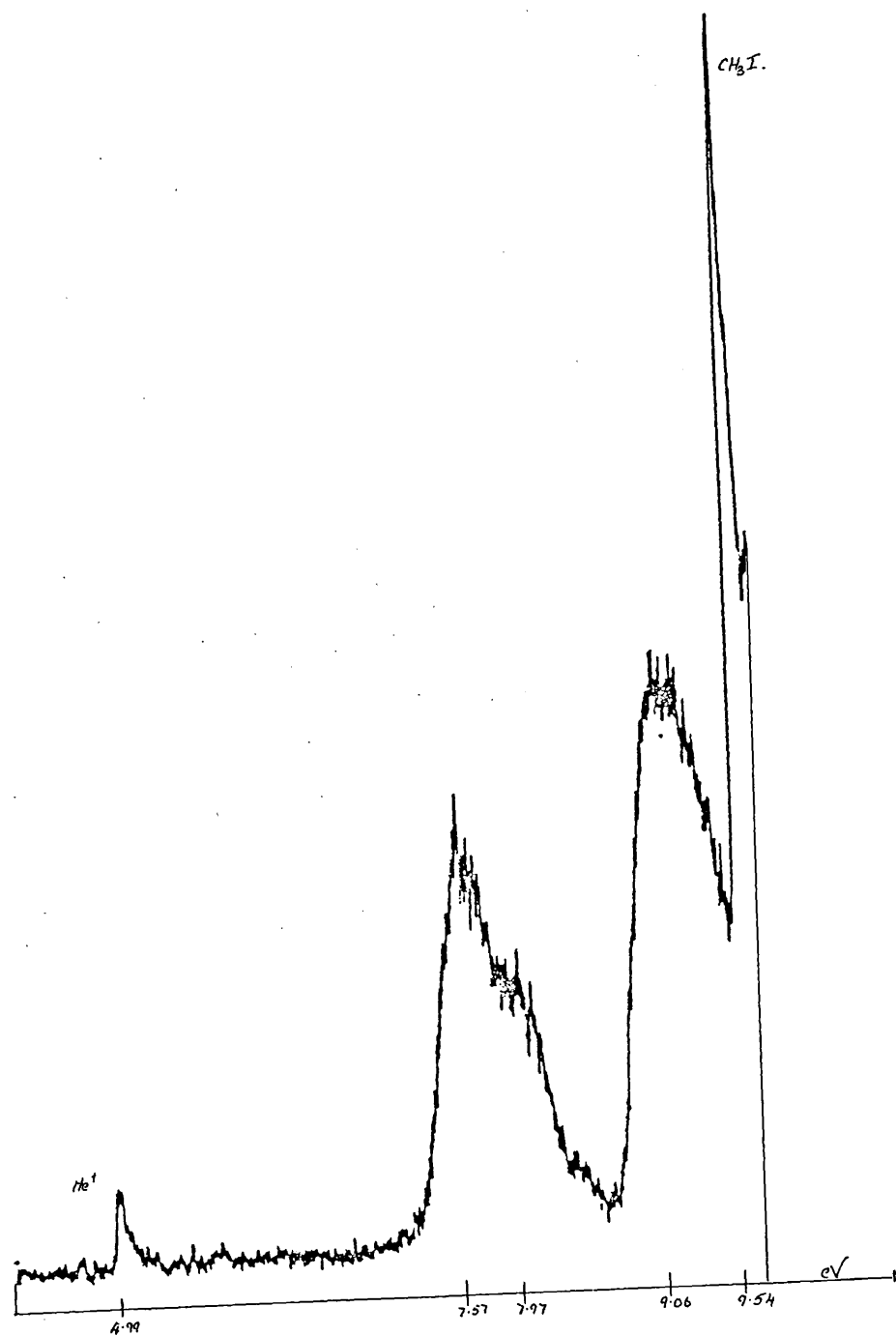
The P.E.S. of cpFecpCOCH<sub>2</sub>CH<sub>2</sub>CO<sub>2</sub>H

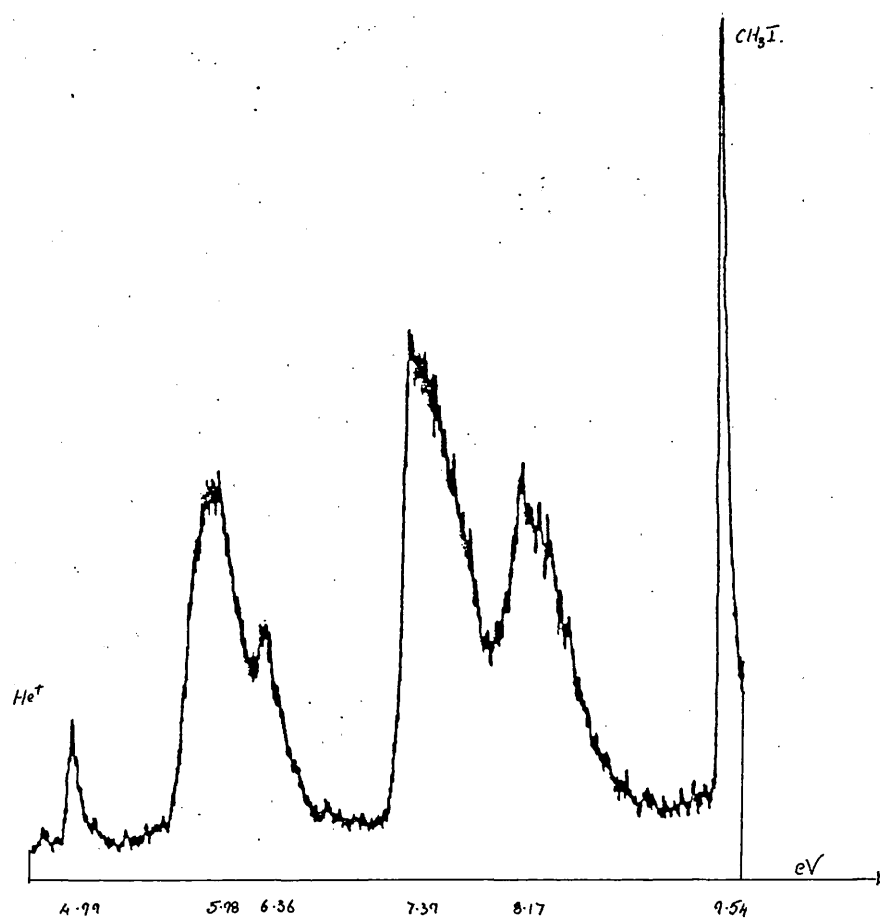


The P.E.S. of 1,1'-dichloroferrocene



The P.E.S. of 1,1',2,2'-tetrachloroferrocene



The P.E.S. of decamethylferrocene

7.4 THE CORRELATION OF OXIDATION POTENTIALS,  
IONISATION ENERGIES (AND  $\sigma$  HAMMETT VALUES)

The results obtained from the oxidation and ionisation spectra [Table 7.2] were correlated graphically [Graph 7.1]. The available data appear to lie on two distinct lines.

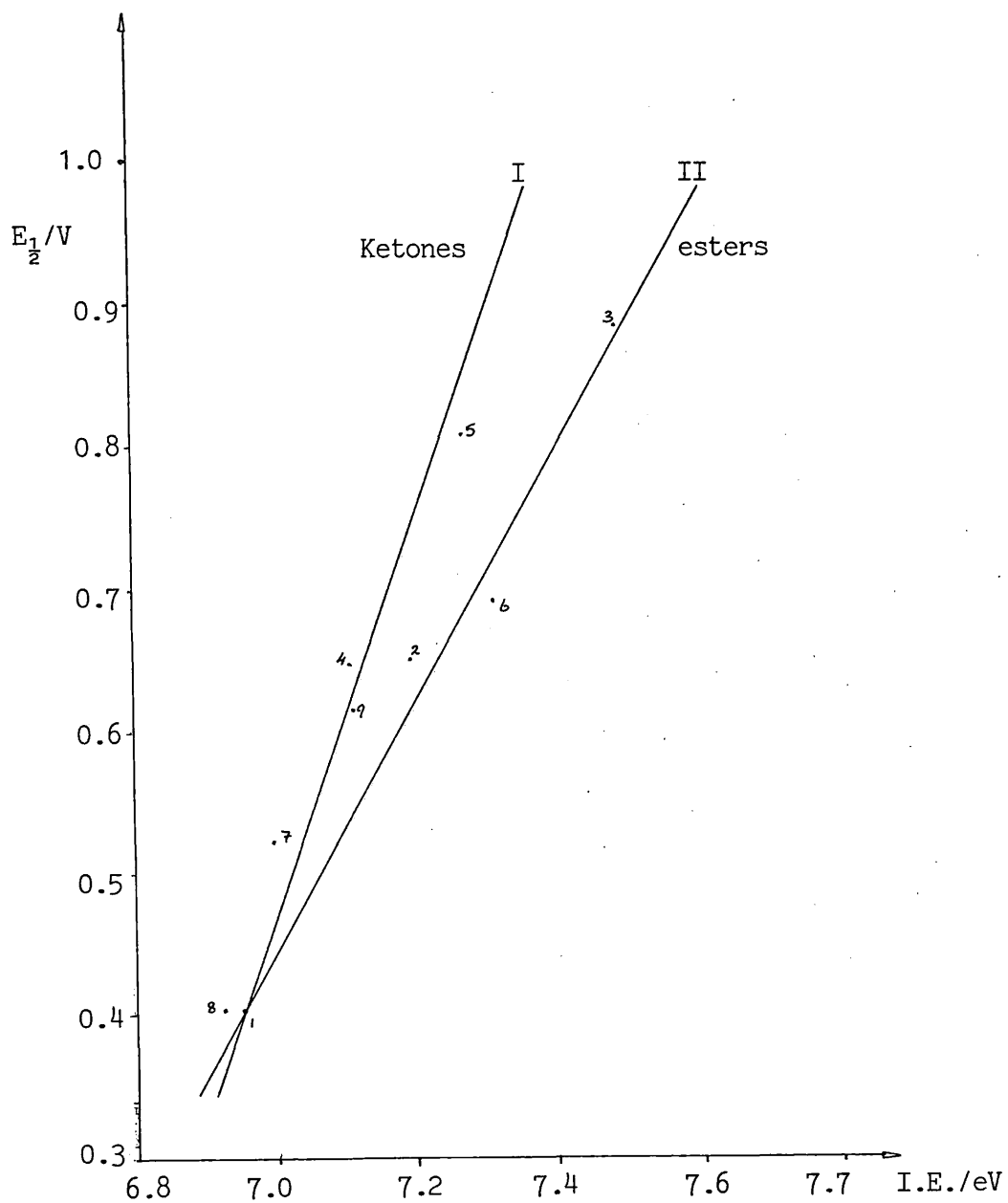
Table 7.2

Compound	$E_{\frac{1}{2}}$ .V(vs SHE)	I.E. eV	Graph 7.1 Point
Ferrocene	0.39	6.95	1
1-Acetyl ferrocene	0.64	7.18	2
1,1'-Diacetyl ferrocene	0.87	7.47	3
1-Methyl ferrocene carboxylate	0.64	7.10	4
1,1'-Dimethyl ferrocene carboxylate	0.79	7.27	5
Formyl ferrocene	0.68	7.31	6
-Ferrocene acrylic acid	0.52	7.00	7
Ferrocene propionic acid	0.40	6.93	8
cp.Fe cp COCH <sub>2</sub> CH <sub>2</sub> CO <sub>2</sub> H	0.62	7.11	9

It has been suggested by W.C. Neikam<sup>184</sup> that if a straight line is obtained, the free energy change in solvation upon oxidation is constant for that range of compounds and independent of their structure. Since this is not the case with the results [Graph 7.1], it seems that for substituted ferrocenes the solvation energy change is structurally dependent.

Graph 7.1

Oxidation potential vs ionisation energy for various substituted ferrocenes listed in Table 7.2



Two other metallocene systems have been reported  $[\text{Cr}(\text{arene})_2]^{185}$  and  $[\text{Fe}(\text{C}_5\text{R}_5)(\text{arene})]^{186}$ . A linear correlation was found in the chromium study but, the importance of this was limited due to the restricted number of derivatives investigated. In the iron study it was found that the oxidation potentials obtained in aqueous lithium hydroxide and dimethylformamide solutions did not correlate with the first ionisation energies. It was argued that this was due to large solvation effects.

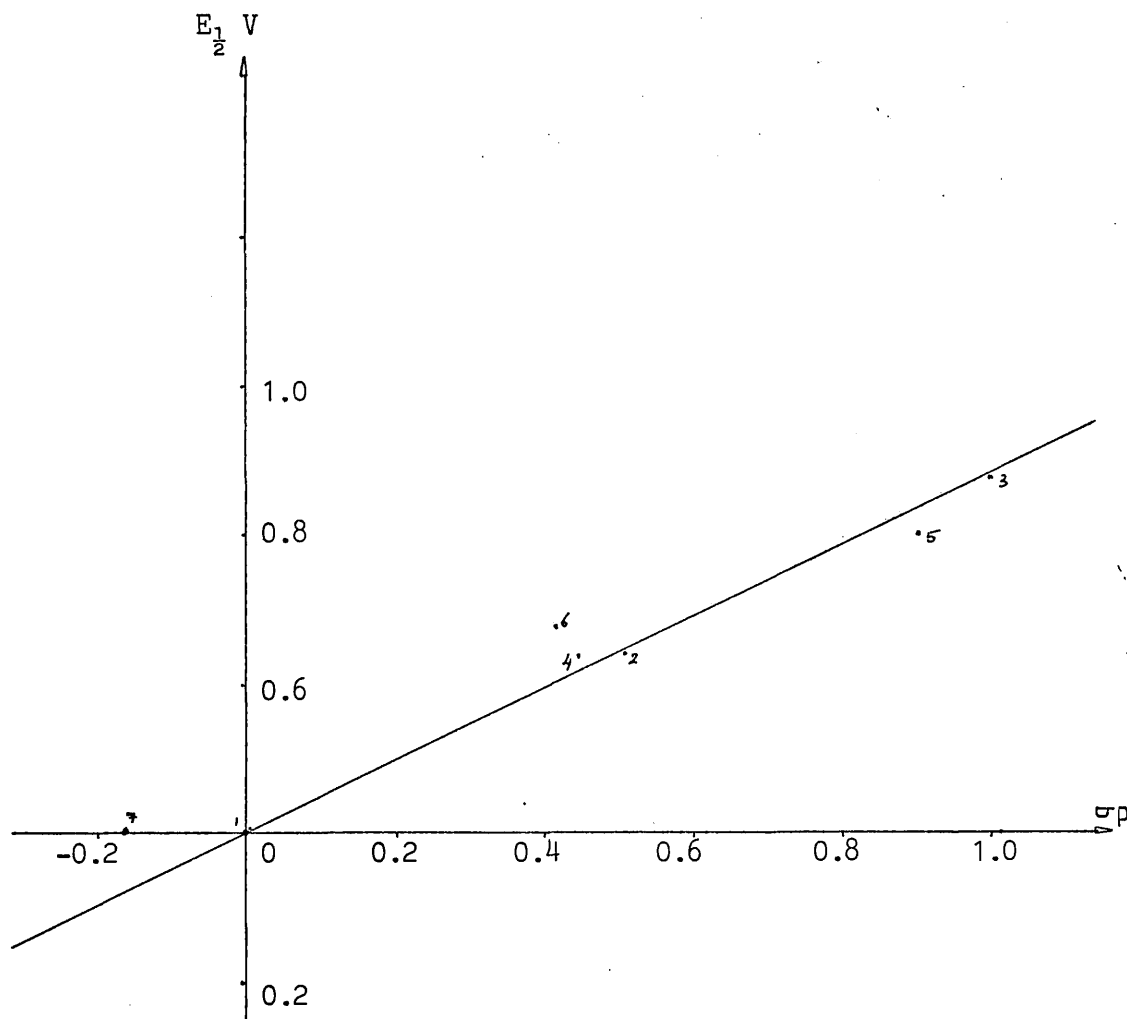
A mathematical relationship between the first ionisation energy level and the half-wave potential may be seen in Appendix 2.

In an attempt to analyse the data further, a correlation of ionisation energies and oxidation potentials with  $\sigma$  Hammett values was attempted.

Table 7.3

Substituent	$E_{\frac{1}{2}}$ V(vs SHE)	Hammett op value	Graph 7.2
Ferrocene	0.39	0.00	1
1-Acetylferrocene	0.64	0.50	2
1,1'-Diacetylferrocene	0.87	1.00	3
1-Methylferrocene carboxylate <sup>+</sup>	0.64	0.45	4
1,1'-Dimethylferrocene carboxylate <sup>+</sup>	0.79	0.90	5
Formyl ferrocene	0.68	0.42	6
Ferrocenepropionic acid	0.40	-0.17 <sup>+</sup>	7
<sup>+</sup> taken as a methyl op value	<sup>+</sup> taken as CO <sub>2</sub> Et op value		

GRAPH 7.2

Oxidation potentials vs. Hammett  $\sigma_p$  values

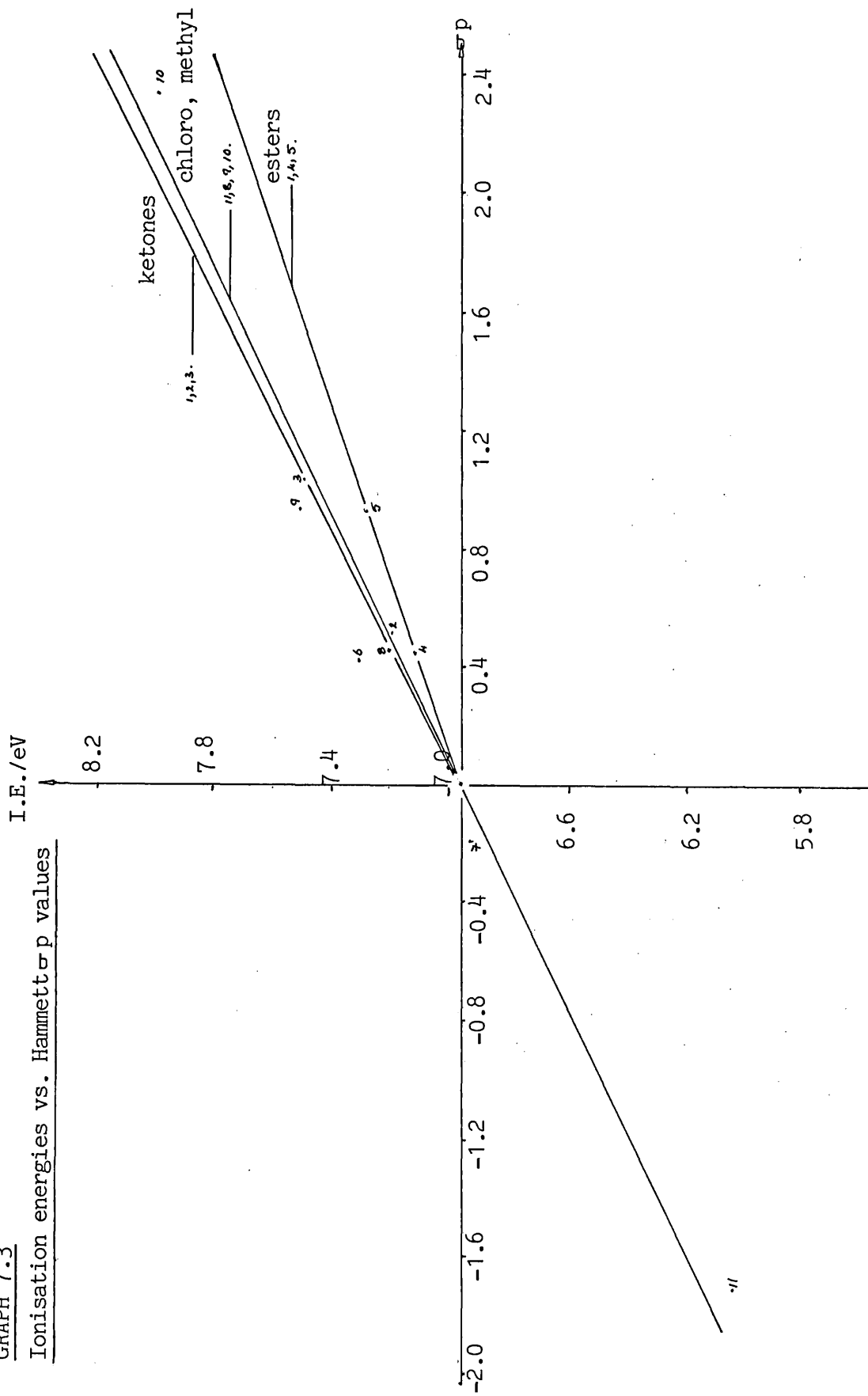
The oxidation potentials of the substituted ferrocenes were found to correlate best with the Hammett  $\sigma_p$  values [Table 7.3] as may be seen in Graph 7.2. This indicates that there is some relationship between the mesomeric (resonance) effects of the substituents (which involves a transfer of charge between the ring and substituent via the  $\pi$  system) with the oxidation potentials. Correlations with other Hammett values  $\sigma_{R^+}$ ,  $\sigma_I$  and  $\sigma_p$  proved inconclusive.

A similar analysis was attempted for the ionisation energy data [Table 7.4].

Table 7.4

Substituent	I.E./eV	Hammett $\sigma_p$ value	Graph 7.3
Ferrocene	6.95	0.00	1
1-Acetylferrocene	7.18	0.60	2
1,1'-Diacetylferrocene	7.48	1.00	3
1-Methylferrocene carboxylate <sup>+</sup>	7.10	0.45	4
1,1'-Dimethylferrocene carboxylate <sup>+</sup>	7.27	0.90	5
Formylferrocene	7.31	0.42	6
Ferrocene propionic acid <sup>+</sup>	6.93	-0.17	7
1,1'-Dichloroferrocene	7.20	0.46	8
1,1',2,2'-Tetrachloroferrocene	7.51	0.92	9
Decachloroferrocene	7.97	2.30	10
Decamethylferrocene	5.99	-1.70	11
<sup>+</sup> taken as methyl $\sigma_p$ value		<sup>+</sup> taken as CO <sub>2</sub> Et $\sigma_p$ value	

GRAPH 7.3  
Ionisation energies vs. Hammett  $\sigma$  p values





A reasonable correlation was found with the Hammett  $\rho$  values [Graph 7.3]. However, when individual series of functional groups were investigated it was found that the correlation was good. This seems to be indicative of a substituent effect similar to that occurring on the ionisation and additional evidence for this is being sought from a study of the ferrocene amides prepared in this thesis. The conclusions drawn from the Hammett plots should be treated with some caution due to the limited number of similarly substituted ferrocenes investigated.

**CHAPTER 8: FUTURE DEVELOPMENTS AND CONCLUSIONS**

CHAPTER 8FUTURE DEVELOPMENTS AND CONCLUSIONS

A general synthetic route to macrocyclic metallocene cryptands has been established in this thesis and a number of properties of these materials have been investigated. The synthetic approach to these macrocycles allows alteration of the heteroatom. It is thus possible to manipulate the ionic preference of the molecule. Such "ion design" gives the cryptand cavity some structural recognition with fixed receptor sites of defined dimensions. This would only give effective inclusion complexes with specific cations. A wide variety of cryptands containing different heteroatoms are now known, Chapter 2, and therefore the synthesis of new metallocene macrocycles should be relatively easy.

Tri-substituted metallocenes may be prepared by lithiation or acetylation and thus give the macrocycle a free functional group which could be utilised in a number of ways. The formation of polymers, or bond formation with other functional groups attached to molecules which are physically active, (porphyrins, phenanthrolines) could have numerous applications as outlined in Chapter 2. Of particular interest to us is the attachment of these selective ion-binding cavities to electrodes and their incorporation into electronic sensors.

The detailed n.m.r. investigation of the ferrocene and ruthenocene cryptands (38), (41) and in particular dynamic n.m.r. studies of these molecules have given an insight into the various molecular motions and conformations of these compounds. Attempts to study metal ion-binding in the ruthenocene cryptands via  $^{99}\text{Ru}$  and  $^{101}\text{Ru}$  n.m.r., Appendix 3, have been hampered by the insensitivity of the ruthenium resonance, the broadness of the ruthenium lines and the fact that ruthenium resonates near the low frequency limit of the currently available spectrometer probes. Nonetheless, this would provide a convenient and direct method by which any interaction between the ruthenium atom and a cation held in the cryptand could be monitored.

The complexation of these metallocene macrocycles was also examined by the Peterson method and simple  $^1\text{H}$  n.m.r., Chapter 5.3. It was seen that the ferrocene [2.2]cryptand (38) is selective in its binding properties and shows a strong preference for complexation with calcium ions. Similar selectivity has been observed in ferrocene[2.2]cryptands containing a longer bridging chain between the metallocene and cryptand.<sup>190,192</sup> The solid state  $^1\text{H}$  n.m.r. of ferrocene complexed inside a cyclodextrin molecule<sup>191</sup> has recently been reported. This new technique is widely available and should offer a valuable probe into ion binding in the absence of solvent.

An X-ray diffraction study of a single crystal of ruthenium(2.2)cryptand (41) was attempted, Chapter 5, but the results merit further investigation despite the apparent instability of the crystal.

The cyclic voltammetry and photoelectron studies on materials prepared are being continued. In particular data on the cryptands are being sought for correlation with electronic interactions between the metallocene moiety and bound metal ions as determined by other spectroscopic methods (u.v./vis. spectroscopy). Such results are crucial for the evaluation of these materials for use in ion-selective electrodes and other electrochemical phenomenon.

## CHAPTER 9: EXPERIMENTAL

CHAPTER 9  
EXPERIMENTAL

Preparation of diaza[24]crown-8 and diaza[21]crown-7

(A-G, Scheme 4.10)

A. Dibromotetraethylene glycol

A solution of freshly distilled tetraethylene glycol (85.5 g, 0.44 mol) in dry pyridine (53.3 g, 0.68 mol) was added drop-wise with stirring to a cooled (0°C) solution of phosphorus tribromide (100 g, 0.37 mol) in dry pyridine (20 ml). The mixture was stirred for four hours and was then left to stand overnight at room temperature. The solution was poured onto ice and the organic phase was decanted. The organic layer was washed with dilute hydrochloric acid and then dried (MgSO<sub>4</sub>). The dibromotetraethylene glycol was then purified by fractional distillation under reduced pressure to give a colourless oil (b.p. 128°C @ 1 mm Hg) (LIT: b.p. 123-125°C @ 0.4 mm Hg). (LIT: b.p. 156-159°C @ 8 mm Hg).<sup>162</sup>

Yield: 89.1 g (63%)

<sup>1</sup>H n.m.r. (60 MHz, CDCl<sub>3</sub>): δ 3.76 (CH<sub>2</sub>, 16H, m.).

B. Tetraethylene glycol diphthalamide

Potassium phthalimide (9.0 g, 0.049 mol) and dimethylformamide (30 ml) was heated for one hour at 100°C with vigorous stirring. The dibromotetraethylene glycol (8.9 g, 0.028 mol) was added and the heating and stirring continued for three hours. The mixture was then allowed to cool, filtered and water (50 ml) was added to the filtrate which was then filtered again. The combined residues were washed with dilute KOH and water before extracting with dichloromethane. (Care must be taken with the dilute KOH as hydrolysis may occur). The extracts were dried (MgSO<sub>4</sub>) and evaporated to yield 12.1 g (95%). The tetraethylene glycol diphthalamide was then recrystallised from glacial acetic acid.

Yield: 11.5 g (90%), m.p. 108°C (LIT: m.p. 108-109°C).<sup>61</sup>

<sup>1</sup>H n.m.r. (60 MHz, CDCl<sub>3</sub>): δ 7.78 (aromatic, H, m.);

δ 3.55 (OCH<sub>2</sub>, 12H, m.); δ 2.05 (NCH<sub>2</sub>, 4H, s.).

C. Diaminotetraethylene glycol (1,1-Diamino-3,6,9-trioxadecane)

Tetraethylene glycol diphthalamide (33 g, 0.073 mol) was suspended in ethanol (absolute 250 ml) and heated under reflux. Hydrazine hydrate (25.9 g, 0.518 mol) (50%) was added and the heating continued for a further two hours. Then concentrated hydrochloric acid (33.2 ml, 12 m) was added dropwise and the mixture heated for a further 30 minutes. The majority of the ethanol was then removed by



distillation (200 ml) and the solution was left to cool and the precipitate was filtered off. The solution was then placed in a liquid/liquid extractor and saturated with KOH. The product was then removed with benzene (48 hr extraction). The benzene solution was then dried ( $\text{MgSO}_4$ ) and evaporated to yield the crude amine, 10.3 g (74%). The amine was distilled from solid KOH under reduced pressure (b.p.  $162-163^\circ\text{C}$  @ 2 mm Hg) (LIT: b.p.  $114-116^\circ\text{C}$  @ 0.2 mm Hg)<sup>61</sup> (Store over KOH).  
Yield: 9.4 g (67%)

$^1\text{H}$  n.m.r. (60 MHz,  $\text{CDCl}_3$ ):  $\delta$  3.24 ( $\text{OCH}_2$ , 12H, m.);  $\delta$  2.40 ( $\text{NCH}_2$ , 4H, t.);  $\delta$  1.60 ( $\text{H}_2\text{N}$ , 4H, s.).

D. 1,11-Ditosyl-1,11-diamino-3,6,9-trioxadecane (34)

p-Toluene sulphonylchloride (13.9 g, 0.073 mol) was suspended in dry pyridine (80 ml) and heated to  $60^\circ\text{C}$  with stirring. The diaminotetraethylene glycol (6.4 g, 0.033 mol) in dry pyridine (25 ml) was added slowly and the mixture was left stirring at  $60^\circ\text{C}$  for  $2\frac{1}{2}$  hours. Pyridine (50 ml) was then removed by distillation and the solution was left to cool to  $45^\circ\text{C}$  and poured onto ice drop-wise with vigorous stirring. A white precipitate was formed which was filtered off and air dried. The tosylate was then dissolved in toluene and further dried in a Dean-Stark apparatus. The toluene was then evaporated and the crude tosylate was recrystallised from toluene.

Yield: 10.9 g (66%) m.p.  $92^\circ\text{C}$ .

Analysis; Calculated: N. 5.6%; C. 52.8%; H. 6.4%.

Found: N. 5.6%; C. 52.7%; H. 6.4%.

$^1\text{H}$  n.m.r. (60 MHz,  $\text{CDCl}_3$ ):  $\delta$ 7.50 (aromatic, 8H, q.);  
 $\delta$ 5.4 (HN, 2H p.s.);  $\delta$ 3.55 ( $\text{OCH}_2$ , 12H, m.);  $\delta$ 3.15 ( $\text{NCH}_2$ ,  
 4H, t.);  $\delta$ 2.88 ( $\text{CH}_3$ , 6H, s.).

E. Tetraethylene glycol ditosylate<sup>144</sup>

p-Toluene sulphonylchloride (22.6 g, 0.119 mol) was suspended in dry pyridine (40 ml) and stirred. Freshly distilled tetragol (10 g, 0.052 mol) in dry pyridine (10 ml) was added slowly. The mixture was stirred for a further 2½ hours and then poured dropwise onto ice with very vigorous stirring. An oil eventually formed, which was quickly separated and taken up in ether. The ether layer was washed once with water and then dried ( $\text{MgSO}_4$ ). The ether was evaporated leaving an oil which was tetraethylene glycol ditosylate.

Yield: 11.94 g (46%)

Analysis; Calculated: C. 52.57%; H. 6.01%

Found: C. 51.70%; H. 6.0%

$^1\text{H}$  n.m.r. (60 MHz,  $\text{CDCl}_3$ ):  $\delta$ 7.50 (aromatic, 8H, q.);  
 $\delta$ 4.10 ( $\text{OCH}_2$ , 4H, t.);  $\delta$ 3.50 ( $\text{OCH}_2$ , 12H, b.s.);  $\delta$ 2.40  
 ( $\text{CH}_3$ , 6H, s.).

F. Ditosyl-diaza[24]crown-8<sup>65</sup>

Sodium (0.22 g, 0.0094 mol) was dissolved in absolute dry ethanol (15 ml) under nitrogen. This was then added to (D) 1,11-ditosyl-1,11-diamino-3,6,9-trioxadecane (2.35 g, 0.047 mol) in 50 ml of dry dimethylformamide over a period of 15 minutes and stirred for a further 45 minutes in a 1 litre creased flask under nitrogen. The solution was

then heated to 100°C. Tetraethylene glycol ditosylate (E) (2.34 g, 0.0047 mol) in dry dimethylformamide (65 ml) was then added over a period of 5½ hours. The solution was then allowed to stir overnight 12¾ hours during which time the temperature fell to 80°C. The solution was then heated to 120°C and stirred for a further 4 hours. The volume of dimethylformamide was then reduced by evaporation (rotorvapor) taking the mixture almost to dryness. Ice (100 g) was then added which resulted in the formation of an oily solid. The aqueous layer was decanted and the oil was taken up in methylene-chloride. The dichloromethane solution was washed with dilute sodiumhydroxide and then water. After drying (MgSO<sub>4</sub>) the dichloromethane was removed by evaporation, leaving the crude ditosylate diazacrown. This was then recrystallised from chloroform and ethanol.

Yield: 0.85 g (28%) m.p. 82°C.

Analysis; Calculated: N. 4.25%; C. 54.67%; H. 7.04%

Found: N. 4.19%; C. 54.62%; H. 7.01%

<sup>1</sup>H n.m.r. (90 MHz, CDCl<sub>3</sub>): δ7.15 (aromatic, 8H, q.); δ3.20 (OCH<sub>2</sub>, 24H, b.s.); δ2.02 (CH<sub>3</sub>, 6H, s.); δ2.20 (NCH<sub>2</sub>, 8H, t.).

G. Diaza[24]crown-8<sup>66,15,61</sup>

Lithium aluminium hydride (0.135 g, 0.0036 mol) in (25 ml) dry tetrahydrofuran was stirred under a nitrogen atmosphere. Ditosyl-diaza[24]crown-8 (0.24 g, 0.00036 mol) was then dripped into the suspension and refluxed for 26 hours. The suspension was allowed to cool and then worked up via the Steinhardt method with successive drops of water

and 15% sodium hydroxide. The white precipitate was filtered off and washed several times with ether. The ether was then dried ( $\text{MgSO}_4$ ) and evaporated to yield the product, an oil (LIT: Oil).<sup>15</sup>

Yield: 0.1 g (79%).

Analysis; Calculated: N. 8.0%; C. 54.8%; H. 9.8%

Found: N. 7.9%; C. 54.9%; H. 9.8%

$^1\text{H}$  n.m.r. (60 MHz,  $\text{CDCl}_3$ ):  $\delta$  3.65 ( $\text{OCH}_2$ , 24H, b.s.);  
 $\delta$  2.80 ( $\text{NCH}_2$ , 8H, t.);  $\delta$  2.32 (HN, 2H, b.s.).

#### H. Triethylene glycolditosylate<sup>144</sup>

Triethylene glycol (5 g, 0.033 mol) was dissolved in (50 ml) dry pyridine and cooled to  $0^\circ\text{C}$ . p-Toluenesulphonyl chloride (25.1 g, 0.132 mol) was then added slowly with stirring. The mixture was stirred for a further 4 hours at  $0^\circ\text{C}$  and then placed in a fridge at  $2^\circ\text{C}$  for 24 hours during which time a precipitate of pyridine hydrochloride was formed. The suspension was poured dropwise onto 300 g of ice with vigorous stirring. The tosylate precipitated as a white solid which was then filtered and washed with water. The tosylate was dried and then recrystallised from petroleum ether  $40\text{-}60^\circ\text{C}$ .

Yield: 9.4 g (69%).

$^1\text{H}$  n.m.r. (90 MHz,  $\text{CDCl}_3$ ):  $\delta$  7.65 (aromatic, 8H, q.);  
 $\delta$  4.13 ( $\text{OCH}_2$ , 4H, t.);  $\delta$  3.64 ( $\text{OCH}_2$ , 4H, t.);  $\delta$  3.51 ( $\text{OCH}_2$ ,  
 4H, s.);  $\delta$  2.40 ( $\text{CH}_3$ , 6H, s.).

Ditosyl-diaza[21]crown-7<sup>64,65</sup>

The same general method was used as for (F) except on a second preparation potassium was used instead of sodium as the cation:

1st Yield: 3.97 g (53.5%)

2nd Yield: 4.31 g (87.9%)

<sup>1</sup>H n.m.r. (60 MHz, CDCl<sub>3</sub>): δ 7.65 (aromatic, 8H, q.);  
δ 3.50 (CH<sub>2</sub>, 24H, b.s.); δ 2.38 (CH<sub>3</sub>, 6H, s.).

Diaza[21]crown-7<sup>66,15</sup>

The same general method was used as for (G).

Yield: 0.88 g (41%) oil (LIT: m.p. < 20°C)<sup>15</sup>

Analysis: Calculated: N. 9.1%; C. 54.9%; H. 9.9%

Found: N. 9.0%; C. 54.9%; H. 10.0%

<sup>1</sup>H n.m.r. (60 MHz, CDCl<sub>3</sub>): δ 3.45 (OCH<sub>2</sub>, 20H, b.s.);  
δ 2.60 (NCH<sub>2</sub>, 8H, t.); δ 2.1 (HN, 2H, b.s.).

Attempted preparation of diaza[12]crown-4 (Scheme 4.11)N-p-Tosylsulphonyldiethanolamine

A solution of diethanolamine (52.5 g, 0.5 mol) in 2 N sodium carbonate (500 ml) was heated to 65-70°C. p-Toluenesulphonylchloride (95.2 g, 0.5 mol) was added slowly and the reaction mixture was heated with stirring at 90-95°C for one hour. The reaction mixture was left to cool and the desired product crystallised. This was then filtered, washed with water and dried. The product was then recrystallised from toluene.

Yield: 104.4 g (81%); m.p. 100°C (LIT: m.p. 100-101°C)<sup>147</sup>

<sup>1</sup>H n.m.r. (60 MHz, CDCl<sub>3</sub>): δ 7.45 (aromatic, 4H, q.); δ 4.00 (HO, 2H, s.); δ 3.84 (OCH<sub>2</sub>, 4H, b.s.); δ 3.24 (NCH<sub>2</sub>, 4H, t.); δ 2.41 (CH<sub>3</sub>, 3H, s.).

Tri-p-Tosylsulphonyldiethanolamine

To a stirred solution of p-toluenesulphonylchloride (191 g, 1 mol) in pyridine (300 ml) was added over 40 minutes diethanolamine (26.3 g, 0.25 mol) at room temperature. After 3½ hours stirring the reaction mixture was dripped into water (2 l) and stirred for 2 hours. The pale yellow solid is filtered and washed with water. This is then dried and recrystallised from methanol to give the product as white crystals.

Yield: 96.3 g (67%) m.p. 78°C (LIT: m.p. 78-79°C)<sup>146</sup>

<sup>1</sup>H n.m.r. (to MHz, CDCl<sub>3</sub>): δ 7.70 (aromatic, 12H, b.s.); δ 4.11 (OCH<sub>2</sub>, 4H, b.s.); δ 3.36 (NCH<sub>2</sub>, 4H, b.s.); δ 2.43 (CH<sub>3</sub>, 6H, s.); δ 2.39 (CH<sub>3</sub>, 3H, s.).

Ditosyl diaza[12]crown-4

N-p-Tosylsulphonyldiethanolamine (13.03 g, 0.05 mol) in dry tetrahydrofuran (250 ml) was added dropwise over 2½ hours to a stirred suspension of sodium hydride (2.53 g, 0.11 mol) in dry tetrahydrofuran (150 ml) and the mixture was stirred for a further 2½ hours at room temperature (N<sub>2</sub> atmosphere). Tri-p-tosylsulphonyldiethanolamine (28.5 g, 0.05 mol) in dry tetrahydrofuran (100 ml) was added to the solution of the dianion and the reaction mixture was stirred at room temperature for two days. Water (200 ml) was added to the mixture, the tetrahydrofuran removed by evaporation, and the product extracted into chloroform. The extract was dried (MgSO<sub>4</sub>) and evaporated and the residue purified by column chromatography.

Yield: No product.

The above method was repeated using lithium instead of sodium hydride.

Yield: No product.

Ferrocenyl derivatives

Ferrocene was obtained from the Aldrich Chemical Company, Inc.

1,1'-ferrocene dicarboxylic acid

Ferrocene (8.8 g, 0.0473 mol) was dissolved in (200 ml) dry O<sub>2</sub>-free hexane in a 500 ml three necked flask under a dry nitrogen atmosphere. n-Butyl-lithium (7.5 g, 0.117 mol) (1.5 m hexane solution) was added to tetramethylethylenediamine (T.M.E.D.A.) (13.6 g, 0.117 mol) in (20 ml) hexane and left to stand for 15 minutes in the dropping funnel under a nitrogen atmosphere. This was then added over a period of 1 hour and the mixture was stirred for 18 hours. The dilithioferrocene suspension was then injected into a CO<sub>2</sub>/ether slush. The dilithium salt was then filtered and washed with ether (LIT: dimer 98%; monomer 1.8%).<sup>59</sup>

The ferrocene salt can be converted into the acid by the addition of water (100 ml) and then dilute acid to precipitate the ferrocene acid. This was then filtered and dried. The traces of ferrocene monocarboxylic acid are removed by extraction with benzene in a Soxhlet, the ferrocene dicarboxylic being insoluble in benzene. This was recrystallised with glacial acetic acid to give the desired product.

Yield: 12.3 g (95%) m.p. 195°C dec (LIT: m.p. 195-205°C dec)<sup>59,36</sup>



1,1'-ferrocene dicarboxyl chloride (26)

Lithium, 1,1'-ferrocene dicarboxylic salt was treated with an 8 fold excess of oxalyl chloride in dry dichloromethane. This was stirred for 1 hour then refluxed for 30 minutes. The excess oxalyl chloride and dichloromethane were removed by evaporation (rotorvapor) and the residue was extracted with benzene (Sohxlet 4 hours). The benzene was then evaporated and the residue was recrystallised from dry hexane.

Yield: (60%) m.p. 98°C (LIT: m.p. 98°C)<sup>67,68</sup>

<sup>1</sup>H n.m.r. (60 MHz, CDCl<sub>3</sub>): δ5.05 (ferrocenyl. H<sub>2,5</sub>, 4H, t.); δ4.75 (ferrocenyl. H<sub>3,4</sub>, 4H, t.).

1,1'-ferrocenedicarboxylate (25)

This was prepared using the method described by A. Bell, Ph.D thesis, 1979, (56%) with one modification which increased the yield by 21%.

Ferrocene (1.0 g, 0.0054 mol) in pentane (50 ml) was lithiated with n-butyl lithium (0.86 g, 0.0134 mol) in the presence of T.M.E.D.A. to give 1,1'-dilithioferrocene. The 1,1'-dilithioferrocene suspension was then syringed under N<sub>2</sub> into a large excess of dimethylformamide (40 ml) stirred at -45°C. After the addition the solution was left at -45°C for 1 hour and then allowed to warm to 0°C. This was then added to a large excess of saturated ammonium chloride (500 ml) at 0°C. The aqueous solution was extracted with ether. The combined extracts were dried (MgSO<sub>4</sub>) and evaporated down to 10 ml. This was washed through a silica

gel column with ether. Two bands were seen, the first contained unreacted ferrocene and the second contained the product. The product was concentrated and recrystallised from O<sub>2</sub>-free pentane.

Yield: 1.0 g (77%) m.p. 183°C (LIT: m.p. 183-184°C)<sup>150</sup>

<sup>1</sup>H n.m.r. (60 MHz, CDCl<sub>3</sub>): δ 9.90 (CHO, 2H, s.); δ 4.80 (ferrocenyl. H<sub>2,5</sub>, 4H, t.); δ 4.60 (ferrocenyl. H<sub>3,4</sub>, 4H, t.).

Preparation of decamethylferrocene2,3,5,6-Tetrahydro-2,3,5,6-tetramethyl-8-pyrone (84)

To a solution of potassium hydroxide (28.1 g in 187 ml methanol) diethylketone (129 g, 1.5 mol) was added. Lithium chloride (4.25 g, 0.1 mol) was added and the solution was warmed to 30°C. Acetaldehyde (196 g, 4.45 mol) was added very slowly over a period of 5 hours. After 14 hours the reaction mixture was neutralized with HCl dil. The organic layer was separated and washed twice with water (150 ml). Simple distillation under reduced pressure up to a boiling point of 100°C @ 16 Torr gave a crude product.

Redistillation through a 20 cm Vigreux-column b.p. 63-69°C @ 13 Torr yields 60.4 g (26%) (LIT: b.p. 63-69°C @ 13 Torr)<sup>164</sup>

<sup>1</sup>H n.m.r. (60 MHz, CDCl<sub>3</sub>): δ 7.2-6.1 (CH, 4H, c.m.);

δ 3.7-0.8 (CH<sub>3</sub>, 12H, c.m.)

2,3,4,5-Tetramethylcyclopent-2-enone (85)

p-Toluenesulfonic acid (7.31 g, 0.039 mol) was added to (84) (60 g, 0.38 mol) in benzene (400 ml). While the mixture is refluxing the formed water is collected in a trap. After 20 hours, the elimination of water is complete. The mixture was neutralised with Na<sub>2</sub>CO<sub>3</sub> solution and the organic layer was washed twice with water (150 ml). The benzene layer was separated and dried (MgSO<sub>4</sub>) and then evaporated. Distillation under reduced pressure through a 20 cm Vigreux-column, b.p. 80-82°C @ 13 Torr yields 41.45 g (78%)

(LIT: b.p. 79-83°C @ 13 Torr)<sup>164</sup>

<sup>1</sup>H n.m.r. (60 MHz, CDCl<sub>3</sub>): δ 3.6-0.8 (CH<sub>3</sub>, CH, 14H, c.m.).

1,2,3,4,5-Pentamethylcyclopentadiene (86)

(85) (12.34 g, 0.089 mol) was treated with methylmagnesium bromide (12.79 g, 0.107 mol) in dry ether (100 ml). The reaction mixture was refluxed for 30 minutes and then left to cool. Dilute acid was added slowly and the ether layer was washed twice with water (150 ml). The ether layer was dried ( $\text{MgSO}_4$ ) and evaporated. The tertiary alcohol was then taken up in benzene (50 ml) and a crystal of iodine was added resulting with a spontaneous loss of water. The water was removed and the benzene evaporated. Distillation of the product b.p.  $59^\circ\text{C}$  @ 14 mm Hg yields: 9.26 g (76%) (LIT: b.p.  $58.5^\circ\text{C}$  @ 13.5 mm Hg)<sup>165</sup>  
 $^1\text{H}$  n.m.r. (60 MHz,  $\text{CDCl}_3$ ):  $\delta$  1.80 ( $\text{CH}_3$ , 15H, s.);  $\delta$  1.05 (CH, 1H, s.).

Decamethylferrocene

A solution of ferrous chloride was obtained by boiling for 5 hours under reflux a mixture of anhydrous ferric chloride (2.16 g, 0.133 mol) with iron powder (0.72 g, 0.013 mol) in tetrahydrofuran (25 ml). This solution was treated with a solution of lithium-pentamethylcyclopentadienide obtained by adding butyllithium in hexane (2.38 g, 0.0372 mol) to a mixture of pentamethylcyclopentadiene (2.74 g, 0.02 mol) in tetrahydrofuran (25 ml) at  $-78^\circ\text{C}$  and allowing to warm to room temperature. The resulting reaction mixture was boiled under reflux for 24 hours to insure complete reaction. After cooling to room temperature the solvent was removed. Direct sublimation of the brown solid ( $100-140^\circ\text{C}$  @ 0.1 mm Hg)

gave the desired product.

Yield: 2.3 g (35%) m.p. 292°C (LIT: m.p. 291-295°C).<sup>186</sup>

<sup>1</sup>H n.m.r. (60 MHz, CDCl<sub>3</sub>): δ 1.62 (CH<sub>3</sub>, 30H, s.).

## Preparation of decachloroferrocene

### 1,1'-dichloroferrocene

A solution of 1,1'-dilithioferrocene (0.027 mol) in hexane was prepared according to the previously described procedure in this ferrocene section. The 1,1'-dilithioferrocene in hexane was cooled to  $-78^{\circ}\text{C}$  and tosyl chloride (11.5 g, 0.06 mol) was added slowly. The resulting solution was stirred at  $-78^{\circ}\text{C}$  for 1 hour after which time it was allowed to warm slowly to room temperature. Water (5.0 ml) was then added and the reaction mixture was filtered free of solid impurities. The precipitate was washed with methylene chloride and the combined filtrate was evaporated to dryness. The residue was chromatographed on a grade II alumina column. Elution with hexane produced a main band containing 1,1'-dichloroferrocene.

Recrystallization from hexane gave the desired product.

Yield: 5.2 g (75%) m.p.  $80^{\circ}\text{C}$  (LIT: m.p.  $80-81^{\circ}\text{C}$ ,<sup>167</sup>  
 $75-77^{\circ}\text{C}$ )<sup>168</sup>

$^1\text{H}$  n.m.r. (60 MHz,  $\text{CDCl}_3$ ):  $\delta$ 4.36 (ferrocenyl.  $\text{H}_{2,5}$ , 4H, t.);  
 $\delta$ 4.09 (ferrocenyl.  $\text{H}_{3,4}$ , 4H, t.).

### 1,1',2,2'-Tetrachloroferrocene

A solution of 1,1'-dichloroferrocene (14.41 g, 0.057 mol) in hexane (700 ml) was stirred at  $23^{\circ}\text{C}$  while a solution of n-butyllithium in hexane (57 mol, 0.141 mol) was added followed by the addition of T.M.E.D.A. (16.39 g, 0.141 mol). The reaction mixture was stirred for 50 minutes

and then added over a 40 minute period to a stirred solution of hexachloroethane (38.61 g, 0.164 mol) in hexane (300 ml). After the addition was complete, the mixture was stirred for a further 5 minutes and then filtered through a bed of alumina. The filtrate was evaporated to dryness and the residue fractionally sublimed. After removal of the hexachloroethane, 90°C @ 1 mm Hg (LIT: 45°C @ 0.25 mm Hg)<sup>169</sup> the product was sublimed, 140°C @ 1 mm Hg (LIT: 120-125°C @ 0.25 mm Hg). Recrystallization from hexane gave 1,1',2,2'-tetrachloroferrocene. This was analysed by G.L.C. and was found to be pure.

Yield: 14.6 g (80%), m.p. 141-142°C (LIT: m.p. 141°C)<sup>169</sup>

<sup>1</sup>H n.m.r. (60 MHz, CDCl<sub>3</sub>): δ 4.40 (ferrocenyl. H<sub>3,4</sub>, 4H, d.); δ 4.10 (ferrocenyl. H<sub>5</sub>, 2H, t.).

1,1',2,2',3,3'-Hexachloroferrocene

A solution of 1,1',2,2'-tetrachloroferrocene (4.08 g, 0.013 mol) in dry tetrahydrofuran (T.H.F.) (300 ml) was stirred at 15°C while a solution of n-butyllithium in hexane (0.079 mol, 32 ml) was added. The reaction mixture was stirred for 2½ hours and then added over a 20 minute period to a solution of hexachloroethane (24.98 g, 0.106 mol) in hexane (400 ml). After the addition was complete the mixture was stirred for a further 5 minutes and then filtered through a bed of alumina. The filtrate was evaporated and the product was fractionally sublimed. G.L.C. analysis of the product showed there to be pentachloroferrocene and heptachloroferrocene present. The product was recrystallized three times from hexane to obtain a pure sample of 1,1',2,2',3,3'-hexachloroferrocene.

Yield: 2.52 g (51%), m.p. 192°C (LIT: m.p. 191°C)<sup>169</sup>

<sup>1</sup>H n.m.r. (60 MHz, CDCl<sub>3</sub>); δ 4.38 (ferrocenyl. H<sub>4,5</sub>, 4H, s.).

1,1',2,2',3,3',4,4'-Octachloroferrocene

The experimental procedure used was the same as for 1,1',2,2',3,3'-hexachloroferrocene, except that the lithiation was carried out for 1½ hours.

Crude yield: 2.07 g (88%).

After repeated recrystallizations a pure sample by G.L.C. was obtained.

m.p. 210°C (LIT: m.p. 212°C)<sup>169</sup>

<sup>1</sup>H n.m.r. (60 MHz, CDCl<sub>3</sub>): δ4.55 (ferrocenyl. H<sub>5</sub>, 2H, s.).

Decachloroferrocene

A solution of 1,1',2,2',3,3',4,4'-octachloroferrocene (1.0 g, 0.002 mol) in dry THF (100 ml) was stirred at 0°C while a solution of n-butyllithium in hexane (0.006 mol, 2.6 ml) was added. The reaction mixture was stirred at 0°C for 1 hour and then hexachloroethane (4.46 g, 0.019 mol) was added. The mixture was stirred for a further 15 minutes and then filtered through a bed of alumina. The filtrate was evaporated to dryness and the hexachloroethane was removed by sublimation. The mixture was dissolved in carbon tetrachloride (25 ml) and stirred with concentrated nitric acid for 24 hours. The layers were separated and the carbon tetrachloride was washed with water and dried (MgSO<sub>4</sub>). This was then passed down a column of alumina to give decachloroferrocene.

Yield: 0.51 g (45%) m.p. 248-250°C dec (LIT: m.p. 245-246°C dec.)<sup>169</sup>



Attempted direct synthesis of decachloroferrocene

A solution of pentachlorocyclopentadienyl-lithium<sup>173</sup> prepared from hexachlorocyclopentadiene (13.5 g, 0.049 mol) in hexane (10 ml) and n-butyllithium in hexane (0.049 mol, 32 ml) at  $-70^{\circ}\text{C}$  was reacted with ferrous chloride (2.84 g, 0.023 mol). The reaction mixture was stirred for 1 hour and then left to warm to room temperature. The solution was then passed through a bed of alumina and the filtrate was evaporated. Chromatography of the product on an alumina column yielded none of the desired metallocene but samples of pentachlorocyclopentadiene and hexachlorocyclopentadiene were obtained.

Formyl ferrocene

A mixture of (11.2 g, 0.06 mol) of ferrocene and (10.7 g, 0.07 mol) of phosphorous oxychloride was heated to  $50^{\circ}\text{C}$  and (8.1 g, 0.06 mol) of N-methylformanilide was added dropwise with stirring over 15 minutes. The mixture was poured onto ice (50 g) and extracted with diethyl ether for 24 hours in a continuous extractor. The extract was washed with water, 5% aqueous sodium carbonate solution and again with water. The washed extracts were dried ( $\text{MgSO}_4$ ) and the ether was removed by distillation. The crude aldehyde was an oil that solidified on standing.

Yield: 4.6 g (36%).

The aldehyde was recrystallized from a mixture of n-heptane and methylene chloride.

Yield: 4.0g (31%), m.p. 124°C (LIT: m.p. 124.5°C)<sup>170</sup>.

<sup>1</sup>H n.m.r. (90 MHz, CDCl<sub>3</sub>): δ 9.95 (CHO, 1H, s.); δ 4.79 (ferrocenyl. H<sub>2,5</sub>, 2H, t.); δ 4.59 (ferrocenyl. H<sub>3,4</sub>, 2H, t.); δ 4.26 (ferrocenyl. ring, 5H, s.).

#### Acetyl ferrocene

A mixture of (10.0 g, 0.054 mol) of ferrocene and (112.2 g, 1.1 mol) of acetic anhydride was stirred and phosphoric acid (20 ml of 85% (8.7 M) was added dropwise. The flask was then heated for 30 minutes on a steam bath. The reaction mixture was poured onto chipped ice (200 g) and then neutralized by adding solid sodium bicarbonate. The orange-brown solid that precipitated was collected and washed with water until the washings were pale orange. The crude product was then air dried.

Yield: 22 g.

This was taken up in a minimal amount of toluene and placed on an alumina column and eluted with light petroleum and then petroleum, diethyl-ether (1:1). The solvent was removed and the acetylferrocene was recrystallized from light petroleum.

Yield: 6.4 g (52%), m.p. 85°C (LIT: m.p. 85-86°C)<sup>170</sup>

<sup>1</sup>H n.m.r. (90 MHz, CDCl<sub>3</sub>): δ 4.77 (ferrocenyl. H<sub>2,5</sub>, 2H, t.); δ 4.50 (ferrocenyl. H<sub>3,4</sub>, 2H, t.); δ 4.20 (ferrocenyl. ring, 5H, s.); δ 2.39 (CH<sub>3</sub>, 3H, s.).

#### β-Ferrocenylacrylic acid

Formylferrocene (10 g, 0.047 mol), malonic acid (10 g, 0.096 mol) and piperidine (20 ml) were dissolved in dry pyridine (150 ml) and heated under nitrogen on a boiling water bath for 4 hours at 85-90°C. The cooled solution was

diluted with water and extracted with chloroform. The chloroform extract was washed with dilute hydrochloric acid and water. The washed extracts were dried ( $\text{MgSO}_4$ ) and the chloroform was evaporated. The crude product was recrystallized from benzene to give deep red crystals. Yield: 6.0 g (50%), m.p.  $185^\circ\text{C}$  (LIT: m.p.  $186-187^\circ\text{C}$ )<sup>171</sup>  
 $^1\text{H}$  n.m.r. (90 MHz,  $\text{CDCl}_3$ ):  $\delta$  8.00 ( $\text{CO}_2\text{H}$ , 1H, s.);  $\delta$  7.50 (CH, 1H, d.);  $\delta$  6.15 (CH, 1H, d.);  $\delta$  4.56 (ferrocenyl.  $\text{H}_{2,5}, \text{H}_{3,4}$ , 4H, 2t.);  $\delta$  4.26 (ferrocenyl. ring, 5H, s.).

Ferrocenylpropionic acid<sup>36</sup>

$\beta$ -Ferrocenylacrylic acid (5 g, 0.012 mol) was dissolved in dry ether (50 ml). Ammonia (250 ml) was condensed onto the solution and a 4 molar equivalence of sodium (1.1 g) was added in small portions. The solution was stirred for 1 hour and 10 molar equivalence of ammonium chloride (6.4 g) was then added. The solution was again stirred for 1 hour. The ammonia was removed and water (100 ml) was added to the solution. Dilute HCl was added until the solution was acidic. The ferrocenyl acid was removed by ether extraction and the extract dried ( $\text{MgSO}_4$ ). The ether was removed by distillation leaving a crude product. Recrystallization from light petroleum and chloroform gave the desired product.

Yield: 4.3 g (86%), m.p.  $120^\circ\text{C}$  (LIT: m.p.  $119-120^\circ\text{C}$ )<sup>172</sup>  
 $^1\text{H}$  n.m.r. (90 MHz,  $\text{CDCl}_3$ ):  $\delta$  4.11 (ferrocenyl., 9H, c.);  $\delta$  2.64 ( $\text{CH}_2$ , 4H, b.s.).

$\alpha$ -Keto-1,1'-trimethyleneferrocene 37

$\beta$ -Ferrocenylpropionic acid (3.5 g, 0.014 mol) was dissolved in dry methylene chloride (75 ml). This was added to a magnetically stirred, ice-cooled solution of trifluoroacetic anhydride (7 g) in methylene chloride (75 ml). The mixture was stirred in the dark at 0°C for 5 hours. The solution was then passed into sodium bicarbonate solution and the organic layer separated. The aqueous layer was washed with ether and the combined organic solution was washed to neutrality and dried ( $\text{MgSO}_4$ ) after the removal of the solvent. The pure ketone was separated on an alumina column and recrystallized from petroleum.

Yield: 0.9 g (27%), m.p. 144-145°C (LIT: m.p. 144-145°C)<sup>172</sup>

$^1\text{H}$  n.m.r. (90 MHz,  $\text{CDCl}_3$ );  $\delta$ 4.83 (ferrocenyl. H, 2H, t.);  $\delta$ 4.60

(ferrocenyl.  $\text{H}_{1,1}$ , 2H, t.);  $\delta$ 4.39 (ferrocenyl.  $\text{H}_2$ , 2H, t.);  $\delta$  4.03

(ferrocenyl.  $\text{H}_{3,1}$ , 2H, t.);  $\delta$ 1.96 ( $\text{CH}_2$ , 4H, s.).

[3]Ferrocenophane

$\alpha$ -Keto-1,1'-trimethyleneferrocene (0.5 g, 0.002 mol) was dissolved in dry ether (15 ml). Lithium aluminium hydride (0.112 g, 0.003 mol) and aluminium chloride anhydrous (0.75 g, 0.0057 mol) were added to the solution. The reaction mixture was refluxed for 45 minutes after which aliquots of methyl formate dissolved in dry ether was added at 0°C until the effervescence ceased. This was followed by the addition of sulphuric acid (20%, 75 ml) at 0°C. The mixture was extracted with ether and the extracts were dried ( $\text{MgSO}_4$ ). The solvent was removed leaving a crude

yellow material. Recrystallization from light petroleum and ether gave the desired product as red crystals.

Yield: 0.46 g (98%), m.p. 108°C (LIT: m.p. 108-109°C)<sup>172</sup>

<sup>1</sup>H n.m.r. (90 MHz, CDCl<sub>3</sub>); δ 4.02 (ferrocenyl, 8H, s.); δ 1.96 (CH<sub>2</sub>, 6H, s.).

Ferrocene amides1,1'-bis(N,N-dimethylamido)ferrocene (58)

Excess dimethylamine (100%) (10 ml) was injected into a solution of 1,1'-ferrocene dicarboxyl chloride (0.5 g, 0.0016 mol) in dry toluene (50 ml) cooled to 0°C. After stirring for 10 minutes the mixture was filtered to remove precipitated dimethylamine hydrachloride, and the solvent evaporated to yield 0.52 g (100%) 1,1'-bis(N,N-dimethylamido)ferrocene. This was then passed down an alumina column with dichloromethane (grade 1) to remove traces of acid which may still be present, after dichloromethane (400 ml) was passed down the column, 1% methanol in dichloromethane was used to remove the amide from the alumina. The solvent was evaporated and the product recrystallised from chloroform.

Yield: 0.5 g (95%), m.p. 130°C (LIT: m.p. 130°C)<sup>153</sup>

Analysis; Calculated: C. 58.58%; N. 8.54%; H. 6.10%

Found: C. 58.58%; N. 8.53%; H. 6.08%

<sup>1</sup>H n.m.r. (90 MHz, CDCl<sub>3</sub>): δ4.66 (ferrocenyl. H<sub>2,5</sub>, 4H, t.);  
δ4.38 (ferrocenyl. H<sub>3,4</sub>, 4H, t.); δ3.06 (CH<sub>3</sub>, 12H, s.).

General Method

An amine, triethylamine mixture (ratio 2+2.2) in dry benzene (20 ml) was added to a solution of 1,1'-ferrocene-dicarbonyl chloride (ratio 1) in dry benzene (50 ml) and stirred for 10 minutes. The mixture was then filtered to remove precipitated trimethylamine hydrachloride and the

solvent evaporated to yield the crude amide. This was dissolved in dichloromethane and put on an alumina column (grade 1). Dichloromethane (400 ml) was passed down the column to remove any amine present. Methanol (1%) in dichloromethane was then passed through the alumina to remove the amide. The solvent was evaporated and the product recrystallised from chloroform.

The following amides were all prepared by the general method outlined above.

1,(N,N-dimethylamido)ferrocene (55)

Yield: 95%, m.p. 110.5°C (LIT: m.p. 111-113°C)<sup>163</sup>

Analysis; Calculated: C. 60.75%; N. 5.45%; H. 5.84%

Found: C. 60.70%; N. 5.40%; H. 5.80%

<sup>1</sup>H n.m.r. (90 MHz, CDCl<sub>3</sub>): δ 4.62 (ferrocenyl. H<sub>2,5</sub>, 2H, t.);  
 δ 4.29 (ferrocenyl. H<sub>3,4</sub>, 2H, t.); δ 4.22 (ferrocenyl. ring, 5H, s.);  
 δ 3.10 (CH<sub>3</sub>, 6H, s.).

1,(N,N-diethylamido)ferrocene (56)

Yield: 94%, m.p. 124°C

Analysis: Calculated: C. 63.21%; N. 4.92%; H. 6.67%

Found: C. 63.31%; N. 4.90%; H. 6.71%

<sup>1</sup>H n.m.r. (90 MHz, CDCl<sub>3</sub>): δ 4.64 (ferrocenyl. H<sub>2,5</sub>, 2H, t.); δ 4.32  
 (ferrocenyl. H<sub>3,4</sub>, 2H, t.); δ 4.22 (ferrocenyl. ring, 5H, s.); δ 2.54  
 (CH<sub>2</sub>, 4H, s.); δ 1.22 (CH<sub>3</sub>, 6H, s.).

1,1'-bis(N,N-diethylamido)ferrocene (60)

Yield: 93%, m.p. 59°C

Analysis; Calculated: C. 62.25%; N. 7.30%; H. 7.29%

Found: C. 62.40%; N. 7.30%; H. 7.30%

<sup>1</sup>H n.m.r. (90 MHz, CDCl<sub>3</sub>): δ 4.64 (ferrocenyl. H<sub>2,5</sub>, 4H, t.); δ 4.36 (ferrocenyl. H<sub>3,4</sub>, 4H, t.); δ 3.45 (CH<sub>2</sub>, 8H, s.); δ 1.20 (CH<sub>3</sub>, 12H, s.).

Ferrocene-1,-carboxylic acid, morpholide (57)

Yield: 90%, m.p. 112°C

Analysis; Calculated: C. 57.55%; N. 8.95%; H. 5.43%

Found: C. 57.51%; N. 8.95%; H. 5.40%

<sup>1</sup>H n.m.r. (90 MHz, CDCl<sub>3</sub>): δ 4.70 (ferrocenyl. H<sub>2,5</sub>, 2H, t.); δ 4.45 (ferrocenyl. H<sub>3,4</sub>, 2H, t.); δ 4.39 (ferrocenyl. ring, 5H, s.); δ 3.86 (CH<sub>2</sub>, 8H, b.s.).

Ferrocene-1,1'-dicarboxylic acid, morpholide (62)

Yield: 90%, m.p. 179.5°C

Analysis; Calculated: C. 58.29%; N. 6.80%; H. 5.83%

Found: C. 58.32%; N. 6.83%; H. 5.88%

<sup>1</sup>H n.m.r. (90 MHz, CDCl<sub>3</sub>): δ 4.60 (ferrocenyl. H<sub>2,5</sub>, 4H, t.); δ 4.40 (ferrocenyl. H<sub>3,4</sub>, 4H, t.); δ 3.66 (CH<sub>2</sub>, 16H, b.s.).

Ferrocene-1,1'-dicarboxylic acid, piperidide (64)

Yield: 96%, m.p. 164.5°C

Analysis; Calculated: C. 64.75%; N. 6.87%; H. 6.86%

Found: C. 64.80%; N. 6.89%; H. 6.89%

<sup>1</sup>H n.m.r. (90 MHz, CDCl<sub>3</sub>): δ 4.58 (ferrocenyl. H<sub>2,5</sub>, 4H, t.); δ 4.38 (ferrocenyl. H<sub>3,4</sub>, 4H, t.); δ 3.65 (NCH<sub>2</sub>, 8H, s.); δ 1.62 (CH<sub>2</sub>, 12H, s.).



Ferrocene-1,1'-dicarboxylic acid, dipyrrolidide (66)

Yield: 90%, m.p. 173°C

Analysis; Calculated: C. 63.20%; N. 7.37%; H. 6.32%

Found: C. 63.24%; N. 7.40%; H. 6.32%

<sup>1</sup>H n.m.r. (90 MHz, CDCl<sub>3</sub>): δ4.76 (ferrocenyl. H<sub>2,5</sub>, 4H, t.); δ4.36  
(ferrocenyl. H<sub>3,4</sub>, 4H, t.); δ3.59 (NCH<sub>2</sub>, 8H, s.); δ1.99 (CH<sub>2</sub>, 8H, s.).

1,1'-bis(N-ethylamido)ferrocene (53)Yield: 70%, m.p. 193°C (LIT: m.p. 196°C)<sup>174</sup>

Analysis; Calculated: C. 62.17%; N. 7.25%; H. 7.84%

Found: C. 62.20%; N. 7.26%; H. 7.86%

<sup>1</sup>H n.m.r. (90 MHz, CDCl<sub>3</sub>): δ7.20 (HN, 2H, s.); δ4.55 (ferrocenyl. H<sub>2,5</sub>,  
4H, t.); δ4.35 (ferrocenyl. H<sub>3,4</sub>, 4H, t.); δ2.80 (CH<sub>2</sub>, 4H, s.);  
δ1.25 (CH<sub>3</sub>, 6H, s.).

1,1'-bis(N-phenylamido)ferrocene (43)Yield: 50%, m.p. 212°C (LIT: m.p. 212°C)<sup>174</sup>

Analysis; Calculated: C. 66.17%; N. 7.02%; H. 4.81%

Found: C. 66.17%; N. 7.04%; H. 4.83%

<sup>1</sup>H n.m.r. (250 MHz, CDCl<sub>3</sub>): δ8.69 (HN, 2H, s.); δ7.80 (aromatic  
H<sub>3</sub>, 4H, d.); δ7.39 (aromatic H<sub>4</sub>, 4H, t.); δ7.15 (aromatic H<sub>5</sub>, 2H, t.);  
δ4.67 (ferrocenyl. H<sub>2,5</sub>, 4H, t.); δ4.49 (ferrocenyl. H<sub>3,4</sub>, 4H, t.).

1,1'-bis(N-benzylamido)ferrocene (51)

Yield: 80%, m.p. 173°C

Analysis; Calculated: C. 69.03%; N. 6.19%; H. 5.36%

Found: C. 69.08%; N. 6.21%; H. 5.38%

<sup>1</sup>H n.m.r. (250 MHz, CDCl<sub>3</sub>): δ7.21 (aromatic, 10H, c.m.); δ7.01 (HN, 2H,  
t.); δ4.57 (CH<sub>2</sub>, 4H, d.); δ4.48 (ferrocenyl. H<sub>2,5</sub>, 4H, t.); δ4.34  
(ferrocenyl. H<sub>3,4</sub>, 4H, t.).

Ferrocene MacrocyclesThe General High Dilution Method1,11-(1,1'-ferrocenediamido)-3,6,9-trioxaunadecane (31)

1,11-diamino-3,6,9-trioxaunadecane (1.1 g, 0.00572 mol) freshly distilled from solid KOH was dissolved in dry benzene (50 ml) containing triethylamine (1.27 g, 0.0126 mol), dried by distillation from solid KOH. Ferrocene bis acid chloride (1.78 g, 0.00572 mol) was dissolved in dry benzene (50 ml). The two solutions were added dropwise, simultaneously to a 1 litre creased flask containing dry benzene (100 ml). The two solutions were added over a period of 2 hours during which time the solution was stirred vigorously under a nitrogen atmosphere. The stirring was then continued for a further 17 hours. The solution was then filtered to remove  $\text{Et}_3\text{NHCl}$ , evaporated to dryness and washed through an alumina column with methylene chloride. The product was then recrystallised from toluene.

Yield: 1.31 g (53%), m.p. 155-6°C

Analysis; Calculated: C. 55.8%; N. 6.5%; H. 6.1%

Found: C. 56.0%; N. 6.4%; H. 6.2%

$^1\text{H}$  n.m.r. (90 MHz,  $\text{CDCl}_3$ ):  $\delta$  7.04 (HN, 2H, t.);  $\delta$  4.66 (ferrocenyl.  $\text{H}_{2,5}$ , 4H, t.);  $\delta$  4.40 (ferrocenyl.  $\text{H}_{3,4}$ , 4H, t.);  $\delta$  3.71 ( $\text{CH}_2\text{O}$ , 12H, b.s.);  $\delta$  3.63 ( $\text{CH}_2\text{N}$ , 4H, c.m.).

Mass Spectra: Calculated: M/e: 430; Found: M/e: 430.

Ferrocene[2.2]cryptand(monomer) (38) and ferrocene[2.2]<sup>cryptand</sup>(dimer)(39)

A 1 litre 3-necked creased flask, equipped with a mechanical stirrer, was flushed with nitrogen and charged with dry benzene (100 ml). A solution of 1,1'-bis(chlorocarbonyl) ferrocene (1.18 g, 0.0030 mol) dissolved in benzene (100 ml) was placed in a pressure equalised dropping funnel. In a second similar dropping funnel were placed 1,4,10,13-tetraoxa-7,16-diazacyclooctadecane (1 g, 0.0038 mol) and triethylamine (0.85 g, 0.0084 mol) in benzene (100 ml). The two solutions were added dropwise, simultaneously over a period of 2½ hours, with vigorous stirring. The mixture became orange and deposited a fine precipitate of triethylamine hydrochloride. When the addition was complete the mixture was stirred for a further 4 hours and left to stand overnight. The solids were separated by filtration and the solvent was then removed to leave an orange residue. This material was chromatographed on a column of alumina using methylene chloride - 0.5% methanol. An orange band was collected, evaporated and the product recrystallised from methylene chloride and pentane.

Yield: (monomer) 0.99 g (52%), m.p. 183-184°C

(LIT: 40%, m.p. 183-184°C)<sup>153</sup>

Analysis; Calculated: C. 57.61%; N. 5.60%; H. 6.44%

Found: C. 57.34%; N. 5.65%; H. 6.50%

Mass Spectra: Calculated M/e: 500; Found M/e: 500.

<sup>1</sup>H n.m.r. (250 MHz, CDCl<sub>3</sub>): Table 5.12.

Further elution of the column using methylene chloride - 2% methanol produced a second orange band which was collected, evaporated and the product recrystallised from methylene chloride and pentane.

Yield: (dimer) 0.29 g (15%), m.p. 244-245°C)

(LIT: 26%, m.p. 244-245°C)<sup>153</sup>

Analysis; Calculated: C. 57.61%; N. 5.60%; H. 6.44%

Found: C. 57.65%; N. 5.47%; H. 6.48%

Mass Spectra: Calculated M/e: 1000, Found M/e: 1000.

<sup>1</sup>H n.m.r. (250 MHz, CDCl<sub>3</sub>): δ 4.63 (ferrocenyl. H<sub>2,5</sub>, 8H, t.); δ 4.35

(ferrocenyl. H<sub>3,4</sub>, 8H, t.); δ 4.0-3.4 (CH<sub>2</sub>, 48H, com.).

Ruthenocene derivativesRuthenocene<sup>35</sup>

A 500 ml flask was purged with nitrogen and dry 1,2-dimethoxyethane (300 ml) was added followed by sodium (7.7 g, 0.355 mol) in small pieces. The solution was stirred and freshly distilled cyclopentadiene (32 ml, 0.388 mol) was added dropwise. After the evolution of hydrogen had stopped the mixture was heated and stirred at slightly below reflux temperature (80°C) for 1½ hours. (In the event that not all the sodium dissolves, the solution should be cooled to room temperature and a little more cyclopentadiene added. The above procedure should then be repeated.)

Ruthenium trichloride (15 g, 0.067 mol) and ruthenium powder (2.4 g, 0.024 mol) was added slowly to the reaction mixture and heated and stirred at (80°C) for 80 hours. The mixture was then allowed to cool to room temperature and worked up via one of the following methods:

Method 1 - The contents of the flask were evaporated to dryness and the flask was filled with nitrogen. The residue was then transferred to a sublimator under nitrogen and this was sublimed (0.1 mm, 130°C). The flask was allowed to cool to room temperature before removing the vacuum and replacing it with a nitrogen atmosphere. The sublimate was dissolved in benzene and passed through a 1 x 12" column of activated alumina. The solvent was evaporated and the product

recrystallised from chloroform.

Yield: 8.9g (57%), m.p. 199°C (LIT: m.p. 199°C)<sup>35</sup>.

Method 2 - Dry methanol (120 ml) was added very slowly to the flask and the contents were then evaporated to dryness and the residue was transferred to a Soxhlet and extracted with benzene for 48 hours. The benzene solution was then concentrated and passed through a 1 x 12" column of activated alumina. The solvent was evaporated and the product recrystallised from chloroform.

Yield: 10.1 g (65%) m.p. 199°C (LIT: m.p. 199°C)<sup>35</sup>

<sup>1</sup>H n.m.r. (90 MHz, CDCl<sub>3</sub>): δ 4.75 (HC, 10H, s.).

<sup>13</sup>C n.m.r. (62.5 MHz, CDCl<sub>3</sub>): δ 83.32 (CH, 10C, s.).

The above preparation was repeated using dry tetrahydrofuran as the solvent and sodium hydride instead of sodium metal.

Yield: 69%.

#### Lithium,1,1'-ruthenocene dicarboxylic salt

Ruthenocene (5 g, 0.022 mol) was dissolved in dry ether (150 ml) and dry tetrahydrofuran (100 ml) in a 500 ml three necked flask under a nitrogen atmosphere maintained at -50°C. n-Butyl lithium (8.3 g, 0.129 mol) in hexane (52 ml) was added slowly to T.M.E.D.A. (15 g, 0.129 mol) in dry hexane (20 ml) and left to stand for 15 minutes in a dropping funnel under a nitrogen atmosphere. This was added to the ruthenocene and stirred at -50°C for 1 hour. The

mixture was allowed to warm to room temperature and stirred for a further 24 hours. The dilithioruthenocene suspension was then injected into a CO<sub>2</sub>/ether slush. After the CO<sub>2</sub> evaporated the dilithium salt was filtered and washed with dry ether yielding the crude lithium 1,1'-ruthenocene dicarboxylic acid.

The salt may be converted into the acid using the method described for 1,1'-ferrocenedicarboxylic acid.

Yield: 4.98 g (71%); m.p. 325° dec.

(LIT: m.p. 325°C dec.)<sup>54,36,38</sup>

#### Dimethyl ruthenocene-1,1'-dicarboxylate (27)

Lithium 1,1'-ruthenocenedicarboxylic salt (0.16 g, 0.00047 mol) was dissolved in dry methanol (10 ml). Dimethylsulphate (0.149 g, 0.00118 mol) in methanol (5 ml) was added to the salt. The mixture was stirred and refluxed for 3 hours. Methanol (10 ml) was then removed by distillation and the solution was allowed to cool to room temperature. Ether (30 ml) was then added and the solution was washed with water (10 ml) and sodium carbonate (10%) (10 ml). The ether layer was washed again with water and then dried (MgSO<sub>4</sub>). The ether was evaporated and the product was recrystallised from pet-ether 40-60° as pale yellow/white fibrous crystals.

Yield: 0.11 g (71%), m.p. 133-134°C

Analysis; Calculated: C. 48.4%; H. 4.1%

Found: C. 48.4%; H. 4.0%

$^1\text{H}$  n.m.r. (60 MHz,  $\text{CDCl}_3$ ):  $\delta$ 5.17 (ruthenocenyl.  $\text{H}_{2,5}$ , 4H, t.);  
 $\delta$ 4.73 (ruthenocenyl.  $\text{H}_{3,4}$ , 4H, t.);  $\delta$ 3.74 ( $\text{CH}_3$ , 6H, s.).

1,1'-Ruthenocene bis acid chloride (28)

Lithium 1,1'-ruthenocenedicarboxylic salt (5.22 g, 0.0153 mol) in dichloromethane (100 ml) was treated with an excess of oxalyl chloride (15.4 g, 0.1225 mol) in dichloromethane (40 ml) under nitrogen. The suspension was stirred for 1 hour then refluxed for 3 hours. The excess oxalyl chloride and dichloromethane were removed by evaporation and the residue extracted with toluene. The toluene was evaporated and the product was recrystallised from dry hexane.

Yield: 2.6 g (47%), m.p.  $67^\circ\text{C}$

Analysis; Calculated: C. 40.5%; H. 2.3%

Found: C. 40.5%; H. 2.4%

$^1\text{H}$  n.m.r. (60 MHz,  $\text{CDCl}_3$ ):  $\delta$ 5.16 (ruthenocenyl.  $\text{H}_{2,5}$ , 4H, t.);  
 $\delta$  4.80 (ruthenocenyl.  $\text{H}_{3,4}$ , 4H, t.).



Ruthenocene amides

The following amides were all prepared by the general method outlined in the ferrocene amides section.

1,1'-bis(N,N-dimethylamido)ruthenocene (59)

Yield: 95%, m.p. 149°C

Analysis; Calculated: C. 51.48%; N. 7.51%; H. 5.36%

Found: C. 51.48%; N. 7.50%; H. 5.35%

<sup>1</sup>H n.m.r. (90 MHz, CDCl<sub>3</sub>): δ5.00 (ruthenocenyl. H<sub>2,5</sub>, 4H, t.);  
δ 4.70 (ruthenocenyl. H<sub>3,4</sub>, 4H, t.); δ3.02 (CH<sub>3</sub>, 12H, s.).

1,1'-bis(N,N-diethylamido)ruthenocene (61)

Yield: 90%, m.p. 154°C

Analysis; Calculated: C. 55.95%; N. 6.53%; H. 6.52%

Found: C. 56.00%; N. 6.56%; H. 6.57%

<sup>1</sup>H n.m.r. (90 MHz, CDCl<sub>3</sub>): δ5.00 (ruthenocenyl. H<sub>2,5</sub>, 4H, t.);  
δ 4.72 (ruthenocenyl. H<sub>3,4</sub>, 4H, t.); δ3.55 (CH<sub>2</sub>, 8H, s.); δ1.20  
(CH<sub>3</sub>, 12H, s.).

Ruthenocene-1,1'-dicarboxylic acid, morpholide (63)

Yield: 75%

Analysis; Calculated: C. 52.53%; N. 6.13%; H. 5.25%

Found: C. 52.54%; N. 6.17%; H. 5.28%

<sup>1</sup>H n.m.r. (90 MHz, CDCl<sub>3</sub>): δ4.96 (ruthenocenyl. H<sub>2,5</sub>, 4H, t.);  
δ 4.76 (ruthenocenyl. H<sub>3,4</sub>, 4H, t.); δ3.74 (CH<sub>2</sub>, 16H, s.).

Ruthenocene-1,1'-dicarboxylic acid, piperidide (65)

Yield: 70%

Analysis; Calculated: C. 58.30%; N. 6.18%; H. 6.18%

Found: C. 58.50%; N. 6.20%; H. 6.20%

$^1\text{H}$  n.m.r. (90 MHz,  $\text{CDCl}_3$ ):  $\delta$  4.85 (ruthenocenyl.  $\text{H}_{2,5}$ , 4H, t.);  
 $\delta$  4.62 (ruthenocenyl.  $\text{H}_{3,4}$ , 4H, t.);  $\delta$  3.58 ( $\text{NCH}_2$ , 8H, s.);  $\delta$  1.60 ( $\text{CH}_2$ ,  
 12H, s.).

Ruthenocene-1,1'-dicarboxylic acid, dipyrrolidide (67)

Yield: 74%

Analysis; Calculated: C. 56.48%; N. 6.59%; H. 5.64%

Found: C. 56.63%; N. 6.61%; H. 5.78%

$^1\text{H}$  n.m.r. (90 MHz,  $\text{CDCl}_3$ ):  $\delta$  4.96 (ruthenocenyl.  $\text{H}_{2,5}$ , 4H, t.);  $\delta$  4.58  
 (ruthenocenyl.  $\text{H}_{3,4}$ , 4H, t.);  $\delta$  3.52 ( $\text{NCH}_2$ , 8H, s.);  $\delta$  1.82 ( $\text{CH}_2$ , 8H, s.).

1,1'-bis(N-ethylamido)ruthenocene (54)

Yield: 75%, m.p. 169°C

Analysis; Calculated: C. 55.66%; N. 6.49%; H. 7.02%

Found: C. 55.59%; N. 6.42%; H. 6.94%

$^1\text{H}$  n.m.r. (90 MHz,  $\text{CDCl}_3$ ):  $\delta$  7.20 (HN, 2H, b.s.);  $\delta$  4.96 (ruthenocenyl.  
 $\text{H}_{2,5}$ , 4H, t.);  $\delta$  4.60 (ruthenocenyl.  $\text{H}_{3,4}$ , 4H, t.);  $\delta$  3.25 ( $\text{CH}_2$ , 4H, q.);  
 $\delta$  1.12 ( $\text{CH}_3$ , 6H, t.).

1,1'-bis(N-benzylamido)ruthenocene (52)

Yield: 72%, m.p. 134°C

Analysis; Calculated: C. 62.76%; N. 5.63%; H. 4.87%

Found: C. 62.70%; N. 5.60%; H. 4.80%

$^1\text{H}$  n.m.r. (90 MHz,  $\text{CDCl}_3$ ):  $\delta$  7.32 (aromatic, 10H, c.);  $\delta$  6.79 (HN, 2H, b.s.);  
 $\delta$  5.09 ( $\text{CH}_2$ , 4H, b.s.);  $\delta$  4.68 (ruthenocenyl.  $\text{H}_{2,5}$ , 4H, t.);  $\delta$  4.46  
 (ruthenocenyl.  $\text{H}_{3,4}$ , 4H, t.).

Ruthenocene macrocyclesRuthenocene[2.2]cryptand (monomer) (41) and ruthenocene[2.2]cryptand (dimer) (42)

A 1 litre 3-necked creased flask, equipped with a mechanical stirrer, was flushed with nitrogen and then charged with dry benzene (100 ml). A solution of 1,1'-bis(chlorocarbonyl)ruthenocene (1.36 g, 0.00382 mol) dissolved in benzene (100 ml) was placed in a pressure-equalised dropping funnel. In a second similar dropping funnel were placed 1,4,10,13-tetraoxa-7,16-diazacyclooctadecane (diaza[18]crown-6) (1 g, 0.00382 mol) and triethylamine (0.85 g, 0.0084 mol) in benzene (100 ml). The two solutions were added dropwise, simultaneously over a period of 4 hours, with vigorous stirring. The mixture became pale yellow and deposited a fine precipitate of triethylamine hydrochloride. When the addition was complete the mixture was stirred for a further 21 hours. The solids were separated by filtration and the solvent was then removed to leave an oily yellow residue. This material was chromatographed on a column of alumina (grade 1) using methylene chloride - 0.5% methanol. A yellow band was collected, evaporated and the product recrystallised from methylene chloride and pentane.

Yield: (monomer) 0.78 g (38%), m.p. 204.5°C

Analysis; Calculated: C. 52.83%; N. 5.13%; H. 5.13%

Found: C. 56.80%; N. 5.11%; H. 5.11%

Mass Spectra; Calculated M/e: 545; Found M/e: 545.

<sup>1</sup>H n.m.r. (250 MHz, CDCl<sub>3</sub>): Table 5.12.

Further elution of the column using methylene chloride-2% methanol produced a second yellow band. This was collected, evaporated and recrystallised from methylene chloride and pentane.

Yield: (dimer) 0.53 g (26%), oil.

Analysis; Calculated: C. 52.83%; N. 5.13%; H. 5.13%

Found: C. 52.77%; N. 5.15%; H. 5.10%

Mass Spectra: Calculated M/e: 1090; Found M/e: 1090

$^1\text{H}$  n.m.r. (90 MHz,  $\text{CDCl}_3$ ):  $\delta$ 4.95 (ruthenocenyl.  $\text{H}_{2,5}$ , 8H, t.);  $\delta$  4.66 (ruthenocenyl.  $\text{H}_{3,4}$ , 8H, t.);  $\delta$ 3.8-3.6 ( $\text{CH}_2$ , 48H, c.m.).

The general high dilution method was used to prepare the following ruthenocene macrocycles.

Ruthenocene[3.2] cryptand monomer (76) and dimer (77)

(76) Yield: 21%

Analysis; Calculated: C. 52.97%; N. 4.75%; H. 6.11%

Found: C. 53.00%; N. 4.80%; H. 6.20%

Mass Spectra: Calculated M/e: 589; Found M/e: 589.

$^1\text{H}$  n.m.r. (250 MHz,  $\text{CDCl}_3$ ): Table 5.14.

(77) Yield: 56%

Analysis; Calculated: C. 52-97%; N. 4.75%; H. 6.11%

Found: C. 53.04%; N. 4.81%; H. 6.17%

Mass Spectra; Calculated M/e: 1178; Found M/e: 1178.

$^1\text{H}$  n.m.r. (250 MHz,  $\text{CDCl}_3$ ): Table 5.16.

Ruthenocene[3.1] cryptand monomer (78) and dimer (79)

(78) Yield: 27%

Analysis; Calculated: C. 52.84%; N. 5.14%; H. 5.87%

Found: C. 52.79%; N. 5.09%; H. 5.80%

Mass Spectra; Calculated M/e: 545; Found M/e: 545.

<sup>1</sup>H n.m.r. (90 MHz, CDCl<sub>3</sub>): Table 5.14.

(79) Yield: 48%.

Analysis; Calculated: C. 52.84%; N. 5.14%; H. 5.87%

Found: C. 52.75%; N. 5.04%; H. 5.78%

Mass Spectra; Calculated M/e: 1090; Found M/e: 1090

<sup>1</sup>H n.m.r. (90 MHz, CDCl<sub>3</sub>): Table 5.16.

Ruthenocene[2.1] cryptand monomer (82) and dimer (83)

(82) Yield: 15% @ 60°C and 5% @ 1°C.

Analysis; Calculated: C. 52.51%; N. 5.61%; H. 5.61%

Found: C. 52.50%; N. 5.59%; H. 5.60%

Mass Spectra; Calculated M/e: 499; Found M/e: 499

<sup>1</sup>H n.m.r. (90 MHz, CDCl<sub>3</sub>): Table 5.14.

(83) Yield: 53% @ 60°C and 40% @ 1°C

Analysis; Calculated: C. 52.51%; N. 5.61%; H. 5.61%

Found: C. 52.53%; N. 5.62%; H. 5.64%

Mass Spectra; Calculated M/e: 998; Found M/e: 998

<sup>1</sup>H n.m.r. (90 MHz, CDCl<sub>3</sub>): Table 5.16.

## Appendix 1

Principal I.R. bands  $\text{cm}^{-1}$  (run as mujol mills).

Assignment	C=O (s.v)	CO-NH Amide II	CH(sv)/(d)					
<u>COMPOUND</u>								
Ferrocene			1800	1160	1102	1000	815	722
1-acetylferrocene	1680		1270	1160	1110	1000	820	722
1,1'-diacetylferrocene	1660		1280	-	-	975	840	720
1-methylferrocene carboxylate	1705		1285	1198	1145	960	895	-
1,1'-dimethylferrocene dicarboxylate	1705, 1700		1290	1198	1145	960	895	720
1-(N,N-dimethylamido)-ferrocene (55)	1610		1300	-	1110	925	815	720
1,1'-bis(N,N-dimethylamido)-ferrocene (58)	1610		1260	-	1110	975	825	720
1,1'-bis(N-ethylamido)-ferrocene (53)	1630	1550	1310	-	1140	975	-	720
1,1'-bis(N-benzylamido)-ferrocene (51)	1630	1550	1295	-	1030	975	-	720
1-(N,N-diethylamido)-ferrocene (56)	1620		1300	1175	1105	975	825	720
1,1'-bis(N,N-diethylamido)-ferrocene (60)	1625		1305	1240	1030	940	830	720
1-(N-morpholine amido)-ferrocene (57)	1620		1300	-	1110	925	825	720
1,1'-bis(N,N-morpholine amido)-ferrocene (62)	1610		1170	1170	1100	1000	820	720
1,1'-bis(N,N-piperidine amido)-ferrocene (64)	1615		1270	1175	-	1000	820	720
1,1'-bis(N,N-pyrolidine amido)-ferrocene (66)	1610		1300	1165	1020	975	830	720
Ferrocene 2.2.cryptand (monomer) (38)	1605, 1610		1305	1140	1110	-	840	720
Ferrocene 2.2.cryptand (dimer) (39)	1620		1310	1140	1095	-	975	720

(s.v) stretching vibrations; (d) deformation

Principal I.R. bands  $\text{cm}^{-1}$

Assignment	N-H (sv)	O-H (sv)	C=O (sv)	CH(sv)/d.				MULL
<u>COMPOUND</u>								
Ruthenocene								MUJOL
1,1'-ruthenocene bis acid chloride (28)			1775				810	720
1,1'-ruthenocene dicarboxylic acid		2925	1765				825	700
1,1'-bis(N-benzylamido)-ruthenocene (52)			1630	1250	1110	1100	865	
1,1'-bis(N,N-dimethylamido)-ruthenocene (59)			1605	1245	1170	1045	940	
1,1'-bis(N-ethylamido)-ruthenocene (54)			1675	1300	1170	1040	985	-
1,1'-bis(N,N-morpholineamido)-ruthenocene (63)	3300		1620	1300	1170	1040	970	720
1,1'-bis(N,N-piperidine amido)-ruthenocene (65)			1610	1300	1145	1100	970	720
1,1'-bis(N,N-pyrrolidine amido)-ruthenocene (67)			1600	1490	1280	1180	1010	
Ruthenocene[2.2]cryptand (monomer) (41)			1605	1480	1280	1180	1015	
Ruthenocene[2.2]cryptand (dimer) (42)			1605	1475	1300	1100	1025	720
Ruthenocene[3.1]cryptand (monomer) (78)			1610	1380	1300	1150	970	720
Ruthenocene[3.1]cryptand (dimer) (79)			1610	1460	1380	1100	930	
Ruthenocene[2.1]cryptand (monomer) (82)			1710	1480	1410	1100	910	
Ruthenocene[2.1]cryptand (dimer) (83)			1600	1460	1370	1040	925	
Ruthenocene[2.3]cryptand (monomer) (76)			1710	1470	1410	1100	910	
Ruthenocene[2.3]cryptand (dimer) (77)			1610	1470	1410	1030	945	
				1480	1410	1100	910	

(sv) stretching vibration; (d) deformation

Appendix 2

Ruthenium has seven isotopes of which only two are magnetically active:  $^{99}\text{Ru}$ , natural abundance 12.7%,  $I = 5/2$  and  $^{101}\text{Ru}$ , natural abundance 17.1%,  $I = 5/2$ . There are two communications<sup>187,188</sup> to date reporting ruthenium n.m.r. observations which show that both ruthenium isotopes are satisfactory n.m.r. probes. We have observed with the aid of Dr. C. Brevard<sup>189</sup> (Bruker Spectrospin Ltd.)  $^{99}\text{Ru}$  resonance of ruthenocene itself on a demonstration Bruker WP200 spectrometer which provided a useful starting point.

Previous studies were able to establish the magnetic moments ( $N$ ) and quadrupole moments ( $Q$ ) of both isotopes. ( $^{99}\text{Ru}$ .  $N = -0.688151 N_N$ ,  $Q = 0.077$  Barn  
 $^{101}\text{Ru}$   $N = -0.715260 N_N$ ,  $Q = 0.460$  Barn. However, some of the other basic parameters were changed from the communication during the search for a ruthenium resonance frequency signal. It was found that  $^{99}\text{Ru}$ , although lower in natural abundance was much more sensitive than  $^{101}\text{Ru}$ .

The first sample investigated using a low frequency probe on a Joel FX90Q spectrometer was ruthenium tetraoxide which provided a high concentration of ruthenium nuclei per molecule. Questionable n.m.r. signals were found for ruthenium tetraoxide and ruthenocene [Table 11.1].



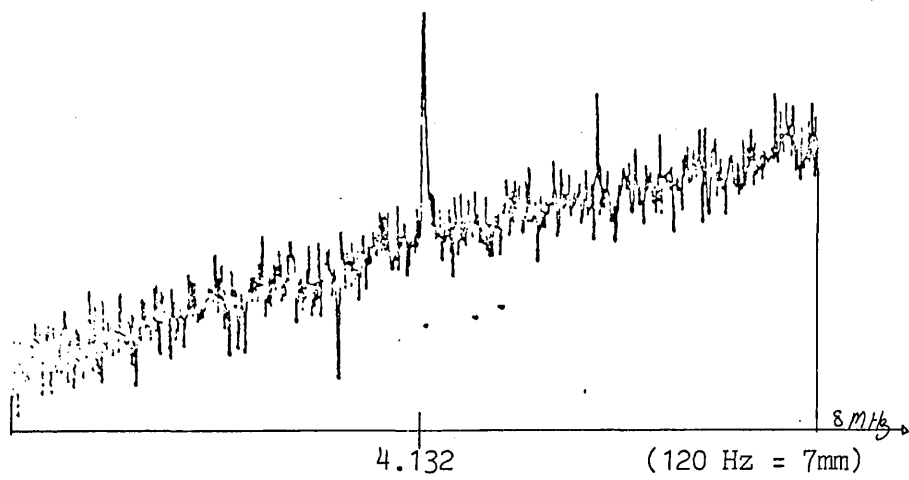
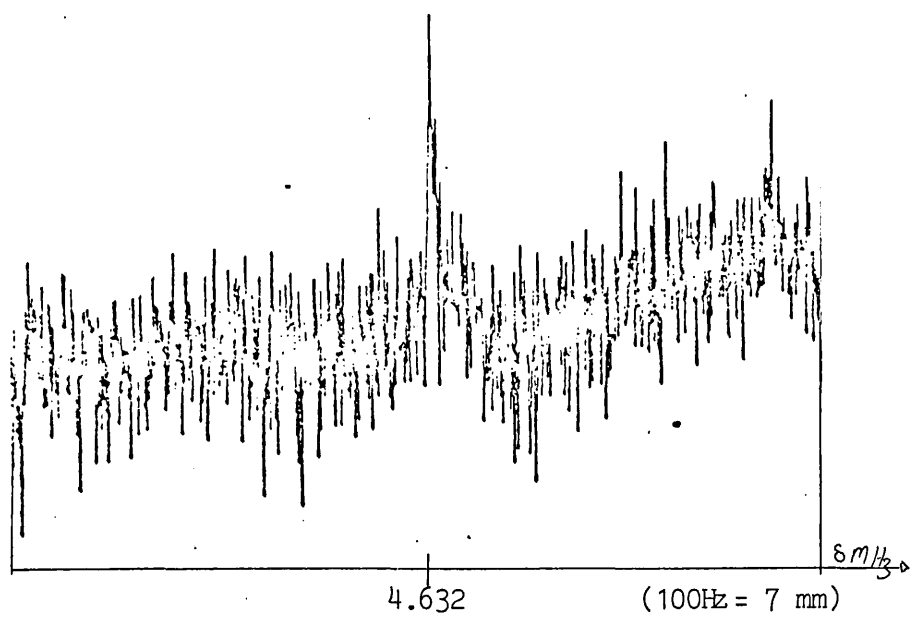
Table 11.1. Ruthenium 99 and 101 n.m.r.

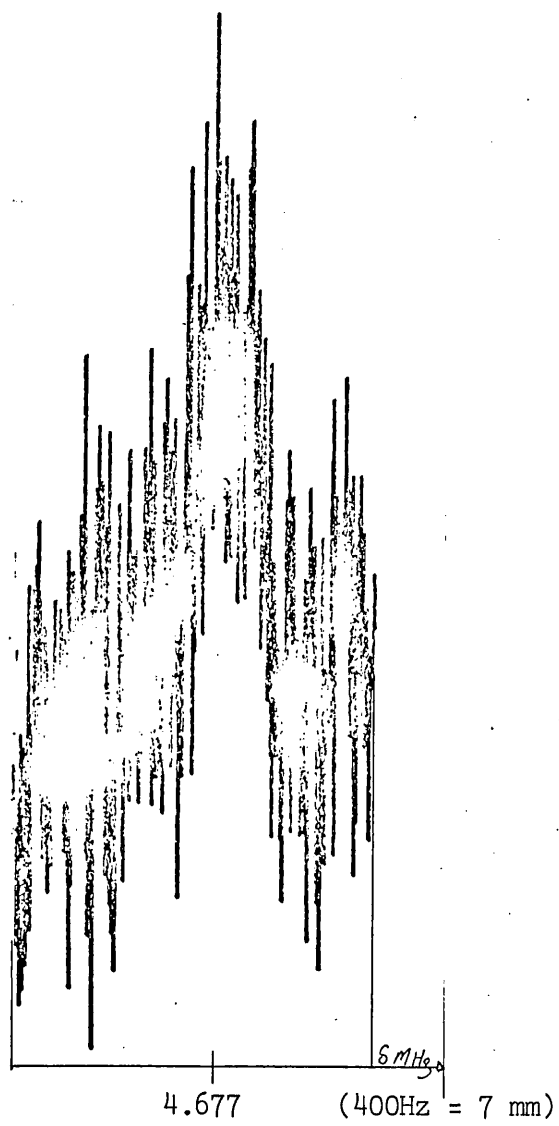
Joel FX909-FT				Bruker MD250 <sup>188</sup>			Varian FT-80A <sup>187</sup>	
	$\delta$ MHz	$\omega$ $\frac{1}{2}$ ht.Hz	$\omega$ Hz	$\delta$ MHz	$\omega$ $\frac{1}{2}$ ht.Hz	$\omega$ Hz	$\delta$ MHz	$\omega$ $\frac{1}{2}$ ht.Hz
<u>Ruthenium tetraoxide</u>								
<sup>99</sup> Ru	4.132176	4.0	14	11.541356	1.0	8	3.778875	1.0
<sup>101</sup> Ru	4.632209	13.0	24	12.935341	10.0	32	4.235296*	-
<u>Ruthenocene</u>								
<sup>99</sup> Ru	4.677716	475		11.734506	Broad			
<sup>101</sup> Ru	5.280923	475		13.151820*	-			
<sup>1</sup> H.TMS 89 MHz			<sup>1</sup> H.H <sub>2</sub> O.250.134741 MHz			<sup>1</sup> H.TMS 79.542111 MHz		

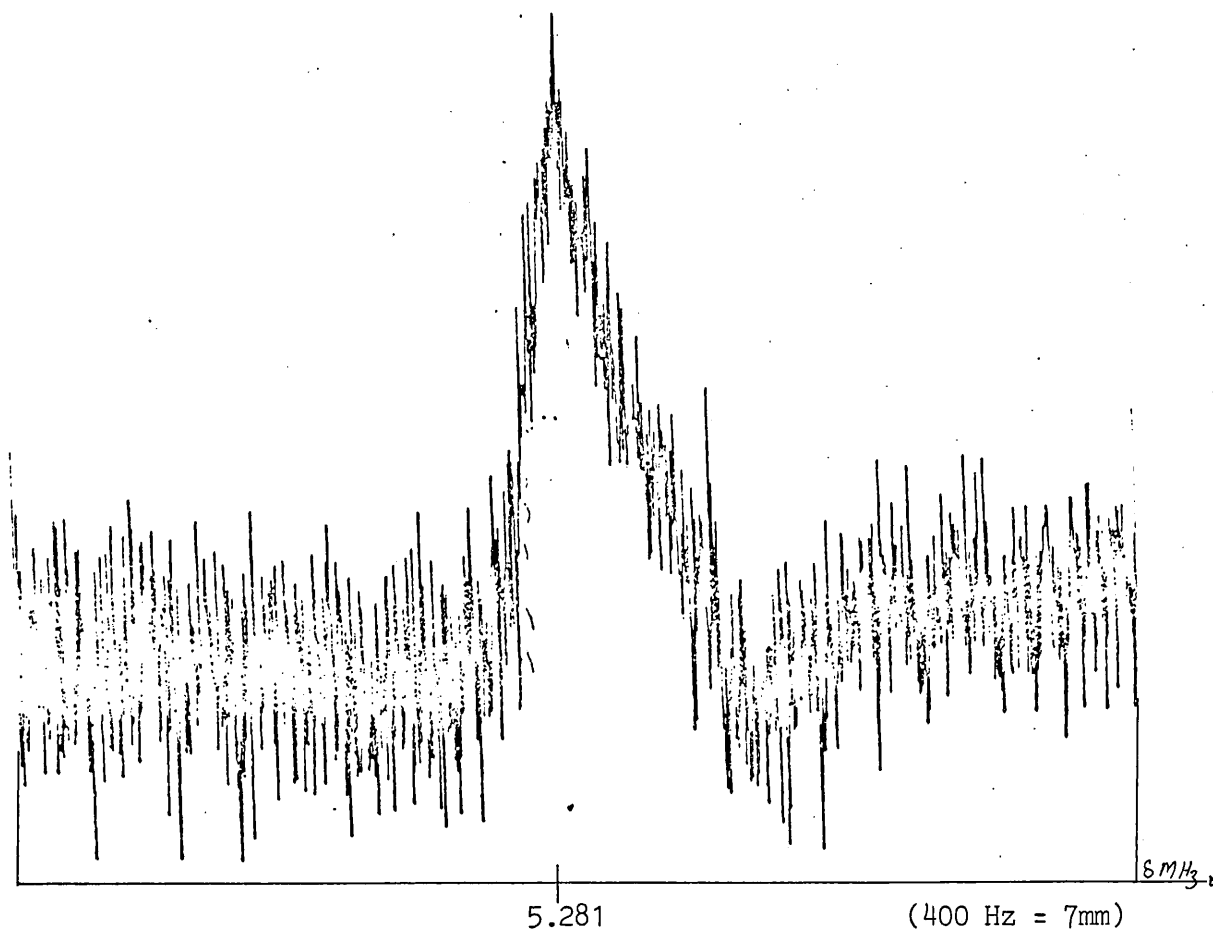
\*Calculated

The tetrahedral symmetry of the ruthenium tetraoxide molecule leads to a sharp resonance in contrast to the ruthenocene resonance which are broad reflecting the much lower symmetry of this molecule and should be treated with some caution.

The FX90Q spectrometer insert is not well designed for the study of insensitive nuclei with long pulse widths and the probe suffers strong acoustic ringing. No other spectrometers were available for the study of ruthenium samples within the University of London during the course of this project.

Ruthenium tetraoxide $^{99}\text{Ru}$  n.m.r. $^{101}\text{Ru}$  n.m.r.

Ruthenocene $^{99}\text{Ru}$  n.m.r.

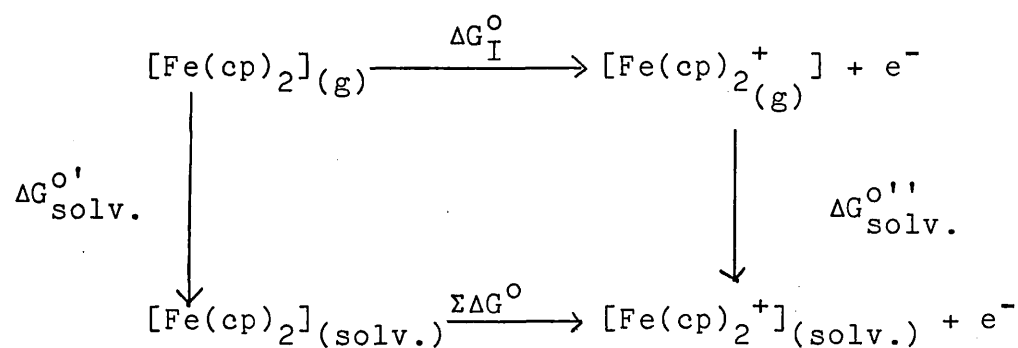
Ruthenocene $^{101}\text{Ru}$  n.m.r.

Appendix 3n.m.r. definitions

t	triplet
d	doublet
s	singlet
c	complex
b	broad
v	very
m	multiplet
q	quartet

Appendix 4. The thermodynamic relationship between the first ionisation energy and the half wave potential

Following the procedure of Buckingham and Sargesson, the redox half cell in question can be represented by the following form of the Born-Haber cycle:

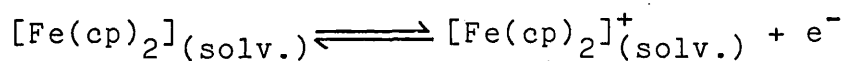


where:  $\Delta G_{\text{I}}^{\circ}$  is the free energy change on ionisation of ferrocene

$\Delta G_{\text{solv.}}^{\circ'}$  is the free energy change on solvation of ferrocene

$\Delta G_{\text{solv.}}^{\circ''}$  is the free energy change on solvation of the ferricenium ion

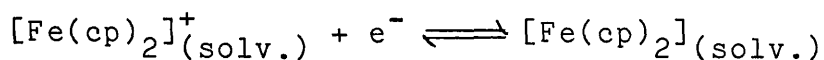
Thus, the overall free energy change for the process



is given by:

$$\Sigma \Delta G^{\circ} = \Delta G_{\text{I}}^{\circ} + \Delta G_{\text{solv.}}^{\circ''} - \Delta G_{\text{solv.}}^{\circ'}$$

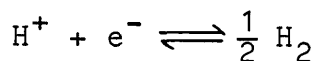
and that of:



is given by:

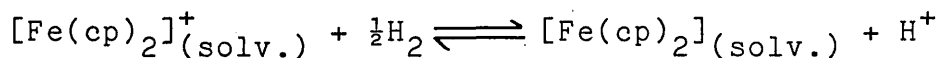
$$-\Sigma \Delta G_{\text{Fer}^+/\text{Fer}}^{\circ} = -\Delta G_{\text{I}}^{\circ} - \Delta G_{\text{solv.}}^{\circ'} + \Delta G_{\text{solv.}}^{\circ'}$$

The overall free energy change for the hydrogen half cell



is  $\Sigma \Delta G_{\text{H}^+/\frac{1}{2}\text{H}_2}$

Thus, overall, combining the two half cell reactions:



and  $\Delta G = -\Sigma \Delta G_{\text{Fer}^+/\text{Fer}}^{\circ} - \Sigma \Delta G_{\text{H}^+/\frac{1}{2}\text{H}_2}^{\circ}$

Now  $\Delta G = -zE^{\circ}F$  and  $z = 1$

Therefore

$$E^{\circ} = \frac{\Sigma \Delta G_{\text{Fer}^+/\text{Fer}}^{\circ}}{F} + \frac{\Sigma \Delta G_{\text{H}^+/\frac{1}{2}\text{H}_2}^{\circ}}{F}$$

As  $E^{\circ}$  for the half cell  $\text{H}^+/\frac{1}{2}\text{H}_2$  is defined as 0, then

$$\Sigma \Delta G_{\text{H}^+/\frac{1}{2}\text{H}_2}^{\circ} = 0$$

Therefore

$$\begin{aligned} E^{\circ} &= \frac{\Sigma \Delta G_{\text{Fer}^+/\text{Fer}}^{\circ}}{F} \\ &= \frac{\Delta G_{\text{I}}}{F} + \frac{\Delta(\Delta G_{\text{solv.}}^{\circ})}{F} \end{aligned}$$

where  $\Delta(\Delta G_{\text{solv.}}^{\circ}) = \Delta G_{\text{solv.}}^{\circ'} - \Delta G_{\text{solv.}}^{\circ}$

For a reversible system:

$$E_{\frac{1}{2}} = E = E^{\circ} + \frac{RT}{zF} \ln - \frac{[\text{Fer}^+]}{[\text{Fer}]}$$

Therefore:

$$E_{\frac{1}{2}} = \frac{RT}{F} \ln \frac{[\text{Fer}^+]}{[\text{Fer}]} + \frac{\Delta G_{\text{I}}^{\circ}}{F} + \frac{\Delta(\Delta G_{\text{solv.}}^{\circ})}{F} \quad (1)$$

The ionisation energy of a gaseous atom or ion is the change in internal energy,  $\Delta U$ , at OK which accompanies the ionisation process.

To convert  $\Delta U_{\text{O}}$  to  $\Delta H_{298}$ :

$$\Delta H_{298} = \Delta U_{\text{O}} + \int_{\text{U}}^{298} \{c_p(\text{M}^+) + c_p(\text{e}^-) - c_p(\text{M})\} dT$$

I.E. refers to the process  $\text{M}_{(\text{g})} \rightarrow \text{M}_{(\text{g})}^+ + \text{e}_{(\text{g})}^-$

If M,  $\text{M}^+$  and  $\text{e}^-$  are all regarded as ideal monatomic gases, then their heat capacities are zero at OK and  $5/2R$  at temperatures above OK.

Therefore:

$$\begin{aligned} \Delta H_{298} &= \Delta U_{\text{O}} + \int_0^{298} 5/2R \\ &= \Delta U_{\text{O}} + 5/2 \cdot R \cdot 298 \\ &= \Delta U_{\text{O}} + 6.2 \text{ (kJ mol}^{-1}\text{)} \end{aligned}$$

$$\Delta G_{\text{I}}^{\circ} = \Delta H_{\text{I}}^{\circ} - T\Delta S$$

i.e.  $\Delta G_{\text{I}} = \Delta U_{\text{O}} + 6.2 - T\Delta S$



As the change in entropy is small and positive, the  $T\Delta S$  term is small and negative.

Therefore:

$$\Delta G_I \approx \Delta U_O$$

i.e.  $\Delta G_I \approx \text{I.E.}$

Substituting into equation (1):

$$\begin{aligned} E_{\frac{1}{2}} &\approx \frac{\text{I.E.}}{F} \text{ (in kJ)} + \frac{RT}{F} \ln \frac{[\text{Fer}^+]}{[\text{Fer}]} + \frac{\Delta(\Delta G_{\text{solv.}}^{\circ})}{F} \\ &\approx \text{I.E. (in eV)} + RT \ln \frac{[\text{Fer}^+]}{[\text{Fer}]} + \Delta(\Delta G_{\text{solv.}}^{\circ}) \end{aligned}$$

REFERENCES

1. C.J. Pedersen, J. Am. Chem. Soc., 1967, 89, 2495.  
C.J. Pedersen, J. Am. Chem. Soc., 1967, 89, 7017.
2. Topics in current chemistry, 1981, 98.
3. Topics in current chemistry, 1982, 101.
4. Structure and Bonding, 1973, 16,  
J.M. Lehn, Chapter 1.  
M.R. Trutor, Chapter 2.  
W. Simon, W.E. Morf and P. Ch. Meier, Chapter 3.  
R.M. Izatt, D.J. Eatough and J.J. Christensen,  
Chapter 4.
5. R.N. Greene, Tetrahedron Lett., 1972, 1793.
6. M. de S. Healy and A.J. Rest, Adv. Inorg. Chem.  
Radiochem., 1978, 21, 1.
7. D.N. Reinhoudt, F. de Jong and H.M.P. Tomassen,  
Tetrahedron Lett., 1979, 2067.
8. B.R. Bowsher and A.J. Rest, J. Chem. Soc., Dalton  
Trans., 1980, 1157.
9. B.L. Shaw, J. Am. Chem. Soc., 1975, 97, 3856.
10. K. Ziegler in Methoden der Organischen Chemie,  
Houben-Wegl, 1981, 4.2, 729.
11. M.G.B. Drew, A. Hamid Bin Othan, S.G. McFall and  
S.N. Nelson, J. Chem. Soc., Chem. Commun., 1975, 818.
12. D.H. Cook and D.E. Fenton, Inorg. Chim. Acta, 1977,  
25, L95.
13. R.M. Izatt and J.J. Christensen (Eds.), 'Synthetic  
Multidentate Macrocyclic Compounds', Academic Press,  
New York, London 1978.
14. B. Dietrich, J.-M. Lehn, J.P. Sauvage and J. Blaazat,  
Tetrahedron, 1973, 29, 1629.
15. B. Dietrich, J.-M. Lehn, J.P. Sauvage, Tetrahedron,  
1973, 29, 1647.
16. P. Seiler, M. Dobler, J.D. Dunitz, Acta Cryst.,  
1974, B30, 2744.
17. P.R. Mallinson and M.R. Turner, J. Chem. Soc.,  
Perkin Trans. II, 1972, 1818.
18. D.L. Hughes, J. Chem. Soc., Dalton Trans., 1975,  
2374.

19. B. Metz, D. Moras, R. Weiss, J. Chem. Soc., Chem Commun., 1970, 217.
20. Y.M. Cahen, J.L. Dye and A.I. Popov, J. Phys. Chem., 1975, 79, 1289.  
Y.M. Cahen, J.L. Dye and A.I. Popov, J. Phys. Chem., 1975, 79, 1292.
21. J.-M. Lehn, Acc. Chem. Res., 1978, 11, 49.  
J.-M. Lehn, Pure Appl. Chem., 1977, 49, 847.
22. D.K. Cabbiness and D.W. Margerum, J. Am. Chem. Soc., 1969, 91, 6540.
23. J.J. Christensen, 'Transport of metal ions by liquid membranes containing macrocyclic carriers', McGraw-Hill, 1978.
24. See 21.
25. B. Metz, D. Moras and R. Weiss, J. Chem. Soc., Perkin Trans. II, 1976, 423.
26. G.W. Gokel and H.D. Durst, Synthesis, 1976, 168.
27. H.K. Frenslorff, J. Am. Chem. Soc., 1971, 93, 600.
28. R.M. Izatt, et al., J. Am. Chem. Soc., 1977, 99, 6134.  
R.M. Izatt, et al., Inorg. Chim. Acta, 1978, 30, 1.
29. M. Ciampolini et al., Inorg. Chim. Acta, 1980, 45, L239.  
J.P. Dutasta, J. Martin, J.B. Robert, Heterocycles, 1980, 14, 1631.
30. E.P. Kyba and S.S.P. Chou, J. Am. Chem. Soc., 1980, 102, 7012.
31. D.H. Buseh, Acc. Chem. Res., 1978, 11, 392.
32. F. Peter and M. Gross, J. Electroanal. Chem., 1974, 53, 307.  
F. Peter and M. Gross, J. Electroanal. Chem., 1975, 61, 245.
33. M. Rosenblum, 'Chemistry of the iron group metallocenes', Wiley Interscience, 1965.
34. A.P. Bell and C.D. Hall, J. Chem. Soc., Chem. Commun., 1980, 163.
35. D.E. Bublitz, et al., Organic Synthesis, 1961, 41, 96.
36. M.D. Rausch, E.O. Fischer and H. Grubert, J. Am. Chem. Soc., 1960, 82, 76.

37. G. Wilkinson, J. Am. Chem. Soc., 1952, 74, 6146.  
E.O. Fischer and H. Grubert, Chem. Ber., 1959, 92,  
2302.
38. L. Bednank and E. Neuse, J. Organomet. Chem., 1979,  
C8-12, 168.
39. P. Pertiei, G. Vitalli, M. Paci and L. Perri, J. Chem.  
Soc., Dalton Trans., 1981, 1961.
40. O. Hoger and K. Schlogl, J. Organomet. Chem., 1968,  
13, 457.
41. J.S. Bodenheimer and W. Low, Spectrochim. Acta,  
1973, 29A, 1733.
42. G. Wilkinson, M. Roseblum, A. Whiting and R.B.  
Woodward, J. Am. Chem. Soc., 1952, 74, 2125.  
G. Woodward, M. Roseblum and A. Whiting, J. Am.  
Chem. Soc., 1952, 74, 3458.
43. T.J. Kealy and P.L. Pauson, Nature, 1951, 168, 1039.
44. E.A. Seddon and K.R. Seddon, 'The Chemistry of  
Ruthenium', Amsterdam Elsevier, 1984.
45. A. Haaland and J.E. Nilsson, Acta Chem. Scand., 1968,  
22, 2653.
46. G.L. Hardgrove and D.H. Templeton, Acta Cryst.,  
1959, 12, 28.
47. E.R. Lippincott and R.D. Nelson, Spectrochim. Acta,  
1958, 10, 307.
48. H.P. Fritz, Adv. Organomet. Chem., 1964, 1, 239.
49. T.V. Long and F.R. Huege, J. Chem. Soc., Chem.  
Commun., 1968, 20, 1239.
50. D. Hartley and M.J. Ware, J. Chem. Soc., 1969, 1A,  
138.
51. M.D. Rausch, M. Vogel and M. Rosenberg, J. Org.  
Chem., 1957, 22, 903.
52. B. Leukart, Chem. Ber., 1885, 18, 873.
53. B. Leukart and M. Schmidt, Chem. Ber., 1885, 18,  
2338.
54. D.W. Mayo, P.D. Shaw and M. Rausch, Chem. and Ind.,  
1957, 1388.
55. J.A. Pople, W.G. Schneider and H.J. Bernstein, 'High  
resolution nuclear magnetic resonance', McGraw-Hill,  
1978, 223.

56. G. Binsch, Topics in stereochemistry, 1968, 3, 122.
57. L.W. Reeves, Adv. Phys. Org. Chem., 1965, 3, 202.
58. W.E. Stewart and T.H. Siddell, Chem. Rev., 1970, 70, 537.
59. M.D. Rausch and D.J. Ciappenelli, J. Organomet. Chem., 1967, 10, 127.
60. J.M. Osgerby and P.L. Pausen, J. Chem. Soc., 1961, 4604.
61. J.-M. Lehn, (CA 74: 100134t) British Patent 1973, 1304367.
62. M. Dale and C. Kristiansen, Acta Chem. Scand., 1972, 26, 1471.
63. F. Vogtle, et al., Chem. Ber., 1976, 112, 1392.
64. C. Richmann and T. Atkins, J. Am. Chem. Soc., 1976, 96, 2268.
65. F. Vogtle, et al., Liebigs Ann. Chem., 1976, 1, 916.
66. F. Vogtle, et al., Liebigs Ann. Chem., 1977, 1, 1344
67. CA 68: 29843a  
CA 68: 87384a
68. R. Elliott, et al., J. Prakt. Chem., 1967, 35, 149.
69. D.N. Hendnekson, Y.S. Sohn, W.H. Morrison and H.B. Gray, Inorg. Chem., 1972, 11, 808.
70. S.P. Gubin and A.A. Lubovich, J. Organomet. Chem., 1970, 22, 183.
71. S.P. Gubin, S.A. Smirnova, L.I. Denisovich and A.A. Lubovich, J. Organomet. Chem., 1971, 80, 243.
72. J.L. Dye, C.W. Andrews and S.E. Mathews, J. Phys. Chem., 1975, 79, 3065.
73. J.L. Dye, C.W. Andrews and J.M. Ceraso, J. Phys. Chem., 1975, 79, 3076.
74. D.G. Adolphson, J.D. Corbett, D.J. Merryman, P.A. Edwards and F.J. Annatis, J. Am. Chem. Soc., 1975, 97, 6267.
75. A. Knochel and R.D. Wilken, J. Radioanal. Chem., 1976, 32, 345.

76. M. Cinquiai, F. Montanari and P. Turido, *J. Chem. Soc., Chem. Commun.*, 1975, 393.
77. B.E. Jepson, 1974, U.S. Patent No. 3,914,373.
78. D. Zucker and J.D. Drury, *J. Chem. Phys.* 1964, 41, 1678.
79. G.D. Klinskii, et al., *Russ. J. Phys. Chem.*, 1974, 48, 880.  
G.D. Klinskii, et al., *Russ. J. Phys. Chem.*, 1974, 48, 880.
80. See 20.
81. J.M. Cernso and J.L. Dye, *J. Am. Chem. Soc.*, 1977, 95, 4432.
82. J.P. Kintzinger and J.-M. Lehn, *J. Am. Chem. Soc.*, 1977, 96, 3313.
83. E. Mei, A.I. Popov and J.L. Dye, *J. Am. Chem. Soc.*, 1977, 99, 6532.
84. S. Villenaux and J.J. Delpaech, *J. Chem. Soc., Chem. Commun.*, 1975, 478.
85. B. Britz and D. Knittel, *Electrochim. Acta*, 1975, 20, 891.
86. F. Peter and M. Gross, *J. Electroanal. Chem.*, 1974, 53, 307.  
F. Peter and M. Gross, *J. Electroanal. Chem.*, 1975, 61, 245.
87. G. Eisenman, 'Glass electrodes for hydrogen and other cations', 1967.
88. J.W. Ross, *Science*, 1967, 156, 1378.
89. J.L. Walker, *Anal. Chem.*, 1971, 43, 89A.
90. E. Eyal and G.A. Rechnitz, *Anal. Chem.*, 1971, 43, 1090.
91. Z. Stefanac and W. Simon, *J. Microchem.*, 1967, 12, 125.
92. W.K. Lutz, P.U. Frieh and W. Simon, *Helv. Chim. Acta*, 1971, 54, 2767.
93. D.F. Reusch and E.L. Cassler, *J. Am. Chem. Soc.*, 1973, 19, 736.
94. M. Mascini and F. Pallozi, *Anal. Chem. Acta*, 1974, 73, 375.

95. W.E. Merf, et al., Pure Appl. Chem., 1973, 36, 421.
96. C. Fuchs, et al. Klin. Wsehr. 1976, 56, 824.
97. E. Weber and F. Vogtle, Kontakte (Merck.), 1978, 2, 16.
98. O.H. Le Blanc, et al., J. Appl. Physiol., 1976, 40, 644.
99. M. Tayaki, H. Nakamura and K. Ueno, Anal. Lett., 1977, 10, 1115.
100. G. Czerwenka and L. Scherrbeck, Anal. Chem., 1975, 34, 276.
101. J.-M. Lehn and J.P. Sauvage, J. Am. Chem. Soc., 1975, 97, 6700.
102. S. Kopolov, J. Smid and T.E. Hoegen-Esch, Macromolecules, 1973, 7, 1015.
103. S. Kopolov, J. Smid and T.E. Hoegen-Esch, Macromolecules, 1973, 6, 133.
104. C.J. Pedersen, et al., Angew. Chem., Int. Ed. Engl., 1972, 11, 16.
105. B.G. Cox, et al., J. Am. Chem. Soc., 1978, 100, 4746.
106. F. Peter, J.P. Gvsselbrecht and M. Gross, J. Electroanal. Chem., 1978, 86, 115.
107. L. Pospisil, J. Electroanal. Chem., 1973, 46, 203.  
L. Pospisil, J. Electroanal. Chem., 1973, 46, 251.
108. T. Kimura, I. Washima and T. Shimaro, Chem. Lett. Jpn., 1977, 1, 563.
109. Y. Takeda and H. Goto, Bull. Chem. Soc. Jpn., 1979, 52, 1920.
110. Y. Takeda and H. Goto, Bull. Chem. Soc. Jpn., 1979, 52, 2501.
111. Y. Takeda and H. Goto, Bull. Chem. Soc. Jpn., 1979, 52, 1027.
112. Y. Marcus and Y.E. Asher, J. Phys. Chem., 1978, 82, 1246.
113. R.C. Helgeson, et al., J. Am. Chem. Soc., 1973, 95, 3023.
114. T. Kimura, et al., Anal. Chem., 1979, 51, 1113.

115. See 103.
116. F. Melson, et al., *J. Chromatogr.*, 1965, 20, 207.
117. W. Smalek and W. Lada, *J. Radioanal. Chem.*, 1977, 30, 199.
118. R.L. Sousa, D.H. Hoffmann, L. Kaplam and D.J. Cram, *J. Am. Chem. Soc.*, 1974, 96, 7100.
119. B. Dietrich, J.-M. Lehn and J. Simon, *Agrew. Chem. Int. Ed. Engl.*, 1974, 13, 406.
120. J.P. Behr, J.-M. Lehn and P. Vierling, *J. Chem. Soc., Chem. Commun.*, 1976, 621.
121. G.A. Russel, G. Walraff and J.L. Gerlock, *J. Phys. Chem.*, 1978, 82, 1161.
122. E. Blasius, et al., *J. Chromatogr.*, 1980, 147, 201.
123. B. Dietrich and J.-M. Lehn, *Tetrahedron Lett.*, 1973, 1225.
124. D. Clement, F. Damm and J.-M. Lehn, *Heterocycles*, 1976, 5, 477.
125. W.P. Weber and G.W. Gokel, 'Phase transfer catalysis in organic synthesis', Springer-Verlag, 1977.
126. D.E. Fenton, *Chem. Rev.* 1973-4, 140.
127. J. Berger, et al., *J. Am. Chem. Soc.*, 1951, 73, 5295.
128. J. Drench, et al., *Nature*, 1984, 218, 929.
129. D.J. Cram, et al., *J. Am. Chem. Soc.*, 1979, 101, 4948.
130. J.P. Behr and J.-M. Lehn, *J. Chem. Soc., Chem. Commun.*, 1978, 143.
131. J.P. Behr and J.-M. Lehn, *Helv. Chim. Acta*, 1980, 63, 2112.
132. R.M. Kellogg, et al., *Tetrahedron*, 1978, 34, 2377.
133. O. Kahn, et al., *J. Am. Chem. Soc.*, 1980, 102, 5935.
134. J.-M. Lehn, J. Simon and J. Wagner, *Nouv. J. Chim.*, 1977, 1, 77.
135. J.F. Stoddart, *Chem. Rev.*, 1979, 8, 85.
136. R. Breslow, *Acc. Chem. Res.*, 1980, 13, 170.



137. E. Kordize, et al., J. Organomet. Chem., 1975, 93, C26.
138. C. Brevard and P. Granger, Inorg. Chem., 1983, 22, 532.
139. S. Brettgonbach, et al., Z. Phy., 1977, A217, 280.
140. J.D. Dunitz, L.E. Orgel, and A. Rich, Acta Cryst., 1956, 9, 373.  
E.A. Seibold and L.E. Sutton, J. Chem. Phys., 1955, 23, 1967.  
E.R. Lippincott and R.D. Nelson, Spectrochim. Acta, 1958, 10, 307. *See reference 194.*
141. M. Rosenblum, 'Chemistry of iron group metallocenes', Interscience New York, part 1, 1965.  
G. Wilkinson and F.A. Cotton, Progress in Inorg. Chem., 1959, 1, 1.
142. R.K. Bohn and A. Haaland, J. Organomet. Chem., 1966, 5, 470.
143. J.W. Edwards, G.L. Kington and R. Mason, J. Chem. Soc., Faraday Trans., 1960, 56, 660.  
L.N. Mulay and A. Attalla, J. Am. Chem. Soc., 1963, 85, 702.  
J.S. Bodenheimer and W. Low, Phys. Lett., 1971, 36A, 253.
144. P. Dale and C.J. Kristiansen, Acta Chem. Scand., 1972, 26, 1471.
145. M.R. Johnson, I.V. Sutherland and R.F. Newton, J. Chem. Soc., Perkin Trans. I, 1979, 1, 357.
146. S.A.G. Hogberg and D.J. Cram, J. Org. Chem., 1975, 40, 151.
147. O. Eisleberg, Chem. Ber., 1941, 74, 1433.
148. D.E. Bublitz and K.L. Rinehart, Organic Reactions, 1963, 17, 213.
149. M.D. Rausch and D.J. Ciapenelli, J. Organomet. Chem., 1967, 1, 127.
150. J.M. Osgerby and P.L. Pauson, J. Chem. Soc., 1961, 1, 4604.
151. H.J. Lorkowski, R. Pannier and A. Vende, J. Prakt. Chem., 1967, 85, 149.
152. M. Rosenblum, et al., J. Am. Chem. Soc., 1963, 85, 316.

153. C.D. Hall and P.J. Hammond, Private commun. 1984.
154. S. Sorrisso and H. Lumbroso, *Tetrahedron*, 1970, 26, 2695.
155. G.L. Palenik, *Inorg. Chem.*, 1969, 8, 2744.  
G.L. Palenik, *Inorg. Chem.*, 1970, 9, 2424.
- 156a. A. Liden, et al., *J. Am. Chem. Soc.*, 1976, 98, 2853.
- 156b. R.G. Jones and J.M. Wilkins, *Org. Mag. Res.*, 1978, 11, 20.
157. H. Fritz, et al., *Org. Mag. Res.*, 1981, 16, 36.
158. M.D. Rausch and A. Siegal, *J. Organomet. Chem.*, 1969, 17, 117.
159. F.A. Bovey, 'Nuclear magnetic resonance spectroscopy', Academic Press, New York, 1965, 75.
160. H.S. Gutowsky and C.H. Holm, *J. Chem. Phys.*, 1956, 25, 1228.
161. Annual reports on n.m.r. spectroscopy, 1968, 14, 71.
162. See 61.
163. P. Reich-Rohnsig and K. Schlögl, *Montash. Chem.*, 1968, 99, 2175.
164. F.X. Kohl and P. Jatzi, *J. Organomet. Chem.*, 1983, 243, 119.
165. L. de Vries, *J. Org. Chem.*, 1960, 25, 1838.
166. R.B. King and M.B. Bisnette, *J. Organomet. Chem.*, 1967, 8, 287.
167. R.F. Rovar, M.D. Rausch and H. Rosenberg, *J. Organomet. Chem.*, 1970, 1, 173.
168. A.N. Nesmeyanov, V.A. Sazonova and V.N. Drozd, *Chem. Ber.*, 1960, 93, 2717.
169. F.L. Hedberg and H. Rosenberg, *J. Am. Chem. Soc.*, 1973, 95, 870.
170. P.J. Graham, R.V. Lindsey, G.W. Parshall, M.L. Peterson and G.M. Whitman, *J. Am. Chem. Soc.*, 1957, 79, 3416.
171. G.D. Broadhead, J.M. Osgerby and P.L. Pauson, *J. Am. Chem. Soc.*, 1958, 1, 650.

172. M. Rosenblum, A.K. Banerjee, N. Danieli, R.W. Fish and V. Schlatter, *J. Am. Chem. Soc.*, 1963, 85, 316.
173. R.L. Schaaf, P.T. Kan and K.L. Rinehart, Wright air development center technical report, 1960, II, 58, (AD243566L).
174. S.V. Sunthakar and S.T. Mahadik, *J. Indian Chem.*, 1973, 11, 1207.
175. D.H. Evans, K.M. O'Connell, R.A. Petersen and M.J. Kelly, *J. Chem. Ed.*, 1983, April, 290.
176. G.A. Mabbott, *J. Chem. Ed.*, 1983, Sept., 697.
177. P.T. Kissinger and W.R. Heineman, *J. Chem. Ed.*, 1983, Sept., 702.
178. J.H.D. Eland, 'Photoelectron spectroscopy', Butterworths, 1974.
179. R.K. Bohn and A. Haaland, *J. Organomet. Chem.*, 1966, 5, 470.
180. R. Prins, *Mol. Phys.*, 1970, 19, 603.
181. F.A. Cotton and G. Wilkinson, 'Advanced inorganic chemistry', 3rd edition, Wiley Interscience, 1972.
182. J.P. Fackler and W.C. Seidel, *Inorg. Chem.*, 1968, 8, 1631.
183. J.P. Fackler and W.J. Zegarski, *J. Am. Chem. Soc.*, 1973, 95, 8566.
184. W.C. Neikam, et al., *J. Am. Chem. Soc.*, 1964, 86, 4811.
185. T.T.T. Li and C.H. Bachaker, *J. Organomet. Chem.*, 1981, 216, 223.
186. See 5.
187. R.W. Dykstra and A.M. Harrison, *J. Mag. Res.*, 1982, 46, 338.
188. C. Brevard and P. Granger, *Inorg. Chem.*, 1983, 22, 532.
189. C. Brevard, Private Commun., 1981.
190. P.D. Beer, et al., *J. Chem. Soc., Chem. Commun.*, 1985, 1115.
191. S.J.Hayes, C.M.Dobson, N.J.Claydon and P.J.Wiseman, '4<sup>th</sup> International Symposium, Inclusion Phenomenon, University of Lancaster, 1986, poster No.8, (see published conference abs. ).

192. P.D. Beer, et al., J. Organomet. Chem., 1985,  
297, 313.
193. P.J. Hammond, P.D. Beer, C. Dudman, C.P. Dankes,  
C.D. Hall, J.P. Knychala and M.C. Grossel,  
J. Organomet. Chem., 1986, 306, 367.
194. P. Seiler, J.D. Dunitz, Acta Cryst., Sect. B, 1982, B(88)6, 17415.

R.H.B.N.C.  
LIBRARY